S-Nitroso-*N*-acetylpenicillamine (SNAP)-Based Antithrombotic and Antimicrobial Polymers for Biomedical Applications: Nitric Oxide (NO) to the Rescue

by

Yaqi Wo

A dissertation submitted in partial fulfillment
of the requirements for the degree of
Doctor of Philosophy
(Chemistry)
in the University of Michigan
2017

Doctoral Committee:

Professor Mark E. Meyerhoff, Chair
Associate Professor Kenichi Kuroda
Associate Professor Anne J. McNeil
Associate Professor Chuanwu Xi

“Stay Hungry, Stay Foolish.”

—Steve Jobs

2017

DEDICATION

To my family and loved ones.

ACKNOWLEDGEMENTS

Throughout my time at the University of Michigan, I have received constant and very much appreciated support from many great individuals. First and foremost, I would like to express my sincere gratitude to my advisor, Dr. Mark E. Meyerhoff. I am grateful for all of his guidance, not only on how to be a diligent, industrious and responsible scientist, but also how to be a person with humility, a sense of humor and perspective. To me, Dr. Meyerhoff is more than an advisor; he is a father figure and a loyal friend. For me, going to lab everyday did not feel like I was going to work, but rather going to a home away from home. It is hard for me to imagine how different I would be as a young scientist had I not been fortunate enough to join his group.

Next, I would like to thank my committee members, Dr. Anne J. McNeil, Dr. Kenichi Kuroda and Dr. Chuanwu Xi for serving on my dissertation committee. I have appreciated their insight, their wisdom and the time they each spent on my research proposal and data meetings. Their invaluable suggestions helped me to better design and conduct my PhD research. Thank you also to Dr. Mohamed ElSayed for being on my candidacy committee and for being a wonderful teacher in the polymer therapeutic class I took.

I would like also thank Dr. Zhan Chen and Dr. Brian Coppola for recruiting me from China. I owe them my deepest gratitude for recommending me for admission to the the Chemistry Graduate program. I can still relive the excitement I felt the day I received my acceptance email; it was truly a dream come true.

I was also very lucky to work with many wonderful collaborators and experts from different fields during the course of my PhD research (see below). Not only did I value the knowledge I learned from them, but also the invaluable experience I had working with people with different expertise and personalities. I truly believe that this experience has

better prepared me for my future scientific career, especially on how to best function as a member of an interdisciplinary research team

I would like to thank Dr. Elizabeth J. Brisbois for being the best mentor I can ever hope to have and for all her support and love throughout both the fortunate and less fortunate times of my research. Thank you Dr. Adam J. Matzger, for all the wonderful collaborations we have had over the past two year period which has truly been the most productive time of my PhD. Thank you also to Dr. Zi Li, for the countless hours we spent on the improving our experiments, deriving equations and preparing figures for our papers. Thank you to Dr. Lichong Xu and Dr. Christopher A. Siedlecki for the great chance to work with your group and for all the time and effort you spent to help me with my research, our collaboration has truly been nothing but a wonderful joy. Thank you Alessandro Colletta for all the late night and weekends we spent together optimizing our catheter formulation and for being a passionate and diligent researcher and a wonderful friend. Thank you Dr. Chuanwu Xi, for allowing me to work in your lab, I have learned so much about microbiology from you and your team. Thank you Dr. Jianfeng Wu and for all the help and time you spent with me culturing bacteria, sterilizing bioreactors and gathering fluorescence images. Thank you Dr. Gergely Lautner and Dr. Joanna Zajda for always unselfishly offering your help, wisdom and support to me whenever I needed them, and for being my friend. Thank you Dr. Robert H. Bartlett and the whole research team in Extracorporeal Membrane Oxygenation (ECMO) lab, especially Mr. Terry C. Major and Dr. Azmath Mohammed, for all the blood compatibility animal experiments you helped me carry out on my new NO release materials. Thank you Xianglong for trouble shooting and staying late for our tensile strength tests. I'd like to also thank all the friends I have made in the Meyerhoff lab over the years including dear Dr. Megan C. Frost, Dr. Yu Qin, Dr. Xuewei Wang, Dr. Hang Ren, Dr. Si Yang, Dr. Alexander K. Wolf, James Phan, Dr. Andrea Bell-Vlasov, Dr. Alex Ketchum, Joshua Doverspike, Aaron Jolliffe, Jeong Hyun Hwang, Kyoung Ha Cha, Madeline McCabe, Dr. Wenyi Cai, Dr. Bo Peng, and Stephen Ferguson. It has been a joy to work with you all over the last 4+ years.

I also want to express my sincere gratitude to many wonderful technicians I have had the luck to work with during the years. Thank you Paul Lennon and James Windak for teaching me how to use LC-MS and troubleshooting tirelessly every time I encountered an issue. Thank you to Roy Wentz for all the help you provided on making all the glass vessels needed for my research. Thank you Steve Donajkowski and James Tice for teaching me how to make a stainless steel saw from scratch in the instrument shop and for being so kindly helping my lab with making the NOA stands.

My sincere thanks also go out to our Chemistry department staff. Thank you to the wonderful Margarita Bekiares for being the thread that connected me to U of M when I was in China and for always being there for us students whenever we needed you. My thanks also go to our lab contract and grant specialist Bo Zhao, current graduate coordinator Elizabeth Oxford, and our department student service coordinator Jacqueline Benczarski and Katie Foster.

I 'd like to thank all my dear friends, many of whom are back in China and some of whom are doing PhD or post-doctoral research in various universities in the States, Boya Cui, Xiaoyu Guan, Bing Fu, Liyu Feng, Wei Li, Xin Wei, Lianjing Chai, Mengying Xie, Xiaoting Yang, Danfeng Wang, Rui Song, Bohan Zhang… I cannot be who I am today without your love and support; and take this from me, the end of the tunnel is worth your wait! Thank you to my dear friend Dr. Panan Pichayapinyo and Prabhakar Pandian, the happiness and love you brought me are and forever will be my most cherished memories.

Thank you to Dr. Dipankar Koley for believing in me when I had my doubts, for cheering me up when I was low, and for bringing me many moments of joy.

Finally, I want to thank my family, especially my parents, Rui Wang and Zhe Wo, for giving me my life as well as your unconditional love, support and trust. I know that you will always have my back wherever I may go in the future. I love you.

TABLE OF CONTENTS

LIST OF FIGURES

LIST OF TABLES

ABSTRACT

S-Nitroso-*N*-acetylpenicillamine(SNAP)-Based Antithrombotic and Antimicrobial Polymers for Biomedical Applications: Nitric Oxide (NO) to the Rescue

by

Yaqi Wo

Chair: Mark E. Meyerhoff

Nitric oxide (NO) is known to be a potent inhibitor of platelet activation and adhesion. NO released by macrophages or other inflammatory cells also serves as a natural antimicrobial agent in the immune system. Therefore, polymeric materials that are capable of stable and long-term NO release should exhibit similar antithrombotic and antimicrobial properties.

In this dissertation, novel polymeric materials that can release NO at physiological relevant levels for extended time periods were examined and evaluated for their potential

biomedical applications. *S*-Nitroso-*N*-acetylpenicillamine (SNAP), the NO donor compound, exhibits unprecedented shelf stability when incorporated into low water uptake polymer CarboSil 20 80A, a tri-copolymer of polyurethane, poly(dimethylsiloxane) and polycarbonate. Solid-state analysis demonstrated that SNAP can partially dissolve in CarboSil polymer (ca. 3.4-4.0 wt%) and the SNAP molecules exceeding the solubility limit crystalize via hydrogen bonding within the polymer phase to form a stable polymer-crystal composite material. The slow dissolution of the crystals ultimately contributes to the long-term NO release upon solution contact (Chapter 2). The unique NO release mechanism also directly correlates with the polymer surface area that is exposed to the aqueous solution, suggesting that a water rich layer in the outermost surfaces of the polymer material is the likely site where most of the NO is liberated from the soluble SNAP within the polymer (Chapter 3). An optimized solvent impregnation process was also developed to transform off-the-shelf medical devices, such as intravascular (IV) catheters, to NO releasing catheters (Chapter 4). For example, dip-coated CarboSil IV catheter tubing can be impregnated with up to 15 wt% SNAP loading in methanol/methyl ethyl ketone (30/70 v/v) within 2 h. Both SNAP-doped and SNAP-impregnated CarboSil catheters exhibit significantly less bacterial biofilm formation *in vitro* and reduced clotting *in vivo* when compared to the controls.

Further, dual-functional antibacterial biomaterial surfaces that combine the physical modification (e.g., topographical texture) and chemical modification (e.g., NO release) were developed, with the aim of achieving a synergistic and/or additive effect on the inhibition of bacterial adhesion. Textured CarboSil surfaces bearing ordered pillar

topographies (400/400/600, 500/500/600 and 700/700/300 nm) were fabricated via a soft lithography two-stage replication process. The NO release concept was introduced either by spin-coating SNAP-doped CarboSil sub-layer in the middle of the polymer film (Chapter 5) or by impregnating SNAP into the bulk of the polymer via solvent impregnation (Chapter 6). The antibacterial results demonstrated that the dual functional polymer surfaces provide a synergistic effect in reducing bacteria adhesion of *S. epidermidis* and *P. aeruginosa*.

Overall, the stable and long-term delivery of NO from biomedical polymers provides an attractive approach to improve the hemocompatibility and antibacterial properties of a wide variety of medical devices that face biocompatibility/microbial infection challenges within the hospital setting.

CHAPTER 1

Recent Advances in Thromboresistant and Antimicrobial Polymers for Biomedical Applications: Just Say Yes to Nitric Oxide (NO)

Wo, Y.; Brisbois, E.J.; Robert, R.H., Meyerhoff, M.E., *Biomater. Sci.*, **2016**; 4: 1161-83. (Highlighted on Front Cover) *

1.1 Challenges for Current Implantable Medical Devices

Blood-contacting biomaterials are an integral part of various biomedical devices, ranging from simple catheters to intravascular grafts to extracorporeal circuits and membrane oxygenators, that offer lifesaving treatments to thousands of patients every day. The incorporation of these blood-contacting materials is usually complicated by foreign body response that is initiated by the coagulation cascade[1] (see Figure 1.1).

* This introduction chapter is primarily comprised of a review article published in *Biomaterials Science*, written mostly by this Ph.D. candidate, with valuable edits, insights, suggestions and proofreading by Dr. Elizabeth J. Brisbois.

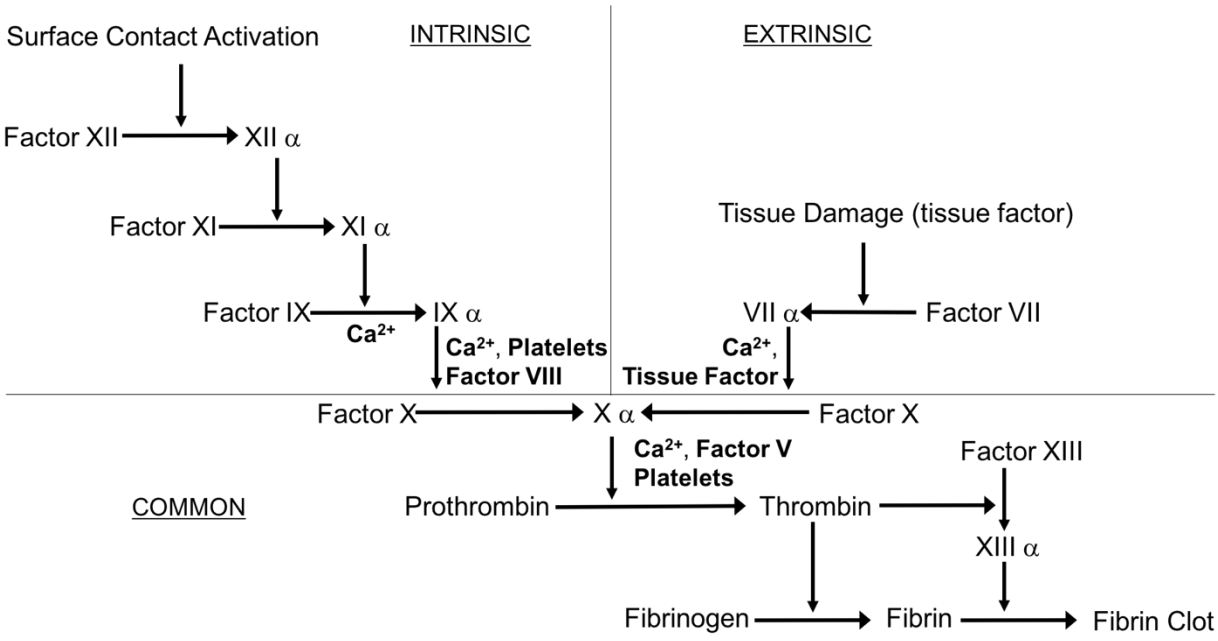

Figure 1.1. Simplified schematic of the blood-coagulation cascade, where both intrinsic (surface contact) and extrinsic (tissue factors) pathways converge and ultimately form thrombus (modified from review by Sefton et al.[2]).

Exposure of blood to foreign materials will cause plasma proteins, such as Factor XII and Factor XI, to be activated and adhere to the polymer surface. The activated protein will interact with platelet surface membrane receptor GPIIb/IIIa, that can bind with fibrinogen, von Willebrand Factors (vWF), fibronectin, and vitronectin, which ultimately leads to platelet conformational changes, subsequent release of intracellular agents (e.g., Factor V, VIII and Ca^{2+}, etc.), and initiates platelet activation and aggregation (intrinsic pathway).[2,3] Further, surgical procedures that utilize these devices have the potential to injure the vessel wall, disrupt blood homeostasis and release tissue factor, also causing platelet activation and concomitant conformational changes as well (extrinsic pathway).[1–6] Both pathways converge and trigger the coagulation cascade as the activated platelets bind with fibrinogen

and other clotting factors. Fibrinogen forms insoluble fibrin, which traps red blood cells and ultimately forms a thrombus within a matter of hours[7,8] (see Figure 1.2).

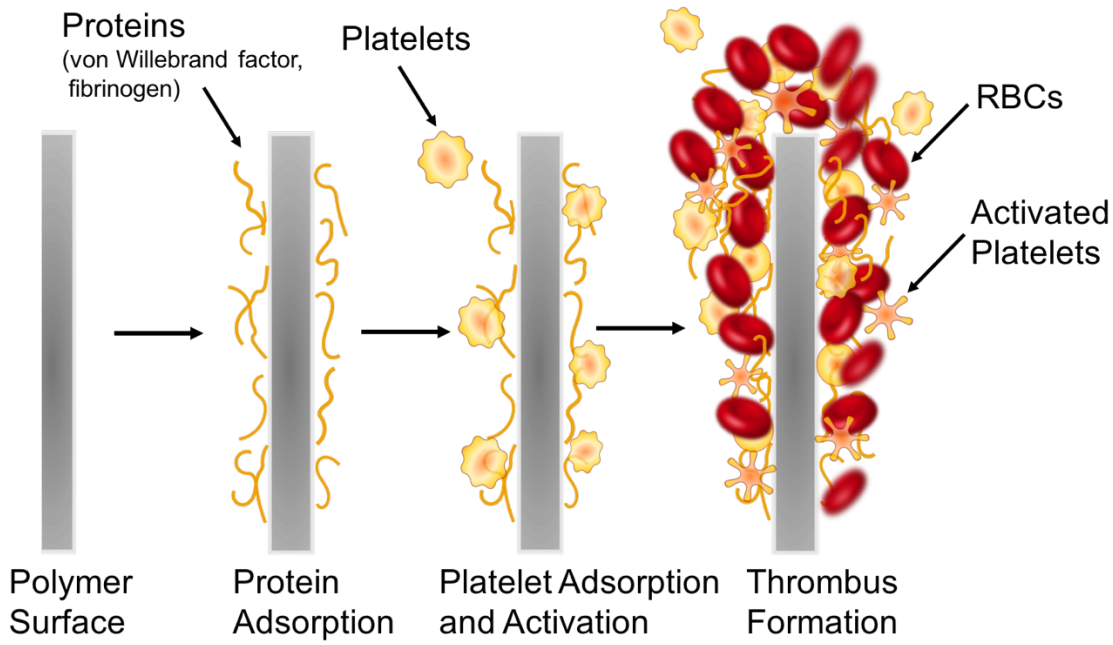

Figure 1.2. Simplified representation of the processes that lead to thrombus formation on the surfaces of blood contacting biomedical devices.

In addition to thrombus formation, bacterial infection is also often associated with the use of many biomedical devices. The rise of hospital-acquired infections, also known as nosocomial infections, is a growing concern in healthcare industry. It was reported that an estimated 1.7 million patients suffered from healthcare-associated infections (HAI) in the U.S. hospitals in 2002 and the number of HAI deaths was 98,987 patients, including 30,665 resulting from bloodstream infections.[9–15] Device-related infections are the result of bacteria adhesion to the biomaterial surface. After planktonic bacteria initially colonize onto the surfaces of polymeric devices, cells start to grow into colonies, and then hydrated

matrices of extracellular polymeric substances (EPS) are formed, also known as biofilms, [16–18] (see Figure 1.3).

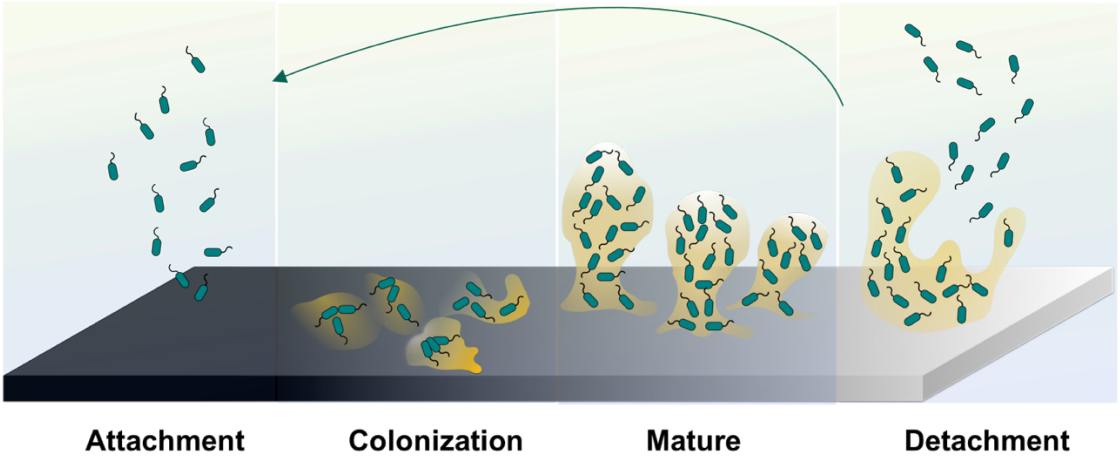

Figure 1.3. Representative processes involved in biofilm formation and bacteria dispersion.

The EPS holds the bacterial cells together in a mass and firmly attaches the cells to the underlying surface. Ultimately, a mature biofilm will periodically release bacteria cells from the biofilm colony into the surrounding medium. Of note, the EPS is both a physical and a chemical barrier to antibiotics and significantly retards their rate of penetration that makes conventional antibiotic treatment for such infections ineffective. Further, the EPS can possibly foster antibiotic-resistant bacterial gene mutations.[19] Ideally, all biomedical devices should be able to prevent bacterial colonization on their surfaces, especially within the first 6 h of blood exposure, which is identified to be the most susceptible and most "decisive period" for the success of a long-term implant.[20] Thrombus and bacteria biofilm formation cause device failure, which in many cases can only be solved by device removal and replacement. Besides patients suffering, the increased healthcare costs associated with these infections has also created a significant economic burden.[20]

The clinical problems of thrombus and infection described above have triggered substantial interest among scientists to develop new and more effective ways to create antithrombotic and antibacterial polymeric surfaces for biomedical devices, especially those in direct contact with blood (e.g., intravascular catheters, vascular grafts, etc.).

1.2 Current Strategies for Prevention of Thrombosis

1.2.1 Actively releasing anticoagulants to block the innate coagulation cascade

In a clinical setting, in order to prevent surface-induced thrombosis during cardiopulmonary bypass, hemodialysis, and angioplasty, anticoagulants are routinely administered, the most commonly used one being heparin.[2,21] However, systemic heparin administration can lead to hemorrhage and thrombocytopenia. Localized release of heparin with concentrations that are not tolerable at the systemic level may be applied with minimal side-effects.[22,23] To date, several approaches have been pursued to achieve localized heparin activity at the surface of implanted devices including the creation of heparin-releasing polymer surfaces via ionic bonding,[22,24–26] physical dispersion[27–30] and solution swelling,[22,31,32] as well as heparin-immobilized polymer surfaces.[33–36] For example, Gutowska et al.[22] described a novel thermosensitive heparin-releasing poly(*N*-isopropylacrylamide) (poly(NiPAAm)) coating for prevention of surface-induced thrombosis on polyurethane catheters. Poly(NiPAAm) has a lower critical solution temperature (LCST) in aqueous solution, around 32 °C, which enables it to swell when immersed in a heparin solution at low temperature (e.g., room temperature, RT) and uptake this polyanionic drug. When the temperature is higher than LCST, the swollen coating will collapse dramatically and release heparin. Both the heparin impregnated and control PU

catheters were inserted into saphenous veins in a canine model for 1.5 h, and the heparin-releasing PU catheter surfaces demonstrated a significant reduction of thrombus formation after contact with the venous blood. This was demonstrated by SEM images of the explanted catheters when compared to the appropriate controls. Heparin typically has low solubility in organic solvents, but this swelling method introduced the possibility of solution absorption in water and loading of a relatively large amount of the drug into the swollen polymer chains. This method also offers flexibility for the amount and type of anticoagulant drugs that can be loaded into various thermosensitive coatings.[22] However, the heparin release kinetics for this system are relatively fast, with the release rates of 1 $\mu g/cm^2$ per h for up to 6 h. Therefore, the potential application of this material is limited to preventing thrombosis formation in short-term applications, such as for angiography catheters, etc.

Heparin has also been covalently linked to the surface of vascular grafts via end-point immobilization and this approach has been commercialized for expanded polytetrafluoroethylene (ePTFE) and Dacron grafts.[37–39] The key to the success of heparin-immobilized polymers depends on the covalently bound heparin remaining flexible enough to bind antithrombin III in order to prevent fibrin formation and the ultimate blood clot.[3] The literature on immobilization of heparin is vast and has been reviewed extensively elsewhere.[37,40] However, due to their very short half-life,[41] heparinized polymer surfaces still suffer a great challenge when it comes to long-term *in vivo* applications. Other anticoagulants such as thrombomodulin,[36] direct thrombin inhibitors (e.g., hirudin[42] and argatroban[43]), or antiplatelet drugs (e.g.: prostacyclin (PGI_2))[36,41,42] have also been

immobilized onto polymer surfaces to increase their hemocompatibility, with varying degrees of success.

1.2.2 Chemical modification of the polymer surface to reduce protein adsorption

It is widely known that the first step that initiates activation of the coagulation cascade is protein adsorption (especially fibrinogen and von Willebrand factor; see Figure 2) to the surface of a blood contacting medical device. This knowledge has led to many years of research in developing approaches to modify polymer surfaces that focus on reducing such non-specific protein adsorption. Some examples include immobilizing a layer of blood-compatible hydrogels on the device surfaces, such as poly(vinyl alcohol) (PVA), polyacrylamide (PAAm), poly(N-vinyl pyrrolidone) (PNVP), poly(hydroxyethyl methacrylate) (PHEMA), poly(ethylene oxide) (PEO), poly(ethylene glycol) (PEG), poly(ethylene glycol) monomethyl ether (PEGME), and cellulose.[3,22,44] Hydrogels are water-swollen polymeric networks containing chemical or physical cross-links and were first used initially as soft contact lenses in the late 1950s.[45] Due to their hydrophilicity and excellent water retention properties, they have the natural tendency to prevent cell and protein adhesion and are considered to be very biocompatible and desirable in biomedical applications. For example, immobilization of PEG ($-CH_2CH_2O-$) is a widely used method to modify traditional polymer surfaces employed in the medical field, such as plasticized poly(vinyl chloride) (PVC) and polyethylene (PE), etc.[46–49] PEG is a non-toxic water-soluble polymer approved by the U.S. Food and Drug Administration (FDA) for internal consumption.[50] Lakshmi et al.[46] were among the first to graft PEG 4000 onto medical grade PVC sheets and conducted thrombogenicity studies to evaluate platelet adhesion

using platelet rich plasma (PRP) and whole blood clotting time with fresh rabbit blood. The scanning electron microscope (SEM) images clearly indicated more platelet adhesion to the bare PVC sheet than the PEG-grafted ones. The PEG grafting also extended the whole blood clotting time from 20 min to more than 70 min as determined by the hemolysis assay. Balakrishnan et al.[47] later demonstrated success using bulk modification of PVC resin with PEG 600 that yielded greatly reduced solid/water interfacial free energy and platelet adhesion in *in vitro* PRP studies. This study expanded the anti-fouling chemistry from surface modification on a finished product to bulk synthesis. However, studies conducted by Sefton and coworkers, who used PEG immobilized PVA hydrogel coated PE tubing in an *ex vivo* canine arteriovenous (AV) shunt, reported that neither the PEG grafted or control PVA tubing could maintain circulating platelet levels after 4 d.[49] Heparin and hydrogel modified surfaces are the most commonly studied approaches for achieving thromboresistant surfaces. For further breadth, readers are guided to reviews that highlight additional approaches developed thus far, such as endothelial cell coated-surfaces, albumin-coated surfaces, pyrolytic carbon-coated surface, phosphorylcholine surfaces, elastin-inspired surfaces, etc.[3,42,51–53]

1.3 Current Strategies for Creating Antibacterial Surfaces

1.3.1 Surfaces that resist bacteria and reduce initial attachment

Bacteria attachment to device surfaces is the first step required for biofilm formation. Therefore, using biomaterial surfaces that resist bacteria attachment is an intuitive solution to this problem.[54] Super-hydrophobic polymer surfaces, such as very smooth silicone, polyurethane, polytetrafluoroethylene (PTFE), poly(vinyl chloride) (PVC), and

polyethylene (PE), that have water contact angles larger than 150°, low surface energy,[55,56] as well as unique water repellent[57] and self-cleaning abilities,[56] are known to have resistance to microbial cell adhesion during short-term applications.[58] Hydrophilic surface modifications, such as the PEG modified surfaces discussed above, have also been widely characterized in the literature and have demonstrated excellent anti-adhesive properties for bacteria cells and proteins.[44] However, the susceptibility of PEG to oxidative damage, especially in the presence of O_2, transition metal ions or certain enzymes *in vivo*, has limited its long-term application in complex media.[59,60] Some studies have demonstrated that polymer surfaces with segmented block co-polymers (hard and soft domains) that result in phase-separated structures also exhibit less bacterial adhesion and cell attachment.[61–63] Overall, however, passive surfaces without functional active agents may not be ideal for long-term applications because these surfaces may eventually become contaminated due to defects during preparation or deterioration of the coating when in contact with physiological fluids.[3,4,64]

1.3.2 Surfaces that disperse or detach biofilms

Biofilm dispersal is a promising area of research that focuses on how to inhibit biofilm formation using dispersal agents, which induce biofilm bacteria to detach and return to their planktonic form. Several studies have found that bacteria naturally produce biofilm dispersal agents when the community senses a quorum, signaling the detachment process.[54] These agents include D-amino acids,[65] cis-2-decenoic acid (C2DA),[16,18,54] peptides and various enzymes (e.g., dispersin B), etc.[54,66] However, most mechanisms of action of these compounds are still unclear, which hinders further development and application in this

field. Many researchers have studied the effects of these dispersal agents *in vitro*, by adding the agents directly to pre-formed biofilm in petri dishes or bioreactors.[67] Jennings et al. attempted to load C2DA into chitosan sponges for localized delivery by initially immersing the sponges into 1 mL of 100 mg/mL C2DA in 10 % enthanol.[68] The release of C2DA was determined by HPLC and its release lasted 5 d (200-1000 μg/mL) with a burst of C2DA release on day 1. The anti-biofilm efficiency of the C2DA loaded chitosan sponge was tested against clinical isolates of methicillin-resistant *Staphylococcus aureus* (MRSA) and the results showed that C2DA at a concentration (in the sponge) at or above 500 μg/mL can inhibit bacterial growth. Current research in this field is aimed at developing vehicles for the controlled and sustained release of such biofilm dispersal agents.[54]

1.3.3 Surfaces that have bactericidal functionalities

The most common mechanism of creating functional antibacterial surfaces is through a bactericidal effect, which includes employing a vast collection of approaches involving quaternary ammonium compounds (QACs)[64,69–71] and other polycations (e.g., organometallic dendrimers[72] and chlorhexidine[73]), metal ions (e.g., silver,[74,75] copper,[76] titanium,[77] etc.), locally released antibiotics (e.g., gentamicin[66,78,79]) or bactericidal agents (e.g., bacteriophages,[54,80,81] protein synthesis inhibitors,[66] antibacterial enzymes such as lysozyme,[64,82] antibacterial peptides,[83–85] natural biomolecules such as chitosan[86–88] and herbal extracts (e.g., flavanones and chalcones),[89] etc.), and inducing oxidative stress.[72,90] In general, the mechanisms of bactericidal surfaces are: 1) contact-based bactericidal activity (e.g., QAC, etc.) which affects the ion-exchange processes and cause general

perturbations that destabilize the cytoplasmic membranes of bacteria, resulting in leakage of the intracellular fluid; and 2) release-based bactericidal (e.g., metal ions, antibiotics, etc.), which damage the bacterial cell membrane as well as disrupt the function of bacterial enzymes, DNA, proteins and cell membranes.[64] A problem, however, with many bactericidal surfaces is the attachment of dead microorganisms remaining on the antibacterial coatings, which can trigger immune response and inflammation, as well as block a given coating's active functional group.

In recent years, in order to achieve improved antibacterial and anti-fouling efficacy, many researchers have developed polymeric surfaces that combine more than one of the antibacterial functionalities mentioned above; for example, creating a surface that not only can attach and kill bacteria but also be able to release any adhered dead bacteria debris. Toward this goal, many pH,[59,82,91] thermo,[92] or electrical voltage[93]-responsive polymers, that can be controllably extended or collapsed or altered in their charge carrying properties have been developed. They are often termed "stimuli-responsive smart antibacterial surfaces". Jiang and coworkers developed a cationic poly(*N*,*N*-dimethyl-*N*-(ethoxycarbonylmethyl)-*N*-[2'-(methacryloyloxy)ethyl]-ammonium bromide) that has a quaternary ammonium group and was grafted onto a gold surface by surface-initiated atom transfer radical polymerization.[59] The cationic surface can kill 99.9% of *E. coli* bacteria when exposed to a suspension of 10^{10} cells/mL for 1 h, and then it hydrolyzes into a nonfouling zwitterionic surface and releases 98 % of the bacterial residue after 8 d at 37 °C and pH 10.0. This is only a one-time transition between cationic and zwitterionic surface; therefore, in order to achieve a fully reversible "kill and release" functional surface, a

surface with morpholinone derivatives that can be switched repeatedly between two equilibrium states was developed by the same authors.[91] In neutral or basic aqueous phase, the surface will release dead bacteria and at the same time resist bacteria adhesion. However, under acidic conditions (e.g., in acetic acid for 20 h), the surface will regenerate bacteria-killing function by reforming the quaternary ammonium functional group.

Of note, there are some limitations of this method of using pH change to alter antimicrobial properties of a surface. These include: 1) this surface can kill bacteria attached on the surface while it is dry, since a wet version of this surface is generally resistant to bacterial attachment, suggesting this method mainly works for applications that prevent airborne bacteria; and 2) the requirement of changing environmental pH to achieve surface functionality may be difficult *in situ* with certain biomedical applications (e.g., blood contacting devices). Most recently, Chen and coworker developed an on-demand switchable and repeatable antibacterial surface. They used a silicone nanowire grafted pH-responsive poly (methacrylic acid) (SiN-PMAA) for loading a natural antibacterial agent (i.e.., lysozyme enzyme), enabling killing of bacteria and releasing dead bacteria debris when alternating the environmental pH between 4, 7 or 10, respectively. The SiN-PMAA surface exhibits a high capacity for binding lysozyme at acidic pH, but can release the majority of the adsorbed lysozyme that serves as biocide to kill bacteria attached to the surface or suspended in solution at neutral pH, and then release the dead bacteria to provide a self-cleaning process when the environment pH is increased to a basic value. This dynamic reservoir concept may serve as the foundation for engineering multifunctional surfaces that could find many practical applications (such as biocatalysis and biosensing)

in both biomedical and biotechnology fields. However, achieving the needed changes in pH within blood, which is a relatively strong buffer, will be more challenging.

Lastly, bacterial interference is a different concept that uses active bacteria (either probiotic bacteria[54,94,95] or bacteria with less virulence[96–98]) to inhibit the targeted bacteria by competing for common resources in the same environment. This approach can be leveraged to prevent infections from exogenous sources. Trautner et al. reported a prospective clinical trial of using nonpathogenic bacteria colonized on urinary catheters in patients who require indwelling catheter drainage, to examine their effect in preventing bacteriuria commonly present in patients with indwelling urinary tract catheters.[98] Commercial urinary catheters were incubated in broth of *Escherichia coli* (*E. coli*) HU2117, a genetic strain that can cause persistent colonization without symptomatic infection,[99] for 48 h before insertion into patients for 28 d. The patients' urine samples were collected at various time points until *E. coli* HU2117 was no longer detected. Ten (83 %) out of 12 subjects were successfully colonized with *E. coli* HU2117 for 14 d or more (range, 15-165 d) after inoculation by insertion of the catheter. One patient had urinary tract infection (UTI) symptoms caused by *Pseudomonas* but none of the patients experienced UTI attributable to the colonization of *E. coli* HU2117. The overall rate of symptomatic UTI for this study was 0.15 cases per 100 patient-days of colonization, compared to the reported rate of 2.72 cases per 100 patient-days, which suggested that this organism may have a protective function in patients who used the *E. coli* colonized catheters.[100] However, a larger study group is needed to test the safety and efficacy of *E. coli* HU2117 coated catheters in highly problematic populations.

1.4 Creating Dual-Functionality Hemocompatible Surfaces

The ultimate truly hemocompatible polymer for blood-contacting biomedical devices should have both antithrombotic and antibacterial functionalities. Many dual-functional materials have been investigated, including zwitterion-based surfaces, submicron-patterned surfaces, and surfaces with multiple functional moieties, etc.

Zwitterionic polymers are polymers with equimolar number of homogeneously distributed anionic and cationic groups on their polymer chains, that form a hydration layer on the surface of the material through electrostatic interaction and therefore resists plasma protein and bacterial cell adhesion.[64,101,102] An alternative strategy towards creating hemocompatible surfaces is to change the polymer's surface topography, thereby mediating subsequent biological responses. Creating a submicron-textured surface can dramatically reduce the accessible contact area for platelets or bacteria to interact with the surface, thereby minimizing the opportunities for bacteria and platelet adsorption.[103–105] Polymers that combine multiple functional groups on one surface have also been tested, such as combining a synthetic heparin-mimetic polymer or hydrophilic polymer brushes (e.g., PEG) with antibacterial quaternary compounds (QAC) or Ag nanoparticles.[106–108]

Despite some successes in the research laboratory with the methods reported above, newer approaches to reduce the possibility of thrombus and/or infection on indwelling device surfaces are still in great demand within the medical community. Therefore, the main focus of the remaining content of this review is the utilization of polymer-based NO delivery to

prepare dual functioning antithrombotic and antibacterial surfaces for biomedical applications.

1.5 Nitric Oxide (NO) to the Rescue

Nitric oxide (NO), a diatomic free radical, was identified as the endothelium-derived relaxation factor (EDRF) in the Nobel Prize-winning discovery by Ignarro, Furchgott, and Murad in 1987.[20,109–114] Many researchers have later unveiled NO's various physiological functions in the human body, including preventing platelet activation and adhesion, inhibiting bacterial proliferation and biofilm formation, enhancing endothelization, signaling in the immune system's response, and promoting angiogenesis and the wound healing process.[113,115–118]

The human body synthesizes a large quantity of bio-regulatory NO from the substrate L-arginine via three distinct isoforms of nitric oxide synthase (NOS), including endothelial NOS (eNOS), neuronal NOS (nNOS) and inducible NOS (iNOS).[119–121] The NO produced by eNOS contributes to the thromboresistant properties of the endothelial lining of blood vessels by inhibiting platelet activation. The activation of platelets is mediated by NO through the soluble guanylate cyclase (sGC) pathway. NO binds to the heme iron moiety of sGC and subsequently increases intracellular concentrations of cyclic guanosine monophosphate (cGMP).[122,123] In addition, the cGMP increases cyclic adenosine monophosphate (cAMP) levels indirectly through phosphodiesterase III, which will also decrease the intracellular calcium concentration. The NO activated sGC ultimately results in reduced intracellular calcium, inhibition of platelet phosphoinositide 3-kinase (PI3), and

reduced affinity as well as number of surface membrane fibrinogen binding sites on platelets (GPIIb/IIIa).[118,122–127] It has also been suggested that many NO-related species are essential for NO's potent antimicrobial effects. First, NO can react with superoxide (O_2^-)[128] and form peroxynitrite ($OONO^-$), which is a lethal oxidizing agent and can induce oxidative stress, nitrosate amino acids and thereby alter protein functionality, oxidize and break DNA strands, and cause cell membrane damage to the bacteria it comes in contact with via lipid peroxidation.[20,128–130] A second possible route reported for NO mediated cytotoxicity relies upon the formation of *S*-nitrosothiols (RSNO) in which after oxidation of NO to N_2O_3 the N_2O_3 can react with sulfhydryl groups on cysteine residues of membrane proteins to create RSNO structures that alter protein functionality, leading to cell stasis or cell death.[109] Indeed, NO released or generated from polymer matrices has been shown to have similar antiplatelet and antimicrobial effects, as further described in detail below.

Some surgery interventions or trauma that destroys the endothelial lining, as well as certain vascular diseases, will lead to an increased level of superoxide anions and that react with NO and reduce its bioavailablity.[120,131] Reduced NO levels are associated with many health complications and/or diseases, such as high blood pressure, deep vein thrombosis, intimal hypertension, restenosis, endothelial dysfunction, and prolonged wound healing times in diabetic patients, etc.[1,132,133] There are three main strategies for increasing NO bioavailability: 1) by participating in physical exercise and controlling certain dietary components (e.g., nitrate-rich diet);[133,134] 2) by administrating drugs that alter the enzymatic production of NO through nitric oxide synthases (NOSs) and increase the biosynthesis of NO endogenously;[118] and 3) by using modified polymeric materials that

can actively deliver NO exogenously to the sites of interest.[3,110,111] Various NO-related drugs have been used in the clinical settings for many years: nitroglycerin (converted to NO by enzymes) for chest pain, sodium nitroprusside for controlling blood pressure, and molsidomine for pulmonary hypertension.[132] This has triggered substantial interest in developing polymers that can be functionalized as an artificial endothelium-like surface to therapeutically deliver NO locally at the polymer/blood interface.

Since NO is highly active *in vivo* (with a short-half life on the order of seconds due to its rapid reaction with oxyhemoglobin, oxygen, and thiols, etc.), many NO donors have been synthesized and used for achieving the goal of prolonged and controlled NO delivery. Some examples include organic nitrates or nitrate esters (e.g., nitroglycerin or glyceryl trinitrate (GTN) and pentaerythrityl tetranitrate (PETN)), metal-NO complexes (e.g., sodium nitroprusside), nitrite, *N*-diazeniumdialates (NONOate), and *S*-nitrosothiols (RSNO),[135–141] (see Figure 1.4). Nitroglycerin, the most commonly used organic nitrate for clinically treating hypertension and angina pain, is known to release 1 mole equivalent of NO upon bioactivation by mitochondrial aldehyde dehydrogenase (mtALDH).[112] However, patients often develop nitrate tolerance (tachyphylaxis) after prolonged use because the reactive oxygen species generated by nitroglycerin can oxidize the thiol group of the mtALDH and result in enzyme dysfunction.[112,142–144] This low bioavailability limits nitroglycerin's use as an efficient NO donor and complicates clinical treatments.

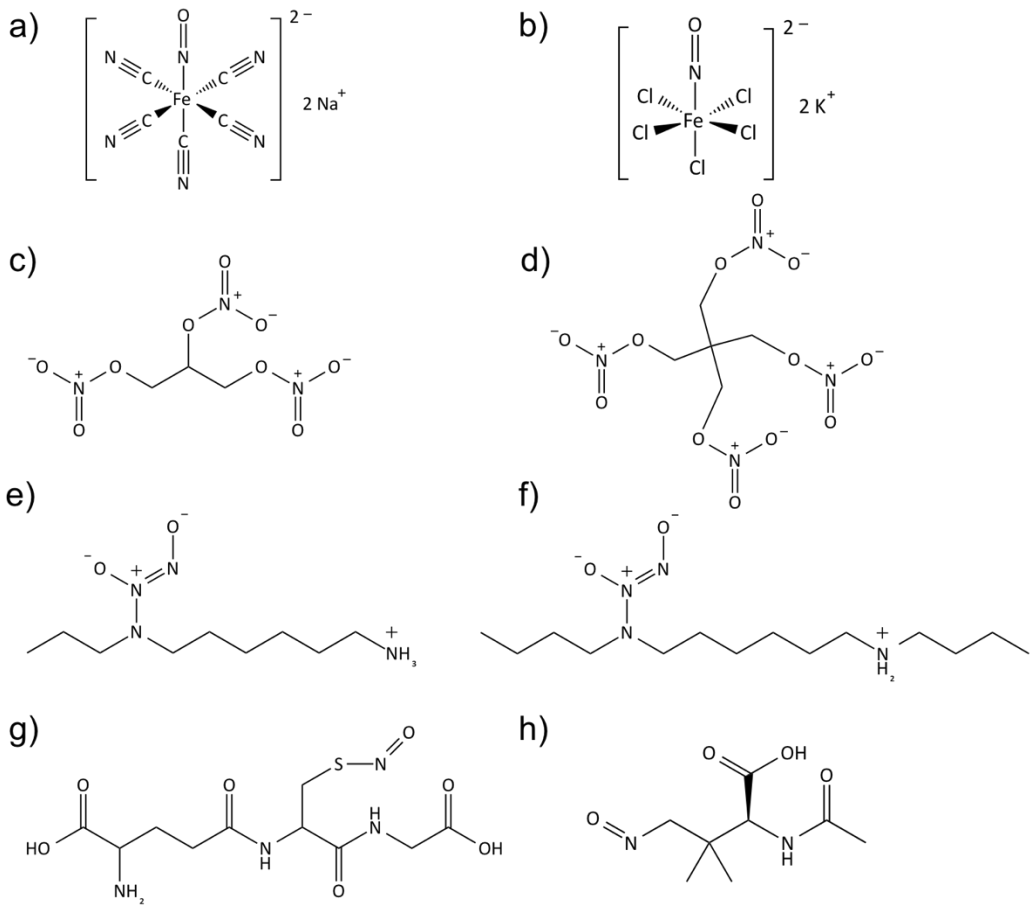

Figure 1.4. Structures of commonly studied NO donors in biomedical applications, a) sodium nitroprusside; b) potassium nitrosylpentachlororuthenate; c) nitroglycerin: d) pentaerythrityl tetranitrate; e) diazeniumdiolated *N*-(6-aminohexyl)aminopropane; f) diazeniumdiolated *N*,*N*'-dibutylhexamethylenediamine; g) *S*-nitrosoglutathione; h) *S*-nitroso-*N*-acetylpenicillamine.

Metal NO complexes (metal nitrosyls) represent another class of NO donors used in biological testing. Many different metal NO complexes have been reported, including manganese,[109,137] iron[145] and ruthenium-NO[109,112,137] complexes, with sodium nitroprusside ($Na_2[Fe(CN)_5NO]$, SNP) being the most common. SNP is often used as a potent vasodilator in hypertensive emergencies,[145] and releases NO in the presence of reducing agents (e.g., thiol-containing compounds such as cysteine or glutathione) or by illumination with near-infrared or visible light.[112,121,145] However, cellular toxicity concerns due to the

release of cyanide and cytotoxic peroxynitrite as byproducts have made metal nitrosyl complexes less attractive as medicinally used NO donors.[112,141]

Reduction of nitrite can generate NO via both enzymatic (nitrite reductase, xanthine oxidoreductase, etc.) and non-enzymatic (gastrointestinal acid, ascorbate, myoglobin, etc.) pathways.[133] Recently, it was demonstrated that nitrite can also be used to generate NO via electrochemical reduction at an electrode surface with either Cu(I) ion generated from oxidation of Cu^0 [146,147] or via the use of Cu(II)-ligand complexes that mimic the active site of nitrite reductase (e.g., Cu(II)-tri(2-pyridylmethyl)amine, Cu(II)TPMA).[148]

Many researchers over the past two decades have focused on using *N*-diazeniumdiolates (NONOates) and *S*-nitrosothiols (RSNOs) as leading candidates for controlled NO delivery due to their relatively high stability, their ability to spontaneously release NO under physiological conditions (e.g., no enzyme required) in a predictable manner, and their higher bioavailability *in vivo*.[3,121,136] Furthermore, the tissue and metabolite independent release also avoids the build-up of tolerance over time, which makes these agents more suitable for biomedical applications.

N-Diazeniumdiolates (1-amino-substituted diazen-1-ium-1,2-diolate) are a class of NO donor molecules formed by reactions between primary or secondary amines with NO under high pressure (e.g., 5 atm) in the presence of base (either an unreacted amine substrate or an added metal alkoxide base) at low temperatures.[1,137] These species are able to generate two mole equivalents of NO per mole of donor, via a proton-driven reaction (hydrolysis),

in the physiological environment such as when the compound is exposed to blood or tissue fluids (see Figure 1.5). NONOates can also release NO via thermal, photochemical or enzymatically (e.g., esterase) reactions.[137,149]

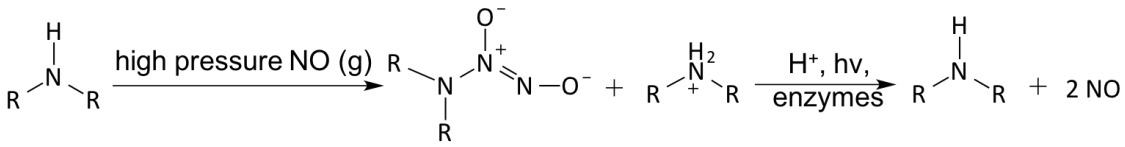

Figure 1.5. *N*-Diazeniumdiolates (NONOates) formation and decomposition.

The half-lives of the synthesized NONOates strongly depend on the structure of the amine precursors and hydrogen bonding stabilization from additional amines within the molecule. It has also been reported that hydroxyl groups within the donor molecule, or the matrix it is within, can also contribute to the hydrogen bonding with the diazeniumdiolates.[150,151] For example, half-lives can range from the shortest reported $t_{1/2}$ of 1.8 s for the diazeniumdiolated amino acid proline (PROLI/NO) to $t_{1/2}$ of 20 h for diethylenetriamine (DETA/NO).[136,137] One drawback of the diazeniumdiolate compounds is that they may potentially form carcinogenic nitrosamines.[152,153] Batchelor et al. synthesized more lipophilic NONOates for use in reducing the NO donor leaching into blood from polymers that had been doped with such NO donors.[154] Since the NO release process produces a lipophilic amine byproduct that increases the pH of organic phase, many additive compounds (such as tetraphenylborate or other borate derivatives[154]) have been included within the organic polymeric phase to serve as counter ions for organic ammonium cations (when amines form after NO release and proton is extracted into the polymer to create the ammonium species) and thereby partly prevent a pH increase within the organic polymer phase. This can greatly prolong the NO release lifetime from such NO donors when incorporated into biomedical polymers. Unfortunately, the borate additives are not ideal

because of their inability to extend the NO release to more than a few days and their cytotoxicity toward endothelial cells.[155,156] Therefore, Handa et al.[155,156] as well as Cai et al.[157] studied various poly(lactic-*co*-glycolic acid) (PLGA) additives with different hydrolysis rates as a means to slowly produce protons within the organic polymer phase that can continue to drive NO release reaction from NONOates. PLGA is a biocompatible and biodegradable polymer, with tunable mechanical properties and wide range of erosion times. Further, it is already approved for use by the FDA for the development of devices for controlled delivery of small molecule drugs, proteins and other macromolecules.[158] These studies demonstrated that the presence of PLGAs in the base polymer containing diazeniumdiolate species can extend NO release under physiological conditions for up to at least 2 weeks.

S-Nitrosothiols (RSNO) represent an endogenous class of NO donors and natural transporters of NO within tissues and blood.[121,159] Such molecules include *S*-nitrosoalbumin (SNO-Alb), *S*-nitrosohemoglobin (SNO-Hb), *S*-nitrosocysteine (SNO-Cys) and *S*-nitrosoglutathione (GSNO).[160] RSNOs can be synthesized via the thiol nitrosation reaction (such as nitrous acid and alkyl nitrite, etc. in an acidic environment).[141] Owing to the natural occurrence of RSNOs *in vivo*, these molecules pose a relatively low risk of toxicity to cells/tissues in comparison to NONOates. The transnitrosation reaction transfers the NO^+ functional group from an RSNO species to another existing free thiol, thus achieving a circulating unlimited supply of NO *in vivo*.[161]

RSNOs have characteristic UV-Vis spectra. In general, they appear green for tertiary RSNOs (such as *S*-nitroso-*N*-acetylpenicillamine, SNAP) or pink for primary and secondary RSNOs (such as SNO-Cys, *S*-nitroso-*N*-acetylcysteine (SNAC) and GSNO). There are two primary bands in the UV-Vis spectra. The strong band in the UV region is between 330 and 350 nm ($\varepsilon \sim 10^3$ M^{-1} cm^{-1}), which is attributed by the $n_0 \rightarrow \pi^*$ transition.[141,162–164] A weak band in the visible region is between 550 to 600 nm ($\varepsilon \sim 20$ M^{-1} cm^{-1}), which is attributed to the $n_N \rightarrow \pi^*$ transition.[141] It is known that RSNOs can release NO via multiple pathways.[164–169] Thermal or photo-initiated decomposition will lead to homolytic cleavage of the S-N bond, and form thiyl and NO radicals, where thiyl radical (RS•) will react with another RSNO and generate disulfide (RSSR) and another NO radical. Metal ions (such as copper or ferrous ions)[170,171] or organoselenium compounds can catalyze RSNO decomposition.[115,172–174] It is reported that Cu^+ (generated from reduction of Cu^{2+} by trace amounts of thiol) can react with RSNO and form the corresponding thiolate and Cu^{2+}, which then react to regenerate Cu^+ and a disulfide to continue the catalytic cascade. RSNOs can also react with ascorbate to generate NO via two pathways. In one, ascorbate (at low concentration) acts as a reducing agent to generate Cu^+ from trace copper ion impurities in solution, or at high concentration ascorbate can act as a nucleophile, attacking the nitroso group to generate NO, a thiolate and dehydroascorbate.[8,175,176] Further, certain enzymes such as copper-containing superoxide dismutase (CuZn-SOD)[141,177] or the selenium-containing enzyme glutathione peroxidase (GPx)[141,172,174] can also convert RSNO to NO in the presence of a reducing agent, such as glutathione (GSH) (see Figure 1.6).

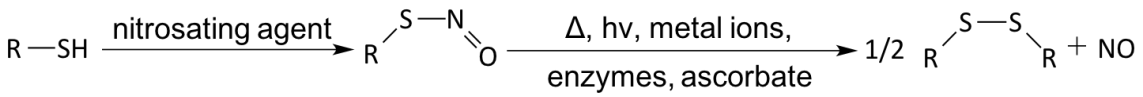

Figure 1.6. *S*-Nitrosothiol (RSNO) formation and decomposition.

GSNO and SNAP are two commonly used RSNOs that have been intensively studied in a variety of biomedical applications. GSNO is present in blood endogenously, which makes it innately more biocompatible and attractive for many applications, such as promoting wound healing process in mice or rats.[178–181] The precursor for SNAP synthesis is *N*-acetylpenicillamine (NAP), whose ultimate hydrolysis product, penicillamine, is already a FDA approved chelator for treating heavy metal poisoning, such as Wilson's disease.[182–185] SNAP is reportedly one of the most stable NO donors available, due to its intermolecular hydrogen bonding,[163,186] and has already been shown to be a very promising candidate for fabricating long-term NO releasing polymeric materials.[162,163,187] Lipophilic analogs of SNAP (such as *N*-substituted derivatives of SNAPs) have also been developed by addition of bulky side-chains to *N*-acetylpenicillamine and preventing Cu^{+} catalysis through steric hindrance.[188,189] Other lipophilic RSNOs (e.g., S-nitroso-*tert*-dodecyl mercaptan (SNTDM), log P = 5.3)[190] (note: P = partition coefficient of a molecule between octanol and water) with a higher Log P value than SNAP (log P = 0.4)[163] have been synthesized for reducing the NO donor leaching from the hydrophobic polymer phase.

1.6 Polymer-Based Strategies for NO Delivery

For the past two decades, many research groups have focused on developing techniques to deliver NO locally, continuously and efficiently from polymeric devices where blood clotting and/or bacteria infection are major complications. To improve the NO payload

and stability, achieve targeted NO delivery through multi-functionalization and elongate NO releasing lifetime, many different scaffolds have been used as NO-releasing or NO-generating vehicles. These include micelles,[139,191,192] microbubbles,[193] proteins,[194–198] liposomes,[127,199] inorganic nanoparticles (such as silica,[71,200–204] gold,[205,206] microparticles,[199,207] zeolites,[208,209]), metal-organic frameworks (MOFs),[210–213] dendrimers,[72,214,215] xerogels,[216–218] electrospun fibers,[89,101,219] natural polymers (chitosan,[86–88,220–222] gelatin,[223] etc.), and other organic polymers (polymethacrylate,[224] polyester,[225,226] polydimethylsiloxane (PDMS),[227] polysaccharides,[228,229] hydrogel,[179,180,230,231] PVA,[49,232,233] polyurethanes,[162,163,234,235] and PVC[155]). The approaches and benefits of different NO-delivery materials have been highlighted in numerous reviews.[1,112,121,132,136–139,236] Here, an overview of the most promising polymer-based NO delivery strategies are discussed, including covalently bound NO donors within/on a polymer matrix, physically dispersed NO donors within a polymer matrix, and catalytically generated NO from various RSNO reservoirs in the body (see Figure 1.7), and their representative examples in antithrombotic and antibacterial applications are described.

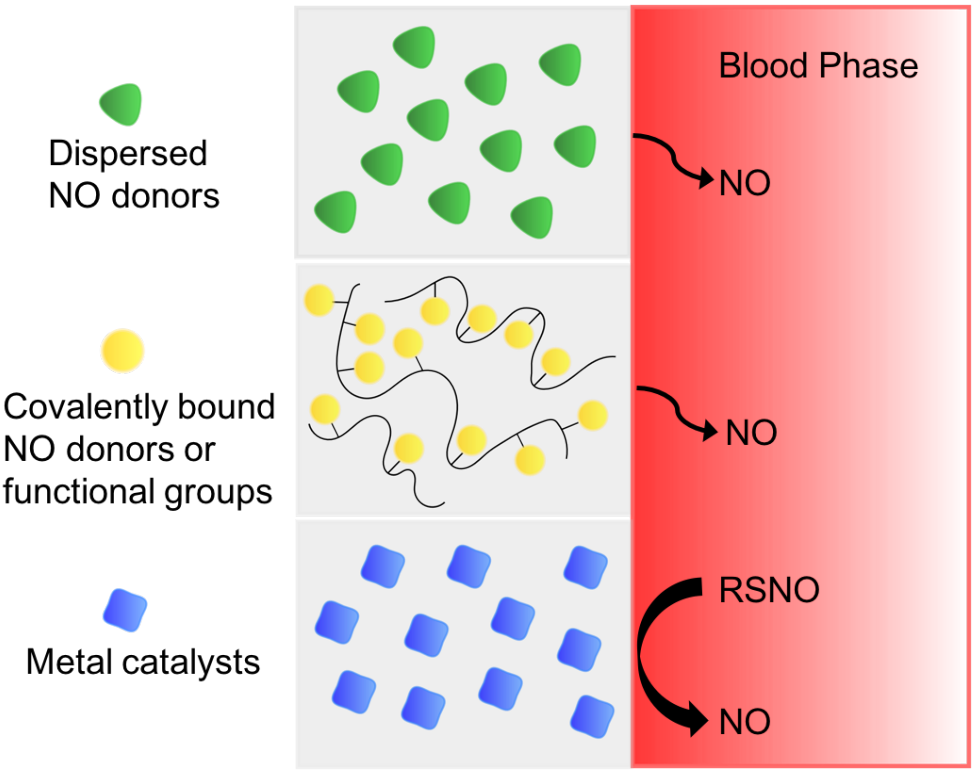

Figure 1.7. Three different strategies to fabricate of polymer surfaces that release or generate NO, including physical dispersion of NO donor into polymeric matrix, covalently bound NO donor functionalities onto polymer backbone, or NO generation from endogenous RSNO species in blood by metal catalysts embedded in or covalently bound to the surface of the polymer.

1.6.1 Covalently bound NO releasing polymers

N-Diazeniumdiolates are one of the most studied NO donors, and many polymers with secondary amine groups have been chemically modified to create the NONOate moiety.[110,111,137] Meyerhoff and coworkers were among the first to link these NO donors to particle fillers (such as fumed silica particles[237]) or to the polymer backbone of polymers such as PVC,[34,238] polyurethane (PU),[34,111,234] and silicone rubber (SR).[239] Zhang et al. synthesized NO-releasing fumed silica (FS) particles (0.2-0.3 μm) by tethering alkylamines onto the surface of the FS particles using amine-containing silylation reagents (coupling efficiency 50-70 %), and then converted them to corresponding NONOate groups with

final NO loading of ca. 0.6 μmol/mg of particle.[237] The half-lives of the particles are significantly longer than the solution phase NO donor analogs, owing to the fact that a large quantity of amines present at the particle surface can increase the local pH, which then reduces the NO release rate. Of note, when local pH decreases significantly, it results in partial release of the stored NO due to the proton-driven NO release mechanism. Therefore, some methods utilize additional acid-generating compounds to facilitate continual release of the entire NO payload.

Keefer and coworkers were one of the earliest groups to covalently attach a diazeniumdiolate species to the backbone of poly(ethylenimine) (PEI) to form PEI/NONOate, which later was used to provide a flexible NO release coating for PTFE vascular grafts.[240] The NO release from the sample was at a relatively constant rate (0.5 pmol min^{-1} mg^{-1}) for 5 weeks in PBS buffer at 37 °C. In subsequent studies, Saavedra et al. prepared methoxymethyl-protected diazeniumdiolated piperazine PVC;[238] however, the NO release rate was slow due to the fact that the NO could only be released from the NONOate group after the hydrolysis of the methoxymethyl protecting group.[34] In addition, this PVC film can concurrently release toxic methanol and formaldehyde as byproducts of the methoxymethyl-protecting group, which is undesirable for use as materials in biomedical applications. Zhang et al. later incorporated diazeniumdiolated functionalities into more biocompatible silicone rubber.[239] Briefly, the diaminoalkyltrimethoxysilane crosslinking agent (DACA) was reacted with the terminal hydroxyl groups of the PDMS, and then the aminated PDMS macromolecules were cross-linked to each other (condensation-curing) in the presence of ambient moisture before forming the NONOates

species at the amine sites (via reaction of the polymer with $NO_{(g)}$ at high pressure). Likewise, *N*-diazeniumdiolated NO donors have been covalently linked to polyester,[241] polymethacrylate,[224] polyurethane (PU),[35,111,234,235] PVA[233] and other hydrogels[242] as well. The synthetic methods are somewhat similar to that described above, with the exception of one type of PU containing a diamine chain extender, where sodium salts (NaX, where X is an anion) are incorporated into the reaction mixture during the NO addition process to facilitate the formation of anionic diazeniumdiolates.[111]

Dendrimers are another class of popular NO delivery vehicles due to their ability to store a large reservoir of NO, have tunable sizes, and to be multi-functionalized for targeted delivery.[215,243] Stasko et al. were the first to modify generation 3 and 5 polypropylenimine dendrimers at their exterior with different amine functionalities that were then converted to diazeniumdiolated dendrimers via reaction with $NO_{(g)}$ at high pressure. The secondary amine/NONOates yield the highest storage capacity for NO, with up to 5.6 μmol NO/mg of polymer, and a NO release duration of >16 h under physiological conditions.[243]

Frost et al. was the first to modify fumed silica particles (7-10 nm in diameter) with an RSNO functionality,[200,201] such as *S*-nitrosocysteine-FS (SNO-Cys-FS), *S*-nitroso-*N*-acetylcysteine-FS (SNAC-FS) and *S*-nitroso-*N*-acetylpenicillamine-FS (SNAP-FS). This was accomplished, by tethering the thiol containing amino acids or *N*-acetylpenicillamine thiolactone onto aminopropyl-FS. In these efforts, a total NO loading of up to $1.38 \pm 0.29 \times 10^{-7}$ mol NO/mg particles was achieved. The SNAC-FS and SNAP-FS particles can be blended into polyurethane (PU) or trilayer silicone rubber (SR) matrices to create films that

release NO at different rates by tuning the chemical identity, water uptake, or thickness of the PU polymer.[201] However, the SR films containing SNAC-FS or SNAP-FS in the middle layer do not release NO upon exposure to copper ions or ascorbate in PBS solution because the very high hydrophobicity of the SR blocks the contact between the buffer and the RSNOs.[200] However, such films are able to release NO at levels proportional to the intensity of visible light that is allowed to shine on the polymer, providing the first hydrophobic materials that have an external on/off trigger that precisely controls the rate of NO release via a photodecomposition reaction. The authors determined that 590 nm light is primarily responsible for the release of NO from the SNAP-FS-SR films. Evidence suggested that 67 % of the photoinitiated NO was accounted for by the longer wavelength (590 nm) and 33 % by shorter wavelengths (centered around 340 nm). SNAP has also been covalently attached to PDMS,[227] gelatin[223] and a macrocycle (e.g., cyclam).[244] The ability to generate programmable sequences of NO flux from these light-sensitive materials can offer precise spatial and temporal control of the NO release and potentially provides a platform to systematically study, at a fundamental level, the *in vivo* physiological response to implanted devices.[227] Of note, SNAP-cyclam is capable of releasing physiological relevant levels of NO for up to 3 months *in vitro* when blended into poly(L-lactic acid) thin films and irradiated by a 385 nm LED, and this represents the longest NO release from SNAP-based polymer films reported to date.[244]

RSNOs have also been used to form functionalized dendrimers[214] or hyperbranched polymers (e.g., hyperbranched polyamidoamine (HPAMAM) or hyperbranched polyethers[241]) to achieve a high NO payload. Stasko et al. functionalized generation 4

polyamidoamine (PAMAM) dendrimers with N-acetylpenicillamine or N-acetylcysteine and both macromolecular scaffolds have an NO storage of ca. 2 μmol NO/mg polymer after the required nitrosation raction.[214]

Another category of NO delivering materials with large NO storage capabilities are xerogel films. Riccio et al. designed thiol-modified xerogels derived from 3-mercaptopropyltrimethoxysilane (MPTMS) and methyltrimethoxysilane (MTMS).[217] The subsequent thiol nitrosation generates xerogels with NO loadings up to 1.31 ± 0.07 μmol NO/mg, and films of these materials are capable of releasing NO for up to 2 weeks under physiological conditions. Similar to *N*-diazeniumdiolates, many other polymer modification studies have been conducted using *S*-nitrosothiols (RSNOs) as well, including those utilizing PDMS,[227] PVA hydrogel,[180] polyester and poly(methylmethacrylate),[225] as the base polymer materials.

Lastly, several biodegradable polymers, such as citrate-based[226] or saccharide-based polymers (e.g., dextran[228,245] and chitosan[87,88,221]) provide very attractive scaffolds for NO delivery because of their natural occurrence, biodegradability, tolerability to mammalian cells and accessibility for NO donor functionalization reactions.[221,245,246] Reynolds and coworkers synthesized two *S*-nitrosated dextran thiomers (dextran-cystamine and dextran-cysteine), with up to 0.205 ± 0.003 μmol/mg NO loading and the capability to release NO for 6 h in PBS buffer at 37 °C. It has been further demonstrated that these dextran-based materials are susceptible to enzymatic degradation by dextranase, and the degradation of

dextran derivatives is slower and partial when compared to the unmodified dextran because of the chemical modification of the dextran backbone.[245]

1.6.2 Physical encapsulation-based NO releasing polymers

Physical encapsulation methods for preparing NO releasing polymers are based on embedding the NO donor within a polymer matrix physically without chemical bonding. This provides a much less complicated method to prepare NO release polymers than covalent attaching NO donors to particle fillers or the polymer backbones. This approach is a more attractive strategy for future commercialization if stable long-term NO release can be achieved by dispersing the NO donor within a polymer matrix. Toward this goal, polymer[193] or phospholipid[247] shelled microbubbles have been developed in recent years to create a hydrophobic microenvironment for NO transportation and therapeutic delivery. Paradossi and co-workers prepared NO-loaded PVA-shelled microbubbles (4.6 μm ± 0.4 μm diameter and 0.4 μm shell thickness) for treating acute vascular disease, such as thrombosis.[193] The microbubbles were loaded with NO by exposing to gas phase NO at 1.5 bar for 2 h. The NO encapsulation is about 1% of the NO present in the reaction vessel during the loading procedure, with the final content being 3.6 μmol/mg microbubbles. The NO release measured by the Griess assay showed that ca. 90% of the NO is released during a 50 min period in phosphate buffer saline solution. Ideally, the NO delivery should be controlled and selective bursts at a specific time and place, but the release can also be spontaneous and nonspecific.[193] Unfortunately, the *in vitro* stability of such NO-loaded microbubbles is relatively low.[247]

Gas storage in porous materials, such as zeolites, is also another attractive method for medicinal applications. Wheatley et al. have used cobalt-exchanged zeolite-A to absorb and store NO (1.2-1.3 μmol NO/mg zeolite). The NO release was triggered by contacting with water at physiological temperature and pH, replacing the gaseous NO with cobalt-water interactions. These NO-zeolite samples were also blended with powdered PTFE or PDMS to increase their mechanical stability and then pressed as disks for *in vitro* testing. The t½ values of NO release from zeolite polymer disks was significantly increased (from 340 s for zeolite powder to 509 s for PTFE disk and 3076 s for PDMS disk).[208] The results obtained in a platelet aggregometry assay also suggested that the NO-zeolites greatly inhibits platelet aggregation *in vitro*.

Liposomes are also a popular choice to protect and deliver gaseous NO. McPherson and coworkers prepared liposomes encapsulated with NO and argon gas (NO/Ar-ELIP) by a pressured-freeze and thawing method. They used these capsules for attenuating intimal hyperplasia and reducing arterial wall thickness.[199] Other researchers have conducted further studies to encapsulate NO donors within pH[127] or thermo-sensitive[248] liposomes to achieve controlled release. In short, when *N*-diazeniumdiolates are encapsulated within liposomes, pH or temperature fluctuations change the proton influx through the biolayer membrane and subsequently induce a significant NO release. Koehler et al. have also encapsulated SNAP within liposome vesicles and then doped the resulting vesicles within xerogels for photosensitive NO release.[249]

Biodegradable poly(ethylene oxide-*co*-lactic acid) (PELA)[250] and poly(lactic-co-glycolic acid) (PLGA)[207,220,250] have also been shown to be suitable vehicles for encapsulating NO donors to prolong the NO release. Yoo and coworkers developed PLGA (5050DLG5E) nanoparticles (NO/PPNPs) with diazeniumdiolated polyethylenimine (PEI) for long term NO release for antimicrobial applications.[220] The average size of the NO/PPNPs was 162 ± 19 nm as confirmed by scanning electron microscopy (SEM), with a NO release capacity of 1.4 μmol NO/mg polymer. The incorporation of PEI/NONOate into hydrophobic PLGA nanoparticle matrix successfully restricts the spontaneous degradation of the NONOate group and extends the NO release lifetime from 12 h to over 6 d.[220] More recently, Lautner et al. demonstrated the encapsulation of SNAP into PLGA (RG 503H and RG 504) microspheres (20-125 μm in diameter) using a solid-oil-in water (S/O/W) method[251] and achieved up to 4 weeks of controlled release of SNAP from PLGA RG 504, which then generates localized NO in the presence of copper (II) and ascorbate.[207]

Mowery et al.[34] prepared diazeniumdiolated *N*,*N*-dimethyl-1,6-hexanediamine (DMHD) or linear PEI and dispersed them into plasticized PVC or PU. Unfortunately, NO donor leaching was observed by HPLC and this raises potential concerns regarding toxicity if nitrosamine formation occurs, and such nitrosamines are also leached into the surrounding aqueous environment. Bachelor et al. [154] synthesized more lipophilic dialkylhexamethylenediamine-based NONOates with different alkyl groups (from methyl to didodecyl) which can enhance the retention of potential byproducts within the hydrophobic PVC films and thereby reduce their toxicity threat to biological systems.

Seabra et al. incorporated GSNO and SNAC into Synperonic F-127 gel using a 'cold method'[252] and formed a hydrogel that contained 0.3 mol of GSNO or 0.6 mol of SNAC per gram of hydrogel.[252] Kinetic studies showed that SNAC releases NO thermally 3.6 times faster than GSNO (11 ± 0.4 min $^{-1}$ vs. 3.1 ± 0.8 min $^{-1}$); however, approximately 50% of both NO donors had decomposed after only 3 h.[232] Kim et al. developed NO-releasing films by dispersing GSNO into biopolymer chitosan, where 75% GSNO remains after storing at room temperature for 4 weeks. The 20 wt% GSNO/chitosan film released NO over 48 h in PBS buffer at 37 °C.[222] Recently, Brisbois et al. discovered that SNAP is exceptionally stable when doped within several low water uptake biomedical grade polymers, such as Elast-eon E2As and CarboSil, and can release NO for up to 3 weeks at physiological conditions.[156,162] Wo et al. later demonstrated that the SNAP in CarboSil mainly exists in crystalline form when the SNAP concentration exceeds its solubility in the polymer. Ultimately, a slow crystal dissolution process leads to its long-term NO release under physiological conditions.[163] Additionally, this crystal-polymer composite is very stable during storage for at least 8 months, not only because of the hydrophobicity of the CarboSil polymer that limits water diffusion primarily to only the polymer surface, but also because the crystalline SNAP is stabilized by intermolecular hydrogen bonds.[163,253]

In order to apply NO release to any pre-made or off the shelf biomedical devices, Colletta et al.[19] developed a simple solvent impregnation method to load SNAP into commercially available silicone Foley urinary tract catheters at room temperature. This impregnation process takes place under very mild conditions, which is beneficial because, like many NO donors, SNAP or its analogs are sensitive to high temperatures used during industrial

catheter extrusion processes. In this approach, SNAP or a SNAP analog is dissolved in an organic solvent that can swell the polymer to a great extent without dissolving it, and as the polymer uptakes the solvent, the NO donors are loaded into the polymers. After drying to remove the solvent, the resulting polymer contains a stabilized form of the SNAP or analog of SNAP. As an initial example, commercial silicone Foley catheters (i.d. of 0.30 cm and o.d. of 0.59 cm) were swelled in a SNAP solution prepared in tetrahydrofuran (THF) (125 mg/mL) for 24 h, resulting in SNAP impregnation of 5.43 ± 0.15 wt% SNAP in the final dried catheter. This level of SNAP loading enabled the catheters to achieve stable NO release above physiological levels for > 4 weeks.[19]

1.6.3 Catalysis-based NO generating polymers

Instead of incorporating NO donors or NO functionalities into polymers, many efforts have been devoted to generate NO from endogenous RNSOs or infusion of RSNO solutions through thiol transnitrosations,[161,254] and subsequent catalytic reactions using immobilized copper or selenium-based species (e.g., copper nanoparticles,[255] copper(II)-cyclen,[171,256] copper-complexes,[257,258] copper-containing metal-organic frameworks (MOFs),[210–213] and organoselenium species[115,172–174]). Meyerhoff and coworkers were the first to covalently attach copper(II)-cyclen onto commercial biomedical grade polyurethane, which can generate physiological levels of NO (1-2 x 10^{-10} mol cm^{-2} min^{-1}) when in contact with endogenous RSNO and RSH species, such as 10 μM GSNO/GSH in PBS buffer containing 3 μM EDTA.[171] This polymer has also been used as an outer coating at the distal end of an amperometric NO sensor that can generate electrochemical response toward the RSNO species in whole blood.[171] However, it was reported that 50 % of copper(II) ion leached

out after soaking in GSNO/GSH containing PBS buffer at RT for 7 d, which may limit the use of such polymers for long-term applications and generate cytotoxicity concerns.

Reynolds and coworkers are developing many MOF-NO generating catalysts with accessible catalytic sites and that have resistance to degradation, including $Cu_3(BTC)_2$ (BTC: 1,3,5-benzenetricarboxylate), Cu(II)1,3,5-benzene-tris-triazole (CuBTTri) and Cu(II)1,3,5-tricarboxylate (CuBTC).[211–213] It has been reported that CuBTC can be extruded within Tecoflex SG80A polyurethane into single lumen tubing while maintaining the catalyst structure and functionality. The *in vitro* NO release generated from endogenous RSNO species ranges from 1 h to 16 h with tunable dosage, depending on the specific RSNO levels present in the soaking solution.[211]

As previously mentioned, Meyerhoff and coworkers have also demonstrated an electrochemical NO generation via a Cu^+ ion mediated reduction reaction of inorganic nitrite. The Cu^+ ion is generated from oxidation of a copper wire[146,147] or the reduction of copper(II)-tri(2-pyridylmethyl)amine (Cu(II)TPMA) complex.[148] The electrochemically generated NO can be modulated by changing the potentials applied to the electrodes and can achieve fluxes between 0.5 and 3.5 x 10^{-10} mol cm^{-2} min^{-1} (for catheter applications), which is in the range of physiological relevant levels of NO released by the endothelial cells. This approach has been utilized to develop a new generation of multi-lumen catheters in which one lumen is dedicated to generating NO electrochemically to reduce thrombus and microbial biofilm formation on the surface of the catheters.[148,259]

1.7 Applications of NO Releasing/Generating Polymers for Preparing Antithrombotic and Antibacterial Biomedical Devices

1.7.1 Inhibition of thrombosis formation

In a healthy vasculature, endothelial NOS (eNOS) in the endothelial cells that line the inner wall of blood vessels produce NO with a surface flux of $0.5 – 4.0 \times 10^{-10}$ mol cm^{-2} min^{-1} to prevent platelet activation and thereby control the balance between thrombosis and hemorrhage.[120] However, many procedures (such as placing stents, grafts, catheters, or other biomedical devices) disrupt the endothelial cells lining and destroy the delicate balance of vascular homeostasis.[133] The tissue factor release and protein absorption trigger the coagulation cascade and the lack of NO production leads to platelet activation, aggregation, and ultimately thrombus formation. Therefore, NO and its unique antiplatelet/antithrombotic activity represents a very promising approach to prevent thrombus associated complications in many biomedical applications.

Mowery et al. reported that PVC- or PU-based polymer films, prepared with NO releasing diazeniumdiolate functionality via either dispersion or covalent bonding of NO donors, can exhibit significant improvements in biocompatibility during *in vitro* platelet adhesion tests using platelet-rich plasma (PRP).[34] Wu et al. prepared PVC films (with borate additives and di(2-ethylhexyl) ester (DOS)) mixed with 0.5, 1.0, 2.0, 4.0 wt% of diazeniumdiolated *N*,*N*'-dibutyl-1,6-hexanediamine (DBHD/N_2O_2) to determine the effect on platelet adhesion at the surface of polymeric films with various NO flux levels.[260] A lactate dehydrogenase (LDH) assay was used to determine the amount of platelets adhered onto the polymer surface. LDH, which is normally stored within intact platelet, is released into

the bulk solution when the platelets are lysed by surfactant and is a very useful for indication of the amount of cells adhered.[260] Fewer platelets adhered on the polymer surfaces with higher NO flux levels, and NO successfully reduced the amount of platelets adhered on the polymer surfaces from $14.0 \pm 2.1 \times 10^5$ cells/cm^2 on the controls to $2.96 \pm 0.18 \times 10^5$ cells/cm^2 on the surfaces with highest NO release of 7.05×10^{-10} mol cm^{-2} min^{-1}.

Thrombosis is also an important risk factor in any blood exposure to synthetic materials, such as grafts, stents, intravascular sensors, catheters, extracorporeal circuits (ECC) or hemodialysis membranes.[120,121,261,262] Efforts to use NO release polymers for these applications are summarized below based on the type of biomedical device.

1.7.1.1 Intravascular grafts

Keefer and coworkers were the first to test the antithrombotic and antiplatelet activity of NO released from a polymer matrix in animal models.[240] Diazeniumdiolated cross-linked PEI coated PTFE vascular grafts were inserted into silicone rubber shunts that were placed between baboons' femoral and artery veins for 1 h. The autologous baboon platelets were labeled with indium-111-oxine before the start of experiment. The number of platelets adhered on the graft surface at the end of experiment was accessed by measuring the radioactivity intensity using a gamma scintillation camera. The NO-releasing grafts were found to be substantially less thrombogenic than the controls, suggesting considerable promise for this approach to improve the performance of vascular graft after implantation.[240] The West[116] and Wang[115] groups both reported that NO

releasing/generating grafts encourage endothelialization/endothelial cell proliferation, which can alleviate the complications of thrombosis and intimal hyperplasia (IH) that cause the failure of small diameter vascular grafts without the use of systemic anticoagulants.

1.7.1.2 Intravascular sensors

Monitoring the levels of chemical species in blood (such as blood gases (PO_2, pH, and PCO_2), electrolytes (K^+, Na^+ Ca^{2+}), glucose, lactate, etc.) can provide invaluable information for diagnosis and treatment of hospitalized patients.[263] Currently, however, measurements are done *in vitro* with point-of-care devices intermittently, leaving large gaps of information between blood draws.[259,264] Therefore, developing intravascular sensors that can monitor key chemical species in real time in critically ill patients is an important avenue of research.[265] However, adhesion of platelets, and eventual thrombus formation on the surface of the sensors can occur within a few hours after blood contact, and such processes can not only isolate the chemical sensing area from the bulk of the blood and lead to false analytical results but also increase the risk of emboli or stroke.[8,266] Many researchers have attempted to address this problem by incorporating continuous NO release/generation into the sensor design to prevent adhesion of metabolically active platelets from adhering to the sensor surface. To increase the biocompatibility of intravascular oxygen sensors, Marxer et al. developed an amperometric sol-gel derived oxygen sensor that consists of a platinum electrode coated with a diazeniumdiolate and polyurethane containing xerogel film.[267] The coating released NO at a flux up to 4.32 x 10^{-10} mol cm^{-2} min^{-1} for the first 12 h and effectively reduced platelet adhesion in the *in vitro* biocompatibility testing when immersed in platelet rich plasma for 1 h at 37 °C.

Instead of directly coating the electrodes with NO release polymers, many catheter-style intravascular oxygen sensors have been developed for testing *in vivo* with NO released or generated through the polymeric material of the catheters. So far, several different NO delivery approaches have been reported for such intravascular oxygen sensors, including coating the catheter surface with NONOates,[268,269] covalently attaching NONOates to catheter polymer surface,[270] catalytically generating NO *in situ* from endogenous RSNOs using embedded copper particles[8,271] and electrochemically modulating NO generation from nitrite.[259] For example, Schoenfisch et al. coated outer surfaces of SR catheters with 2 wt% (*Z*)-1-[*N*-methyl-*N*-[6-(*N*-methylammoniohexyl)amino]] diazeniumdiolate (MAHMA/N_2O_2) and demonstrated that the NO release from the catheter lasted more than 20 h in PBS at 37 ^oC. One control (coated only with MAHMA) and one NO release catheter (coated with MAHMA/N_2O_2) were implanted within the carotid or left femoral arteries in a canine model for 12-23 h. The electrochemical response of the NO-releasing O_2 sensor more closely represented the real arterial blood gas value measured by a benchtop blood-gas analyzer than the control sensor, which had a significant discrepancy starting from the first few hours after the implantation. SEM images also confirmed that a much greater number of platelets adhered and aggregated on the surfaces of the control sensors compared to the NO releasing sensors. In a separate study, Ren et al. recently demonstrated the use of a dual lumen catheter configuration to combine an amperometric oxygen sensor (in one lumen) with the electrochemical NO generation in the other lumen using Cu(II)TPMA as the mediator for reduction of nitrite ions to NO[259] (see Figure 1.8).

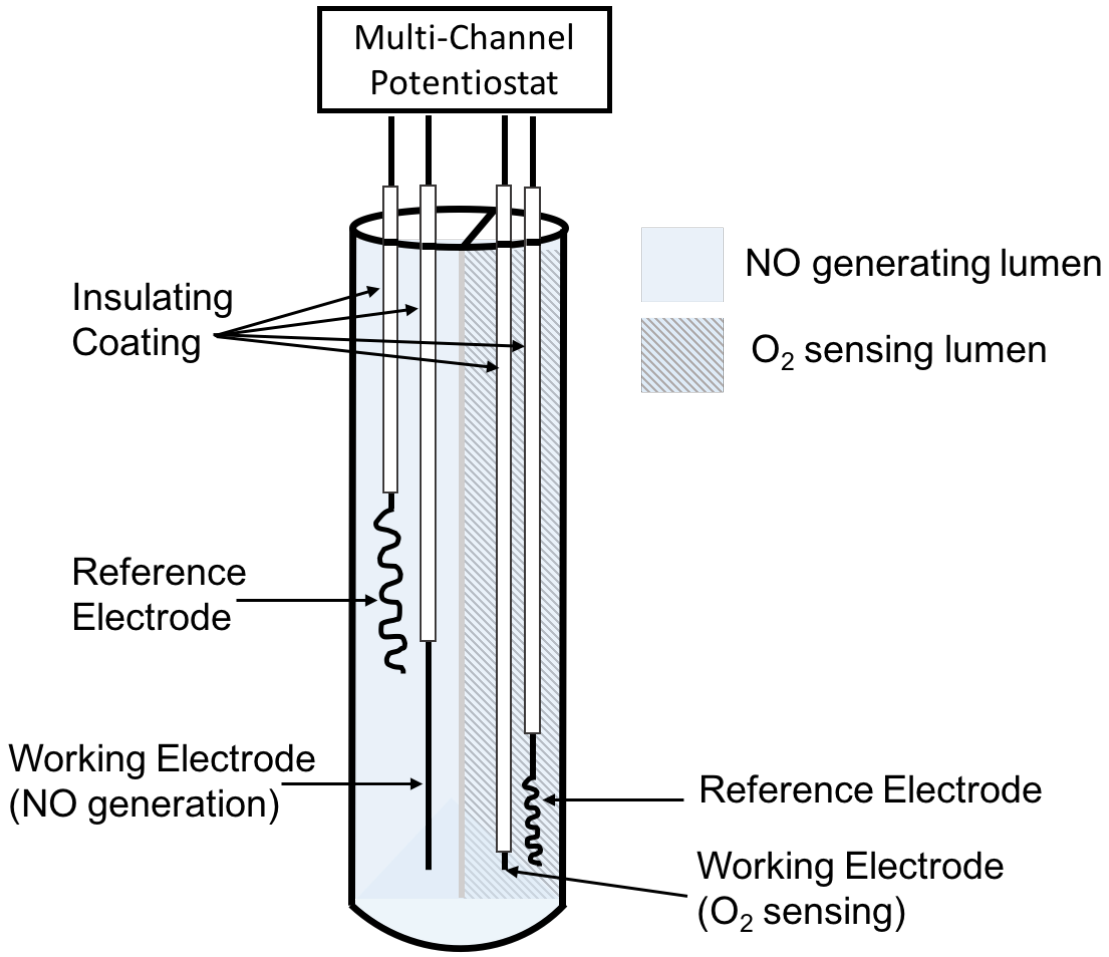

Figure 1.8. Simplified schematic of dual-lumen catheter-type oxygen sensor with electrochemical NO generation from nitrite solution via Cu(II)TPMA (figure not drawn to scale).

Applying different potentials on the electrodes can modulate the rate of NO generation, which offers a steady, controllable, and physiologically relevant flux of NO, compared to the chemically-based NO generation. The performance of the sensor was evaluated in rabbit veins and pig arteries for 7 and 21 h, respectively. The sensors in the arteries were challenged with a wider range of oxygen levels by changing the pig's fraction of inspired oxygen between 100 % and 21 %.[259] In both cases, the sensors with electrochemical NO generation provided very accurate oxygen responses, while control sensors deviated from

the real values by 30-40 % after 5 h of implantation because the local oxygen was consumed by the activated platelets and other cells trapped in the thrombus formed on the surface of the control sensors. Similar to oxygen sensors, NO releasing intravascular glucose,[272–276] pH,[276,277] and CO_2[276,278] sensors using diazeniumdiolated NO donors have also been tested, demonstrating much improved electrochemical responses over the corresponding control sensors.

1.7.1.3 Extracorporeal circulations (ECCs)

Extracorporeal circuits are used for several different types of medical procedures, such as hemodialysis, cardiac bypass surgery, and extracorporeal membrane oxygenation (ECMO). The latter is employed to keep newborn babies alive for weeks at a time, if their lungs are not fully developed. The need for systemic anticoagulation in each of these extracorporeal procedures can be problematic, particularly in patients that have heparin induced thrombocytopenia (HIT). Due to the large surfaces area that is in contact with blood in extracorporeal circulation (ECC), the loss of platelet count and platelet functionality are significant,[162] and many researchers have developed NO releasing[43,155,156,162,237,239,279,280] or NO generating[255] polymeric ECC tubing to prevent platelet activation and consumption during this process (see Table 1.1).

Table 1.1. Summary of NO releasing and NO generating coatings reported to increase the hemocompatibility of extracorporeal circuits (ECC).

Summary		**ECC coating material**	**NO donor, additives, etc.**	**NO level (x 10^{-10} mol min^{-1} cm^2)**	**Platelet count after 4 h (% of initial)**	**Ref**
NO release	covalent attachment	Tygon tubings with Carbonthane 3573A coating	*N*-diazeniumdiolated FS fillers	4.1	ca. 85 ± 15 % (NO) vs. 58 ± 5 % (PU)	237
		Silicone rubber tubings	*N*-diazeniumdiolated PDMS	>4.0 at 23 °C; >10.0 at 37 °C	86 ± 24 % (NO) vs. 65 ± 10 % (SR)	239
	physical dispersion	Tygon tubings with PVC/DOS coating	DBHD/NONOate, borate	12.5	79 ± 7 % (NO) vs. 58 ± 7 % (PVC/DOS)	279
		Tygon tubings with PVC/DOS coating	DBHD/NONOate, PLGA	>20	79 ± 11 % (NO) vs. 54 ± 6 % (PVC/DOS)	155
		Tygon tubings with Elasteon-E2As coating	DBHD/NONOate, PLGA	6	97 ± 10 % (NO) vs. 58 ± 3 % (E2As)	156
		Tygon tubings with Elasteon-E2As coating	DBHD/NONOate, PLGA, argatroban	6.5	ca. 90 % (NO/argatroban) vs. 58 ± 3 % (E2As)	43
		Tygon tubings with Elasteon-E2As coating	SNAP	2	100 ± 7 % (NO) vs. 60 ± 6 % (E2As)	162
NO generation		Tygon tubings with Tecophilic SP-60D-60 coating containing 10 wt% Cu^0 nanoparticle	endogenous RSNO and/or infused SNAP	>10 (in presence of 1 μM GSNO, 30 μM GSH, 5 μM EDTA)	ca. 90% (10 wt% Cu^0 and SNAP) vs. 75 % (10 wt% Cu^0 only) vs. 50 % (SNAP only)	255
Inherent polymer properties		Tygon tubings with Tecoflex SG 80A, Tecophilic SP-60D-60, PVC/DOS coating	N/A	N/A	44 ± 4 % (SG 80A) vs. 41 ± 5 % (SP-60D-60) vs. 46 ± 3 % (PVC/DOS)	156

Zhang et al. prepared PVC tubing with PU coating containing 20 wt% diazeniumdiolated FS particle fillers[237] and SR tubing with covalently attached to DACA/N_2O_2[239] as NO releasing polymer tubing circuits for 4 h ECC experiments in a rabbit model. Both types of NO release tubing exhibited less overall platelet adhesion and thrombus surface coverage compared to the controls. However, it still remains a challenge to achieve long-term NO release at physiologically relevant conditions, stable storage capability at room temperatures and high NO donor loading. Handa et al. recently prepared ECC tubing composed of 25 wt% DBHD/N_2O_2 and 10 wt% PLGA (5050DLG7E) additives in 2:1 PVC/DOS polymer matrix and achieved up to 14 d of NO release between 7-18 x 10^{-10} mol cm^{-2} min^{-1} at 37 °C.[155] This circuit tubing successfully preserved the platelet count during 4 h of experiments, with 79 ± 11 % vs. 54 ± 6 % for the NO release circuits compared to PVC/DOS controls. In a subsequent study by the same authors, four different biomedical grade polymers were evaluated for their inherent hemocompatibility in 4 h ECC experiments in rabbits.[156] The type of polymer material can ultimately influence their efficiency as NO releasing coatings. E2As polymer was found to be the most biocompatible material amongst the four tested. E2As coated ECC tubing can preserve 56% of baseline platelet after 4 h versus 48, 40 and 47 % for PVC/DOS, Tecophilic SP-60D-60 and Tecoflex SG 80A, respectively. Major et al. later used E2As polyurethane with DBHD/N_2O_2 and a direct thrombin inhibitor argatroban (AG) as an ECC coating to better mimic the vascular endothelium. The results showed that the combined AG/DBHD polymer coatings can better prevent thrombus formation after 4 h of blood exposure compared to control ECCs or ECCs with coatings containing only DBHD/N_2O_2 or AG alone.[43]

In addition to diazeniumdiolates, RSNOs has also been used to create NO releasing coatings for ECC applications. Brisbois et al.[162] were the first to discover that SNAP-doped E2As polymer films exhibit unprecedented shelf-life stability, with 82 % of the initial SNAP remaining after 2 months storage at 37 °C. The 10 wt% SNAP/E2As films can release NO for up to 20 d at levels above the physiological NO flux range. In the ECC experiments with rabbits, the inner walls of PVC ECC circuits were coated with the SNAP/E2As polymer. Such coated tubing successfully preserved the platelet count during the 4 h of experiments (at 100 ± 7% % vs. 60 ± 6 % for controls), with 33 % less thrombus formation on the tubings' inner surfaces.

Another related approach to increase the biocompatibility of ECC tubing is to generate NO catalytically using infused RSNOs.[255] Hydrophilic SP-60D-60 polyurethane polymer containing 10 wt% Cu^0 nanoparticles (NP) (80 nm) coated on the inner walls of ECC circuit tubing were tested in the rabbit thrombogenicity model. Experiments were conducted with and without intravenous SNAP infusion (0.1182 μmol/kg/min) over a 4 h period. The Cu^0 NP embedded ECC circuit with SNAP infusion yields considerably less thrombus (0.4 ± 0.2 pixel/cm^2) on the surface of the chamber after 4 h, as compared to the Cu^0 NP circuit without SNAP infusion (3.2 ± 0.2 pixel/cm^2) or the control circuit without Cu^0 NP (4.9 ± 0.5 pixel/cm^2). Of note, since the endogenous RSNO levels are low (e.g., 1-10 μmol/L for SNO-albumin),[281] this approach requires consistent supply of infused RSNOs to provide continuous catalytic generation of NO at the flowing blood/polymer tubing interface.[255]

1.7.2 Prevention bacterial infection or biofilm formation

Nitric oxide (NO) has antimicrobial activity against a growing list of microorganisms, including bacteria, fungi, parasites, viruses, and yeast.[20,112,121,128,178,282,283] However, for medical device applications, the focus has thus far been on its antibacterial/antibiofilm properties, especially for the bacteria that most commonly cause CRBSIs (catheter related bloodstream infections), such as *Staphylococcus epidermidis (S. epidermidis)*, *Staphylococcus aureus (S. aureus)*, and *Pseudomonas aeruginosa (P. aeruginosa)*.[66,104] It has been clearly demonstrated that NO releasing/generating polymers can have strong bactericidal effects,[19,147,148,163,202,228,284,285] even for bacteria that are able to metabolize and deactivate NO, such as *P. aeruginosa*, that possesses NO reductase enzyme that converts NO to nitrous oxide (N_2O) and ultimately nitrogen (N_2).[87,202,220] Of note, NO possesses broad-spectrum antibacterial activity against both gram-positive and gram-negative bacteria, including methicillin-resistant *Staphylococcus aureus* (MRSA).[220,282] Moreover, the dose of NO required to kill bacteria (e.g., 200 ppm of gaseous NO)[282,283,286] does not show any cytotoxic effects in human dermal fibroblasts when exposed for 48 h.[217,221] In addition to its bactericidal activity at high dosage, low levels of NO (picomolar to nanomolar range in solution phase)[287] also serve as a key mediator that minimize planktonic bacteria adhesion and colonization, as well as disperse mature biofilm and release the bacteria trapped in the EPS film back to their planktonic state.[287–289] It has been proposed that exposure to low doses of NO restore the sensitivity of biofilm and dispersed bacteria towards several types of antibiotics, greatly increasing their efficacy.[287] Overcoming bacteria colonization on the surfaces of biomedical devices through continuous NO release represents an innovative and highly desirable approach to reduce

risk of infections, which can ultimately increase device functionality and success rates, reduce morbidity and mortality, and improve patient outcomes..

Frost et al. successfully develop a *S*-nitroso-*N*-acetyl-D-penicillamine functionalized polymer matrix (e.g., PDMS,[227] cyclam[244] and gelatin[223]) that can release NO via light-initiated SNAP decomposition. SNAP modified purified gelatin can release NO up to 1 x 10^{-8} μmol mg^{-1} s^{-1} under a 527 nm wavelength light-emitting diode (LED,) and it also shows continuous and light intensity-responsive NO release over 24 h, with a total payload of 0.06 μmol NO mg^{-1}.[223] The antibacterial activity of SNAP/gelatin was tested against *S. aureus* (3 x 10^5 CFU/mL) and it demonstrated the ability to create a zone of inhibition of 1.2 ± 0.7 mm and 0.75 ± 0.3 mm, when exposed to the 4.5 V and 3 V LED light, respectively, over 24 h. Schoenfisch and coworkers have evaluated the antibacterial characteristics of NO releasing sol-gel coatings[290] and xerogel films[217] which are capable of releasing NO for 5 and 14 d, respectively, against a 10^8 colony forming units (CFU)/mL saline suspension of *P. aeruginosa* for up to 4 h. NO successfully reduced bacterial cell coverage on these surfaces by up to 40 %. Recently, Reynolds and coworkers developed a water-soluble NO-releasing polysaccharide derivative that can release 100 % of its NO storage capacity (49.5 ± 5.0 μmol/g) over 24 h.[228] The bactericidal activity of this species was evaluated against *E. coli*, *Acinetobacter baumannii* (*A. baumannii*) and *S. aureus* and the reported data demonstrated an 8-log unit reduction in viable bacteria cell counts for all three types of bacteria after 24 h of incubation. The absence of CFU counts after 72 h corroborated that there was no bacterial growth recovery after exposure to NO. This is the

first time a water-soluble antibacterial agent has reached an industrially relevant level of antimicrobial activity.[228]

Further, it is also well known that bacteria in mature biofilms are much harder to eradicate than when they are in planktonic stage. Meyerhoff and coworkers have conducted many experiments where the antibacterial properties of NO releasing polymer were evaluated against mature biofilm, developed in CDC bioreactors prior to contacting with NO.[146,148] Electrochemical NO generating catheters using inner copper wire working electrode and inorganic nitrite salt solution can generate NO through the walls of the catheters with a flux $> 1.0 \times 10^{-10}$ mol cm^{-2} min^{-1} for more than 60 h.[147] First, the catheters were mounted in a drip-flow bioreactor, which is a standardized model that allows growth of high biomass-biofilm of *E. coli* at the air liquid interface when incubated with in LB (Luria Bertani) broth for 2 d and 4 d without the NO turned on. After allowing biofilm to form on catheter surfaces, the electrochemical NO release was "turned on" for only 3 h at the end of the experiments. The short period of NO release was effective at dispersing and killing the *E. coli* biofilm, and could lower the number of live bacteria adhered on the catheter surfaces by > 99.9%. In a separate study, Backlund et al.[215] synthesized diazeniumdiolated PAMAM dendrimers with different alkyl chain modifications and examined their antibacterial properties against 24 h old *Streptococcus mutans* biofilm (*S. mutans*) at pH 7.4 and 6.4. The bactericidal action of the NO releasing dendrimers was reported to increase with alkyl chain length of the dendrimer and lower pH. In another experiment conducted by Schoenfisch and coworkers, a Center for Disease Control (CDC) bioreactor, that mimics bacterial growth under different sheer force conditions, was used to grow *P.*

aeruginosa biofilms over a 48 h period. The biofilms were then exposed to a water-soluble NO releasing chitosan oligosaccharide (0.17-0.46 μmol NO/mL) for 24 h. The presence of the NO release elicited a 5-log unit reduction in viable bacterial counts with a minimal bactericidal concentration (MBC) of the dendrimer preparation as low as 400 μg/mL.[221]

Continuous NO release during bacterial proliferation has also been proven to prevent biofilm formation. Cai et al. fabricated NO releasing silicone rubber films containing DBHD/N_2O_2 along with PLGA (RG 502H) additives that can release NO for 10 d at physiological conditions. pH sensitive dyes were incorporated in the films to help visualize the pH change within the polymeric matrix due to slow hydrolysis of the PLGA that promotes the extended NO release.[157] Both the NO release and control films were incubated in a CDC bioreactor for 7 d at 37 °C and the number of live bacteria on the surfaces of the silicone rubber was assessed. The NO release films exhibited substantial antibiofilm properties against both gram-positive *S. aureus* (98.4 % reduction) and gram-negative *E. coli* (99.9% reduction) when compared to controls.[157] In subsequent studies, Colletta et al.[19] and Ketchum et al.[190] used the solvent impregnation method previously described above (see Section 1.6.2) to load silicone-based tubing with NO donors (SNAP and lipophilic SNAP derivatives, respectively) and demonstrated that they have antibacterial effects toward several microorganisms (e.g., *Staphylococcus epidermis*, *Proteus mirabilis* or *S. aureus*). These results offer a new strategy to reduce bacterial infections associated with not only intravascular catheters but also urinary catheters.

In addition to *in vitro* experiments, NO releasing polymers (e.g., catheters) have also exhibited both antithrombotic and antibacterial properties *in vivo*. Brisbois et al. conducted experiments where both SNAP-doped E2As catheter and control E2As catheters were implanted in sheep jugular veins for 7 d.[187] At the end of the 7 d period, the catheters were carefully explanted and both the clot area as well as the number of live bacteria adhered on the catheter surfaces were assessed. The 10 wt% SNAP/E2As catheters exhibited enhanced hemocompatibility (70% less thrombus formation) and bactericidal activity (90% reduction of bacteria adhesion) when compared to the controls.

Nitric oxide releasing polymers have also provided a potential strategy for use as active wound healing dressings, capable of reducing bacterial infections at wound sites and accelerating the wound healing process for incisional and excisional wounds,[180,220,222] burn wounds,[291] and diabetic wounds.[233] While normal fibroblasts do not synthesize NO, it has been demonstrated that fibroblasts isolated from the regular wound can release NO.[292] The iNOS is synthesized in the early phase of wound healing by inflammatory cells, such as macrophages, monocytes, and other immune lineage cells.[120,121,293] The NO released through iNOS enhances angiogenesis, regulates collagen formation, cell proliferation and wound contractions.[112,293] Studies using induced NOS (iNOS) knock out mice showed diminished collagen deposition, with the restoration of normal collagen deposits upon exposure to SNAP, indicating the important relationship between NO production and wound healing.[294] Therefore, elevating the local NO concentration at a wound site by an exogenous NO supply represents a promising strategy to facilitate the wound healing process.

Yoo and coworkers developed PEI/NONOate nanoparticles (NPs) capable of prolonged NO release, which were then used to treat MRSA-infected excisional wounds (5 mm diameter, full thickness) in mice.[220] MRSA was inoculated in the wound for 1 d to develop infection and then the wounds were treated with the NO releasing NPs or control NPs over 6 d. The photographs of the wounds taken at day 0, 1, 4 and 7 clearly showed an accelerated wound healing process for mice treated with NPs, with wound area reduced to 25% at the end of 7 d. The untreated wounds showed a thicker scab with no reduction in the wound area. In a subsequent study, GSNO-doped chitosan films, which exert strong antimicrobial activity against a broad spectrum of bacteria, were evaluated as a wound healing dressing on full thickness excisional wounds (1.5 m x 1.5 cm) in a rat model for 15 d.[222] Comparing the NO-treated and untreated wounds, those treated with the GSNO/Chitosan dressing were almost completely healed at the end of the 15 d, with less bacterial burden and decreased inflammatory cell infiltration, but enhanced re-epithelialization.[121,222] Brisbois et al. tested the antibacterial efficacy of DBHD/N_2O_2 and PLGA (5050DLG1A) doped biomedical grade PU films as a dressing for burn wounds (10 cm^2 and partial thickness) in a mouse model.[291] Burn wounds are quite common, but difficult to treat and often lead to infections.[112] The burn wounds in mice were inoculated by *A. baumannii* for 24 h prior to application of the NO and control wound dressings. After 24 h of treatment, the wound area skin tissue was harvested and assessed for number of viable bacteria adhered at the wound sites. A 4-log unit bacterial reduction was observed for the NO treated wounds when compared to the control would sites.

1.8 Summary

As detailed above, there are many approaches that have been examined to improve the biocompatibility and antimicrobial activity of biomedical polymers/devices. Most of the conventional approaches, (e.g., creating heparin-releasing surfaces, bacteria-resistant or biocide-releasing surfaces, etc.), can only improve either the hemocompatibility or the antibacterial properties of the devices. However, NO release or generating polymers have demonstrated very positive effects in terms of preventing both platelet activation and thrombus formation as well as exhibiting significant antimicrobial activity toward infection/biofilm formation without bacterial resistance. Although this review mainly focused on the use of NO release polymers for antithrombotic and antibacterial applications, these polymers also have many other potential applications for use on skin, bones, connective tissue, gastroenterology, or studying NO-induced cellular responses.[112,178,295,296]

Recently, considerable effort has been devoted to develop combination therapy and hybrid drugs that combine NO release functionality with other active agents for increased efficacies, including anticoagulants,[35,127] direct thrombin inhibitors,[36,43] antimicrobial metal ions,[216] quaternary ammonium compounds,[71] PEG,[116] antibiotics,[297] and non-steroidal anti-inflammatory drugs (NSAIDs), such as ibuprofen.[141] The remaining challenge for NO delivery polymers in order to be used in clinical settings lies in the development of more stable NO donors and polymer scaffolds and delivering the desired amount NO in a controlled spatial and temporal manner. In many cases, long-term NO release is desired, especially for using NO-releasing, blood compatible polymeric materials

for preparing intravascular grafts, stents, catheters, and other vascular access devices. Further research should focus on the dose-dependent biological responses to different NO concentrations and aim towards developing clinically relevant NO delivery materials for that purpose, that can ultimately expedite the translation of these materials from the laboratory to clinical use. Overall, both *in vitro* and *in vivo* (animals) studies of some of the NO releasing/generating polymers developed to date have clearly demonstrated the immense potential of this approach to improve the hemocompatibility/antimicrobial activity of a variety of biomedical devices that are required to improve patient care. Hopefully, the first commercial devices that employ this strategy will soon become available for routine use within hospitals.

1.9 Statement of Research

As previously described in this chapter, since SNAP is soluble in water, it is often covalently attached to filler particles which are then filled into polymer matrix in order to reduce leaching when the polymer is in contact with physiological solutions. Yet in recent studies, SNAP was found to be exceptionally stable when doped into low water uptake biomedical polymers, such as Elast-eon E2As. However, the reason for this enhanced stability still remains unclear. Therefore, the first goal of this dissertation work is to further examine different SNAP-incorporated polymeric materials and conduct solid-state analysis to understand the origin of the high stability of SNAP-doped polymers. The purpose of developing NO releasing polymers is to mimic the antithrombotic and antimicrobial functions of NO released by the endothelial cells, macrophage and other cells. Hence, it is very essential to develop materials that can release NO in a similar flux range. Therefore,

the second purpose of this research is to understand the various factors that control the NO release rates from these new composite biomaterials. Furthermore, this thesis introduces the concept of a simple solvent impregnation process to incorporate SNAP into pre-made polymeric devices. The successful adaptation of this technology may facilitate the process of developing commercial biomedical devices that can employ this NO release technique to prevent thrombus formation and bacterial biofilm infection. This dissertation also includes results from a research collaboration with Dr. Lichong Xu and Dr. Christopher A. Siedlecki's laboratory at Penn State University Medical Center with the aim to develop dual-functional antibacterial biomaterial surfaces. It should be noted that this dissertation is prepared using a multiple manuscript/publication format, and hence the introduction sections in each of the chapters may be somewhat repetitive.

Chapter 1 summarizes and reviews in detail the research efforts to date in designing and creating antithrombotic and antimicrobial biomaterials for potential biomedical applications, with an emphasis on the use of NO releasing/generating polymeric materials. This portion of the chapter was published in *RSC Biomaterials Sciences* and was highlighted on the cover of the journal. (Y. Wo, E. J. Brisbois, R. H. Bartlett, M. E. Meyerhoff, *RSC Biomaterials Sciences*, **2016**, *4*, 1161-1183).

Chapter 2 reports on fundamental solid-state studies that examine the origin of the high stability of SNAP-doped CarboSil 20 80A polymer-crystal composites and their potential in reducing bacterial biofilm formation *in vitro* and reducing thrombus formation *in vivo*. This work was published in *ACS Applied Materials & Interfaces* (Y. Wo, Z. Li, E. J.

Brisbois, A. Colletta, J. Wu, T. C. Major, C. Xi, R. H. Bartlett, A. J. Matzger, M. E. Meyerhoff, *ACS Applied Materials & Interfaces*, **2015**, *7* (40), 22218-22227).

Chapter 3 focuses on examining the NO release mechanism from SNAP-doped CarboSil polymer with respect to SNAP concentration, water-contacting polymer surface area and polymer thickness. This chapter also includes a kinetics study of SNAP decomposition in various solution phases. Finally, it demonstrates the antibacterial properties of SNAP-doped CarboSil catheters are solely from the effect of NO released from the catheter surface. This work has been submitted to *Composite Part B: Bio-inspired Nano-engineered Materials*.

Chapter 4 introduces the solvent impregnation approach to prepare SNAP-impregnated CarboSil 20 80A catheters. This chapter details the optimization of the impregnation process and reports on the solid-state analysis of the new material. It also includes the results and discussions regarding the *in vitro* anti-biofilm experiments and *in vivo* testing in an animal model. This work has been submitted to *ACS Biomaterials Science & Engineering*.

Chapter 5 summarizes our collaborative studies with Penn State Medical School to design and spin-coat a dual-functional antibacterial surface that combines the physical modification of material surface with submicron textures (e.g, pillars) and the chemical modification of the material by incorporating NO release functionality. We have demonstrated there is synergy between NO release and surface textures against

Staphylococcus epidermidis bacterial adhesion. The work presented in this chapter has been accepted for publication in *Acta Biomaterialia*.

Chapter 6 describes the use of the solvent impregnation technique reported in Chapter 4 to create SNAP-impregnated NO releasing CarboSil biomaterial surface that also has surface texturing. This approach provides a more efficient and cost-effective approach to create dual-functionality biomaterials in which the antibacterial properties of the resulting materials increase with impregnated SNAP concentration. Statistical analysis of the bacterial adhesion suggests that either NO release and surface texturing has a significant effect in reducing bacterial adhesion alone. However, there is synergy when the NO release approach is combined with surface texturing against *Staphylococcus epidermidis* and *Pseudomonas aeruginosa*, not *Staphylococcus aureus* and *Escherichia coli*. This work will be submitted to *Biomaterials Science*.

Chapter 7 summarizes the major findings/conclusion from this dissertation research and provides suggestions for future directions that will build upon the studies reported herein.

1.10 References

1 N. Naghavi, A. De Mel, O. S. Alavijeh, B. G. Cousins and A. M. Seifalian, *Small*, 2013, **9**, 22–35.

2 M. B. Gorbet and M. V Sefton, *Biomaterials*, 2004, **25**, 5681–703.

3 E. J. Brisbois, H. Handa and M. E. Meyerhoff, in *Advanced Polymers in Medicine*, ed. F. Puoci, Springer International Publishing, Cham, 2015, pp. 481–511.

4 M. V.Sefton, C. H. Gemmell and M. B. Gorbet, *J. Biomater. Sci. Polym. Ed.*, 2000, **11**, 1165–1182.

5 M. B. Gorbet and M. V. Sefton, in *The Biomaterials: Silver Jubilee Compendium*, Elsevier, 2004, vol. 25, pp. 219–241.

6 T. A. Horbett, *Cardiovasc. Pathol.*, 1993, **2**, 137–148.

7 J. D. Andrade and V. Hlady, in *Advances in Polymer Science*, 1986, vol. 79, pp. 1–63.

8 Y. Wu and M. E. Meyerhoff, *Talanta*, 2008, **75**, 642–50.

9 R. M. Klevens, J. R. Edwards, C. L. Richards, T. C. Horan, R. P. Gaynes, D. A. Pollock and D. M. Cardo, *Public Health Rep.*, 2007, **122**, 160–6.

10 C. Abad and N. Safdar, *Infect. Dis. Spec. Ed.*, 2011.

11 H. Shah, W. Bosch, K. M. Thompson and W. C. Hellinger, *The Neurohospitalist*, 2013, **3**, 144–151.

12 L. A. Mermel, M. Allon, E. Bouza, D. E. Craven, P. Flynn, N. P. O'Grady, I. I. Raad, B. J. Rijnders, R. J. Sherertz and D. K. Warren, *Clin. Infect. Dis.*, 2009, **49**, 1–45.

13 A. Sitges-Serra and M. Girvent, *World J. Surg.*, 1999, **23**, 589–595.

14 M. R. Goede and C. M. Coopersmith, *Surg. Clin. North Am.*, 2009, **89**, 463–474.

15 R. Gahlot, C. Nigam, V. Kumar, G. Yadav and S. Anupurba, *Int. J. Crit. Illn. Inj. Sci.*, 2014, **4**, 162–167.

16 M. Chen, Q. Yu and H. Sun, *Int. J. Mol. Sci.*, 2013, **14**, 18488–18501.

17 R. M. Donlan, *Clin. Infect. Dis.*, 2001, **33**, 1387–1392.

18 J. B. Kaplan, *J. Dent. Res.*, 2010, **89**, 205–218.

19 A. Colletta, J. Wu, Y. Wo, M. Kappler, H. Chen, C. Xi and M. E. Meyerhoff, *ACS Biomater. Sci. Eng.*, 2015, **1**, 416–424.

20 E. M. Hetrick and M. H. Schoenfisch, *Chem. Soc. Rev.*, 2006, **35**, 780–789.

21 J. Hirsh, *N. Engl. J. Med.*, 1991, **324**, 1565–1574.

22 A. Gutowska, Y. H. Bae, H. Jacobs, F. Mohammad, D. Mix, J. Feijen and S. W. Kim, *J. Biomed. Mater. Res.*, 1995, **29**, 811–821.

23 T. E. Warkentin, C. P. Hayward, C. A. Smith, P. M. Kelly and J. G. Kelton, *J. Lab. Clin. Med.*, 1992, **120**, 371–379.

24 H. Tanzawa, Y. Mori, N. Harumiya, H. Miyama, M. Hori, N. Ohshima and Y. Idezuki, *ASAIO J.*, 1973, **19**, 188–194.

25 V. L. Gott, J. D. Whiffen and R. C. Dutton, *Science (80-.).*, 1963, **142**, 1297–1298.

26 R. Shibuta, M. Tanaka, M. Sisido and Y. Imanishi, *J. Biomed. Mater. Res.*, 1986, **20**, 971–987.

27 C. A. Hufnagel, P. W. Conrad, J. F. Gillespie, R. Pifarre, A. Llano and T. Yokoyama, *Ann. N. Y. Acad. Sci.*, 1968, **146**, 262–270.

28 J. Y. Lin, C. Nojiri, T. Okano and S. W. Kim, *ASAIO Trans.*, 1987, **33**, 602–605.

29 P. W. Heyman, C. S. Cho, J. C. McRea, D. B. Olsen and S. W. Kim, *J. Biomed. Mater. Res.*, 1985, **19**, 419–436.
30 C. Ebert, J. McRea and S. W. Kim, in *Controlled Release of Bioactive Materials*, Elsevier, 1980, pp. 107–122.
31 A. Gutowska, Y. H. Bae, J. Feijen and S. W. Kim, *J. Control. Release*, 1992, **22**, 95–105.
32 S. Wan Kim and H. Jacobs, *Blood Purif.*, 1996, **14**, 357–372.
33 N. Ayres, D. J. Holt, C. F. Jones, L. E. Corum and D. W. Grainger, *J. Polym. Sci. A. Polym. Chem.*, 2008, **46**, 7713–7724.
34 K. A. Mowery, M. H. Schoenfisch, J. E. Saavedra, L. K. Keefer and M. E. Meyerhoff, *Polymer (Guildf).*, 2000, **21**, 9–21.
35 Z. Zhou and M. E. Meyerhoff, *Biomaterials*, 2005, **26**, 6506–6517.
36 B. Wu, B. Gerlitz, B. W. Grinnell and M. E. Meyerhoff, *Biomaterials*, 2007, **28**, 4047–55.
37 S. E. Sakiyama-Elbert, *Acta Biomater.*, 2014, **10**, 1581–1587.
38 P. C. Begovac, R. C. Thomson, J. L. Fisher, A. Hughson and A. Gallhagen, *Eur. J. Vasc. Endovasc. Surg.*, 2003, **25**, 432–437.
39 C. Devine and C. McCollum, *J. Vasc. Surg.*, 2004, **40**, 924–931.
40 P. Olsson, J. Sanchez, T. E. Mollnes and J. Riesenfeld, *J. Biomater. Sci. Polym. Ed.*, 2000, **11**, 1261–1273.
41 A. G. Kidane, H. Salacinski, A. Tiwari, K. R. Bruckdorfer and A. M. Seifalian, *Biomacromolecules*, 2004, **5**, 798–813.
42 S. W. Jordan and E. L. Chaikof, *J. Vasc. Surg.*, 2007, **45**, 104–115.
43 T. C. Major, E. J. Brisbois, A. M. Jones, M. E. Zanetti, G. M. Annich, R. H. Bartlett and H. Handa, *Biomaterials*, 2014, **35**, 7271–7285.
44 N. A. Peppas, Y. Huang, M. Torres-Lugo, J. H. Ward and J. Zhang, *Annu. Rev. Biomed. Eng.*, 2000, **2**, 9–29.
45 O. WichterleI and D. LÍm, *Nature*, 1960, **185**, 117–118.
46 S. Lakshmi and A. Jayakrishnan, *Artif. Organs*, 1998, **22**, 222–229.
47 B. Balakrishnan, D. S. Kumar, Y. Yoshida and A. Jayakrishnan, *Biomaterials*, 2005, **26**, 3495–3502.
48 C. R. Blass, C. Jones and J. M. Courtney, *Int. J. Artif. Organs*, 1992, 15, 200–203.
49 G. R. Llanos and M. V Sefton, *J. Biomed. Mater. Res.*, 1993, **27**, 1383–91.
50 J. M. Harris, *Poly(Ethylene Glycol) Chemistry*, Springer US, Boston, MA, Netherlands, 1992, vol. 11.
51 M. C. Tanzi, *Expert Rev. Med. Devices*, 2005, **2**, 473–492.
52 S. K. Williams, D. G. Rose and B. E. Jarrell, *J. Biomed. Mater. Res.*, 1994, **28**, 203–212.
53 P. Zilla, M. Deutsch, J. Meinhart, R. Puschmann, T. Eberl, E. Minar, R. Dudczak, H. Lugmaier, P. Schmidt and I. Noszian, *J. Vasc. Surg.*, 1994, **19**, 540–548.
54 S. R. Shah, A. M. Tatara, R. N. D'Souza, A. G. Mikos and F. K. Kasper, *Mater. Today*, 2013, **16**, 177–182.
55 S.-H. Park, S. Lee, D. Moreira, P. R. Bandaru, I. Han and D.-J. Yun, *Sci. Rep.*, 2015, **5**, 15430.
56 W. Ye, Q. Shi, J. Hou, J. Jin, Q. Fan, S.-C. Wong, X. Xu and J. Yin, *J. Mater. Chem. B*, 2014, **2**, 7186–7191.

57 X. Gao and L. Jiang, *Nature*, 2004, **432**, 36.
58 U. Nydegger, R. Rieben and B. Lämmle, *Transfus. Sci.*, 1996, **17**, 481–488.
59 G. Cheng, H. Xue, Z. Zhang, S. Chen and S. Jiang, *Angew. Chemie Int. Ed.*, 2008, **47**, 8831–8834.
60 E. Ostuni, R. G. Chapman, R. E. Holmlin, S. Takayama and G. M. Whitesides, *Langmuir*, 2001, **17**, 5605–5620.
61 S.-H. Hsu, Y.-C. Kao and Z.-C. Lin, *Macromol. Biosci.*, 2004, **4**, 464–470.
62 S.-H. Hsu and Y.-C. Kao, *Macromol. Biosci.*, 2005, **5**, 246–253.
63 L. C. Xu, P. Soman, J. Runt and C. a Siedlecki, *J. Biomater. Sci. Polym. Ed.*, 2007, **18**, 353–368.
64 Q. Yu, Z. Wu and H. Chen, *Acta Biomater.*, 2015, **16**, 1–13.
65 I. Kolodkin-Gal, D. Romero, S. Cao, J. Clardy, R. Kolter and R. Losick, *Science*, 2010, **328**, 627–629.
66 M. R. Kiedrowski and A. R. Horswill, *Ann. N. Y. Acad. Sci.*, 2011, **1241**, 104–21.
67 S. Sepehr, A. Rahmani-Badi, H. Babaie-Naiej and M. R. Soudi, *PLoS One*, 2014, 9.
68 J. A. Jennings, H. S. Courtney and W. O. Haggard, *Clin. Orthop. Relat. Res.*, 2012, **470**, 2663–2670.
69 M. C. Jennings, L. E. Ator, T. J. Paniak, K. P. C. Minbiole and W. M. Wuest, *Chembiochem*, 2014, **15**, 2211–2215.
70 M. C. Jennings, K. P. C. Minbiole and W. M. Wuest, *ACS Infect. Dis.*, 2015, 288–303.
71 A. W. Carpenter, B. V. Worley, D. L. Slomberg and M. H. Schoenfisch, *Biomacromolecules*, 2012, **13**, 3334–3342.
72 A. S. Abd-El-Aziz, C. Agatemor, N. Etkin, D. P. Overy, M. Lanteigne, K. McQuillan and R. G. Kerr, *Biomacromolecules*, 2015, **16**, 3694–3703.
73 N. D. Allan, K. Giare-Patel and M. E. Olson, *J. Biomed. Biotechnol.*, 2012, **2012**.
74 K. Wu, Y. Yang, Y. Zhang, J. Deng and C. Lin, *Int. J. Nanomedicine*, 2015, **10**, 7241–7252.
75 L. Mei, Z. Lu, X. Zhang, C. Li and Y. Jia, *ACS Appl. Mater. Interfaces*, 2014, **6**, 15813–15821.
76 S. K. Sehmi, S. Noimark, J. Weiner, E. Allan, A. J. MacRobert and I. P. Parkin, *ACS Appl. Mater. Interfaces*, 2015, **7**, 22807–22813.
77 L. Zhang, C. Ning, T. Zhou, X. Liu, K. W. K. Yeung, T. Zhang, Z. Xu, X. Wang, S. Wu and P. K. Chu, *ACS Appl. Mater. Interfaces*, 2014, **6**, 17323–17345.
78 S. Rossi, A. O. Azghani and A. Omri, *J. Antimicrob. Chemother.*, 2004, **54**, 1013–1018.
79 L. Zhao, P. K. Chu, Y. Zhang and Z. Wu, *J. Biomed. Mater. Res. B. Appl. Biomater.*, 2009, **91**, 470–480.
80 R. Cademartiri, H. Anany, I. Gross, R. Bhayani, M. Griffiths and M. A. Brook, *Biomaterials*, 2010, **31**, 1904–1910.
81 U. Puapermpoonsiri, J. Spencer and C. F. van der Walle, *Eur. J. Pharm. Biopharm.*, 2009, **72**, 26–33.
82 T. Wei, Q. Yu, W. Zhan and H. Chen, *Adv. Healthc. Mater.*, 2016, **5**, 449–456.
83 G. Cado, R. Aslam, L. Séon, T. Garnier, R. Fabre, A. Parat, A. Chassepot, J.-C. Voegel, B. Senger, F. Schneider, Y. Frère, L. Jierry, P. Schaaf, H. Kerdjoudj, M.-H. Metz-Boutigue and F. Boulmedais, *Adv. Funct. Mater.*, 2013, **23**, 4801–4809.

84 K. V Holmberg, M. Abdolhosseini, Y. Li, X. Chen, S.-U. Gorr and C. Aparicio, *Acta Biomater.*, 2013, **9**, 8224–8231.
85 J. Li, Z. Chen, M. Zhou, J. Jing, W. Li, Y. Wang, L. Wu, L. Wang, Y. Wang and M. Lee, *Angew. Chem. Int. Ed. Engl.*, 2016, **55**, 2592–2595.
86 W. J. Yang, T. Cai, K. G. Neoh, E. T. Kang, G. H. Dickinson, S. L. M. Teo and D. Rittschof, *Langmuir*, 2011, **27**, 7065–7076.
87 K. P. Reighard and M. H. Schoenfisch, *Antimicrob. Agents Chemother.*, 2015, **59**, 6506–6513.
88 K. P. Reighard, D. B. Hill, G. A. Dixon, B. V. Worley and M. H. Schoenfisch, *Biofouling*, 2015, **31**, 775–787.
89 J. Choi, B. J. Yang, G. N. Bae and J. H. Jung, *ACS Appl. Mater. Interfaces*, 2015, **7**, 25313–25320.
90 J. Dolanský, P. Henke, P. Kubát, A. Fraix, S. Sortino and J. Mosinger, *ACS Appl. Mater. Interfaces*, 2015, **7**, 22980–22989.
91 Z. Cao, L. Mi, J. Mendiola, J. R. Ella-Menye, L. Zhang, H. Xue and S. Jiang, *Angew. Chemie - Int. Ed.*, 2012, **51**, 2602–2605.
92 Q. Yu, J. Cho, P. Shivapooja, L. K. Ista and G. P. Lopez, *ACS Appl. Mater. Interfaces*, 2013, **5**, 9295–9304.
93 M. Dargahi, Z. Hosseinidoust, N. Tufenkji and S. Omanovic, *Colloids Surfaces B Biointerfaces*, 2014, **117**, 152–157.
94 S. Tamura, H. Yonezawa, M. Motegi, R. Nakao, S. Yoneda, H. Watanabe, T. Yamazaki and H. Senpuku, *Oral Microbiol. Immunol.*, 2009, **24**, 152–161.
95 S. A. Ishijima, K. Hayama, J. P. Burton, G. Reid, M. Okada, Y. Matsushita and S. Abe, *Appl. Environ. Microbiol.*, 2012, **78**, 2190–2199.
96 B. W. Trautner, R. A. Hull and R. O. Darouiche, *Urology*, 2003, **61**, 1059–1062.
97 B. W. Trautner, R. A. Hull and R. O. Darouiche, *Curr. Opin. Infect. Dis.*, 2005, **18**, 37–41.
98 B. W. Trautner, R. a Hull, J. I. Thornby and R. O. Darouiche, *Infect. Control Hosp. Epidemiol.*, 2007, **28**, 92–94.
99 P. Andersson, I. Engberg, G. Lidin-Janson, K. Lincoln, R. Hull, S. Hull and C. Svanborg, *Infect. Immun.*, 1991, **59**, 2915–2921.
100 A. Esclarin De Ruz, E. Garcia Leoni and R. Herruzo Cabrera, *J. Urol.*, 2000, **164**, 1285–1289.
101 A. R. Unnithan, A. Ghavami Nejad, A. R. K. Sasikala, R. G. Thomas, Y. Y. Jeong, P. Murugesan, S. Nasseri, D. Wu, C. H. Park and C. S. Kim, *Chem. Eng. J.*, 2016, **287**, 640–648.
102 A. Vaterrodt, B. Thallinger, K. Daumann, D. Koch, G. M. Guebitz and M. Ulbricht, *Langmuir*, 2016, **32**, 1347–1359.
103 L. C. Xu and C. a Siedlecki, *Biomed. Mater.*, 2014, **9**, 035003.
104 L. C. Xu and C. a. Siedlecki, *Acta Biomater.*, 2012, **8**, 72–81.
105 L. chong Xu, J. W. Bauer and C. a Siedlecki, *Colloids Surfaces B Biointerfaces*, 2014, **124**, 49–68.
106 L. Wang, H. Li, S. Chen, C. Nie, C. Cheng and C. Zhao, *ACS Biomater. Sci. Eng.*, 2015, **1**, 1183–1193.
107 Z.-Q. Shi, H.-F. Ji, H.-C. Yu, X.-L. Huang, W.-F. Zhao, S.-D. Sun and C.-S. Zhao, *Colloid Polym. Sci.*, 2016, **294**, 441–453.

108 J. Deng, L. Ma, X. Liu, C. Cheng, C. Nie and C. Zhao, *Adv. Mater. Interfaces*, 2016, **3**, 1500473.
109 A. B. Seabra and N. Durán, *J. Mater. Chem.*, 2010, **20**, 1624.
110 M. C. Frost, M. M. Reynolds and M. E. Meyerhoff, *Biomaterials*, 2005, **26**, 1685–1693.
111 M. M. Reynolds, M. C. Frost and M. E. Meyerhoff, *Free Radic. Biol. Med.*, 2004, **37**, 926–936.
112 S. P. Nichols, W. L. Storm, A. Koh and M. H. Schoenfisch, *Adv. Drug Deliv. Rev.*, 2012, **64**, 1177–88.
113 E. M. Hetrick and M. H. Schoenfisch, *Annu Rev Anal Chem (Palo Alto Calif)*, 2009, **2**, 409–33.
114 M. M. Reynolds and G. M. Annich, *Organogenesis*, 2011, **7**, 42–49.
115 Y. Wang, S. Chen, Y. Pan, J. Gao, D. Tang, D. Kong and S. Wang, *J. Mater. Chem. B*, 2015, **3**, 9212–9222.
116 L. J. Taite, P. Yang, H.-W. Jun and J. L. West, *J. Biomed. Mater. Res. Part B Appl. Biomater.*, 2007, **84B**, 108–116.
117 I. L. A. Geenen, D. G. M. Molin, N. M. S. van den Akker, F. Jeukens, H. M. Spronk, G. W. H. Schurink and M. J. Post, *J. Tissue Eng. Regen. Med.*, 2015, **9**, 564–576.
118 A. W. Carpenter and M. H. Schoenfisch, *Chem. Soc. Rev.*, 2012, **41**, 3742–52.
119 M. Vaughn, L. Kuo and J. Liao, *Am. J. Physiol.*, 1998, **274**, 2163–2176.
120 K. M. Vural and M. Bayazit, *Eur. J. Vasc. Endovasc. Surg.*, 2001, **22**, 285–293.
121 M. C. Jen, M. C. Serrano, R. van Lith and G. A. Ameer, *Adv. Funct. Mater.*, 2012, **22**, 239–260.
122 J. Loscalzo, *Circ. Res.*, 2001, **88**, 756–762.
123 G. Walford and J. Loscalzo, *J. Thromb. Haemost.*, 2003, **1**, 2112–2118.
124 J. S. Isenberg, M. J. Romeo, C. Yu, C. K. Yu, K. Nghiem, J. Monsale, M. E. Rick, D. A. Wink, W. A. Frazier and D. D. Roberts, *Blood*, 2008, **111**, 613–623.
125 A. Gries, C. Bode, K. Peter, A. Herr, H. Böhrer, J. Motsch and E. Martin, *Circ.* , 1998, **97** , 1481–1487.
126 M. W. Radomski, R. M. Palmer and S. Moncada, *Proc. Natl. Acad. Sci. U. S. A.*, 1990, **87**, 5193–5197.
127 D. J. Suchyta, H. Handa and M. E. Meyerhoff, *Mol. Pharm.*, 2014, **11**, 645–650.
128 D. O. Schairer, J. S. Chouake, J. D. Nosanchuk and A. J. Friedman, *Virulence*, 2012, **3**, 271–9.
129 H. Rubbo, R. Radi, M. Trujillo, R. Telleri, B. Kalyanaraman, S. Barnes, M. Kirk and B. A. Freeman, *J. Biol. Chem.*, 1994, **269**, 26066–26075.
130 F. C. Fang, *Nat. Rev. Microbiol.*, 2004, **2**, 820–832.
131 L. Ignarro and G. Buga, *Proc. Natl. Acad. Sci. U. S. A.*, 1987, **84**, 9265–9269.
132 S. R. Hanson, T. C. Hutsell, L. K. Keefer, D. L. Mooradian and D. J. Smith, *Adv. Pharmacol.*, 1995, **34**, 383–98.
133 J. O. Lundberg, M. T. Gladwin and E. Weitzberg, *Nat. Rev. Drug Discov.*, 2015, **14**, 623–41.
134 J. O. Lundberg, E. Weitzberg and M. T. Gladwin, *Crit. Care Med.*, 2008, **7**, 156–167.
135 R. Scatena, P. Bottoni, G. E. Martorana and B. Giardina, *Expert Opin. Investig. Drugs*, 2005, **14**, 835–846.

136 D. a Riccio and M. H. Schoenfisch, *Chem. Soc. Rev.*, 2012, **41**, 3731–41.
137 J. a Hrabie and L. K. Keefer, *Chem. Rev.*, 2002, **102**, 1135–54.
138 V. N. Varu, N. D. Tsihlis and M. R. Kibbe, *Vasc. Endovascular Surg.*, 2009, **43**, 121–131.
139 J. Saraiva, S. S. Marotta-Oliveira, S. A. Cicillini, J. D. O. Eloy and J. M. Marchetti, *J. Drug Deliv.*, 2011, **2011**.
140 S. Sortino, *Chem. Soc. Rev.*, 2010, **39**, 2903–13.
141 P. G. Wang, M. Xian, X. Tang, X. Wu, Z. Wen, T. Cai and A. J. Janczuk, *Chem. Rev.*, 2002, **102**, 1091–1134.
142 T. Münzel, A. Daiber and A. Mülsch, *Circ. Res.*, 2005, **97**, 618–28.
143 K. Sydow, A. Daiber, M. Oelze, Z. Chen, M. August, M. Wendt, V. Ullrich, A. Mülsch, E. Schulz, J. F. Keaney, J. S. Stamler and T. Münzel, *J. Clin. Invest.*, 2004, **113**, 482–489.
144 A. Daiber, M. Oelze, M. Coldewey, M. Bachschmid, P. Wenzel, K. Sydow, M. Wendt, A. L. Kleschyov, D. Stalleicken, V. Ullrich, A. Mulsch and T. Munzel, *Mol. Pharmacol.*, 2004, **66**, 1372–1382.
145 L. Grossi and S. D'Angelo, *J. Med. Chem.*, 2005, **48**, 2622–6.
146 L. Höfler, D. Koley, J. Wu, C. Xi and M. E. Meyerhoff, *RSC Adv.*, 2012, **2**, 6765–6767.
147 H. Ren, A. Colletta, D. Koley, J. Wu, C. Xi, T. C. Major, R. H. Bartlett and M. E. Meyerhoff, *Bioelectrochemistry*, 2015, **104**, 10–16.
148 H. Ren, J. Wu, C. Xi, N. Lehnert, T. Major, R. H. Bartlett and M. E. Meyerhoff, *ACS Appl. Mater. Interfaces*, 2014, **6**, 3779–3783.
149 J. R. Hwu, C. S. Yau, S.-C. Tsay and T.-I. Ho, *Tetrahedron Lett.*, 1997, **38**, 9001–9004.
150 A. Wan, Q. Gao and H. Li, *J. Mater. Sci. Mater. Med.*, 2009, **20**, 321–327.
151 S. Hong, J. Kim, Y. S. Na, J. Park, S. Kim, K. Singha, G. Il Im, D. K. Han, W. J. Kim and H. Lee, *Angew. Chemie - Int. Ed.*, 2013, **52**, 9187–9191.
152 C. M. Maragos, D. Morley, D. A. Wink, T. M. Dunams, J. E. Saavedra, A. Hoffman, A. A. Bove, L. Isaac, J. A. Hrabie and L. K. Keefer, *J. Med. Chem.*, 1991, **34**, 3242–3247.
153 L. K. Keefer, R. W. Nims, K. M. Davies and D. A. Wink, *Methods Enzymol.*, 1996, **268**, 281–293.
154 M. M. Batchelor, S. L. Reoma, P. S. Fleser, V. K. Nuthakki, R. E. Callahan, C. J. Shanley, J. K. Politis, J. Elmore, S. I. Merz and M. E. Meyerhoff, *J. Med. Chem.*, 2003, **46**, 5153–61.
155 H. Handa, E. J. Brisbois and T. C. Major, *J. Mater. Chem. B*, 2013, **1**, 3578–3587.
156 H. Handa, T. C. Major, E. J. Brisbois, K. A. Amoako, M. E. Meyerhoff and R. H. Bartlett, *J. Mater. Chem. B*, 2014, **2**, 1059–1067.
157 W. Cai, J. Wu, C. Xi and M. E. Meyerhoff, *Biomaterials*, 2012, **33**, 7933–44.
158 H. K. Makadia and S. J. Siegel, *Polymers (Basel).*, 2011, **3**, 1377–1397.
159 J. S. Stamler, O. Jaraki, J. Osborne, D. I. Simon, J. Keaney, J. Vita, D. Singel, C. R. Valeri and J. Loscalzo, *Proc. Natl. Acad. Sci. U. S. A.*, 1992, **89**, 7674–7677.
160 D. Giustarini, A. Milzani, R. Colombo, I. Dalle-Donne and R. Rossi, *Clin. Chim. Acta*, 2003, **330**, 85–98.
161 X. Duan and R. S. Lewis, *Biomaterials*, 2002, **23**, 1197–1203.

162 E. J. Brisbois, H. Handa, T. C. Major, R. H. Bartlett and M. E. Meyerhoff, *Biomaterials*, 2013, **34**, 6957–66.
163 Y. Wo, Z. Li, E. J. Brisbois, A. Colletta, J. Wu, T. C. Major, C. Xi, R. H. Bartlett, A. J. Matzger and M. E. Meyerhoff, *ACS Appl. Mater. Interfaces*, 2015, **7**, 22218–22227.
164 D. L. H. Williams, *Chem. Commun.*, 1996, 1085–1091.
165 D. L. H. Williams, *Transit. Met. Chem.*, 1996, **21**, 189–191.
166 D. L. Williams, *Acc. Chem. Res.*, 1999, **32**, 869–876.
167 K. Szacilowski and Z. Stasicka, *Prog. React. Kinet. Mech.*, 2001, **26**, 1–58.
168 R. J. Singh, N. Hogg, J. Joseph and B. Kalyanaraman, *J. Biol. Chem.*, 1996, **271**, 18596–18603.
169 C. T. Aravindakumar, M. M. Veleeparampil and U. K. Aravind, *Adv. Phys. Chem.*, 2009, **2009**.
170 J. McAninly, D. L. H. Williams, S. C. Askew, A. R. Butler and C. Russell, *J. Chem. Soc. Chem. Commun.*, 1993, 1758–1759.
171 S. Hwang and M. E. Meyerhoff, *Biomaterials*, 2008, **29**, 2443–2452.
172 W. Cha and M. E. Meyerhoff, *Biomaterials*, 2007, **28**, 19–27.
173 J. Yang, J. L. Welby and M. E. Meyerhoff, *Langmuir*, 2008, **24**, 10265–10272.
174 W. Cai, J. Wu, C. Xi, A. J. Ashe and M. E. Meyerhoff, *Biomaterials*, 2011, **32**, 7774–84.
175 A. J. Holmes and D. L. H. Williams, *Chem. Commun.*, 1998, 1711–1712.
176 A. J. Holmes and D. L. H. Williams, *J. Chem. Soc. Trans. 2*, 2000, 1639–1644.
177 D. Jourd'heuil, F. S. Laroux, A. M. Miles, D. A. Wink and M. B. Grisham, *Arch. Biochem. Biophys.*, 1999, **361**, 323–330.
178 A. B. Seabra, in *Nanocosmetics and Nanomedicines*, eds. R. Beck, S. Guterres and A. Pohlmann, Springer Berlin Heidelberg, Berlin, Heidelberg, 2011, pp. 253–268.
179 R. Vercelino, T. M. Cunha, E. S. Ferreira, F. Q. Cunha, S. H. Ferreira and M. G. De Oliveira, *J. Mater. Sci. Mater. Med.*, 2013, **24**, 2157–2169.
180 F. S. Schanuel, K. S. Raggio Santos, A. Monte-Alto-Costa and M. G. De Oliveira, *Colloids Surfaces B Biointerfaces*, 2015, **130**, 182–191.
181 M. G. de Oliveira, *Basic Clin. Pharmacol. Toxicol.*, 2016, n/a–n/a.
182 T. R. Borthwick, G. D. Benson and H. J. Schugar, *J. Lab. Clin. Med.*, 1980, **95**, 575–580.
183 V. Parameshvara, *Br. J. Ind. Med.*, 1967, **24**, 73–76.
184 K. A. Graeme and C. V Pollack, *J. Emerg. Med.*, 1998, 16, 45–56.
185 M. M. Jones, A. D. Weaver and W. L. Weller, *Res. Commun. Chem. Pathol. Pharmacol.*, 1978, **22**, 581–588.
186 N. Arulsamy, D. S. Bohle, J. A. Butt, G. J. Irvine, P. A. Jordan and E. Sagan, *J. Am. Chem. Soc.*, 1999, **121**, 7115–7123.
187 E. J. Brisbois, R. P. Davis, A. M. Jones, T. C. Major, R. H. Bartlett, M. E. Meyerhoff and H. Handa, *J. Mater. Chem. B*, 2015, **3**, 1639–1645.
188 I. L. Megson, S. Morton, I. R. Greig, F. A. Mazzei, R. A. Field, A. R. Butler, G. Caron, A. Gasco, R. Fruttero and D. J. Webb, *Br. J. Pharmacol.*, 1999, **126**, 639–648.
189 I. L. Megson, *Drugs Future*, 2002, **27**, 777.
190 A. Ketchum, M. Kappler, J. Wu, C. Xi and M. E. Meyerhoff, *J. Mater. Chem. B*,

2015, **4**, 422–430.
191 Y. S. Jo, A. J. van der Vlies, J. Gantz, T. N. Thacher, S. Antonijevic, S. Cavadini, D. Demurtas, N. Stergiopulos and J. A. Hubbell, *J. Am. Chem. Soc.*, 2009, **131**, 14413–14418.
192 N. Kanayama, K. Yamaguchi and Y. Nagasaki, *Chem. Lett.*, 2010, **39**, 1008–1009.
193 F. Cavalieri, I. Finelli, M. Tortora, P. Mozetic, E. Chiessi, F. Polizio, T. B. Brismar and G. Paradossi, *Chem. Mater.*, 2008, **20**, 3254–3258.
194 J. A. Hrabie, J. E. Saavedra, P. P. Roller, G. J. Southan and L. K. Keefer, *Bioconjug. Chem.*, 1999, **10**, 838–842.
195 D. I. Simon, M. E. Mullins, L. Jia, B. Gaston, D. J. Singel and J. S. Stamler, *Proc. Natl. Acad. Sci. U. S. A.*, 1996, **93**, 4736–4741.
196 J. F. Ewing, D. V Young, D. R. Janero, D. S. Garvey and T. A. Grinnell, *J. Pharmacol. Exp. Ther.*, 1997, **283**, 947–954.
197 Y. Ishima, T. Akaike, U. Kragh-Hansen, S. Hiroyama, T. Sawa, A. Suenaga, T. Maruyama, T. Kai and M. Otagiri, *J. Biol. Chem.*, 2008, **283**, 34966–34975.
198 H. Katsumi, M. Nishikawa, F. Yamashita and M. Hashida, *J. Pharmacol. Exp. Ther.*, 2005, **314**, 1117–1124.
199 S.-L. Huang, P. H. Kee, H. Kim, M. R. Moody, S. M. Chrzanowski, R. C. Macdonald and D. D. McPherson, *J. Am. Coll. Cardiol.*, 2009, **54**, 652–659.
200 M. C. Frost and M. E. Meyerhoff, *J. Am. Chem. Soc.*, 2004, **126**, 1348–9.
201 M. C. Frost and M. E. Meyerhoff, *J. Biomed. Mater. Res. A*, 2005, **72**, 409–19.
202 A. W. Carpenter, D. L. Slomberg, K. S. Rao and M. H. Schoenfisch, *ACS Nano*, 2011, **5**, 7235–44.
203 M. H. Kafshgari, A. Cavallaro, B. Delalat, F. J. Harding, S. J. McInnes, E. Mäkilä, J. Salonen, K. Vasilev and N. H. Voelcker, *Nanoscale Res. Lett.*, 2014, **9**, 333.
204 D. L. Slomberg, Y. Lu, A. D. Broadnax, R. A. Hunter, A. W. Carpenter and M. H. Schoenfisch, *ACS Appl. Mater. Interfaces*, 2013, **5**, 9322–9329.
205 A. R. Rothrock, R. L. Donkers and M. H. Schoenfisch, *Society*, 2005, **127**, 9362–9363.
206 M. A. Polizzi, N. A. Stasko and M. H. Schoenfisch, *Langmuir*, 2007, **23**, 4938–4943.
207 G. Lautner, M. E. Meyerhoff and S. P. Schwendeman, *J. Control. Release*, 2016, **225**, 133–139.
208 P. S. Wheatley, A. R. Butler, M. S. Crane, S. Fox, B. Xiao, A. G. Rossi, I. L. Megson and R. E. Morris, *J. Am. Chem. Soc.*, 2006, **128**, 502–509.
209 M. Neidrauer, U. K. Ercan, A. Bhattacharyya, J. Samuels, J. Sedlak, R. Trikha, K. A. Barbee, M. S. Weingarten and S. G. Joshi, *J. Med. Microbiol.*, 2014, **63**, 203–209.
210 J. L. Harding and M. M. Reynolds, *J. Am. Chem. Soc.*, 2012, **134**, 3330–3333.
211 J. L. Harding and M. M. Reynolds, *J. Mater. Chem. B*, 2014, **2**, 2530–2536.
212 J. L. Harding, J. M. Metz and M. M. Reynolds, *Adv. Funct. Mater.*, 2014, **24**, 7503–7509.
213 M. J. Neufeld, J. L. Harding and M. M. Reynolds, *ACS Appl. Mater. Interfaces*, 2015, **7**, 26742–26750.
214 N. A. Stasko, T. H. Fischer and M. H. Schoenfisch, *Biomacromolecules*, 2008, **9**, 834–841.

215 C. J. Backlund, B. V. Worley and M. H. Schoenfisch, *Acta Biomater.*, 2016, **29**, 198–205.
216 W. L. Storm, J. a Johnson, B. V Worley, D. L. Slomberg and M. H. Schoenfisch, *J. Biomed. Mater. Res. A*, 2014, 1–11.
217 D. a Riccio, K. P. Dobmeier, E. M. Hetrick, B. J. Privett, H. S. Paul and M. H. Schoenfisch, *Biomaterials*, 2009, **30**, 4494–502.
218 P. Nacharaju, C. Tuckman-Vernon, K. E. Maier, J. Chouake, A. Friedman, P. Cabrales and J. M. Friedman, *Nitric Oxide*, 2012, **27**, 150–160.
219 P. N. Coneski, J. A. Nash and M. H. Schoenfisch, *ACS Appl. Mater. Interfaces*, 2011, **3**, 426–432.
220 J.-W. Yoo, H. Nurhasni, J. Cao, M. Choi, I. Kim, B. Luel Lee and Y. Jung, *Int. J. Nanomedicine*, 2015, **10**, 3065–3080.
221 Y. Lu, D. L. Slomberg and M. H. Schoenfisch, *Biomaterials*, 2014, **35**, 1716–1724.
222 J. O. Kim, J. K. Noh, R. K. Thapa, N. Hasan, M. Choi, J. H. Kim, J. H. Lee, S. K. Ku and J. W. Yoo, *Int. J. Biol. Macromol.*, 2015, **79**, 217–225.
223 C. Vogt, Q. Xing, W. He, B. Li, M. C. Frost and F. Zhao, *Biomacromolecules*, 2013, **14**, 2521–2530.
224 P. G. Parzuchowski, M. C. Frost and M. E. Meyerhoff, *J. Am. Chem. Soc.*, 2002, **124**, 12182–12191.
225 A. B. Seabra, R. Da Silva, G. F. P. De Souza and M. G. De Oliveira, *Artif. Organs*, 2008, **32**, 262–267.
226 J. P. Yapor, A. Lutzke, A. Pegalajar-Jurado, B. H. Neufeld, V. B. Damodaran and M. M. Reynolds, *J. Mater. Chem. B*, 2015, **3**, 9233–9241.
227 G. E. Gierke, M. Nielsen and M. C. Frost, *Sci. Technol. Adv. Mater.*, 2011, 12, 055007.
228 A. Pegalajar-Jurado, K. A. Wold, J. M. Joslin, B. H. Neufeld, K. A. Arabea, L. A. Suazo, S. L. McDaniel, R. A. Bowen and M. M. Reynolds, *J. Control. Release*, 2015, **220**, 617–623.
229 A. Wan, Q. Gao and H. Li, *J. Mater. Sci. Mater. Med.*, 2008, **20**, 321–327.
230 J. Park, J. Kim, K. Singha, D. K. Han, H. Park and W. J. Kim, *Biomaterials*, 2013, **34**, 8766–8775.
231 J. Kim, Y. Lee, K. Singha, H. W. Kim, J. H. Shin, S. Jo, D. K. Han and W. J. Kim, *Bioconjug. Chem.*, 2011, **22**, 1031–1038.
232 A. B. Seabra, A. Fitzpatrick, J. Paul, M. G. De Oliveira and R. Weller, *Br. J. Dermatol.*, 2004, **151**, 977–983.
233 K. Masters, S. Leibovich, P. Belem, J. L. West and L. Poole-Warren, *Wound Repair Regen.*, 2002, **10**, 286–294.
234 M. M. Reynolds, J. a Hrabie, B. K. Oh, J. K. Politis, M. L. Citro, L. K. Keefer and M. E. Meyerhoff, *Biomacromolecules*, 2006, **7**, 987–94.
235 M. M. Reynolds, J. E. Saavedra, B. M. Showalter, C. A. Valdez, A. P. Shanklin, B. K. Oh, L. K. Keefer and M. E. Meyerhoff, *J. Mater. Chem.*, 2010, **20**, 3107–2114.
236 B. Parzuchowska and P. Parzuchowski, *Polimery*, 2014, **59**, 105–194.
237 H. Zhang, G. M. Annich, J. Miskulin, K. Stankiewicz, K. Osterholzer, S. I. Merz, R. H. Bartlett and M. E. Meyerhoff, *J. Am. Chem. Soc.*, 2003, **125**, 5015–24.
238 J. E. Saavedra, M. N. Booth, J. A. Hrabie, K. M. Davies and L. K. Keefer, *J. Org. Chem.*, 1999, **64**, 5124–5131.

239 H. Zhang, G. M. Annich, J. Miskulin, K. Osterholzer, S. I. Merz, R. H. Bartlett and M. E. Meyerhoff, *Biomaterials*, 2002, **23**, 1485–1494.
240 D. J. Smith, D. Chakravarthy, S. Pulfer, M. L. Simmons, J. A. Hrabie, M. L. Citro, J. E. Saavedra, K. M. Davies, T. C. Hutsell, D. L. Mooradian, S. R. Hanson and L. K. Keefer, *J. Med. Chem.*, 1996, **39**, 1148–56.
241 Y. Kou and A. Wan, *Bioorg. Med. Chem. Lett.*, 2008, **18**, 2337–2341.
242 Y. Kang, J. Kim, Y. M. Lee, S. Im, H. Park and W. J. Kim, *J. Control. Release*, 2015, **220**, 624–630.
243 N. A. Stasko and M. H. Schoenfisch, *J. Am. Chem. Soc.*, 2006, **128**, 8265–8271.
244 C. W. McCarthy, J. Goldman and M. C. Frost, *ACS Appl. Mater. Interfaces*, 2016, **8**, 5898–5905.
245 V. B. Damodaran, L. W. Place, M. J. Kipper and M. M. Reynolds, *J. Mater. Chem.*, 2012, **22**, 23038.
246 T. Kean and M. Thanou, *Adv. Drug Deliv. Rev.*, 2010, **62**, 3–11.
247 C. Wang, F. Yang, Z. Xu, D. Shi, D. Chen, J. Dai, N. Gu and Q. Jiang, *Thromb. Res.*, 2013, **131**, e31–e38.
248 L. A. Tai, Y. C. Wang and C. S. Yang, *Nitric Oxide - Biol. Chem.*, 2010, **23**, 60–64.
249 J. J. Koehler, J. Zhao, S. S. Jedlicka, D. M. Porterfield and J. L. Rickus, *J. Phys. Chem. B*, 2008, **112**, 15086–15093.
250 H. S. Jeh, S. Lu and S. C. George, *J. Microencapsul.*, 2004, **21**, 3–13.
251 C. Wischke and S. P. Schwendeman, *Int. J. Pharm.*, 2008, **364**, 298–327.
252 S. M. Shishido, A. B. Seabra, W. Loh and M. G. de Oliveira, *Biomaterials*, 2003, **24**, 3543–3553.
253 M. G. de Oliveira, S. M. Shishido, A. B. Seabra and N. H. Morgon, *J. Phys. Chem. A*, 2002, **106**, 8963–8970.
254 H. Gappa-Fahlenkamp and R. S. Lewis, *Biomaterials*, 2005, **26**, 3479–3485.
255 T. C. Major, D. O. Brant, C. P. Burney, K. a Amoako, G. M. Annich, M. E. Meyerhoff, H. Handa and R. H. Bartlett, *Biomaterials*, 2011, **32**, 5957–69.
256 S. C. Puiu, Z. Zhou, C. C. White, L. J. Neubauer, Z. Zhang, L. E. Lange, J. A. Mansfield, M. E. Meyerhoff and M. M. Reynolds, *J. Biomed. Mater. Res. B. Appl. Biomater.*, 2009, **91**, 203–212.
257 B. K. Oh and M. E. Meyerhoff, *Biomaterials*, 2004, **25**, 283–293.
258 V. Wonoputri, C. Gunawan, S. Liu, N. Barraud, L. H. Yee, M. Lim and R. Amal, *ACS Appl. Mater. Interfaces*, 2015, **7**, 22148–22156.
259 H. Ren, M. a. Coughlin, T. C. Major, S. Aiello, A. Rojas Pena, R. H. Bartlett and M. E. Meyerhoff, *Anal. Chem.*, 2015, 8067–8072.
260 Y. Wu, Z. Zhou and M. E. Meyerhoff, *J. Biomed. Mater. Res. A*, 2007, **81**, 956–63.
261 A. M. Skrzypchak, N. G. Lafayette, R. H. Bartlett, Z. Zhou, M. C. Frost, M. E. Meyerhoff, M. M. Reynolds and G. M. Annich, *Perfusion*, 2007, **22**, 193–200.
262 C. W. McCarthy, R. J. Guillory, J. Goldman and M. C. Frost, *ACS Appl. Mater. Interfaces*, 2016, **8**, 10128–10135.
263 B. M. Bloom, J. Grundlingh, J. P. Bestwick and T. Harris, *Eur. J. Emerg. Med.*, 2014, **21**, 81–88.
264 D. S. Martin and M. P. W. Grocott, *Crit. Care Med.*, 2013, **41**, 423–432.
265 The Juvenile Diabetes Research Foundation Continuous Glucose Monitoring Study Group, *N. Engl. J. Med.*, 2008, **359**, 1464–1476.

266 K. E. A. Burns and A. McLaren, *Can. Respir. J.*, 2009, **16**, 163–165.
267 S. M. Marxer, M. E. Robbins and M. H. Schoenfisch, *Analyst*, 2005, **130**, 206–212.
268 K. A. Mowery, M. H. Schoenfisch, N. Baliga, J. A. Wahr and M. E. Meyerhoff, *Electroanalysis*, 1999, **11**, 681–686.
269 M. H. Schoenfisch, K. A. Mowery, M. V. Rader, N. Baliga, J. A. Wahr and M. E. Meyerhoff, *Anal. Chem.*, 2000, **72**, 1119–1126.
270 M. C. Frost, S. M. Rudich, H. Zhang, M. A. Maraschio and M. E. Meyerhoff, *Anal. Chem.*, 2002, **74**, 5942–5947.
271 Y. Wu, A. P. Rojas, G. W. Griffith, A. M. Skrzypchak, N. Lafayette, R. H. Bartlett and M. E. Meyerhoff, *Sensors Actuators, B Chem.*, 2007, **121**, 36–46.
272 Q. Yan, T. C. Major, R. H. Bartlett and M. E. Meyerhoff, *Biosens. Bioelectron.*, 2011, **26**, 4276–4282.
273 A. K. Wolf, Y. Qin, T. C. Major and M. E. Meyerhoff, *Chinese Chem. Lett.*, 2015, **26**, 464–468.
274 J. H. Shin, S. M. Marxer and M. H. Schoenfisch, *Anal. Chem.*, 2004, **76**, 4543–4549.
275 M. C. Frost, A. K. Wolf and M. E. Meyerhoff, in *Detection Challenges in Clinical Diagnostics*, 2013, pp. 129–155.
276 R. K. Meruva and M. E. Meyerhoff, *Biosens. Bioelectron.*, 1998, **13**, 201–212.
277 K. P. Dobmeier, G. W. Charville and M. H. Schoenfisch, *Anal. Chem.*, 2006, **78**, 7461–7466.
278 M. C. Frost, M. M. Batchelor, Y. Lee, H. Zhang, Y. Kang, B. Oh, G. S. Wilson, R. Gifford, S. M. Rudich and M. E. Meyerhoff, *Microchem. J.*, 2003, **74**, 277–288.
279 T. C. Major, D. O. Brant, M. M. Reynolds, R. H. Bartlett, M. E. Meyerhoff, H. Handa and G. M. Annich, *Biomaterials*, 2010, **31**, 2736–45.
280 T. C. Major, H. Handa, G. M. Annich and R. H. Bartlett, *J. Biomater. Appl.*, 2014, **29**, 479–501.
281 J. S. Stamler, *Circ. Res.*, 2004, **94**, 414–417.
282 A. Ghaffari, C. C. Miller, B. McMullin and A. Ghahary, *Nitric Oxide*, 2006, **14**, 21–29.
283 D. P. Arora, S. Hossain, Y. Xu and E. M. Boon, *Biochemistry*, 2015, **54**, 3717–3728.
284 Y. Lu, D. Slomberg, B. Sun and M. Schoenfisch, *Small*, 2013, **9**, 2189–98.
285 R. Vumma, C. S. Bang, R. Kruse, K. Johansson and K. Persson, *J. Antibiot. (Tokyo).*, 2015, 1–4.
286 B. B. McMullin, D. R. Chittock, D. L. Roscoe, H. Garcha, L. Wang and C. C. Miller, *Respir. Care*, 2005, **50**, 1451–6.
287 N. Barraud, M. J. Kelso, S. A. Rice and S. Kjelleberg, *Curr. Pharm. Des.*, 2015, **21**, 31–42.
288 N. Barraud, D. J. Hassett, S.-H. Hwang, S. a Rice, S. Kjelleberg and J. S. Webb, *J. Bacteriol.*, 2006, **188**, 7344–53.
289 N. Barraud, M. V. Storey, Z. P. Moore, J. S. Webb, S. A. Rice and S. Kjelleberg, *Microb. Biotechnol.*, 2009, **2**, 370–378.
290 B. J. Nablo and M. H. Schoenfisch, *J. Biomed. Mater. Res. A*, 2003, **67**, 1276–83.
291 E. J. Brisbois, J. Bayliss, J. Wu, T. C. Major, C. Xi, S. C. Wang, R. H. Bartlett, H. Handa and M. E. Meyerhoff, *Acta Biomater.*, 2014, 4136–42.
292 M. R. Schäffer, P. A. Efron, F. J. Thornton, K. Klingel, S. S. Gross and A. Barbul, *J. Immunol.*, 1997, **158**, 2375–81.

293 M. B. Witte and A. Barbul, *Am. J. Surg.*, 2002, **183**, 406–412.
294 H. P. Shi, D. T. Efron, D. Most and A. Barbul, *Surgery*, 2001, **130**, 225–229.
295 G. Richardson and N. Benjamin, *Clin. Sci.*, 2002, **105**, 99–105.
296 G. E. Romanowicz, W. He, M. Nielsen and M. C. Frost, *Redox Biol.*, 2013, **1**, 332–339.
297 T.-K. Nguyen, R. Selvanayagam, K. K. K. Ho, R. Chen, S. K. Kutty, S. A. Rice, N. Kumar, N. Barraud, H. T. T. Duong and C. Boyer, *Chem. Sci.*, 2016, **7**, 1016–1027.

CHAPTER 2

Origin of Long-Term Storage Stability and Nitric Oxide Release Behavior of CarboSil Polymer Doped with *S*-Nitroso-*N*-acetyl-D-penicillamine

Wo, Y.; Li, Z.; Brisbois, E.J.; Colletta, A.; Wu, J.; Major, T.C.; Xi, C.; Bartlett, R.H.; Matzger, A.J.; Meyerhoff, M.E. *ACS Appl. Mater. Interfaces* **2015**; 7 (40): 22218-27 [*]

2.1 Introduction

Blood-contacting biomedical devices ranging from simple catheters to complex extracorporeal life support systems [1] are central for everyday medical care. For example, the use of intravascular catheters, which enables direct vascular access, is crucial for patient diagnosis and treatment. However, despite substantial efforts to better understand blood/surface interactions, complications like pulmonary embolism, stroke and deep vein thrombosis are still associated with the use of indwelling blood-contacting medical devices.[2] In a clinical setting, a systemic anticoagulation agent, such as heparin is often

[*] The principal experiments of this chapter were conducted by Yaqi Wo, with the help of Dr. Zi Li in conducting the solid-state PXRD measurements, Dr. Jianfeng Wu in carrying out the microbiology experiments, and Mr. Terry C. Major in helping perform the animal testing.

given to patients in order to reduce the risk of surface induced thrombus formation.[3] However, heparin treatment should be conducted with extreme care, as an inadvertent overdose of heparin can lead to hemorrhage and thrombocytopenia.[4] Although heparin preferentially binds to antithrombin (ATIII), preventing fibrin formation and hindering the development of the hemostatic plug, platelet activation and reduced platelet count is inevitable when foreign surfaces are in contact with blood for a prolonged period. Moreover, biofilm-associated infections are a significant cause of morbidity and death. *Staphylococcus aureus* (*S. aureus*) is the most prevalent cause of the high incidence of nosocomial bloodstream infections, specifically, biofilm-associated infections on indwelled biomedical devices.[5,6] *S. aureus* biofilms form embedded matrixes which resist both antimicrobials and host defense, thus leading to chronic infections.[7] Therefore, new approaches to reduce the possibilities of these complications and to create truly nonthrombogenic and antimicrobial prosthetic surfaces are still in needed within the medical community.[2]

Nitric oxide (NO), the endothelium-derived relaxing factor, is a gaseous signaling molecule that has been extensively studied over the past two decades for its role in inhibiting platelet activation and adhesion, preventing bacterial growth, reducing smooth cell proliferation and regulating complex biological processes, etc.[8–31] The ubiquity and apparent chemical simplicity of NO have made it a promising therapeutic agent. The production of NO can be accomplished through either enzymatic or nonenzymatic pathways.[11,32] Nitric oxide can be either synthesized enzymatically by nitric oxide synthase (NOS) that catalyze the conversion of L-arginine to L-citrulline, or it can be formed nonenzymatically from the

reduction of nitrite[11] or nitrosothiols. The flux of NO released from a healthy endothelium lining, which constitutes the inner walls of all blood vessels, has been estimated to be between 0.5 and 4.0 x 10^{-10} mol cm^{-2} min^{-1}.[3,10,33,34] Therefore, a potential approach to increase the hemocompatibility of blood-contacting devices is to develop polymeric materials or coatings with sustained NO release at this physiological flux level. Indeed, it has been demonstrated that surfaces capable of releasing NO at these levels can significantly reduce thrombus formation on the surface of implantable chemical sensors,[35] intravascular catheters,[14,15] as well as extracorporeal circuits (ECC).[3,10,33]

Since NO is highly reactive under physiological conditions and has a very short half-life *in vivo*,[10,36] a wide range of NO donors, such as S-nitrosothiols (RSNO) and *N*-diazeniumdiolates (NONOate), have been used to prepare NO releasing polymeric matrixes. Such NO donors have been incorporated into various polymers, including polyethylene glycol,[37] Pluronic F127 hydrogel,[12] polyurethanes,[38] poly(dimethylsiloxane) (PDMS),[9] xerogel[39] and poly(vinyl chloride),[23] and these materials can provide continuous and localized NO delivery to specific sites of interest. *S*-Nitrosoglutathione (GSNO), *S*-nitrosohemoglobin (SNO-Hb) and other endogenous RSNOs are considered NO donors *in vivo*. However, in recent years, researchers have studied synthetic RSNOs, such as *S*-nitroso-*N*-acetylpenicillamine (SNAP).[9,10,18] SNAP is a synthetic tertiary RSNO and it is more stable than most endogenous primary RSNOs due to the steric hindrance of the sulfur atom.[40,41] SNAP, like other RSNOs, can decompose and release NO via thermal decomposition, metal ion catalysis (e.g., Cu^{+}) and photolysis when the light energy

corresponds with the SNAP absorption bands at 340 nm and/or 590 nm (see equation 2.1 for overall reaction).[10,42]

2 SNAP → 2 NO + NAP disulfide [2.1]

Previous work by our group has suggested that SNAP is stable when doped within low water uptake polymers, such as Elast-eon E2As, a siloxane-base polyurethane elastomer.[10] Doping SNAP into the E2As polymer using a solvent evaporation method produced a homogeneous and transparent film, which exhibits relatively high stability during shelf-life studies (82% of the initial SNAP remains after 2 months of dry storage at 37 °C).[10] However, the details of the NO release mechanism from SNAP within the polymer phase and the reason SNAP is so stable in certain polymer materials still remains unclear.

In this study, three different SNAP-doped biomedical grade polymers, including CarboSil 20 80A (a thermoplastic silicone-polycarbonate-urethane with a mix of soft segments of poly(dimethylsiloxane) and polycarbonate as well as a hard segment of methylene diphenyl isocyanate (MDI)), Elast-eon 5-325 (a copolymer of mixed soft segments of poly(dimethylsiloxane) and poly(hexamethylene oxide) as well as the MDI hard segment), and silicone rubber (poly(dimethylsiloxane)) are investigated and further evaluated for their ability to store SNAP for extended periods at 37 °C. CarboSil 20 80A possesses the innate biocompatibility and biostability of conventional silicone elastomers but has the processing capability and toughness of thermoplastic polycarbonate-urethanes. Therefore, the SNAP/CarboSil system is further examined for its NO releasing properties, and leaching of SNAP as well as concomitant NAP and NAP disulfide (NAP dimers) with time from the polymer phase into the PBS soaking buffer. Raman spectroscopy and powder X-

ray diffraction are utilized to conduct in-situ solid-state analysis of SNAP/CarboSil system to better understand the origin of the high stability and long-term NO release properties of this new composite material. Further, catheters fabricated with SNAP-doped CarboSil polymer are evaluated for their efficacy in reducing microbial biofilm formation after 7 d of exposure to flowing media containing *S. aureus*, the common bacteria that causes intravascular infections within a drip-flow bioreactor. Finally, these NO release catheters are also investigated for their potential as antithrombotic devices via 7 h implantation within the veins of rabbits.

2.2 Experimental Section

2.2.1 Materials

N-Acetyl-D-penicillamine (NAP), sodium nitrite, L-cysteine, sodium chloride, potassium chloride, sodium phosphate dibasic, potassium phosphate monobasic, copper (II) chloride, ethylenediaminetetraacetic acid (EDTA), tetrahydrofuran (THF) and *N*,*N*-dimethylacetamide (DMAc) were purchased from Sigma-Aldrich (St. Louis, MO). *N*-Acetyl-D,L-penicillamine disulfide (NAP disulfide) was purchased from Enzo Life Science, Inc. (New York, NY). Methanol, hydrochloric acid, sulfuric acid, Luria Bertani (LB) broth and LB agar were obtained from Fisher Scientific (Hampton, NH). CarboSil 20 80A was obtained from DSM Biomedical Inc. (Berkeley, CA). Elast-eon 5-325 (E5-325) was from AorTech International plc (Scoresby, Victoria, Australia). Dow Corning RTV 3140 silicone rubber (SR) was a product of Ellsworth Adhesives (Germantown, WI). An Agilent ZORBAX rapid resolution high definition (RRHD) Eclipse Plus C18 column (2.1 x 50mm, 1.8 µm particle size) was purchased from Altmann Analytik GmbH & Co.KG

(Munich, Germany). All aqueous solutions were prepared with 18.2 MΩ-deionized water using a Milli-Q filter from EMD Millipore (Billerica, MA). Phosphate buffered saline (PBS), pH 7.4, containing 138 mM NaCl, 2.7 mM KCl, 10 mM sodium phosphate, and 100 μM EDTA was used for all *in vitro* experiments. *S. aureus* ATCC 25923 was obtained from the American Type Culture Collection (ATCC) (Manassas, VA).

2.2.2 SNAP Synthesis

SNAP was synthesized as previously reported.[1,2] In brief, an equimolar ratio of NAP and sodium nitrite was added to a 1:3 mixture of water and methanol containing 2 M H_2SO_4 and 2 M HCl. The reaction vessel was cooled in an ice bath for 5 h and the green SNAP crystals precipitated. The crystals were collected by vacuum filtration, washed by iced DI water and allowed to air dry for 24 h before being storage at -20 °C. The entire synthesis process was performed in the absence of ambient light.

2.2.3 Polymer Film Fabrication

Polymer films containing different wt% SNAP (1-15 wt%) were prepared by solvent evaporation, based on a modified version of the previously reported method.[2] Briefly, 3 different biomedical grade polymers (CarboSil 20 80A, Elast-eon 5-325 and Dow Corning RTV silicone rubber) were dissolved in THF to prepare the casting solution. For the 10 wt% SNAP films, 200 mg of CarboSil and E5-325 were dissolved in 3 mL of THF and SR was dissolved in 1 mL THF. Then, 22.5mg of SNAP was added and dissolved into the polymer solution. After 5 min of stirring, the solutions were cast in Teflon rings (d=2.5 cm) on a Teflon surface, and the films were allowed to dry overnight under ambient

conditions. Small film disks (d=0.7 cm) were cut from the parent films and weighed individually. These disks were then dip coated twice in non-SNAP containing topcoat solution; i.e. the CarboSil topcoat solution (200 mg polymer in 4 mL THF), the E5-325 topcoat solution (200 mg polymer in 4 mL) or the SR topcoat solution (800 mg polymer in 4 mL THF), respectively. The SNAP-doped polymer films that were subjected to Raman spectroscopy and powder X-ray diffraction (PXRD) studies were not coated with any topcoats in order to more easily study the chemical properties of the SNAP-doped CarboSil matrix directly. All films were dried under vacuum for additional 48 h to remove any residual THF before storage at -20 °C. All SNAP-doped films and SNAP containing solutions were protected from ambient light during preparation. The thickness of the SNAP-doped film layer was ca. 250 μm and the thickness of the two topcoat layers was ca. 45 μm, as measured with a Mitutoyo micrometer.

2.2.4 Preparation of SNAP-doped CarboSil Catheters

The SNAP/CarboSil solution was prepared by dissolving SNAP (450 mg) and CarboSil (1800 mg) in THF (18 mL). The CarboSil control solution consisted of CarboSil (2250 mg) in THF (18 mL). The topcoat solution was prepared with SR (1600 mg) in THF (8 mL). For the 20 wt% SNAP-doped CarboSil catheters, layers of SNAP/CarboSil were coated onto the stainless-steel mandrels (McMaster-Carr, IL). as the active coats and dried overnight before removal. Then, the SNAP/CarboSil catheters were then dipcoated in the SR topcoat solution (which coats both the inside and outside surfaces). The topcoats were prepared with two-minute intervals in between. For the CarboSil control catheters, coatings were applied in similar methods using non-SNAP containing CarboSil polymer

solution and the SR top-coating solution. For the dripflow biofilm experiments (*in vitro*), the final catheters had an i.d. of 2.0 mm and an o.d. of 4.0 mm (SR : CB : SR = 7:30:7). However, because of the size limit of rabbit vein, catheters with 1.1 mm i.d. and 2.2 mm o.d. (SR : CB : SR = 3:10:3) were fabricated for the *in vivo* experiments.

2.2.5 Polymer Water Uptake

Control films (without SNAP) made from the 3 different biomedical grade polymers (CarboSil, E5-325 and SR) were cast as described above. The weight of each film was recorded before immersing them in 1 mL DI water for 48 h at 37 °C and after taking them out and wiping the surface dry. The polymer water uptake was calculated and represented as weight percent: wt% = $(W_{after} - W_{before})/(W_{before})$ x 100, where W_{before} and W_{after} are the weights of the same film before and after soaking.[2]

2.2.6 Shelf-life Storage Stability Study

To simulate the harsh environments that could potentially occur during actual storage and shipping, 10 wt% SNAP-doped CarboSil/E5-325/SR films were prepared and stored in amber vials with desiccant at 37 °C. After various time points over an 8-month period, the total NO release of the films were measured by the NOA to determine the wt% of SNAP remaining in the film, as compared to the initial amount of SNAP. Films were cut into smaller pieces and immersed in a clear glass vial containing 50 mM $CuCl_2$ and 10 mM L-Cysteine, which led to the rapid catalytic decomposition of SNAP and the release of NO. Meanwhile, a 100 W halogen floodlight (GE model 17986), a broad-spectrum light source, was placed 20 cm away from the sample vessel and utilized to further enhance the NO

release rate via a photoinitiated decomposition process. The corresponding NO release measured by a Sievers chemiluminescence Nitric Oxide Analyzer (NOA) 280i (Boulder, CO). The total moles of NO released was integrated and used to calculate the amount of SNAP remaining in the films.

2.2.7 Ethylene Oxide (EtO) Sterilization

Ten wt% SNAP-doped CarboSil/E5-325/SR films were prepared and sent to the University of Michigan hospital sterilization facility for ethylene oxide treatment, which is a standardized procedure for many devices used in clinical applications. Briefly, the films went through 1 h of preconditioning and humidification process, followed by 2-3 h of EtO gas exposure, both performed at a high temperature (54 °C) and high humidity environment (40-80 %). After the 1-2 h of EtO gas evacuation (54 °C), the films were subjected to 12 h of air washes (54 °C). The amount of SNAP remaining in the films was determined as described above.

2.2.8 UV-Vis

All UV-Vis spectra were recorded in the wavelength range of 250 nm - 650 nm with a UV-Vis spectrophotometer (Lambda 35, Perkin-Elmer, MA) at room temperature. The molar absorptivity of SNAP in PBS at 340 nm was determined as ε_{SNAP}= 1075 M^{-1} cm^{-1}. The characteristic absorbance at 340 and 590 nm correlated to the $\pi \rightarrow \pi^*$ and $n_N \rightarrow \pi^*$ electronic transitions of the S-NO functional group.[2–6]

2.2.9 Cumulative SNAP, NAP, and NAP disulfide leaching from SNAP-doped CarboSil polymer films immersed in PBS

Ten wt% SNAP-doped CarboSil films with no topcoat, 2 layers of CarboSil topcoats, and 2 layers of SR topcoats, respectively, were fabricated (see the Supporting Information) and placed in individual vials containing 1 mL 10 mM PBS, pH 7.4, with 100 μM EDTA to minimize trace metal catalyzed decomposition of SNAP. All films were incubated in the dark at 37 °C at all times. After various time points, aliquots (15 μL) of the individual soaking solutions were analyzed by liquid chromatography-tandem mass spectrometry (6520 Accurate-Mass Q-TOF LC/MS, Agilent Technologies, CA) for quantification of SNAP, NAP, and NAP disulfide present in the soaking solution. The studies were conducted using a reversed-phase column (ZORBAX RRHD Eclipse Plus C18, 1.8 μm, 2.1 x 50 mm). The gradient was obtained with eluent A (water with 0.1% formic acid) and eluent B (95% acetonitrile, 0.1% formic acid). After sample injection (15 μL), a linear change of eluent mixtures from 100% A to 0% A over 10 min was carried out with a flow rate of 0.4 mL/min. The mass spectrometer used electrospray ionization in the negative ion mode, and the detected species were $[M-H]^-$. All films were placed in fresh PBS buffer immediately after each measurement while the previous soaking solutions were analyzed. The results were compared between films with different topcoats. The amount of total SNAP ($[SNAP]_{total}$) that had diffused into the PBS after time *t* was calculated as follows (equation 2.2):

$$[SNAP]_{total} = [SNAP]_t + [NAP]_t + 2 \times [NAP\ disulfide]_t \qquad [2.2]$$

The amount of total SNAP leached into the buffer was compared with the initial amount SNAP in the polymer film.

2.2.10 Cumulative NO release from SNAP-doped CarboSil films/catheters

Nitric oxide release from the polymer films or catheters was measured using a Sievers chemiluminescence Nitric Oxide Analyzer (NOA) 280i (Boulder, CO). For example, a 10 wt% SNAP-doped CarboSil film with 2 SR topcoats was placed in the sample vial containing 4 mL of 10 mM PBS, pH 7.4, with 100 μM EDTA at 37 °C to mimic the physiological conditions. Nitric oxide was continuously generated and immediately purged and swept into the chemiluminescence detection chamber by N_2 sweeping gas and bubbler. All films were placed in fresh PBS buffer during NO release measurements and incubated at 37 °C in the absence of ambient light after each measurement. Cumulative NO release ($[NO]_{total}$) of a given SNAP-doped CarboSil film after various time points was determined by the sum of the NO release amount in fresh PBS measured by NOA ($[NO]_{NOA}$) and total amount of SNAP ($[SNAP]_{total}$) leached into previous soaking solutions (equation 2.3):

$$[NO]_{total} = [NO]_{NOA} + [SNAP]_{total} \quad [2.3]$$

Cumulative NO release ($[NO]_{total}$) was also compared with the initial amount SNAP in the polymer film.

2.2.11 Polarized Optical Microscopy

Five wt% SNAP-doped CarboSil films and a blank CarboSil film, both without topcoats, were prepared as described above. Optical images were captured by a Leica DMLP

polarization microscope equipped with an N Plan 20× objective under crossed polarizers in combination with a quarter-wave plate, and were then taken with a SPOT Flex Mosaic 15.2 camera using SPOT 5.2 Software from Diagnostic Instruments, Inc.

2.2.12 Raman spectroscopy characterization

Raman spectra were collected by using a Renishaw inVia Raman microscope equipped with a Leica microscope, a RenCam CCD detector and a 633 nm laser employing an 1800 lines/nm grating and a 50 μm slit. Spectra were obtained using the WiRE 3.4 software package. Calibration was performed using a silicon standard in static mode. Full spectra of blank CarboSil (without SNAP), pure SNAP crystals and 15 wt% SNAP-doped CarboSil were collected through an Olympus SLMPlan 20× objective in extended scan mode in the range of 100-4000 cm^{-1} and further analyzed by ACD/SpecManager Version 12.01 software from Advanced Chemistry Development, Inc. For Raman mapping characterization, SNAP-doped CarboSil samples were cut into thin strips and laid down on the stage with the cross section facing upward. Raman cross-section mapping data were obtained by using an Olympus SLMPlan 100× objective in combination with an automatic Renishaw MS20 encoded stage in static scan mode. The exposure time was 40 s with a static scan centered at 720 cm^{-1}. The mapping data were analyzed using the Wire 3.4 software package component direct classical least-squares (DCLS) analysis routines with the full spectra of blank CarboSil and pure SNAP crystals as references.

Raman mapping characterization in the low wavenumber regions, where SNAP and polymer peaks can be distinguished readily, was conducted on a randomly selected 32 μm

× 24 μm rectangular regions of the SNAP-doped CarboSil film cross section, with 1 μm steps in both the x and y dimensions to create a fine grid. Raman spectra of all steps were compared with the orthorhombic SNAP spectrum using direct classical least squares (DCLS) analysis.[7]

2.2.13 Powder X-ray diffraction (PXRD) measurements

Powder X-ray diffraction (PXRD) patterns of SNAP-doped (1-15 wt%) and blank CarboSil films (without topcoats) were collected at room temperature using a Rigaku R-Axis Spider diffractometer with an image plate detector and graphite monochromated Cu-Kα radiation (λ = 1.54187 Å) at 40 kV and 44 mA. Synthesized SNAP crystals were finely ground to eliminate preferred orientation, whereas blank CarboSil and SNAP-doped CarboSil samples were cut into cubes with dimensions of approximately 250 μm. All samples were mounted on a CryoLoop™ using heavy mineral oil, and images were collected for 15 min with a 0.3 mm collimator. The ω-axis was oscillated between 120° and 180° at 1°/secs, the ϕ-axis was rotated at 10°/secs, and the χ-axis was fixed at 45°. The obtained images were integrated from 2.5 to 70° with a 0.1° step size in AreaMax 2.0 software from Rigaku. All powder patterns were processed using Jade 9 XRD Pattern Processing, Identification & Quantification analysis software from Materials Data, Inc. The simulated powder patterns of monoclinic and orthorhombic SNAP crystals were calculated in Mercury 3.3 from the CCDC and were compared with the experimental SNAP powder pattern in Jade 9. Linear least squares regression for quantitation of peak area ratios versus doped-SNAP weight percentage was performed in MATLAB. PXRD measurements of 5 wt% and 15

wt% SNAP/CarboSil film (both freshly made and 10 d old under ambient environment at RT) were taken and compared.

2.2.14 In vitro characterization of SNAP-doped CarboSil catheters against microbial biofilm

A drip-flow biofilm reactor system (Biosurface Technologies Corp., Bozeman, MT),[15] which mimics the catheter environment and bacteria growth condition (at air-liquid interface) *in vivo* [8,9], was used to test the antibiofilm properties of SNAP/CarboSil catheters against biofilm formed by *Staphylococcus aureus* ATCC 25923. The catheters were secured in the center of the bottom surface. The biofilm chambers were first inoculated with 10 mL of bacteria culture (diluted with overnight culture, ~1 x 10^6 CFU/mL) for 1 h to allow bacterial cell adhere on the catheter surfaces. Then the biofilm chambers were supplemented with continuous sterile nutrient medium (10% Luria Broth) at the flow rate of 100 mL/h (controlled by a peristaltic pump) for 7 days at 37 °C. Finally, the catheters were aseptically removed and each catheter was cut into two 1 cm pieces, which was used for plate counting and imaging, respectively. For plate counting, the catheter segment was homogenized (OMNI TH, Omni International, kenesaw, GA) for 30 s in 2 mL of 10 mM sterile PBS (pH 7.4) in order to disintegrate the biofilm to single cell suspension, which was later diluted by 10-fold each time and plated onto LB agar plates. For imaging, the catheter segment was stained with fluorescent dyes by using Live/Dead BacLight Bacterial Vaiability kit (Invitrogen, Carlsbad, CA) for 20 min in the dark, exactly per the kit's instructions. Fluorescent images were acquired with an inverted fluorescence microscope (Olympus IX71, Center Valley, PA) equipped with Fluorescence Illumination System (X-

Cite 120, EXFO) and filters for SYTO-9 (excitation = 488 nm/emission = 520 nm) and Propidium Iodide (excitation = 535 nm/emission = 617 nm). Images were obtained using an oil immersed 60× objective lens, in which red indicates dead bacteria while green indicates live ones.

2.2.15 In vivo characterization of SNAP-doped CarboSil catheters in the veins of rabbits

All animal handling and surgical procedures employed in this research were approved by the University Committee on the Use and Care of Animals in accordance with university and federal regulations. A total of 3 New Zealand white rabbits (Covance, Battle Creek, MI) were used in this study. All rabbits (2.5-3.5 kg) were initially anesthetized with intramuscular injections of 5 mg/kg xylazine injectable (AnaSed® Lloyd Laboratories Shenandoah, Iowa) and 30 mg/kg ketamine hydrochloride (Hospira, Inc. Lake Forest, IL). Maintenance anesthesia was administered via isoflurane gas inhalation at rate of 1.5-3% by mechanical ventilation via a tracheotomy and using an A.D.S 2000 Ventilator (Engler Engineering Corp. Hialeah, FL). Peek inspiratory pressure was set to 15 cm of H_2O) and the ventilator flow rate was 8 L/min. To facilitate the maintenance of blood pressure stability, IV fluids of Lactated Ringer's were given at a rate of 10 mL/kg/h. In order to monitor blood pressure and to collect intermittent blood samples for analysis during the experiment, the rabbit's right carotid artery was cannulated using a 16-gauge IV angiocatheter (Jelco®, Johnson & Johnson, Cincinnati, OH). The blood pressure and derived heart rate were monitored by a Series 7000 monitor (Marquette Electronics Milwaukee, WI) while the animal body temperature was monitored with a rectal probe and maintained at 40 °C using a water-jacketed heating blanket. Sample blood gas analysis

(arterial blood pH, PCO_2, PO_2, total hemoglobin and methemoglobin) was conducted using an ABL 825 blood-gas analyzer and an OSM3 Hemoximeter (Radiometer Copenhagen, DK). Prior to the placement of catheters, the rabbit left and right external jugular veins were isolated. Five cm lengths of the catheters (one SNAP and one control) were inserted into the veins. The animals were not treated with anticoagulant systemically during the experiments.

During the experiment, the mean arterial pressure (MAP) of the rabbit was maintained at 38 ± 2 mmHg for 7 h by continuous IV fluid maintenance. The heart rate average was 228 ± 4 beats/min and no significant change was noted for the duration of experiments. The blood gas was measured once every hour and the results were all within the normal ranges.

After 7 h of catheter implantation, all animals were first given (400 U/kg) sodium heparin (APP Pharmaceuticals, LLC Schaumburg, IL) systemically to prevent thrombosis during necropsy and were then euthanized with a dose of Fatal Plus (130 mg/kg sodium pentobarbital) (Vortech Pharmaceuticals, Dearborn, MI). The jugular veins were clamped and the catheters were carefully removed from the vein, leaving the thrombus intact on the catheter surface. After rinsing the catheter with saline, any residual thrombus was photographed and quantitated using Image J imaging software provided by the National Institutes of Health (Bethesda, MD).

Rabbit whole blood samples were collected in non-anticoagulated 1 cc syringes for activated clotting times (ACT) analysis at the beginning of the experiments. The whole

blood samples were also collected by 1 cc heparinized syringes (40 U/mL of sodium heparin) for blood gas analysis every hour for 7 h.

2.2.16 Statistical analysis

All experiments were conducted in triplicate. Data are all expressed as mean ± SEM (standard error of the mean). Comparison of means using student's t-test was utilized to analyze the statistical differences between SNAP-doped catheters and control catheters. Values of $p < 0.05$ were considered statistically significant for all tests.

2.3 Results and Discussion

2.3.1 Preliminary shelf-life study of various SNAP-doped biomedical grade polymer films

Three biomedical grade polymers (CarboSil, E5-325, and SR) with low water uptake (see Table 2.1) were chosen as matrixes for incorporating SNAP. Ten wt% SNAP-doped polymer films were prepared to evaluate their shelf-life during dry storage. To simulate the actual storage and/or shipping environments, the SNAP-doped SR, E5-325, and CarboSil films were stored in the dark with desiccant at 37 °C over a period of 8 months. The amount of SNAP remaining in different polymer films was determined at various time points to find the best polymer matrix for maintaining SNAP functionality during storage. The SNAP remaining in the film was decomposed through both the Cu (I) mediated catalytic decomposition pathway and the photoinitiated decomposition pathway by the broad-spectrum 100 W halogen light source. The corresponding NO release measured by the NOA was integrated to determine the total amount of SNAP present in the polymer. The results indicate that SNAP is the most stable in the CarboSil polymer matrix, with 88.5

± 4.3% of the initial SNAP remaining after 8 months, compared to 86.8 ± 4.9% in SR and 68.3 ± 3.2% in E5-325 (see Figure. 2.1). Though the conventional silicone elastomer also exhibits equivalent stability, its lack of processability together with the prolonged polymer curing process (for cross-linking to occur) makes CarboSil a more promising material in terms of NO release properties.

Table 2.1. The water uptakes of 3 biomedical grade polymer films. Blank polymer films were soaked in DI water for 48 hours at 37 °C. Water uptake was calculated in the percentage representation, wt % = $(W_{after} - W_{before})/(W_{before})$ x 100, where W_{before} and W_{after} are the weights of the same film before and after soaking. Data are mean ± SEM (n=3).

Polymer	Water Uptake [wt%]
Silicone Rubber	1.5 ± 0.5
Elast-eon 5-325	0.8 ± 0.2
CarboSil 20 80A	0.7 ± 0.2

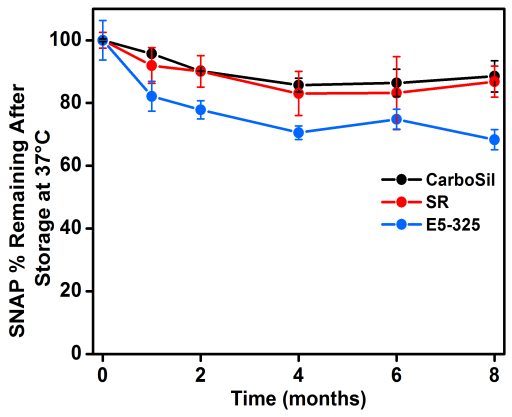

Figure 2.1. Shelf-life study of 10 wt% SNAP-doped CarboSil, SR, and E5-325 films stored dry (with desiccant) in the dark at 37 °C. The SNAP remaining in the films after various time points is determined and compared with the initial level. Data are mean ± SEM (n=3).

2.3.2 Ethylene oxide (EtO) sterilization of various SNAP-doped biomedical grade polymer films

Ethylene oxide sterilization is a routine procedure for sterilizing clinical appliances inside hospitals, during which the devices are subjected to high temperature and high humidity level.[43,44] Ten wt% of SNAP-doped SR, E5-325 and CarboSil were sterilized in order to evaluate the SNAP stability in these materials when undergoing ETO sterilization. The results parallel the shelf-life studies, indicating that SNAP is most stable within the CarboSil polymer matrix. Indeed, the CarboSil films maintain 91.8 ± 3.2% of the initial SNAP after ETO sterilization, compared to 82.7 ± 3.8% for the E5-325 films and 78.7 ± 3.1% for the SR films (see Table 2.2). These data suggest that the SNAP-doped CarboSil polymer matrix is the most attractive of all formulations as a NO release material for fundamental studies and eventually for potential biomedical applications.

Table 2.2. Stability of 10 wt% SNAP-doped CarboSil, SR and E5-325 films after ethylene oxide sterilization process. The SNAP remaining in the films after the sterilization were determined and compared with the initial level. Data are mean ± SEM (n=3).

10 wt% SNAP/CarboSil films	% SNAP remaining after EtO sterilization
Silicone Rubber	78.7 ± 3.1
Elast-eon 5-325	82.7 ± 3.8
CarboSil 20 80A	91.8 ± 3.2

2.3.3 Cumulative leaching and NO release of SNAP-doped CarboSil films

Although SNAP is reported to be slightly hydrophobic and should preferentially stay within the polymer phase,[45] some SNAP is likely to diffuse from the polymer to the soaking solution. Thus, *in vitro* studies were conducted with SNAP-doped CarboSil films

to examine the effects of different topcoat polymers by analyzing the amount of total SNAP leached into the PBS during soaking. Ten wt% SNAP-doped CarboSil films with no topcoat, 2 layers of CarboSil topcoat, and 2 layers of SR topcoat were soaked in 1 mL of PBS at 37 °C. Although SNAP can absorb light in the UV range (see Figure 2.2),[37,42] it is not practical to quantify its decomposition species (e.g., NAP and NAP disulfide) by UV-Vis.[37,46]

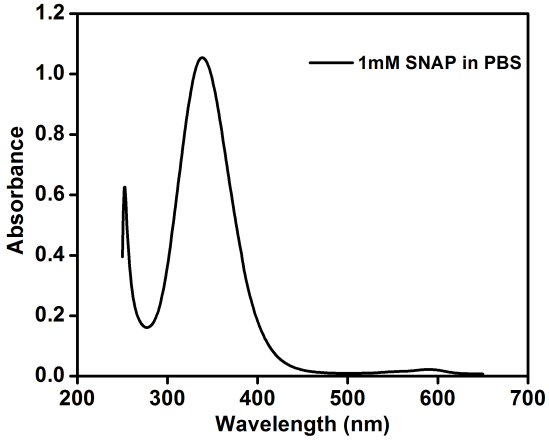

Figure 2.2. The UV-Vis spectrum of 1mM SNAP dissolved in PBS buffer. The molar absorptivity of SNAP in PBS at 340 nm is εSNAP= 1075 M^{-1} cm^{-1}.

Therefore, the concentrations of SNAP, NAP and NAP disulfide in PBS solution buffers at each time point were monitored by LC-MS. Standard solutions of NAP, NAP disulfide and SNAP (1, 5, 10, 20, 40 and 60 μM) were prepared and analyzed for the individual elution times and concentration-peak area calibration curves (see Figure 2.3).

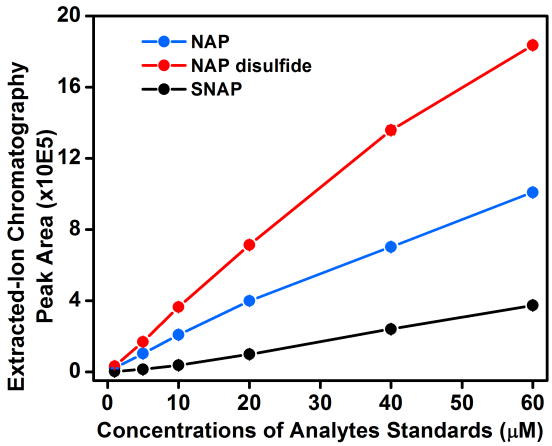

Figure 2.3. The calibration curves of peak area vs analytes concentration. 1, 5, 10, 20, 40 and 60 μM standard solutions of SNAP, NAP and NAP disulfide were prepared using Miili-Q Millipore purified water (18.2 MΩ) and analyzed by LC-MS. Data are mean ± SEM (n=3).

The elution times of NAP, NAP disulfide and SNAP from the C18 column are determined to be 3.45, 4.25, and 4.5 min, respectively, which correspond with the increasing log P values of three molecules (-0.07, 0.01, and 0.40, respectively). The log P values were calculated using Marvin Sketch software, where a higher value means greater lipophilicity and hence a longer retention time. Ten wt% SNAP films initially contain ca. 450 nmol of SNAP per mg of polymer. When SNAP films are in contact with the soaking solutions, water starts to diffuse into the polymer outer surface; SNAP begins to leach into the soaking buffer; and at the same time, SNAP (both from the PBS buffer and within the polymer) starts to release NO and form the NAP disulfide byproduct. The detection of NAP thiolate ion in the soaking solutions can be from two possible sources. It is known that, for solid RSNO samples, contamination of thiols is likely and such thiols can react with the trace amount of Cu (II) in solution and form Cu (I) (equation. 2.4). Then, Cu (I), acting as a catalyst, can react with RSNOs (e.g., SNAP), and form RS^- (e.g., NAP thiolate) and Cu (II)

(equationo 2.5).[47,48] Alternatively, it is conceivable that small amounts of thiolate can be generated by hydrolysis of RSNOs (equation 2.6).[48]

$$Cu^{2+} + RS^{-} \rightarrow Cu^{+} + \tfrac{1}{2}\ RSSR \qquad [2.4]$$

$$Cu^{+} + RSNO \rightarrow Cu^{2+} + RS^{-} + NO \qquad [2.5]$$

$$RSNO + 2\ OH^{-} \rightarrow RS^{-} + NO_2^{-} + H_2O \qquad [2.6]$$

As shown in Figure 2.4A, 47% of the initial SNAP (210 nmol/mg polymer) diffuses out of the CarboSil films without any topcoat over the period of 22 d, compared to 35% for the films with CarboSil topcoat and only 19% for the films with SR topcoat. For each type of film, the rate of SNAP leaching is the fastest in the first few hours, and then significantly lower amounts of SNAP continue to diffuse into the PBS over sequential days. The SR topcoat, which is a cross-linked polymer, can reduce the amount of SNAP diffusion into the soaking solution better than the non-cross-linked CarboSil topcoat. Similar leaching patterns are observed for the NAP and NAP disulfide species from the films with different topcoats (Figure 2.4B and 2.4C). NAP is a widely used chelating and detoxifying agent for treatment of heavy metal poisoning (e.g., mercury, cadmium, and arsenic, etc.).[49–54] Indeed, it hastens the excretion of poisons out of human body without inducing toxic effects, and it represents a protective measure against free radical induced organ injury.[53] Therefore, it is reasonable to believe that small amounts NAP and/or the dimer of NAP (NAP disulfide) emitted from the polymer into the contacting buffer or blood would not likely cause any toxic response in clinical applications.[10]

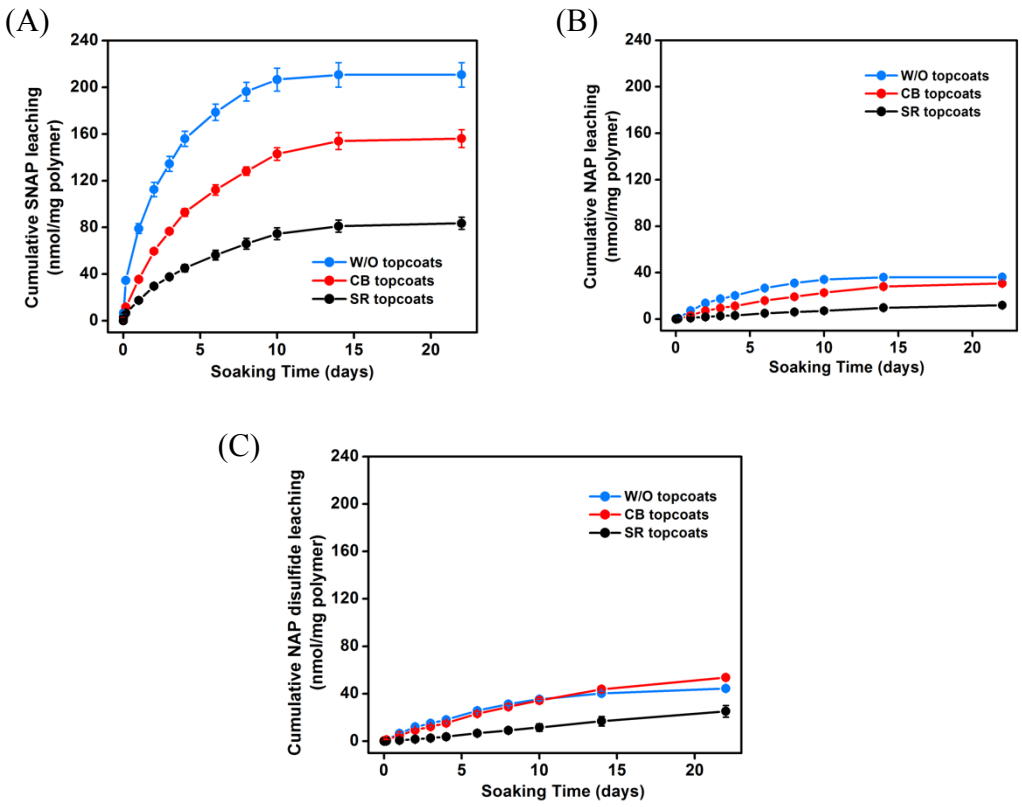

Figure 2.4. Cumulative leaching of SNAP (A), NAP (B), and NAP disulfide (C) into 1 mL of PBS (soaking buffer) from 10 wt% SNAP-doped CarboSil films with different coating conditions: without topcoats, CarboSil topcoats and SR topcoats, over the period of 22 days, at 37 °C in the dark. Data are mean ± SEM (n=3).

The 10 wt% SNAP-doped CarboSil film with SR topcoats releases NO above 0.5 x 10^{-10} mol cm^{-2} min^{-1}, the lower end of endothelial NO flux levels, for more than 3 weeks under physiological conditions (see Figure 2.5A). A large burst of NO release was observed by the NOA (via chemiluminescence) on day 0 that correlates with the rapid SNAP leaching into the PBS buffer in the first few hours. The cumulative amount of SNAP that releases NO was calculated based on the NOA measurements and compared to the initial amount doped within the film. The total NO release from polymer films can originate from the SNAP decomposing and releasing NO inside the polymer phase as well as from SNAP

molecules that diffuse out of the polymer into the PBS buffer. Assuming that the NAP and NAP disulfide detected in the buffer are reaction products of the original SNAP leached from the polymer, the total amount of SNAP that leaches out after time *t* should be $[SNAP]_{total} = [SNAP]_t + [NAP]_t + 2 \times [NAP\ disulfide]_t$. Since the films were placed into fresh PBS during NOA measurements, the NO release detected by the NOA can be only attributed to the SNAP decomposing and releasing NO from inside the polymer phase ($[NO]_{NOA}$) (assuming the amount of SNAP leaching during the measurement was negligible). Therefore, the total NO release ($[NO]_{total}$) from the polymer film is $[NO]_{total} = [NO]_{NOA} + [SNAP]_{total}$, which was compared with the initial SNAP in the CarboSil film. As shown in Figure 2.5B, the total moles of SNAP ($[SNAP]_{total}$) leached out over 22 d, the time period of the leaching experiment, is approximately 38.5% of the total NO released ($[NO]_{total}$) and, therefore, more than 60% of the total NO is, in fact, released from the polymer phase. This suggests that the leaching process is much slower than the rate of NO release from the polymers, so it is likely that, after the first day, NO release from within the polymer (primarily in the water rich regions near the outer surfaces of the polymers) is the primary source of NO emission. The ability of the SNAP/CarboSil polymer system to deliver localized NO continuously and sufficiently to sites of interest makes it a very promising material for biomedical applications.

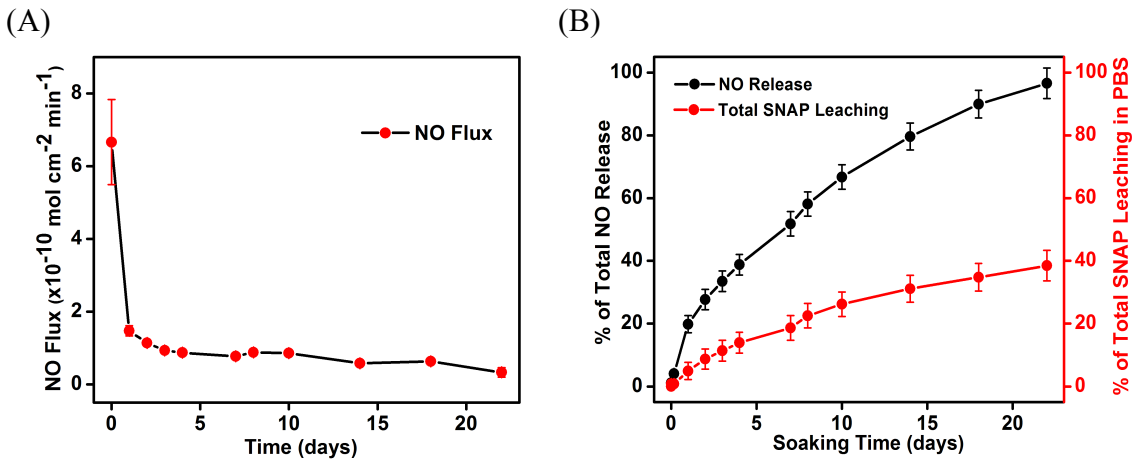

Figure 2.5. (A) NO flux from 10 wt% SNAP-doped CarboSil films with SR topcoats in PBS at 37 °C for 22 days. Data are mean ± SEM (n=3). (B) Comparison of total NO release and total SNAP leaching (sum of SNAP, NAP, and disulfide species) from the 10 wt% SNAP-doped CarboSil films with SR coatings soaking in PBS at 37 °C. The cumulative/total NO release comes from the thermal decomposition of the SNAP in polymer phase as well as the SNAP leached into the buffer. The SNAP leached in PBS accounts for 38.5 % of the total NO release. Data are mean ± SEM (n=3).

2.3.4 Solid-state analysis of SNAP-doped CarboSil polymer systems

To better understand the fundamental reasons for which SNAP is so stable in CarboSil and is able to release NO for 3 weeks, a series of solid phase characterization has been conducted. Films of 5 wt% SNAP-doped CarboSil and blank CarboSil were viewed under a polarized optical microscope. Distinguished crystalline patterns were found in the SNAP/CarboSil film in comparison with the blank film (see Figure 2.6).

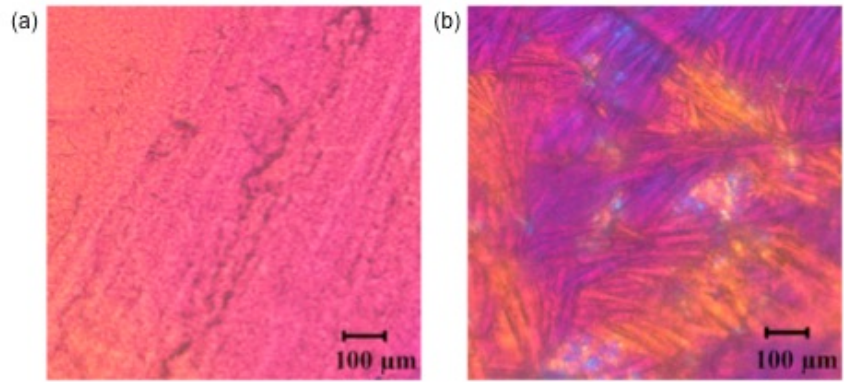

Figure 2.6. Optical image of (a) blank CarboSil and (b) 5 wt% SNAP-doped CarboSil film surface taken under crossed polarizers in combination with a quarter-wave plate. The 5 wt% film clearly shows patterns which suggest the presence of crystalline structures. The scale bars are both 100 µm.

Therefore, it is hypothesized that SNAP crystallized in the polymer matrix during the solvent evaporation process, as opposed to all dissolving in the polymer and forming a homogeneous matrix as previously suggested.[10] We further compared the Raman spectra of SNAP crystals, blank CarboSil film and 15 wt% SNAP/CarboSil film. The spectrum of 15 wt% SNAP/CarboSil (Figure 2.7.) showed characteristic peaks of both CarboSil and crystalline SNAP that further substantiates the existence of crystalline SNAP within the polymer film.

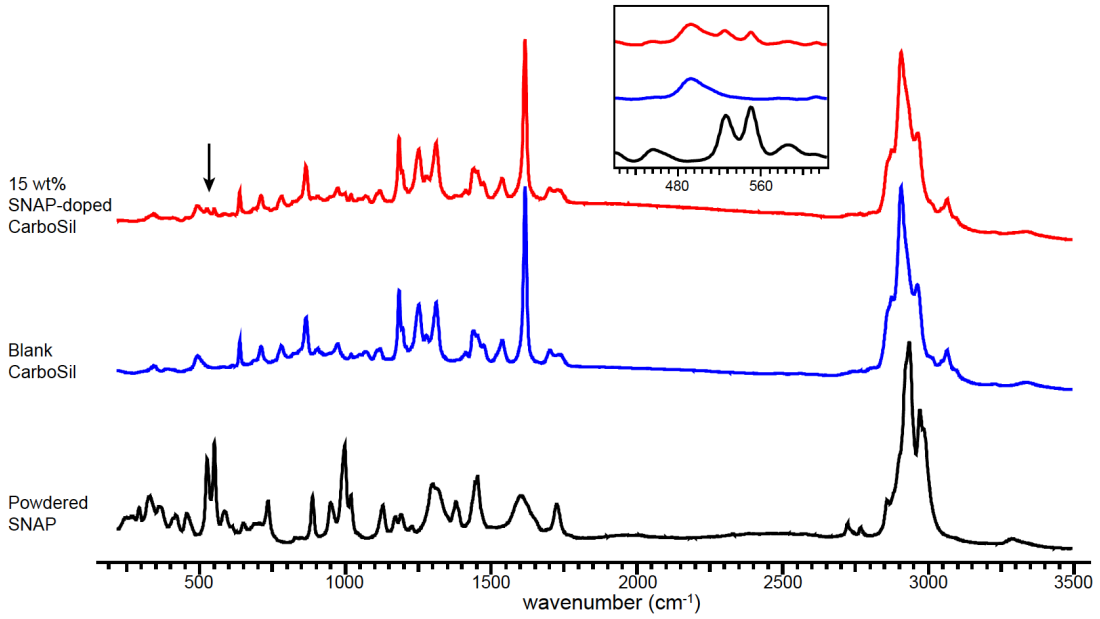

Figure 2.7. Raman spectra comparison of SNAP powder (black), blank CarboSil (blue) and 15 wt% SNAP-doped CarboSil (red). The existence of SNAP crystals in SNAP-doped CarboSil is verified by the characteristic peaks of crystalline SNAP between 500-600 cm^{-1} (see inset).

In order to identify the form of crystalline SNAP detected in the Raman spectroscopy characterization, powder X-ray diffraction (PXRD) analysis of the synthesized SNAP crystals was conducted, and the results agree with the patterns of the orthorhombic SNAP reported in the literature (see Figure 2.8).

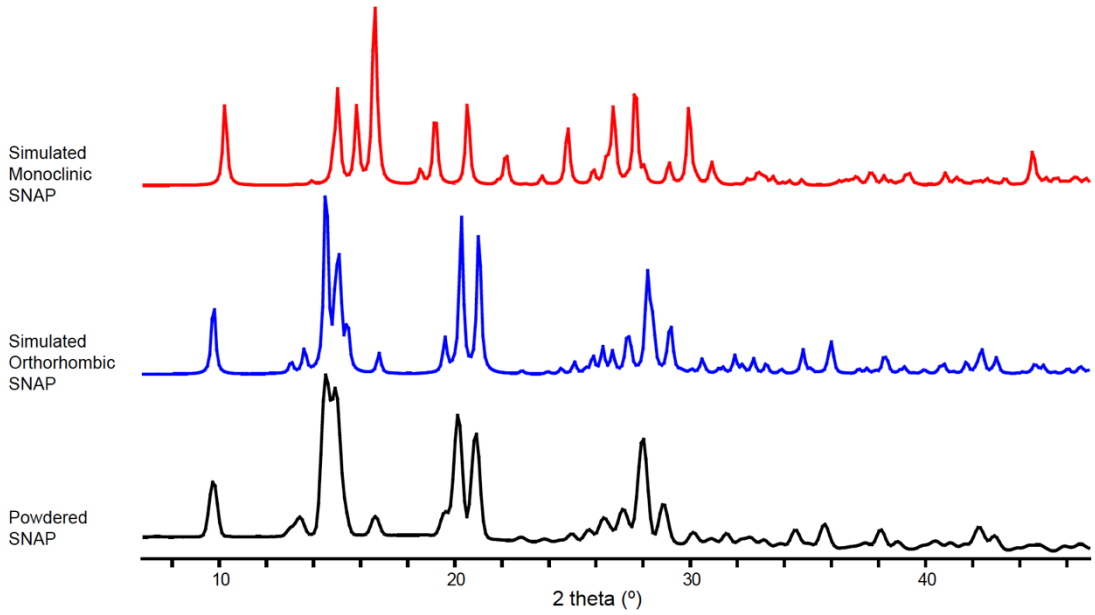

Figure 2.8. The PXRD patterns comparison for grounded SNAP powder, simulated orthorhombic SNAP powder[10] and simulated monoclinic[11,12] SNAP powder suggests that the SNAP crystal synthesized is orthorhombic. The consistent difference in peak positions of powdered SNAP and simulated orthorhombic SNAP patterns (2θ values of powdered SNAP peaks are always slightly smaller than those of the simulated pattern) can be attributed to the difference in operating temperature. Powdered SNAP samples were tested at room temperature while the simulated patterns were based on single crystal XRD patterns taken at low temperature (-100 °F).

It has been suggested that, in orthorhombic SNAP, one SNAP molecule can form 4 intermolecular hydrogen bonds with 4 surrounding SNAP molecules (Figure 2.9).[55]

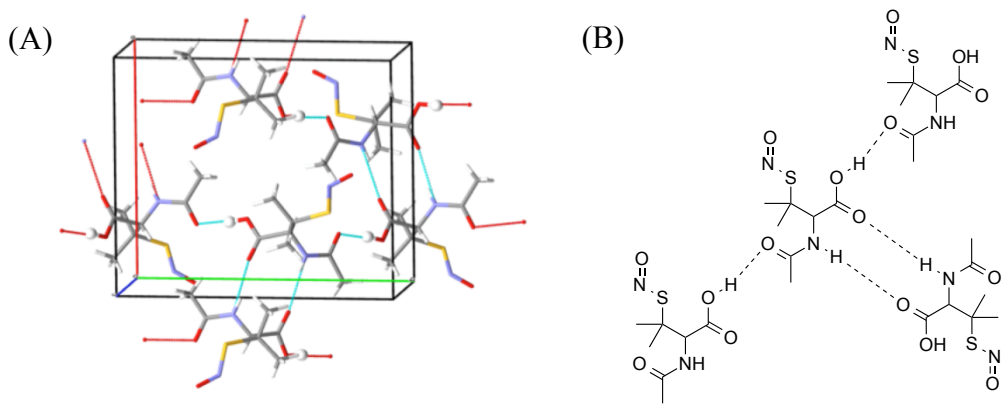

Figure 2.9. (A) The orthorhombic SNAP crystal structure shown in 3D representation, suggesting that one SNAP molecule can form 4 intermolecular hydrogen bonds with 4 surrounding SNAP. (B) The elaboration of the number and position of the hydrogen bonds of one SNAP molecule in 2D schematic.

The PXRD results of SNAP-doped CarboSil films (1-15 wt%) indicate that the characteristic film diffraction patterns are convolutions of blank Carbosil and the crystalline SNAP powder patterns (see Figure 2.10).

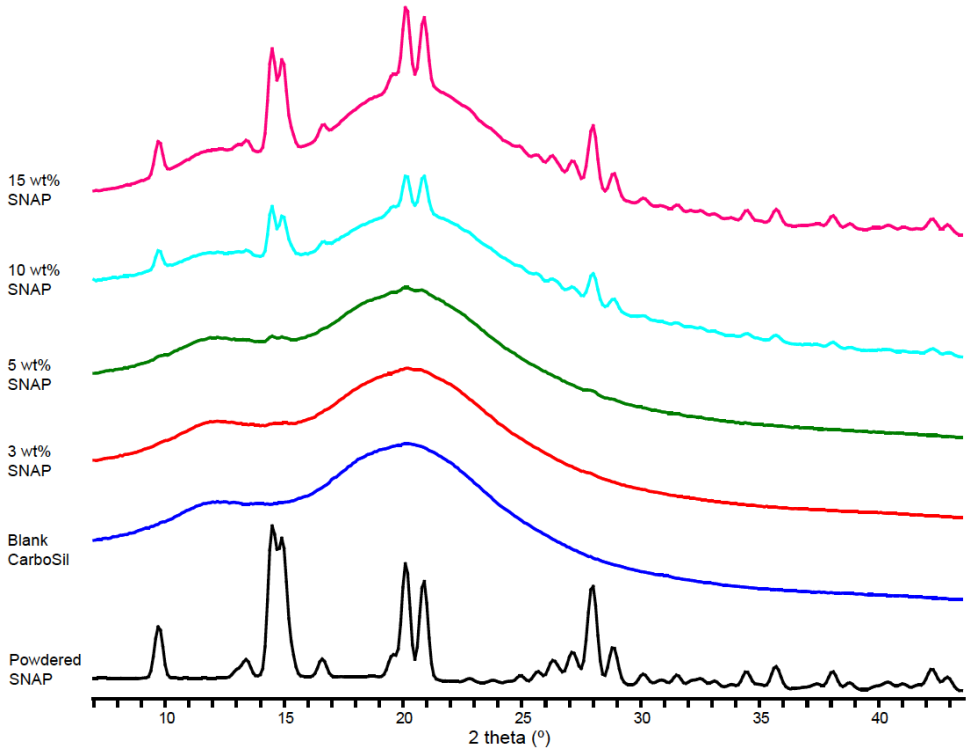

Figure 2.10. Representative PXRD patterns of SNAP powder, blank CarboSil and SNAP-doped CarboSil film samples of different weight percentages (1-15 wt%) were tested. Sample peaks were able to be clearly distinguished when the wt% SNAP doping is no less than 4 wt%.

The results also suggest that as the amount of doped SNAP increases (for films with greater than 4 wt% SNAP), the intensity of orthorhombic SNAP peaks in the obtained PXRD pattern is enhanced, indicating a greater percentage of crystalline SNAP within the polymer films. However, SNAP peaks could barely be detected in PXRD patterns for samples with < 4 wt% doped SNAP, indicating an apparent threshold for formation of the crystalline form of SNAP within CarboSil. Since all SNAP-doped CarboSil films (including those with <4 wt%) have a light green color, it is speculated that SNAP partially dissolves in the polymer, forming a polymer solution, and any excess SNAP beyond the polymer solubility limit crystallizes in the orthorhombic form during the THF evaporation and embeds in the

polymer. This explanation is in agreement with the Raman spectroscopy and PXRD results that orthorhombic SNAP crystals are detected only when the SNAP concentration exceeds the solubility of SNAP in the CarboSil polymer. To calculate the SNAP solubility in the CarboSil polymer, a linear least-squares regression was conducted using three main PXRD peaks. Based on the following assumptions that (1) crystalline SNAP is uniformly distributed in CarboSil and that (2) the preferred orientation of SNAP crystals in CarboSil could be eliminated by cutting samples into cubes and rotating the samples during PXRD characterization, the ratio of peak areas (at a chosen 2θ angle) of a specific SNAP PXRD peak over the total area of the obtained pattern would be proportional to the weight percentage of crystalline SNAP in the sample. In fact, by using the area ratio as a quantitative representation, all the other factors that could influence the peak area (e.g., the volume of the sample irradiated by the X-ray source, the exposure time of sample under the X-ray, etc.) can be eliminated. Here, we set the doped SNAP weight percentage as x and the ratio of the k^{th} orthorhombic SNAP peak area over the SNAP-doped CarboSil pattern total area as y_k, and then y_k can be calculated as (equation 2.7):

$$y_k = \frac{k^{th}\ \text{SNAP peak area}}{\text{total SNAP peaks area+CarboSil pattern area}} = \frac{a_k(x-x_0)}{a(x-x_o)+b(1-x)} \quad [2.7]$$

For a PXRD pattern of a sample with a unit volume and taken with a unit exposure time, a_k, a and b correspond to the area of the k^{th} peak in the orthorhombic SNAP pattern, the total area of all orthorhombic SNAP peaks, and the total area of blank CarboSil pattern, respectively. The term x_o is the SNAP solubility in SNAP-CarboSil solid solution system in the percentage representation. As a result, for any SNAP-doped CarboSil sample, $a_k(x - x_0)$ represents the area of the k^{th} orthorhombic SNAP peak in the pattern, $a(x - x_o)$ represents the area of all signals from orthorhombic SNAP, and $b(1 - x)$ represents

the area of all signals from CarboSil in this sample. Since y_k is a ratio of areas, which is independent of sample volume and exposure time, etc., the only factor that influences y_k is the SNAP weight percentage x in the prepared CarboSil films. By substituting various x and y_k at chosen 2θ angles (three main SNAP peaks, 2θ = 9.5, 14.5, 14.9), a_k, a, b and x_o can be determined. The a values calculated using three different SNAP peaks were 0.099, 0.082 and 0.102, respectively, and the b values were 12.996, 12.934 and 12.985, respectively. As both values are within the error of tolerance, it suggests that the derived equation and the fitting model are successful quantitative representations of the doped polymer system. The calculated solubility is 3.6, 3.5 and 3.9 wt%, respectively (see Figure 2.11), indicating that the solubility of SNAP in CarboSil was ca. 3.4-4.0 wt%.

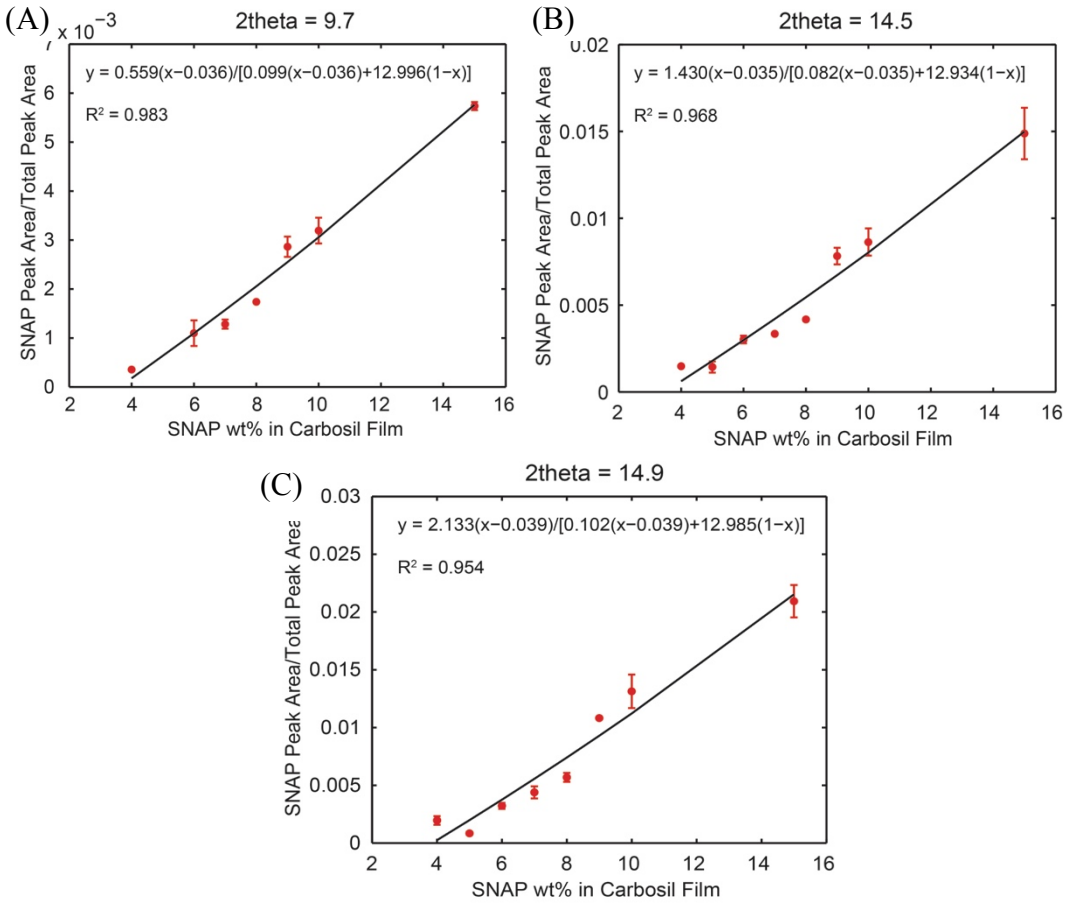

Figure 2.11. Correlation of data obtained by powder X-ray diffraction for SNAP in CarboSil. Linear regression lines were fitted using least squares approach. The 3 most prominent orthorhombic SNAP peaks were chosen to do the fitting (2 theta = 9.5 (A), 14.5 (B) and 14.9 (C)) and the calculated SNAP solubility in CarboSil polymer was 3.6 wt%, 3.5 wt% and 3.9 wt%, respectively.

Characterizing the stabilities of SNAP-doped CarboSil films using PXRD further verifies the dissolution hypothesis. We compared the PXRD patterns of freshly prepared 5 and 15 wt% SNAP-doped CarboSil samples as well as the samples stored under ambient light at room temperature for 10 d under the same conditions. We hypothesize that the solubilized SNAP behaves as a solute, dissolving in the CarboSil polymer that acts as the solvent, and it is less stable at room temperature and decomposes faster than the crystalline SNAP. As the solubilized SNAP in the polymer decomposes and the SNAP in the polymer is under

saturation, the crystalline SNAP is driven to gradually dissolve into the CarboSil polymer. For 5 wt% fresh samples, most of the SNAP added during preparation is dissolved in the polymer, which is labile and more likely to decompose via thermal decomposition. However, for the 15 wt% SNAP films, most of the SNAP in the film (ca. 11-12 wt%) is stabilized by the intermolecular hydrogen bonding.[55] The percentage of SNAP remaining in the 5 and 15 wt% films after 10 d under ambient light is 19.8 and 83.2 wt% of the initial amount, respectively. The attenuation of orthorhombic SNAP peaks in 5 wt% SNAP-doped CarboSil films relative to the fresh samples is indeed much greater than that of the 15 wt% samples (see Figure 2.12) where the SNAP peak changes are almost undetectable, thus validating our hypothesis.

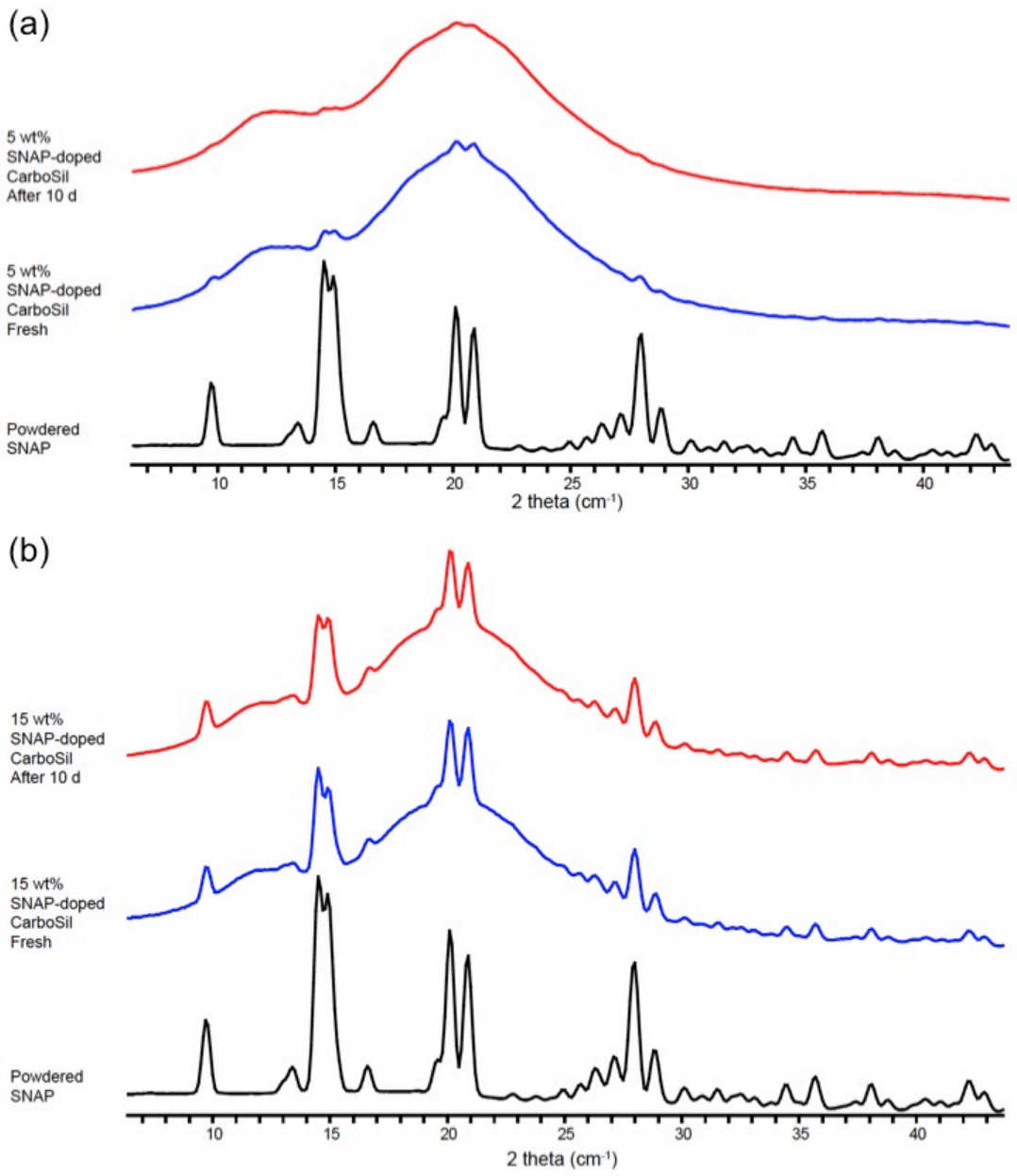

Figure 2.12. PXRD pattern comparison between freshly prepared (blue spectra) and 10 d old (red spectra) of (a) 5 wt% and (b) 15 wt% SNAP-doped CarboSil films. The crystal peaks intensity of 5 wt% films (19.8 wt% SNAP remained) decreased significantly while the 15 wt% one has minimal decrease in intensity (83.2 wt% SNAP remained) after storage under ambient light at room temperature for 10 d.

Intermolecular hydrogen bonding in the SNAP crystals is one of the key reasons for the elevated stability of SNAP-doped CarboSil films during dry storage for 8 months. In addition, as a tertiary nitrosothiol, the SNAP molecule itself is more stable with respect to the loss of NO than other primary and secondary RSNOs due to the steric hindrance effect imposed by the gem methyl group on the dimerization of the radicals that leads to the formation of the sulfur bridge[10,40,41,45] and the hindered rotation of the R—S—N—O linkage at room temperature.[55] The literature also suggests that the acetamide group in SNAP plays a key role in increasing the S—NO bond strength and reducing the NO liability.[46] Moreover, it has also been reported that the viscosity of the polymer imposes an important cage effect on the S—NO bond cleavage and radical pair formation. Specifically, the restricted mobility of soluble SNAP molecules in the CarboSil microenvironment may favor the recombination of the primary radicals rather than radicals escaping from the solvent cage.[10,12,37] Therefore, doping SNAP into the polymer represents a viable option for storage and handling for long-term NO release applications. Further studies comparing SNAP solubility in different polymer matrixes and examining the relationship between the SNAP crystallization/dissolution process and the stability of SNAP in certain polymers could be quite useful in designing additional NO release polymers with enhanced stability and long-term shelf life.

Lastly, Raman mapping characterization using static scans was employed to determine the 2D representation of the SNAP crystal distribution in 3 and 5 wt% SNAP-doped CarboSil films. The green spots in Figure 2.13 represent regions where the orthorhombic SNAP peaks are detected and are found in large quantities only in the 5 wt% SNAP/CarboSil film

but not in 3 wt% films. This finding correlates with the PXRD peak area fitting results that indicate the solubility of SNAP in polymer is ca. 3.4-4.0 wt%. However, the exact grain sizes of the SNAP crystals could not yet be quantified by this method because the focal depth of the laser is likely to exceed the grain size of the crystal. Thus, the green spots could represent crystals from both the surface and deeper within the polymer phase, which results in difficulty in distinguishing any individual crystal from overlaid crystals.

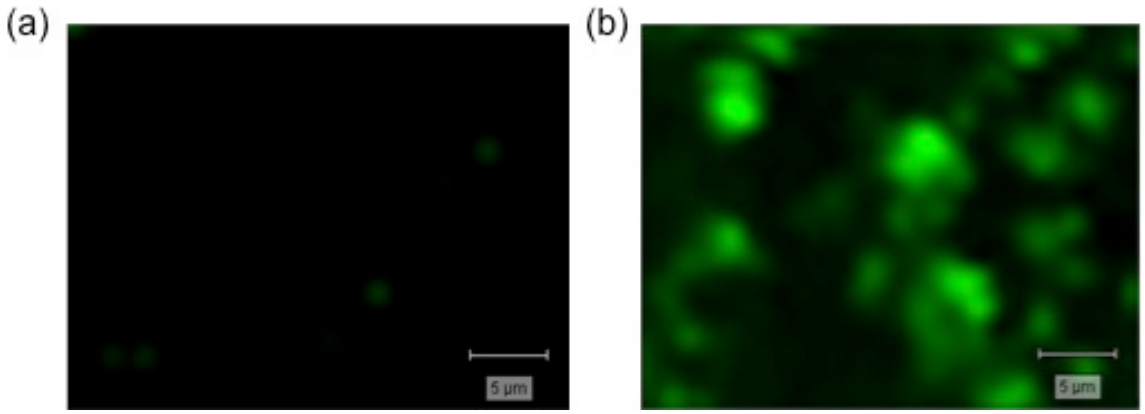

Figure 2.13. Raman mapping results for fitting of (a) 3 wt% and (b) 5 wt% SNAP-doped Carbosil with pure orthorhombic SNAP spectrum as the reference under 100x objective. Green represents areas fitting the crystalline SNAP spectrum.

2.3.5 In vitro antibiofilm experiments

In order to generate NO release (at the higher end of the normal physiological flux level) for longer periods, 20 wt% SNAP-doped CarboSil catheters were prepared as described in the Experimental Section. These devices can release physiological levels of NO for 28 d at 37 °C (see Figure 2.14).

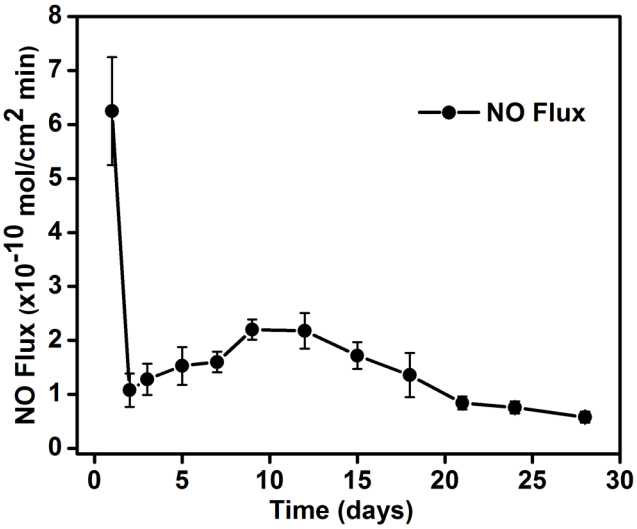

Figure 2.14. Long-term (28d) NO release from the 20 wt% SNAP-doped CarboSil catheter for antibiofilm studies (o.d. 4mm). NO release was measured in PBS via chemiluminescence at 37 °C.

Because stable NO releasing devices can abate bacterial adhesion and colonization associated with catheterization, we examined the antibiofilm properties of catheter segments with *S. aureus* for 7 d in a drip-flow biofilm reactor at 37 °C. The drip-flow bioreactor was chosen because it promotes the growth of the bacteria that grows at the air-liquid interface, which mimics the condition of the surface of indwelling intravascular catheters. Results for 7 d *S. aureus* biofilms shows a 5 logarithmic unit reduction in viable cell count on the surfaces of NO release catheters segments when compared to the control segments (see Figure 2.15A). This finding is further corroborated by the fluorescent images (Figure 2.15B), which illustrates the live/dead bacteria as well as the bacterial

surface coverage on the surfaces of both catheters, respectively. These results demonstrate that the SNAP/CarboSil catheter provides an approach that can potentially reduce/prevent catheter-related bloodstream infections.

(A)

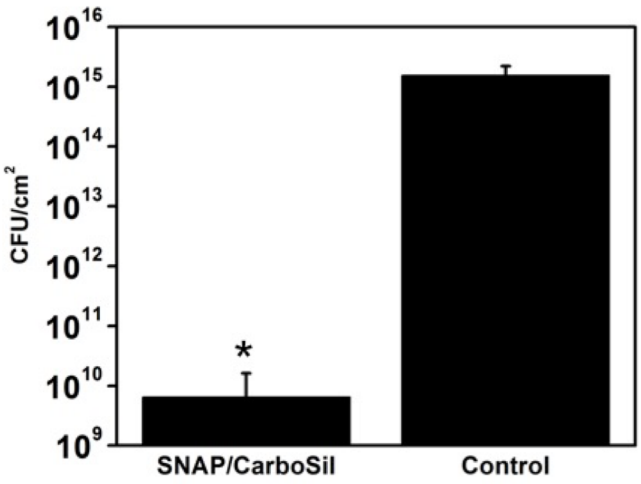

(B)

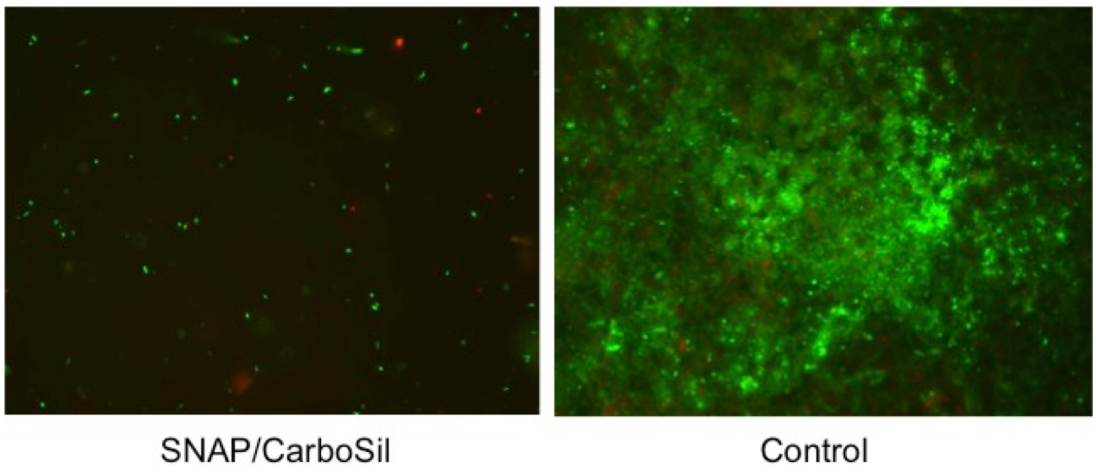

Figure 2.15. *S. aureus* biofilms developed on catheter segments in a drip-flow bioreactor for 7 d. (A) Plate count of the number of viable bacteria adhered to the catheter surface. (B) Representative fluorescence images with oil immersion 60X objective lens of the biofilms on the surface of the catheter.

2.3.6 In vivo antithrombotic experiments in rabbits

In order to demonstrate the potential benefits of using SNAP-doped CarboSil polymer as a thromboresistant material, acute 7 h rabbit experiments were conducted to study the effect of NO release from CarboSil catheters on the thrombus formation area. The NO release from the SNAP/CarboSil catheter maintains an average flux of approximately 5.5 x 10^{-10} mol cm^{-2} min^{-1} for 7 h at 37 °C (see Figure 2.16).

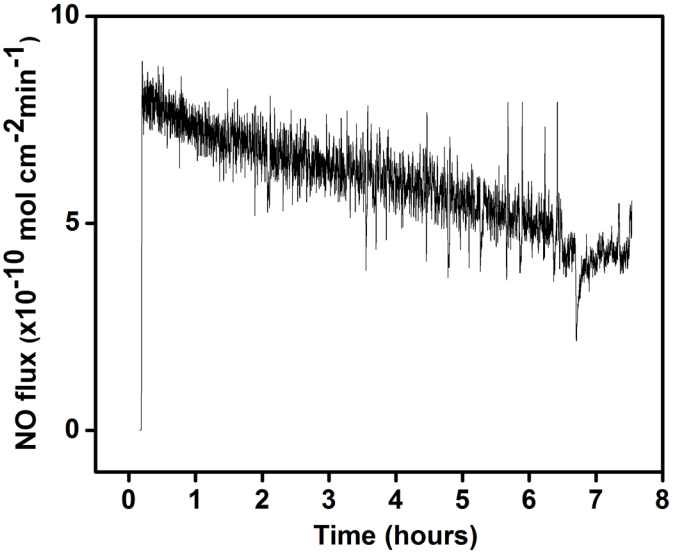

Figure 2.16 Representative NO surface flux profile from a section of the SNAP/CarboSil rabbit catheter for 7h (o.d. 2.2mm). NO release was measured in PBS via chemiluminescence at 37 °C.

One SNAP/CarboSil and one control catheter (non-SNAP) were placed into the external jugular veins of each rabbit for 7 h. Owing to the very slow loss of SNAP from the catheter reservoir (given the composite nature of the material), the dose of SNAP leached from the catheters is significantly below the threshold that can induce the adverse reactions.[10]

After 7 h of implantation, the catheters were carefully removed from the rabbit veins, leaving the thrombus formation intact on the surface. To determine whether the NO release reduced the clotting on the catheter surface, digital images of the catheter surfaces were taken, and the two-dimensional (2D) representation of the thrombus area was quantitated using ImageJ software from the NIH. As shown in Figure 2.17, the thrombus formation is significantly reduced for the SNAP/CarboSil catheters with NO release ability when compared to the controls (n = 3 rabbit experiments). The SNAP/CarboSil catheters were also examined for NO release rates via chemiluminescence after explantation, and they still exhibit an average flux of 3.8 ± 0.2 mol cm^{-2} min^{-1}. This clearly demonstrates that the localized NO release from the catheter surface can significantly reduce platelet activation and thrombus formation.

(A)

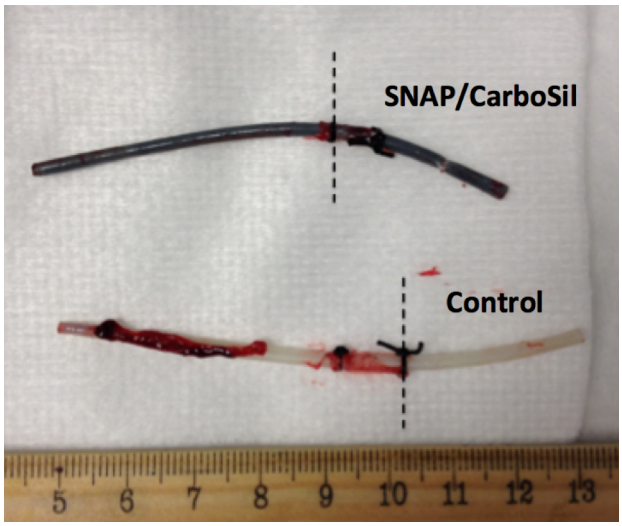

(B)

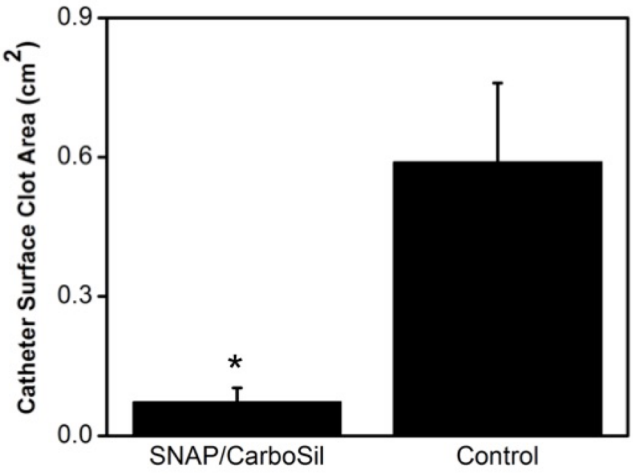

Figure 2.17. (a) Five cm of the catheters (left of the dash line) were inserted into the rabbit external jugular veins for 7 h. Representative pictures of thrombus formation on the SNAP/CarboSil and control catheters after removal from veins. (b) Two-dimensional representation of clot area (cm^2) on SNAP/CarboSil and control catheters in rabbit veins for 7 h, as quantitated using ImageJ software from NIH. Data are mean ± SEM (n=3). * = $p<0.05$, SNAP/CarboSil vs control catheters.

2.4 Conclusion

In this study, we have shown that SNAP doped into the CarboSil 20 80A polymer forms a polymer-crystal composite during solvent evaporation and can locally release NO over a 22 d period via thermal decomposition. Utilizing a cross-linked silicone rubber topcoat can greatly reduce the amount of SNAP, NAP, and NAP disulfide leaching as measured by LC-MS. The 10 wt% SNAP/CarboSil has excellent stability during the 8 month shelf-life study at 37 °C as well as during ethylene oxide sterilization, where 88.5% and 91.8% of the initial SNAP remain in the polymer, respectively. These data suggest the practicality of sterilizing, storing and shipping biomedical devices made with or coated with this material. Raman spectroscopy and PXRD characterization of SNAP-doped CarboSil films demonstrate that the solubility of SNAP in CarboSil is ca. 3.4-4.0 wt%. However, when the SNAP doping wt% is higher than this solubility threshold, SNAP exists in an orthorhombic crystal form within the bulk of the polymer, in which intermolecular hydrogen bonds between SNAP molecules play a key role in maintaining the RSNO stability and functionality over a long period of time. Solubilized SNAP in the polymer phase behaves like a solute in the solid solution polymer system and is less stable and decomposes faster than the crystalline SNAP. When the solubilized SNAP in polymer decomposes/releases NO and the SNAP within the polymer phase is under saturation, the crystalline SNAP in the bulk of the polymer is driven to gradually dissolve into the polymer and further release NO. The NO release process ceases after 22 d when all the SNAP crystals are depleted. The catheters fabricated with this SNAP composite are shown to exhibit significant antibiofilm properties against *S. aureus*, and such catheters could eventually be used to reduce the rate of nosocomial catheter related bloodstream infections.

The SNAP/CarboSil catheters also greatly reduce thrombus formation during 7 h implantation within the veins of rabbits when compared to the corresponding control catheters. Given its excellent stability and long-term NO release capability, the new SNAP-doped CarboSil composite system offers many new opportunities to improve the biocompatibility of biomedical devices for many applications.

2.5 Reference

1 B. D. Ratner, *Biomaterials*, 2007, **28**, 5144–5147.
2 D. J. Suchyta, H. Handa and M. E. Meyerhoff, *Mol. Pharm.*, 2014, **11**, 645–650.
3 H. Handa, E. J. Brisbois and T. C. Major, *J. Mater. Chem. B*, 2013, **1**, 3578–3587.
4 T. M. Robinson, T. S. Kickler, L. K. Walker, P. Ness and W. Bell, *Crit. Care Med.*, 1993, **21**, 1029–1034.
5 N. D. Allan, K. Giare-Patel and M. E. Olson, *J. Biomed. Biotechnol.*, 2012, **2012**.
6 M. Otto, *Annu. Rev. Med.*, 2013, **64**, 175–188.
7 M. R. Kiedrowski and A. R. Horswill, *Ann. N. Y. Acad. Sci.*, 2011, **1241**, 104–21.
8 G. K. Kolluru, X. Shen and C. G. Kevil, *Redox Biol.*, 2013, **1**, 313–318.
9 G. E. Gierke, M. Nielsen and M. C. Frost, *Sci. Technol. Adv. Mater.*, 2011, 12, 55007.
10 E. J. Brisbois, H. Handa, T. C. Major, R. H. Bartlett and M. E. Meyerhoff, *Biomaterials*, 2013, **34**, 6957–66.
11 G. K. Kolluru, S. Yuan, X. Shen and C. G. Kevil, *Hydrog. Sulfide Redox Biol. Part A*, 2015, 271–297.
12 S. M. Shishido, A. B. Seabra, W. Loh and M. G. de Oliveira, *Biomaterials*, 2003, **24**, 3543–3553.
13 L. Höfler, D. Koley, J. Wu, C. Xi and M. E. Meyerhoff, *RSC Adv.*, 2012, **2**, 6765–6767.
14 H. Ren, A. Colletta, D. Koley, J. Wu, C. Xi, T. C. Major, R. H. Bartlett and M. E. Meyerhoff, *Bioelectrochemistry*, 2015, **104**, 10–16.
15 H. Ren, J. Wu, C. Xi, N. Lehnert, T. Major, R. H. Bartlett and M. E. Meyerhoff, *ACS Appl. Mater. Interfaces*, 2014, **6**, 3779–3783.
16 K. S. Bohl and J. L. West, *Biomaterials*, 2000, **21**, 2273–2278.
17 E. J. Brisbois, J. Bayliss, J. Wu, T. C. Major, C. Xi, S. C. Wang, R. H. Bartlett, H. Handa and M. E. Meyerhoff, *Acta Biomater.*, 2014, 4136–42.
18 E. J. Brisbois, R. P. Davis, A. M. Jones, T. C. Major, R. H. Bartlett, M. E. Meyerhoff and H. Handa, *J. Mater. Chem. B*, 2015, **3**, 1639–1645.
19 M. C. Frost, M. M. Reynolds and M. E. Meyerhoff, *Biomaterials*, 2005, **26**, 1685–1693.
20 M. M. Reynolds, M. C. Frost and M. E. Meyerhoff, *Free Radic. Biol. Med.*, 2004, **37**, 926–936.
21 M. M. Reynolds, J. E. Saavedra, B. M. Showalter, C. A. Valdez, A. P. Shanklin, B. K. Oh, L. K. Keefer and M. E. Meyerhoff, *J. Mater. Chem.*, 2010, **20**, 3107–2114.
22 M. M. Reynolds, J. a Hrabie, B. K. Oh, J. K. Politis, M. L. Citro, L. K. Keefer and M. E. Meyerhoff, *Biomacromolecules*, 2006, **7**, 987–94.
23 M. M. Simões and M. G. de Oliveira, *J. Biomed. Mater. Res. B. Appl. Biomater.*, 2010, **93**, 416–24.
24 A. B. Seabra, A. Fitzpatrick, J. Paul, M. G. De Oliveira and R. Weller, *Br. J. Dermatol.*, 2004, **151**, 977–983.
25 Y. Li and P. Lee, *Mol. Pharm.*, 2010, 3855–3859.
26 E. Keyaerts, L. Vijgen, L. Chen, P. Maes, G. Hedenstierna and M. Van Ranst, *Int. J. Infect. Dis.*, 2004, **8**, 223–226.
27 E. M. Hetrick and M. H. Schoenfisch, *Annu Rev Anal Chem (Palo Alto Calif)*, 2009,

2, 409–33.
28 D. a Riccio and M. H. Schoenfisch, *Chem. Soc. Rev.*, 2012, **41**, 3731–41.
29 A. Colletta, J. Wu, Y. Wo, M. Kappler, H. Chen, C. Xi and M. E. Meyerhoff, *ACS Biomater. Sci. Eng.*, 2015, **1**, 416–424.
30 A. W. Carpenter and M. H. Schoenfisch, *Chem. Soc. Rev.*, 2012, **41**, 3742–52.
31 P. N. Coneski and M. H. Schoenfisch, *Chem. Soc. Rev.*, 2012, **41**, 3753–8.
32 J. O. Lundberg, E. Weitzberg and M. T. Gladwin, *Crit. Care Med.*, 2008, **7**, 156–167.
33 H. Handa, T. C. Major, E. J. Brisbois, K. A. Amoako, M. E. Meyerhoff and R. H. Bartlett, *J. Mater. Chem. B*, 2014, **2**, 1059–1067.
34 M. Vaughn, L. Kuo and J. Liao, *Am. J. Physiol.*, 1998, **274**, 2163–2176.
35 Y. Wu and M. E. Meyerhoff, *Talanta*, 2008, **75**, 642–50.
36 T. S. Hakim, K. Sugimori, E. M. Camporesi and G. Anderson, *Physiol. Meas.*, 1996, **17**, 267–77.
37 S. M. Shishido and M. G. de Oliveira, *Photochem. Photobiol.*, 2007, **71**, 273–280.
38 P. N. Coneski and M. H. Schoenfisch, *Polym. Chem.*, 2011, **2**, 906.
39 D. A. Riccio, P. N. Coneski, S. P. Nichols, A. D. Broadnax and M. H. Schoenfisch, *ACS Appl. Mater. Interfaces*, 2012, **4**, 796–804.
40 P. G. Wang, M. Xian, X. Tang, X. Wu, Z. Wen, T. Cai and A. J. Janczuk, *Chem. Rev.*, 2002, **102**, 1091–1134.
41 C. E. Lin, S. K. Richardson, W. Wang, T. Wang and D. S. Garvey, *Tetrahedron*, 2006, **62**, 8410–8418.
42 M. C. Frost and M. E. Meyerhoff, *J. Am. Chem. Soc.*, 2004, **126**, 1348–9.
43 G. C. Mendes, T. R. Brandão and C. L. Silva, *Am. J. Infect. Control*, 2007, **35**, 574–581.
44 I. P. Matthews, C. Gibson and A. H. Samuel, *Clin. Mater.*, 1994, **15**, 191–215.
45 I. L. Megson, S. Morton, I. R. Greig, F. A. Mazzei, R. A. Field, A. R. Butler, G. Caron, A. Gasco, R. Fruttero and D. J. Webb, *Br. J. Pharmacol.*, 1999, **126**, 639–648.
46 M. G. de Oliveira, S. M. Shishido, A. B. Seabra and N. H. Morgon, *J. Phys. Chem. A*, 2002, **106**, 8963–8970.
47 K. Szacilowski and Z. Stasicka, *Prog. React. Kinet. Mech.*, 2001, **26**, 1–58.
48 D. L. Williams, *Acc. Chem. Res.*, 1999, **32**, 869–876.
49 R. Aronow and L. E. Fleischmann, *Clin. Pediatr. (Phila).*, 1976, **15**, 936-937-945.
50 M. M. Jones, A. D. Weaver and W. L. Weller, *Res. Commun. Chem. Pathol. Pharmacol.*, 1978, **22**, 581–588.
51 R. A. Kark, D. C. Poskanzer, J. D. Bullock and G. Boylen, *N. Engl. J. Med.*, 1971, **285**, 10–16.
52 V. Parameshvara, *Br. J. Ind. Med.*, 1967, **24**, 73–76.
53 P. Srivastava, A. J. Arif, C. Singh and V. C. Pandey, *Pharmacol. Res.*, 1997, **36**, 305–7.
54 K. A. Graeme and C. V Pollack, *J. Emerg. Med.*, 1998, 16, 45–56.
55 N. Arulsamy, D. S. Bohle, J. A. Butt, G. J. Irvine, P. A. Jordan and E. Sagan, *J. Am. Chem. Soc.*, 1999, **121**, 7115–7123.

CHAPTER 3

Study of Crystal Formation and Nitric Oxide (NO) Release Mechanism from *S*-Nitroso-*N*-acetylpenicillamine (SNAP)-Doped CarboSil Polymer Composites for Potential Antimicrobial Applications

Wo, Y.; Li, Z.; Colletta, A.; Wu, J.; Xi, C.; Matzger, A.J.; Brisbois, E.J.; Bartlett, R.H.; Meyerhoff, M.E. "Development of *S*-Nitroso-*N*-acetylpenicillamine (SNAP)-Doped CarboSil Polymer Composites for Antimicrobial Biomedical Applications." *Composite Part B, Bio-Inspired special issue*, *Submitted.* [*]

3.1 Introduction

Microorganisms commonly attach to living and nonliving surfaces, including those of a variety of indwelling medical devices.[1] After the initial colonization on the abiotic surfaces, bacteria form extracellular polysaccharide substance (EPS), also known as biofilm, that creates a physical and chemical barrier for the bacteria, preventing conventional antibiotic

[*] The key experiments of this chapter were conducted by Yaqi Wo, with help from Dr. Zi Li in the conducting the SNAP kinetics studies and the use of optical microscope, and Dr. Jianfeng Wu in assisting with the microbiology experiments.

treatment or appropriate activation of the host defense system.[2,3] Infection due to bacterial adhesion and biofilm formation represents a major complication associated with the long-term use of indwelling biomedical devices, such as intravascular and urinary tract catheters. Intravascular catheters are utilized for management of hospitalized patients, where catheters are placed into the blood vessel for direct vascular access and used for infusion of fluids, drug administration, removal of blood samples, and patient monitoring, etc. Meanwhile urinary catheters serve an indispensable role in patient care, including preventing patient urine retention as well as providing a solution to chronic urinary incontinence. However, external bacteria can access the blood vessel or urinary tract despite the routine antiseptic procedures used when implanting these devices, and both catheter-related bloodstream infections (CRBSIs) and catheter-associated urinary tract infections (CAUTIs) cause lengthy hospital stays, increased healthcare costs and high mortality rates.[4–6] Current antimicrobial approaches for use with biomedical catheters include using catheters impregnated with antibiotics, employing antibiotic lock solutions, or utilizing catheters that possess a silver alloy coating that is capable of releasing Ag^+ ions to prevent bacterial infection.[7–10] Even though these antimicrobial catheters have been demonstrated in the laboratory to reduce bacterial adhesion and inhibit bacterial growth with some success,[11–14] clinical results and efficiencies with such catheters have been less than satisfactory owing to the polysaccharide matrix that protects the bacteria and the increased level the microbial mutations (that prevents given antibiotic from proper functioning) within the biofilm.[15,16] Therefore, efforts aimed at devising novel solutions to effectively prevent biofilm-induced infections associated with the long-term use of indwelling catheters are still needed.

Nitric oxide (NO) was identified as the endothelium-derived relaxation factor (EDRF) by Ignarro, Furchgott, and Murad in 1987, and these scientists were awarded the Nobel Prize in Physiology or Medicine for their discovery in 1998.[17,18] NO is an endogenous gas molecule synthesized from the amino acid L-arginine via three distinct isoforms of nitric oxide synthases (NOS): endothelial NOS (eNOS), neuronal NOS (nNOS) and inducible NOS (iNOS).[19–21] The NO released by the endothelium cells that line the inner wall of all blood vessels helps to prevent platelet activation/adhesion and serves to control blood pressure, and the rate of release into the blood stream is typically at a surface flux rate of $0.5 - 4 \times 10^{-10}$ mol cm^{-2} min^{-1}.[19,22–24] The human body also synthesizes greater amounts of NO from macrophages, upper airway epithelial cells, and other cells to serve as a potent antimicrobial agent to fight against bacterial infections *in vivo*.[25,26] In this regard, NO has been reported to kill both gram-positive and gram-negative bacteria.[27–32] It has also been reported that NO can modulate biofilm metabolism and make bacteria within biofilm more susceptible to antibiotics.[33,34]

Because NO has a very short half-life, a wide variety of NO donors that are capable of releasing NO via different mechanisms/stimuli have been studied for therapeutic and targeted NO release.[17,35–43] One very promising NO release compound is *S*-nitroso-*N*-acetylpenicillamine (SNAP). SNAP is a tertiary *S*-nitrosothiol species, which is much more stable in storage than primary *S*-nitrosothiols (e.g., *S*-nitrosoglutathione) and it is also considered very biocompatible because NAP and its ultimate degradation product, penicillamine, have been used as chelators to treat heavy metal poisoning, such as Wilson's

disease in humans, for many years.[44–48] Our group recently reported that SNAP is exceptionally stable when incorporated into CarboSil, a low water-uptake thermoplastic silicone-polycarbonate-urethane biomedical polymer.[6] The low water uptake nature of CarboSil enables minimized SNAP leaching when in contact with solution. Moreover, CarboSil itself has enhanced inherent biocompatibility over many previously studied polymer systems,[35,49] such as poly(vinyl chloride)(PVC)-based materials. Solid state x-ray diffraction studies demonstrated that SNAP can partially dissolve in the CarboSil polymeric matrix (solubility: ca. 3.4-4.0 wt%), while the proportion exceeding this solubility limit crystallizes in its orthorhombic form. It was proposed that the hydrogen bonding between crystalline SNAP molecules contributes to its excellent shelf stability and slow dissolution of crystalline SNAP within the bulk of the CarboSil polymer determines the rate of NO release and ultimately leads to its long-term release under physiological conditions.[6] However, more detailed studies are needed to further understand the polymer/crystal composite formation and the NO release mechanism from the SNAP-doped CarboSil polymer matrix. Herein, we report our effort to prepare *S*-nitroso-*N*-acetylpenicillamine (SNAP)-doped CarboSil 20 80A polymer films and observe, in real time, the crystal formation process within the bulk of the polymer phase. The NO release mechanism of this composite material when it is in contact with physiological solutions and its correlation with respect to film surface area and polymer thickness are also carefully examined. SNAP/CarboSil catheters are also fabricated and evaluated for their long-term antimicrobial activity toward *Pseudomonas aeruginosa* (*P. aeruginosa*) and *Proteus mirabilis* (*P. mirabilis*) in a CDC (Center for Disease Control) bioreactor for 14 days.

3.2 Experimental Section

3.2.1 Materials

N-Acetyl-D-penicillamine (NAP), sodium nitrite, L-cysteine, sodium chloride, potassium chloride, sodium phosphate dibasic, potassium phosphate monobasic, copper (II) chloride, ethylenediaminetetraacetic acid (EDTA), and tetrahydrofuran (THF) were purchased from Sigma-Aldrich (St. Louis, MO). Methanol, hydrochloric acid, sulfuric acid, Luria Bertani (LB) broth and LB agar were obtained from Fisher Scientific (Hampton, NH). CarboSil 20 80A was obtained from DSM Biomedical Inc. (Berkeley, CA). All aqueous solutions were prepared with 18.2 MΩ-deionized water using a Milli-Q filter from EMD Millipore (Billerica, MA). Phosphate buffered saline (PBS), pH 7.4, containing 138 mM NaCl, 2.7 mM KCl, 10 mM sodium phosphate, and 100 μM EDTA was used for all *in vitro* experiments. *P. aeruginosa* ATCC 27853 and *P. mirabilis* ATCC 29906 was obtained from the American Type Culture Collection (ATCC) (Manassas, VA).

3.2.2 Study of SNAP decomposition reaction in solution

SNAP was synthesized as previously reported.[6,50] SNAP solutions (2 mM) in various solvents were prepared. The solvents chosen in this experiment were PBS with EDTA (100 μM), PBS without EDTA, ethanol, THF and methanol-methyl ethyl ketone (30/70 v/v) solvent mixture. The decomposition experiments of SNAP in solution were conducted at 60 °C. The concentration of SNAP in solution were monitored by UV-Vis absorbance spectroscopy at 380 nm (in order to avoid any absorbance overlapping with solvents) using an Agilent 8453 UV-visible spectrophotometer from Agilent Technologies. Two hundred UV-Vis spectra were taken at 5 min intervals for each decomposition experiment. The

absorbance data were fit into a first order reaction equation by KaleidaGraph 3.5 Synergy Software.

3.2.3 Real-time monitoring of SNAP crystallization process in CarboSil

An 8 wt% SNAP-CarboSil solution was prepared by dissolving 17.4 mg SNAP and 200 mg CarboSil in 2 mL THF. A clean glass cover slide was weighed. Three drops of solution were then dispensed on the glass slide and the total weight was measured immediately, followed by weight measurements every 10 min. Optical images of the sample were captured every 10 min by a Leica DMLP polarization microscope equipped with a N Plan 2.5× objective under crossed polarizers in combination with a quarter-wave plate, and were then taken with a SPOT Flex Mosaic 15.2 camera using SPOT 5.2 Software from Diagnostic Instruments, Inc.

3.2.4 Preparation of SNAP-doped CarboSil films

Ten wt % SNAP was doped into CarboSil 20 80A polymer by solvent casting method using a Teflon plate.[6] After curing fully, small disks (0.7 cm diameter and 260 μm thickness) were punched from the 10 wt% parent films. To actively control the surface area of the films that are in contact with buffer during NO release measurements, SNAP/CarboSil films were separated into two groups and sputter coated with a 400 Å thick of gold film by gold sputtering (Denton Vacuum Inc., Desk II) for 120 s on either the front or the back side of the film (see Figure 3.1), to reduce the film water-contacting surface area by 50 %.

Figure 3.1. The images of 10 wt% SNAP-doped CarboSil film with no gold sputtering (left), front side gold sputtering (middle) and back side gold sputtering (right).

Meanwhile, another set of the cured films (all with 0.7 cm in diameter), but with different wt% levels of SNAP within (5 wt% or 10 wt%) or different thicknesses (260 μm or 520 μm thick) were also prepared for NO release measurements. Films with the following configurations (5 wt% and 260 μm thick, 10 wt% and 260 μm thick, and 10 wt% and 520 μm thick) were coated with plain CarboSil polymer topcoats by dip-coating (45 μm thick) to reduce SNAP leaching. The NO release from all polymeric films was measured in PBS buffer at 37 °C using a nitric oxide analyzer (NOA) (General Electric Analytical Instruments, Boulder, CO) via chemiluminescence measurements. The NO release profiles were recorded and compared between films with no gold coating, with only front side gold coating, and only back side gold coating, as well as between films with the same diameter but different SNAP concentration or thicknesses.

3.2.5 Evaluation of the antimicrobial activities of NO release CarboSil catheters

All SNAP catheters and control catheters were sterilized by ethylene oxide in the University of Michigan Central Sterile Processing Department [6] prior to testing. In order to determine whether the bactericidal effect of SNAP-doped catheter is directly related to the nitric oxide that is being released, three control groups were used in the study. These

included NAP-doped CarboSil catheters, plain CarboSil catheters, and a commercial silicone tubing. This combination allowed us to evaluate the whether the precursor NAP or the polymer CarboSil itself has any effect on bacterial adhesion. SNAP-doped, NAP-doped or plain CarboSil catheters were fabricated by a dip-coating method using a stainless steel mandrel [6] and the final catheters had dimensions of 2 mm i.d. and 4 mm o.d. (see Figure 3.2).

Figure 3.2. The images of SNAP-doped (top), NAP-doped (middle) and plain control CarboSil catheters, all with blank CarboSil topcoats.

The NO release from SNAP-doped catheters with CarboSil topcoats was measured using the NOA, as described in Section 3.2.4. All CarboSil catheter segments and commercial silicone tubing segments were mounted on coupon holders within a CDC bioreactor (see Figure 3.3) and the bioreactor was kept at 37 °C and supplemented with 10% Luria Bertani medium via a peristaltic pump with a continuous flow rate of 100 mL/h.

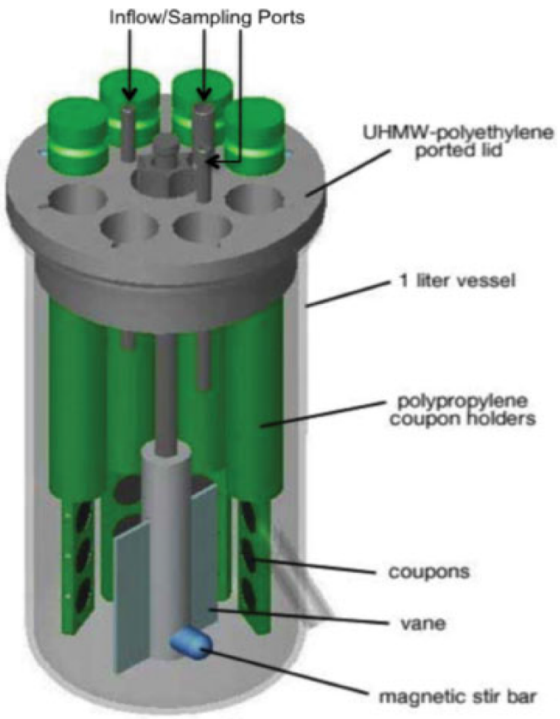

Figure 3.3. Schematic of the CDC bioreactor in which the different catheters were tested for bacterial biofilms formation. [51]

First, the media in the bioreactor in contact with the catheter/tubing segments was inoculated with overnight bacteria culture (~1 × 10^8 colony forming unit/mL) for 1 h without stirring. Then the bacteria, *P. aeruginosa* ATCC 27853 or *P. mirabilis* ATCC 29906, respectively (for two different studies), were cultured and grown onto surfaces of catheters for 14 d, with stirring. Finally, all the catheter/tubing segments were removed from the bioreactor and cut into halves, and one half of each was homogenized in sterile PBS buffer, 10-folds serially diluted and then subjected to bacteria plate counting. The other half of all the segments were used for fluorescence imaging of live bacteria on the surface of the tubing. Briefly, control and SNAP impregnated catheter segments were stained with LIVE/DEAD BacLight Bacterial Viability kit (L7012, Invitrogen, Carlsbad, CA) according to the instructions, where green color indicates live bacteria and red color

indicates dead bacteria. All fluorescence images were acquired with an inverted fluorescence microscope (Olympus IX71, Center Valley, PA) equipped with Fluorescence Illumination System (X-Cite 120, EXFO) and filters for SYTO-9 (excitation = 488 nm/emission = 520 nm) and propidium iodide (excitation = 535 nm/emission = 617 nm). Images were obtained using an oil immersed 60× objective lens.

3.2.6 Statistical analysis

All experiments were conducted in triplicate. Data reported herein are all expressed as mean ± SEM (standard error of the mean). Comparison of means using student's t test was utilized to analyze the statistical differences between SNAP-doped catheters and control catheters. Values of $p < 0.05$ were considered statistically significant for all tests.

3.3 Theory

In solution, the decomposition of solubilized SNAP is a pseudo-first-order reaction proportional to the SNAP concentration, resulting in a relatively short half-life and rapid decomposition at room temperature. The stability of SNAP can be improved by doping SNAP into low water uptake polymers, such as CarboSil 20 80A, where SNAP will form crystals and embed within the polymer matrix. The intermolecular interactions between SNAP molecules in the crystal lattice stabilize this NO donor, and leads to long-term NO release via slow crystal dissolution process into the solid polymer. If this mechanism is correct, the NO release profile (such as NO release rates and longevity of the release) from SNAP-doped CarboSil polymer should be dictated by three factors: 1) the SNAP concentration in the polymer matrix; 2) the water-contacting polymer surface area exposed

to the test solution; and 3) the film thickness of the specific SNAP-doped CarboSil polymer formulation. In theory, NO release rates are controlled by SNAP concentration in the polymer and the water-contacting polymer surface area. The longevity of NO release, on the other hand, should be directly proportional to the SNAP loading/concentration and the film thickness of a specific SNAP-doped CarboSil polymeric material.

3.4 Results and Discussion

3.4.1 NO release mechanism

It has been previously reported that SNAP is stable when doped into low-water uptake polymers such as CarboSil 20 80A,[6] which is a polyurethane-based triblock copolymer. The elevated stability of SNAP in this polymer during storage has been previously ascribed to the strong intermolecular interactions between SNAP molecules that forms crystals in the bulk of the polymer phase when SNAP concentration exceeds its solubility limit in the polymer. However, the process of how the polymer-crystal composites are formed during the casting and drying of the polymer phase as well as understanding what key parameters dictate the observed NO release rates from the polymer crystal composites still remains unclear.

We hypothesize that the NO release profile of the certain SNAP-doped polymer films are related to several factors: the film surface area in contact with aqueous phase, the film thickness, and the SNAP concentration within the polymeric film (see Section 3.3 above). In this work, to better understand the properties of this new composite material we first compared the NO release rates between 10 wt% SNAP-doped CarboSil films (all with 0.7

cm diameter) with thicknesses of 260 and 520 μm in PBS buffer. Of note, all the NO release data from CarboSil films were recorded until when the release rate was no longer above 0.5 x 10 -10 mol min $^{-1}$ cm $^{-2}$, which is the lower end of physiological NO release levels by the endothelial cells.[19,22–24] As shown in Figure 3.4A, the results demonstrate that the NO release levels are not significantly different between the 10 wt% films with 260 or 520 μm thickness, but the NO release lifetime is much longer for the films with twice the thickness. The overall thickness of the films tested is very small compared to their diameter, and increasing the thickness of films to 520 μm only increases the total surface area of the films by 6 % when compared to the original films, a relatively small increase. However, the NO release levels of the 5 wt% SNAP-doped films are nearly half of the levels observed for films doped with 10 wt% SNAP (see Figure 3.4B).

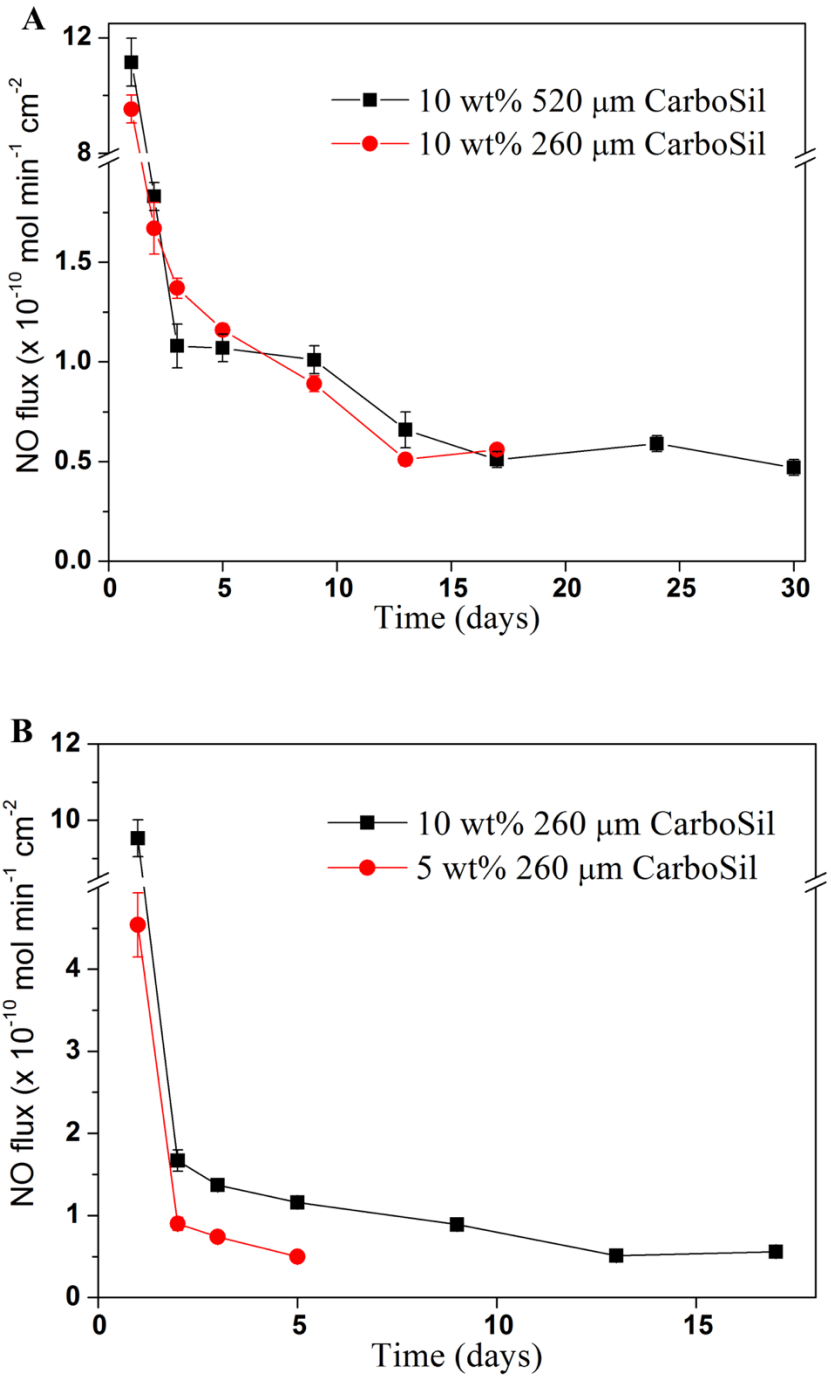

Figure 3.4. The NO release comparison between 10 wt% SNAP-doped CarboSil films with thickness of 260 or 520 µm (A); and 260 µm thick SNAP-doped films with 5 wt% or 10 wt% SNAP concentration (B).

Further, to understand whether the NO release rate is determined by the water-contacting surface area of the film or simply by the total surface area of the film, the NO release rates from three identical 10 wt% SNAP-doped CarboSil films were compared with no gold sputtering, one with 400 Å gold film sputtered on its front side, and one with 400 Å gold film sputtered on its back side. The gold coating on either side of the film will prevent direct water contact on that side of the films when they are immersed in solution. As shown in Figure 3.5, both of the gold sputtered CarboSil films exhibited half the NO release rate when compared to the non-coated films. This demonstrates that the NO release rate from SNAP-doped CarboSil films is controlled by the total water-contacting surface area of the polymer film. It also suggests that the water rich layer in the outermost surfaces of the polymers is the likely site where most of the NO is liberated from soluble SNAP within the polymer.

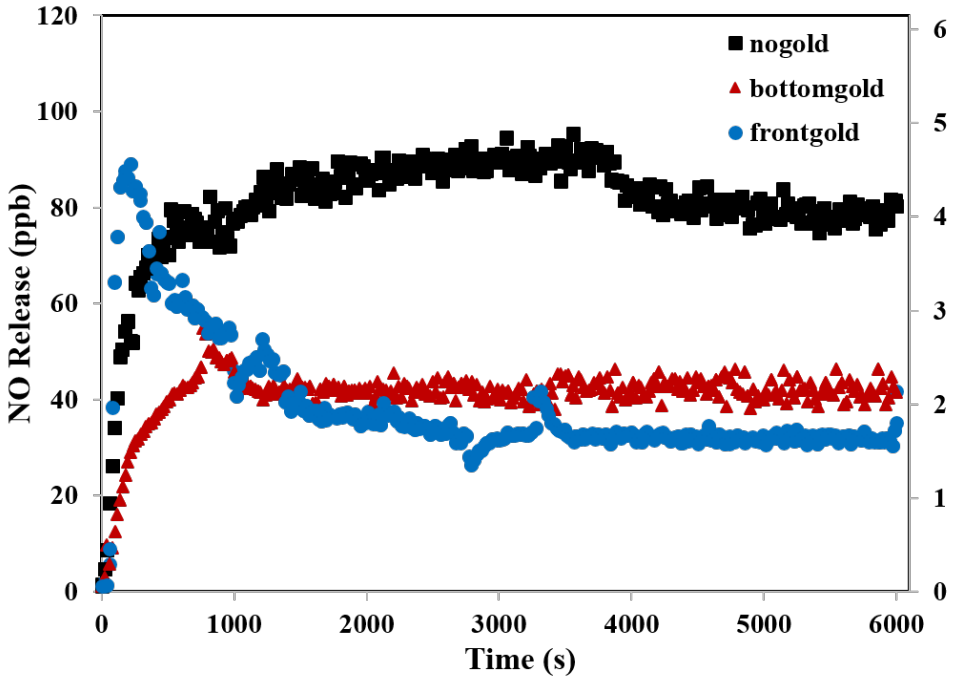

Figure 3.5. The NO release comparison between 10 wt% SNAP-doped CarboSil films with no gold film coating (square), front side 400 Å gold coating (triangle) and back side 400 Å gold coating (circle).

From the results described above, the factors that control the NO release levels and longevity of release are summarized as follows. Firstly, the results indicate that NO release levels do not increase as the thickness of the film increases, because the water-contacting surface area and the SNAP concentration in the film are the rate determining factors dictating the observed NO release kinetics. Secondly, if the water-contacting surface area remains the same, the NO release rate decreases as the SNAP concentration decreases. Thirdly, the longevity of NO release from a given film is determined by the SNAP concentration within the film, as well as the thickness of SNAP-doped polymeric film.

3.4.2 SNAP decomposition in solution

We recently reported that when SNAP is doped into CarboSil 20 80A, 3.4-4.0 wt% of SNAP is dissolved in the polymer phase while any additional SNAP above this solubility threshold exists as crystals embedded within the polymer matrix [6]. It appears that the SNAP that is solubilized in the polymer matrix, analogous to SNAP dissolved in a solvent, is more reactive and more likely to decompose and releases NO, than crystalline SNAP that is stabilized by strong hydrogen bonding [6] as well as the low water uptake nature in the bulk region of the polymeric phase. SNAP decomposition in liquid solution is investigated herein to determine SNAP stability in various solvents. Such, solution phase decomposition experiments of SNAP in various solvents were conducted at 60 °C, in order to accelerate the decomposition and observe obvious signal changes over a short time period. The SNAP concentrations in various solvent solutions were monitored by UV-Vis absorbance spectroscopy. As illustrated in Figure 3.6, all decomposition reactions exhibited pseudo-first-order behavior relative to SNAP levels at low concentrations. All experimental data fit into first-order reaction equation $A_t = A_0 e^{-kt} + c$, where A_t is the concentration of reactant at time t, A_0 is the initial concentration, k is the first-order reaction rate constant, and c is the instrumental system error.

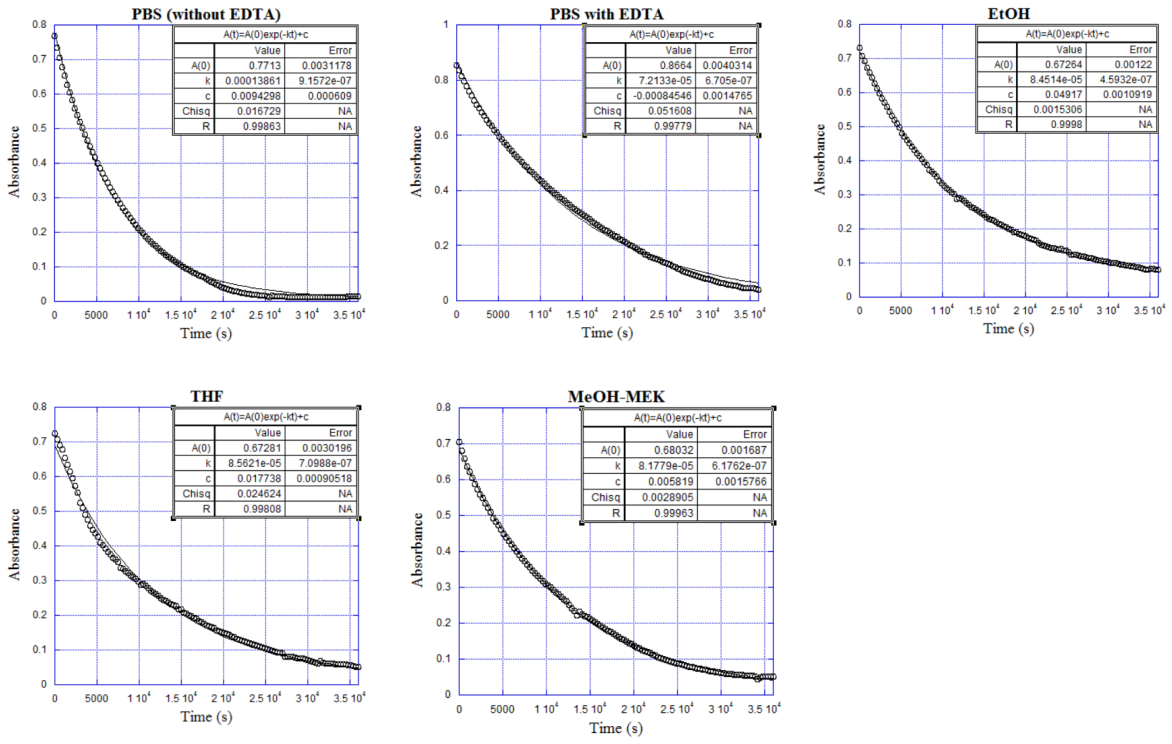

Figure 3.6. SNAP decomposition (formation of NO) in various solvents at 60 °C represented by absorbance of SNAP at 380 nm versus time (s). The decomposition of SNAP in solvent is a pseudo-first-order reaction. All decomposition reactions were fit into the equation $A(t) = A(0)\exp(-kt) + c$, where $A(t)$ represents the concentrations of SNAP at time t, $A(0)$ represents the initial concentration, k is the reaction rate coefficient, and c is the correct constant for instrumental system error.

In agreement with previously reported results, in PBS without EDTA, the decomposition of SNAP is accelerated, due to the presence of trace levels of metal catalysts, such as Cu^{2+} ions.[52,53] In PBS-EDTA solution, EDTA chelates any copper ions, and as a result, the rate constant of SNAP decomposition in PBS-EDTA is comparable to those in the other selected organic solvents, with half-lives all within a 3 h period (see Table 3.1). When SNAP is in the CarboSil polymer "solid solution", the SNAP decomposition is primarily through thermal and photochemical decomposition, instead of metal ion catalysis.[54]

Table 3.1. The reaction rate constants of SNAP decomposition in various solvents at 60 °C.

Solvent	Reaction rate constant (10^{-7} s^{-1})	Half-life (min)
PBS (without EDTA)	1389 ± 3	83 ± 0
PBS with EDTA	721 ± 0	160 ± 0
EtOH	852 ± 7	136 ± 1
THF	845 ± 11	137 ± 2
MeOH-MEK	820 ± 2	141 ± 3

3.4.3 SNAP crystallization process in CarboSil polymer

It was proposed in our previous work [6] that during solvent evaporation, as the amount of the solvent decreases, SNAP eventually reaches to its saturation in CarboSil and then crystallizes. As a follow-up, the crystallization of SNAP within CarboSil polymer was observed *in situ* by optical microscopy while the evaporation of the THF solvent was monitored by weight measurements. Significant loss of weight was observed in the first half hour due to the THF evaporation (see Figure 3.7).

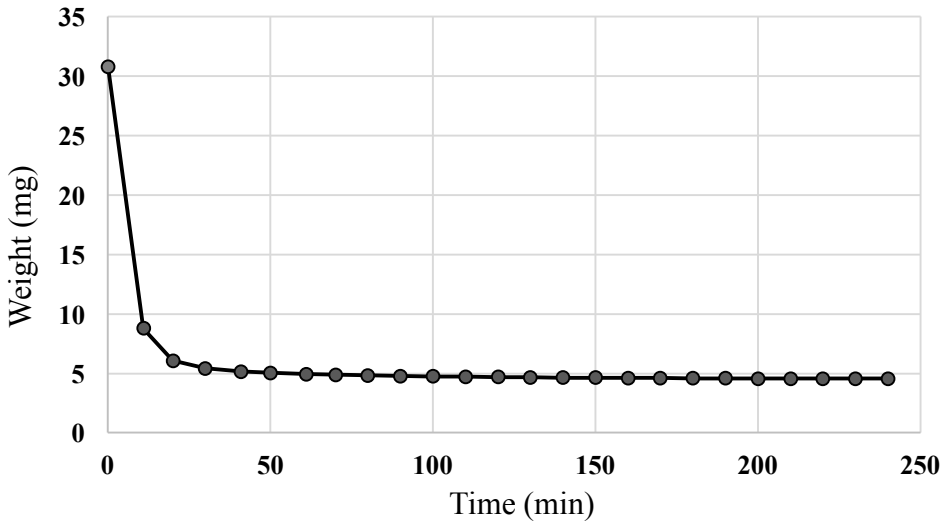

Figure 3.7. The weight of 8 wt% SNAP-CarboSil (dissolved in THF) droplet (mg) decreases over time, as the polymer-crystal composite forms during the solvent evaporation.

Formation of SNAP crystals was first visually detected after 40 min, when most of THF has evaporated, followed by rapid crystal growth. Such behavior is analogous to crystallization in a supersaturated liquid solution, except that the "solvent" for SNAP is the solid CarboSil polymer, once most of the THF has evaporated. As THF evaporates, SNAP reaches its solubility limit in CarboSil and then forms a supersaturated solid "solution". Once crystalline seeds form, crystal growth is relatively fast, as shown in Figure 3.8, which can stem from the mobility of SNAP molecule in the presence of any remaining THF solvent in the polymer.[55–57] This crystallization process observed experimentally in real time helps to verify our previous theory.[6]

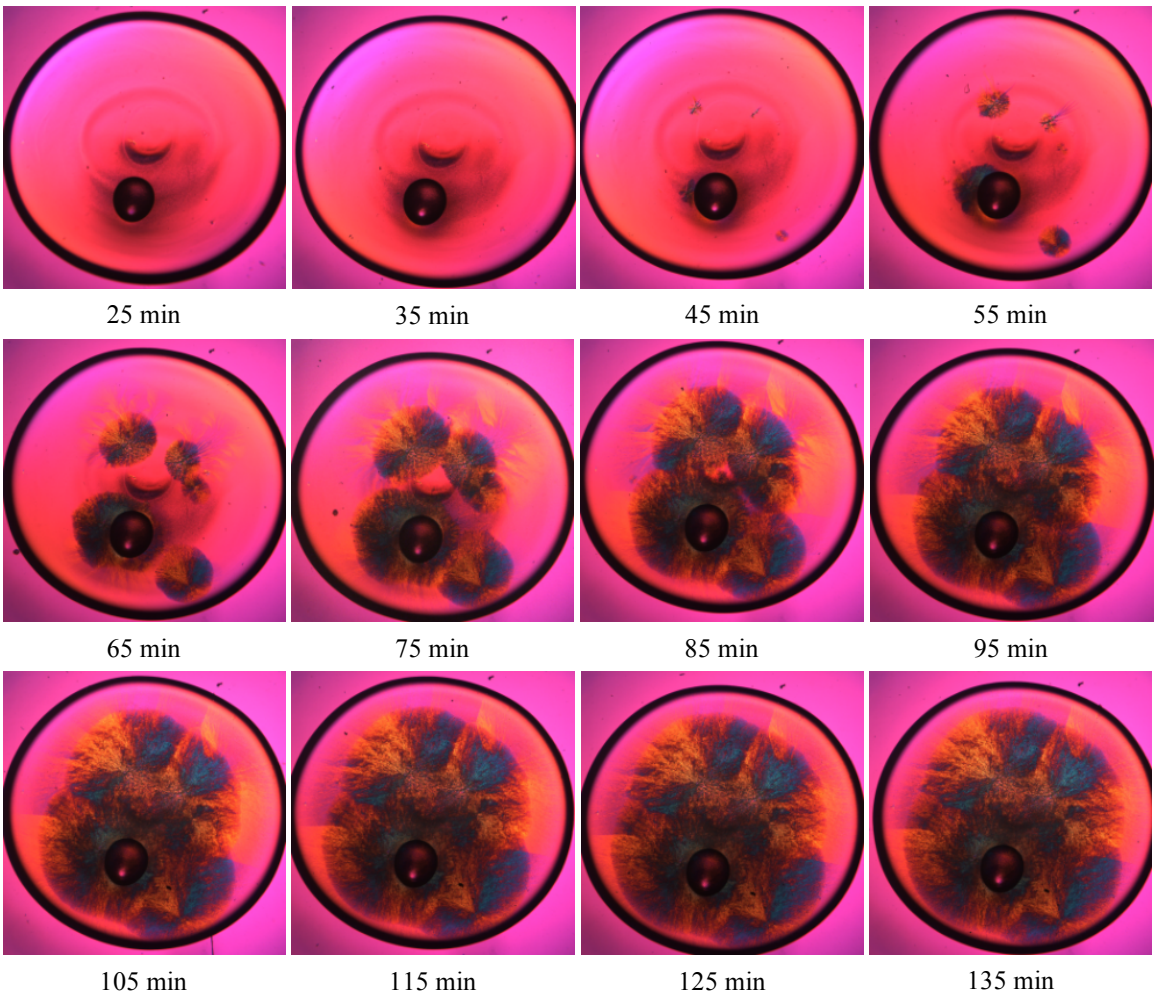

Figure 3.8. Optical images of SNAP crystallization in CarboSil by evaporation. The first image was the one taken after 25 min of solvent evaporation, followed by images captured at 10 min interval.

3.4.4 Study of antimicrobial efficiencies

To evaluate the potential of NO releasing catheters being used as antimicrobial devices, including both intravascular and urinary catheters, we examined the antimicrobial properties of CarboSil catheters (2 mm i.d. and 4 mm o.d.) containing 20 wt% SNAP against two common infection-causing bacteria: *P. aeruginosa* and *P. mirabilis*. *P. aeruginosa* has been reported to be one of the leading bacterium that causes catheter-related blood stream infections, and represents 16% of all the CRBSI cases.[58,59] Infections caused

by *P. aeruginosa* also often occur in patients already battling with more severe illness, e.g., extensive trauma, burns, or malignancy.[60] It is very important to examine the antimicrobial effect of NO against this particular strain of bacteria because *P. aeruginosa* possesses NO reductase enzyme that may enable the bacteria cells to metabolize and deactivate NO, by converting NO to nitrous oxide (N_2O) and ultimately to nitrogen.[61–63] On the other hand, the primary bacterium associated with persistent and complicated catheter-associated urinary tract infections (CAUTIs) is *P. mirabilis*,[3,64,65] which is also known for its ability to elevate urine pH, induce calcium/magnesium phosphate precipitation and produce mature crystalline biofilms.[3,64,66] The CDC biofilm reactor, a laboratory biofilm reactor system, was used in this study since it provides a good model system that offers an environment that mimics the bacterial growth on the polymer surface under moderate fluid sheer stress.[67] The 20 wt% SNAP-doped CarboSil catheters can release NO at levels > 0.5 x 10^{-10} mol cm^{-2} min^{-1}, the lower end of endothelial NO flux levels, for 3 weeks under physiological conditions (Figure 3.9). Such long-term (21 d) continuous and stable NO release can greatly inhibit the development of mature biofilm on the surface of NO release catheters.

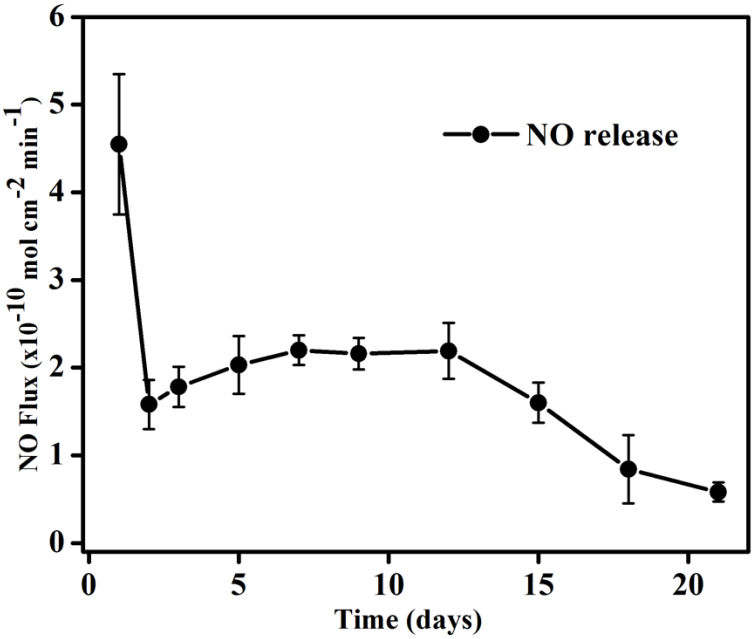

Figure 3.9. NO release from 20 wt% SNAP-doped CarboSil catheters with CarboSil topcoats in PBS at 37 °C for 21 d. Data are mean ± SEM (n=3).

As shown in Figure 3.10, for *P. aeruginosa,* there was a 2 log-unit reduction in the number of viable bacteria adhered on the surface of the SNAP catheters after 14 d compared with other groups and there was no significant difference in the adhesion of bacteria on the three control groups, including NAP-doped catheters, indicating the bactericidal effect of the SNAP CarboSil catheter is solely related to the NO being released during the experiments. These findings were substantiated by the fluorescence imaging data, in which all three control catheter surfaces were covered by high biomass mature biofilm formed by live bacteria (green) while the SNAP catheter surfaces had noticeably less bacterial coverage and most of bacteria on SNAP catheter surfaces were either single or dead (red) bacteria cells. It should be noted that during the process of forming mature biofilm, bacteria cells

that are located within the biofilm experience nutrient limitation, which can result in a stationary phase-like dormancy [68,69] or irregular shapes.[70]

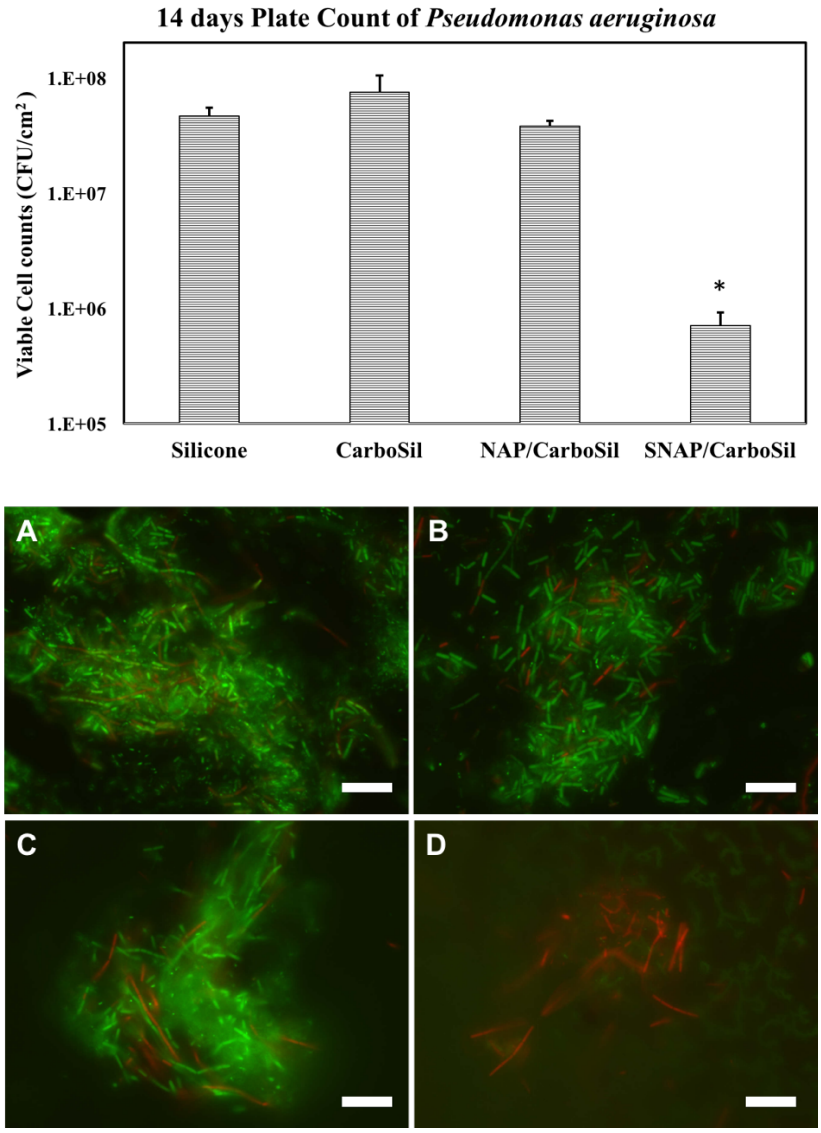

Figure 3.10. Upper image: Bar graph of plate count data for adhesion of viable *P. aeruginosa* bacteria to the surfaces of silicone/CarboSil catheters run in CDC bioreactor for 14 d. Lower images: fluorescence microscopic images of surface live (green) and dead (red) bacteria on different catheters, silicone catheters (A), CarboSil catheters (B), NAP-doped CarboSil catheters (C), and SNAP-doped CarboSil catheters (D) (n=4 for each condition) and their representative fluorescence images; scale bar 20 μm.

Results for the 14 d *P. mirabilis* biofilm culture experiments exhibited a 3 log-unit difference in adhered bacterial cell viability between SNAP catheters and the three different groups of control catheters (see Figure 3.11). The fluorescence imaging data also show that bacterial coverage on the NO releasing catheter is noticeably less than the three controls. Clearly, these results demonstrate that overcoming bacteria colonization and biofilm formation on the surfaces of NO releasing catheter through continuous NO release represents an innovative and highly desirable approach to prevent bacterial biofilm formation, reduce risks associated with catheter-related bloodstream infections and urinary catheter infections. Hence, the use of SNAP-doped CarboSil catheters should ultimately lead to improved device performance and patient outcomes.

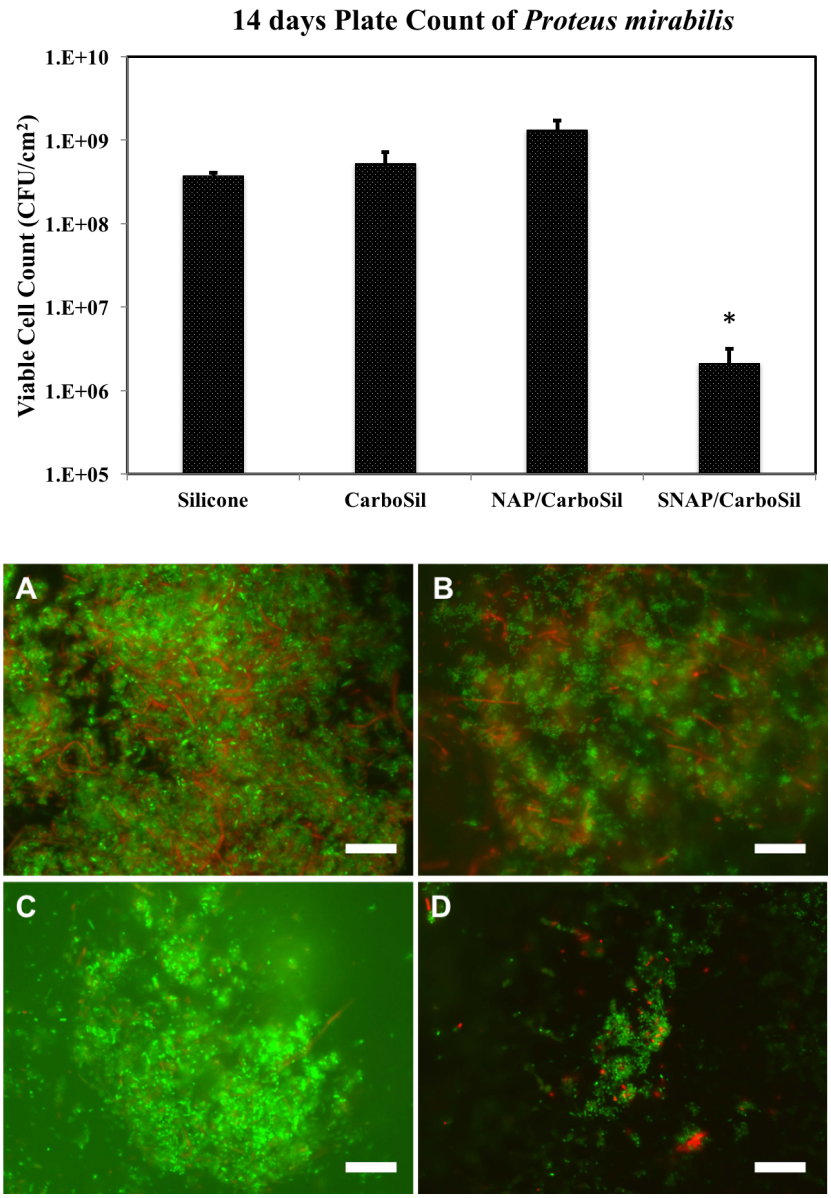

Figure 3.11. Upper image: Bar graph of plate count data for adhesion of viable *P. mirabilis* bacteria to the surfaces of silicone/CarboSil catheters run in CDC bioreactor for 14 d. Lower images: fluorescence microscopic images of surface live (green) and dead (red) bacteria on different catheters, silicone catheters (A), CarboSil catheters (B), NAP-doped CarboSil catheters (C), and SNAP-doped CarboSil catheters (D) (n=4 for each condition) and their representative fluorescence images; scale bar 20 μm.

3.5 Conclusion

In summary, in this work we have provided the first real-time observation of the formation of SNAP crystallization within a polymer phase that creates a unique composite material

for potential biomedical applications. SNAP crystals form and become embedded within CarboSil polymer when the SNAP concentration increases and exceeds its solubility during organic solvent (e.g., THF) evaporation. It is also clear that in addition to the SNAP concentration in the polymer matrix, the NO release profile (level of NO release and longevity of NO release) from such polymers is directly related to the water-contacting polymer surface area and the thickness of specific SNAP-doped CarboSil polymeric material. The decomposition of solubilized SNAP is a pseudo-first-order reaction proportional to the SNAP concentration. The SNAP-doped CarboSil catheters were also shown to exhibit significant antimicrobial properties against the bacteria *P. aeruginosa* and *P. mirabilis*, which are known to be associated with high rates of hospital infections for intravascular and urinary catheters, respectively. Such an NO release composite material provides a cost-effective strategy to potentially improve the antimicrobial properties of indwelling intravascular and urinary catheters, as well as other implantable medical devices.

3.6 References

1 R. M. Donlan, *Emerg. Infect. Dis.*, 2001, **7**, 277–81.
2 T. F. C. Mah and G. A. O'Toole, *Trends Microbiol.*, 2001, 9, 34–39.
3 S. M. Jacobsen, D. J. Stickler, H. L. T. Mobley and M. E. Shirtliff, *Clin. Microbiol. Rev.*, 2008, **21**, 26–59.
4 P. J. Pronovost, C. A. Goeschel, E. Colantuoni, S. Watson, L. H. Lubomski, S. M. Berenholtz, D. A. Thompson, D. J. Sinopoli, S. Cosgrove, J. B. Sexton, J. A. Marsteller, R. C. Hyzy, R. Welsh, P. Posa, K. Schumacher and D. Needham, *BMJ*, 2010, **340**, c309.
5 P. Pronovost, D. Needham, S. Berenholtz, D. Sinopoli, H. Chu, S. Cosgrove, B. Sexton, R. Hyzy, R. Welsh, G. Roth, J. Bander, J. Kepros and C. Goeschel, *N. Engl. J. Med.*, 2006, **355**, 2725–2732.
6 Y. Wo, Z. Li, E. J. Brisbois, A. Colletta, J. Wu, T. C. Major, C. Xi, R. H. Bartlett, A. J. Matzger and M. E. Meyerhoff, *ACS Appl. Mater. Interfaces*, 2015, **7**, 22218–22227.
7 N. Fernandez-Hidalgo, B. Almirante, R. Calleja, I. Ruiz, A. M. Planes, D. Rodriguez, C. Pigrau and A. Pahissa, *J. Antimicrob. Chemother.*, 2006, **57**, 1172–1180.
8 M. Pollini, F. Paladini, M. Catalano, A. Taurino, A. Licciulli, A. Maffezzoli and A. Sannino, *J. Mater. Sci. Mater. Med.*, 2011, **22**, 2005–2012.
9 D. Roe, B. Karandikar, N. Bonn-Savage, B. Gibbins and J. baptiste Roullet, *J. Antimicrob. Chemother.*, 2008, **61**, 869–876.
10 E. M. Hetrick and M. H. Schoenfisch, *Chem. Soc. Rev.*, 2006, **35**, 780–789.
11 S. Rossi, A. O. Azghani and A. Omri, *J. Antimicrob. Chemother.*, 2004, **54**, 1013–1018.
12 N. D. Allan, K. Giare-Patel and M. E. Olson, *J. Biomed. Biotechnol.*, 2012, **2012**.
13 M. Fischer, M. Vahdatzadeh, R. Konradi, J. Friedrichs, M. F. Maitz, U. Freudenberg and C. Werner, *Biomaterials*, 2015, **56**, 198–205.
14 N. Gatter, W. Kohnen and B. Jansen, *Zentralblatt für Bakteriol.*, 1998, **287**, 157–169.
15 P. Ramritu, K. Halton, P. Collignon, D. Cook, D. Fraenkel, D. Battistutta, M. Whitby and N. Graves, *Am. J. Infect. Control*, 2008, **36**, 104–117.
16 N. Høiby, T. Bjarnsholt, M. Givskov, S. Molin and O. Ciofu, *Int. J. Antimicrob. Agents*, 2010, **35**, 322–332.
17 A. W. Carpenter and M. H. Schoenfisch, *Chem. Soc. Rev.*, 2012, **41**, 3742–52.
18 L. Ignarro and G. Buga, *Proc. Natl. Acad. Sci. U. S. A.*, 1987, **84**, 9265–9269.
19 M. Vaughn, L. Kuo and J. Liao, *Am. J. Physiol.*, 1998, **274**, 2163–2176.
20 K. M. Vural and M. Bayazit, *Eur. J. Vasc. Endovasc. Surg.*, 2001, **22**, 285–293.
21 M. C. Jen, M. C. Serrano, R. van Lith and G. A. Ameer, *Adv. Funct. Mater.*, 2012, **22**, 239–260.
22 M. C. Frost, S. M. Rudich, H. Zhang, M. A. Maraschio and M. E. Meyerhoff, *Anal. Chem.*, 2002, **74**, 5942–5947.
23 M. A. Starrett, M. Nielsen, D. M. Smeenge, G. E. Romanowicz and M. C. Frost, *Nitric Oxide - Biol. Chem.*, 2012, **27**, 228–234.
24 M. M. Reynolds and G. M. Annich, *Organogenesis*, 2011, **7**, 42–49.

25 C. Bogdan, *Nat. Immunol.*, 2001, **2**, 907–16.
26 C. Nathan, *FASEB J. Off. Publ. Fed. Am. Soc. Exp. Biol.*, 1992, **6**, 3051–3064.
27 B. B. McMullin, D. R. Chittock, D. L. Roscoe, H. Garcha, L. Wang and C. C. Miller, *Respir. Care*, 2005, **50**, 1451–6.
28 A. Pegalajar-Jurado, K. A. Wold, J. M. Joslin, B. H. Neufeld, K. A. Arabea, L. A. Suazo, S. L. McDaniel, R. A. Bowen and M. M. Reynolds, *J. Control. Release*, 2015, **220**, 617–623.
29 Y. Lu, D. Slomberg, B. Sun and M. Schoenfisch, *Small*, 2013, **9**, 2189–98.
30 A. Colletta, J. Wu, Y. Wo, M. Kappler, H. Chen, C. Xi and M. E. Meyerhoff, *ACS Biomater. Sci. Eng.*, 2015, **1**, 416–424.
31 C. J. Backlund, B. V. Worley and M. H. Schoenfisch, *Acta Biomater.*, 2016, **29**, 198–205.
32 A. W. Carpenter, B. V. Worley, D. L. Slomberg and M. H. Schoenfisch, *Biomacromolecules*, 2012, **13**, 3334–3342.
33 R. N. Allan, S. Morgan, S. Brito-Mutunayagam, P. Skipp, M. Feelisch, S. M. Hayes, W. Hellier, S. C. Clarke, P. Stoodley, A. Burgess, H. Ismail-Koch, R. J. Salib, J. S. Webb, S. N. Faust and L. Hall-Stoodley, *Antimicrob. Agents Chemother.*, 2016, **60**, 2456–2466.
34 H. Ren, J. Wu, A. Colletta, M. E. Meyerhoff and C. Xi, *Front. Microbiol.*, 2016, **7**, 1–8.
35 Y. Wo, E. J. Brisbois, R. H. Bartlett and M. E. Meyerhoff, *Biomater. Sci.*, 2016, **4**, 1161–1183.
36 D. a Riccio and M. H. Schoenfisch, *Chem. Soc. Rev.*, 2012, **41**, 3731–41.
37 A. B. Seabra and N. Durán, *J. Mater. Chem.*, 2010, **20**, 1624.
38 H. Handa, E. J. Brisbois and T. C. Major, *J. Mater. Chem. B*, 2013, **1**, 3578–3587.
39 H. Handa, T. C. Major, E. J. Brisbois, K. A. Amoako, M. E. Meyerhoff and R. H. Bartlett, *J. Mater. Chem. B*, 2014, **2**, 1059–1067.
40 E. J. Brisbois, J. Bayliss, J. Wu, T. C. Major, C. Xi, S. C. Wang, R. H. Bartlett, H. Handa and M. E. Meyerhoff, *Acta Biomater.*, 2014, 4136–42.
41 E. J. Brisbois, T. C. Major, M. J. Goudie, R. H. Bartlett, M. E. Meyerhoff and H. Handa, *Acta Biomater.*, 2016, **37**, 111–119.
42 Y. Kang, J. Kim, Y. M. Lee, S. Im, H. Park and W. J. Kim, *J. Control. Release*, 2015, **220**, 624–630.
43 J. Kim, Y. Lee, K. Singha, H. W. Kim, J. H. Shin, S. Jo, D. K. Han and W. J. Kim, *Bioconjug. Chem.*, 2011, **22**, 1031–1038.
44 W. H. Lyle, *J. Rheumatol. Suppl.*, 1981, **7**, 96–99.
45 V. Parameshvara, *Br. J. Ind. Med.*, 1967, **24**, 73–76.
46 K. A. Graeme and C. V Pollack, *J. Emerg. Med.*, 1998, 16, 45–56.
47 M. M. Jones, A. D. Weaver and W. L. Weller, *Res. Commun. Chem. Pathol. Pharmacol.*, 1978, **22**, 581–588.
48 G. Lautner, M. E. Meyerhoff and S. P. Schwendeman, *J. Control. Release*, 2016, **225**, 133–139.
49 M. L. Clarke, J. Wang and Z. Chen, *J. Phys. Chem. B*, 2005, **109**, 22027–22035.
50 E. J. Brisbois, H. Handa, T. C. Major, R. H. Bartlett and M. E. Meyerhoff, *Biomaterials*, 2013, **34**, 6957–66.
51 D. L. Williams, B. S. Haymond and R. D. Bloebaum, *Res. J. Microbiol.*, 2011, **6**,

425–429.
52 D. L. H. Williams, *Transit. Met. Chem.*, 1996, **21**, 189–191.
53 D. L. H. Williams, *Chem. Commun.*, 1996, 1085–1091.
54 D. a Riccio, P. N. Coneski, S. P. Nichols, A. D. Broadnax and M. H. Schoenfisch, *ACS Appl. Mater. Interfaces*, 2012, **4**, 796–804.
55 G. Coquerel, *Chem. Soc. Rev.*, 2014, **43**, 2286–2300.
56 J. W. Mullin, in *Crystallization Fourth Edition*, Butterworth-Heinemann, Oxford, 2001, pp. 216–288.
57 J. W. Mullin, in *Crystallization Fourth Edition*, Butterworth-Heinemann, Oxford, 2001, pp. 181–215.
58 R. Gahlot, C. Nigam, V. Kumar, G. Yadav and S. Anupurba, *Int. J. Crit. Illn. Inj. Sci.*, 2014, **4**, 162–167.
59 R. Parameswaran, J. B. Sherchan, D. Muralidhar Varma, C. Mukhopadhyay and S. Vidyasagar, *J. Infect. Dev. Ctries.*, 2011, **5**, 452–458.
60 D. L. Dunn, *Surg. Clin. North Am.*, 1994, **74**, 621–635.
61 K. P. Reighard and M. H. Schoenfisch, *Antimicrob. Agents Chemother.*, 2015, **59**, 6506–6513.
62 A. W. Carpenter, D. L. Slomberg, K. S. Rao and M. H. Schoenfisch, *ACS Nano*, 2011, **5**, 7235–44.
63 J.-W. Yoo, H. Nurhasni, J. Cao, M. Choi, I. Kim, B. Luel Lee and Y. Jung, *Int. J. Nanomedicine*, 2015, **10**, 3065–3080.
64 S. M. Jacobsen and M. E. Shirtliff, *Virulence*, 2011, **2**, 1–6.
65 B. V Jones, E. Mahenthiralingam, N. a Sabbuba and D. J. Stickler, *J. Med. Microbiol.*, 2005, **54**, 807–13.
66 D. J. Stickler and S. D. Morgan, *J. Med. Microbiol.*, 2006, **55**, 489–94.
67 D. M. Goeres, L. R. Loetterle, M. A. Hamilton, R. Murga, D. W. Kirby and R. M. Donlan, *Microbiology*, 2005, **151**, 757–762.
68 M. C. Walters, F. Roe, A. Bugnicourt, M. J. Franklin and P. S. Stewart, *Antimicrob. Agents Chemother.*, 2003, **47**, 317–323.
69 M. R. Brown, D. G. Allison and P. Gilbert, *J. Antimicrob. Chemother.*, 1988, **22**, 777–780.
70 K. D. Young, *Microbiol. Mol. Biol. Rev.*, 2006, **70**, 660–703.

CHAPTER 4

Reduction of Thrombosis and Bacterial Infection via Controlled Nitric Oxide (NO) Release from *S*-Nitroso-*N*-acetylpenicillamine (SNAP) Impregnated CarboSil Intravascular Catheters

Wo, Y.; Brisbois, E.J.; Wu, J.; Li, Z.; Major, T.C.; Mohammed, A; Wang, X; Colletta, A.; Bull, J.W.; Matzger, A.J.; Xi, C.; Bartlett, R.H.; Meyerhoff, M.E., *ACS Biomater. Sci. Eng., Submitted* [*]

4.1 Introduction

Intravascular (IV) catheters are indispensable in modern-day medical practice, especially within hospital intensive care units.[1,2] They provide necessary vascular access that allows doctors to withdraw blood samples, monitor patients, and administrate medicine in a simple

[*] The principal experiments of this chapter were conducted by Yaqi Wo, with the help of Dr. Zi Li in conducting the solid-state measurements, Dr. Jianfeng Wu in assisting with the microbiology experiments, Mr. Terry C. Major and Dr. Azmath Mohammed in carrying out the animal testing, and Mr. Xianglong Wang for performing the mechanical strength testing of the NO release materials.

fashion; however, their frequent and prolonged use increase patients' risk for complications such as thrombosis and local or systematic infections.[3] Catheter-related thrombosis (CRT) is a common complication in patients with long-term indwelling catheters,[4] and it becomes symptomatic in about 5% of the patients.[5] Device-initiated thrombus formation can lead to thrombi detachment from the device surface that can travel through the vasculature and cause life-threatening obstructions such as pulmonary embolism, deep vein thrombosis, stroke or heart attack.[2,5,6] Use of systemic anticoagulants to prevent CRT is common but not always effective,[5] and can increase the risk of causing hemorrhage[7,8] and/or inducing thrombocytopenia.[7] Another major complication associated IV catheter placement is infection.[1,9–11] Bacterial biofilm, commonly formed on surfaces by microbes sticking to each other, are surrounded and protected by a self-produced extracellular polymeric matrix. The presence of biofilm is one of the main causes of catheter-related blood stream infections (CRBSIs).[3,11,12] Bacterial cells within biofilm are significantly more resistant to antibiotics as well as the patient's innate immune defense system than planktonic phase microbes, and the minimal concentration of antibiotics for eradication of mature biofilm is typically 10-1000 times higher than for the planktonic cells.[13,14]. CRBSIs are the most common cause of nosocomial bacteremia,[10] and each year 150 million IV catheters are implanted in the United States,[15,16] and 250,000 CRBSIs occur annually due to their use.[9,16,17] As a result, it has been reported that CRBSIs dramatically increase the length of hospital stays,[18] mortality rates[19] and overall treatment cost[9,20] per episode.

Many strategies have been suggested in the past to prevent thrombosis and infections from occurring on IV catheters, such as using a catheter lock solution that contains anticoagulant (e.g., heparin) and/or high concentration of antimicrobial agents (e.g., antibiotics).[7,21] Although there have been some success in clinical trials using these methods,[21] others have reported no significant differences in thrombosis reduction between when using heparin lock solution vs. saline solution.[7,22,23] And for most of the studies evaluating antimicrobial lock solutions, the treatment was only evaluated based on negative blood sample cultures, not the presence or absence of biofilm on the catheter itself, a much more specific infection risk indicator.[11] Moreover, there are many concerns emerging from the potential toxicity to the patient resulting from the diffusion or inadvertent flushing of the lock solution into blood circulation,[11,24] as well as the development of antimicrobial resistance.[11,25]

Nitric oxide (NO) is synthesized in the human body from the substrate L-arginine[26] and participates in a variety of physiological processes, including vasodilation, blood pressure regulation, inhibiting platelet activation, maintaining hemostasis in the vasculature, immune response, and wound healing.[27–30] Nitric oxide can prevent activation of platelets, the first step in the coagulation cascade that ultimately leads to thrombus formation.[29,31] Nitric oxide has also been shown to exhibit broad-spectrum antibacterial activity against both gram-positive and gram-negative bacteria, including methicillin-resistant *Staphylococcus aureus* (MRSA).[27,32] NO serves as a bactericidal agent at high levels (200 ppm of gaseous NO),[33–35] but low levels of NO (picomolar to nanomolar range in solution phase) are also a key signaling molecule and mediator in bacterial quorum sensing to minimize bacterial adhesion and disperse biofilm formation.[36,37] Various *S*-nitrosothiols

(RSNOs) are leading candidates as NO donors for incorporation into biomaterials for controlled NO delivery, due to their relatively high stability, and ability to release NO under physiological conditions.[38–40] *S*-nitroso-*N*-acetylpenicillamine (SNAP) is a particularly attractive RSNO species for creating NO releasing biomedical devices because of its low cost, safety (e.g., penicillamine is an FDA approved drug[41]), and potential for long-term NO release applications when it is incorporated into biomedical polymers with very low water uptake.[42,43]

Recently, our lab has developed a very simple impregnation procedure in which SNAP can be impregnated into commercial silicone rubber Foley urinary catheters to achieve long-term NO release capabilities (> 30 d).[44] In this previous work, Colletta et al. obtained 5.43 wt% of SNAP-within the silicone Foley catheter by impregnating the tubing for 24 h in a 125 mg/mL SNAP solution prepared in THF. The antimicrobial efficiency of the NO releasing Foley catheters was demonstrated toward several strains of bacteria associated with catheter associated urinary tract infections. In follow-up work, Brisbois et al. reported the impregnation of commercial Tygon formula 3350 silicone tubing using 25 mg/mL of SNAP in THF for 24 h and then used the tubing for preparing extracorporeal circuits (ECC). These NO releasing ECC loops exhibited improved blood compatibility over corresponding controls without NO release in a 4 h rabbit thrombogenicity model.[45]

It is well known that molecular interactions between polymer surfaces and protein molecules determine the biocompatibility of a polymer[46] and the innate hemocompatibility of the polymer that contacts blood can greatly influence its ultimate efficacy in preventing

thrombus formation.[47] Indeed, Handa et al. evaluated the intrinsic hemocompatibility of four different biomedical grade polymers *in vivo* and the results demonstrated that polyurethane copolymers (such as Elast-eon E2As, a block copolymer of polyurethane and polydimethylsiloxane) have enhanced inherent hemocompatibility compared to the other polymers, including polyurethanes (e.g., Tecoflex SG-80A) and poly (vinyl chloride) (PVC).[47] CarboSil 20 80A, similar to Elast-eon E2As, is a tri-block copolymer of polyurethane, poly(dimethylsiloxane) and polycarbonate, synthesized from hard segments 4,4'-methylene bisphenyl diisocyanate with glycol chain extender and soft segments of aliphatic polycarbonate and poly(dimethylsiloxane).[46] Studies have shown that there is a strong interaction between fibrinogen and CarboSil polymer surface when fibrinogen is adsorbed onto CarboSil and very few conformational changes of the adsorbed fibrinogen is observed,[46] which is an important step in preventing thrombus formation in the coagulation cascade initiated by protein adsorption.[27] Therefore, CarboSil is a very attractive material for preparing IV catheters owing to its enhanced innate hemocompatibility.[43,46] IV catheters or other biomedical devices made with NO releasing CarboSil should have more enhanced efficacy in reducing platelet activation and thrombus formation than CarboSil alone. Of note, the impregnation method described earlier[44,45] was developed for silicone rubber and THF is a good solvent for silicone since it can swell the tubing to ca. 1.3 times its original size.[45] However, the compatibility between various solvents and polymers are quite different in different scenarios.[48] For example, since THF is known to be able to dissolve instead of swell CarboSil polymer,[43] different solvents need to be selected in order to adapt this methodology to CarboSil. Moreover, many other aspects of the previously reported impregnation process (e.g., the SNAP concentration,

impregnation time, etc.) needs to be optimized to achieve the best efficiency for SNAP impregnation into CarboSil. Herein, we report our effort to modify the SNAP impregnation method to transform premade dip-coated CarboSil 20 80A IV catheters into NO releasing catheters. The optimized SNAP impregnation process and material characterization (including solid-state analysis of the SNAP within the CarboSil polymer) are described in detail. The resulting catheters are further evaluated for their antimicrobial efficacies *in vitro* against *Staphylococcus epidermidis* [16,49,50] and *Pseudomonas aeruginosa*,[10] two bacteria that are commonly reported to cause CRBSIs. In addition, the IV CarboSil catheters are also evaluated within the jugular veins of rabbits to examine their effectiveness at preventing thrombus formation.

4.2 Experimental Section

4.2.1 Materials

N-Acetyl-D-penicillamine (NAP), sodium nitrite, L-cysteine, sodium chloride, potassium chloride, sodium phosphate dibasic, potassium phosphate monobasic, copper (II) chloride, ethylenediaminetetraacetic acid (EDTA), tetrahydrofuran (THF) and *N*,*N*-dimethylacetamide (DMAc) were purchased from Sigma-Aldrich (St. Louis, MO). *N*-Acetyl-D,L-penicillamine disulfide (NAP disulfide) was obtained from Enzo Life Science, Inc. (New York, NY). Methanol (MeOH), methyl ethyl ketone (MEK), hydrochloric acid, sulfuric acid, Luria Bertani (LB) broth and LB agar were products of Fisher Scientific (Hampton, NH). CarboSil 20 80A was obtained from DSM Biomedical Inc. (Berkeley, CA). An Agilent ZORBAX rapid resolution high definition (RRHD) Eclipse Plus C18 column (2.1 x 50mm, 1.8 μm particle size) was purchased from Altmann Analytik GmbH

& Co.KG (Munich, Germany). All aqueous solutions were prepared with 18.2 MΩ-deionized water using a Milli-Q filter from EMD Millipore (Billerica, MA). Phosphate buffered saline (PBS), pH 7.4, containing 138 mM NaCl, 2.7 mM KCl, 10 mM sodium phosphate, and 100 μM EDTA was used for all *in vitro* experiments. *S. epidermidis* ATCC 14990 and *P. aeruginosa* ATCC 27853 were obtained from the American Type Culture Collection (ATCC) (Manassas, VA).

4.2.2 Preparation of SNAP-impregnated films and catheters

SNAP was synthesized as previously reported.[42,43,51] In brief, an equimolar ratio of NAP and $NaNO_2$ was added to a 1:3 mixture of water and methanol containing 2 M H_2SO_4 and 2 M HCl. The reaction vessel was placed in an ice bath for 5 h while the green SNAP crystals precipitated. The crystals were collected by vacuum filtration, rinsed with iced DI water to remove any residues and allowed to air dry for 24 h before being stored in the freezer at -20 °C. The entire synthesis process was performed in the absence of ambient light.

In order to determine the ideal solvent combination for optimal SNAP impregnation into CarboSil, a series of solvents were screened for their ability to swell CarboSil polymer pellets and dissolve SNAP. The swelling capability of the solvents was reported in percent as equation 4.1:

$$\text{swelling ratio (\%)} = (R_{after}-R_{before})/R_{before} \times 100 \quad [4.1]$$

where R_{before} and R_{after} are the radius of the polymer pellets before and after the solvent impregnation process, respectively.

Polymer films containing various wt% of SNAP were prepared by solvent impregnation. First, 200 mg of the CarboSil polymer was dissolved in 2 mL THF and then cast in a Teflon ring (d = 2.5 cm) on a Teflon plate and left to dry overnight under ambient condition to obtain the blank polymer films. Small disks (d = 0.7 cm) were cut from the parent films and used as blank films. Some blank CarboSil films were impregnated in SNAP solutions (120 mg/mL) in 30 % MeOH and 70 % MEK for different lengths of time and the amount of SNAP (wt %) in the final films were analyzed to obtain time needed to achieve maximum SNAP impregnation into the polymer films. The CarboSil films were also treated with solutions containing different concentrations of SNAP (5.5 – 120 mg/mL) for 2 h to achieve a polymer impregnation profile in regard to the SNAP concentration in the impregnation solution.

The catheters used in the *in vitro* and *in vivo* experiments were prepared by dip coating CarboSil polymer solution on 20 cm long stainless steel mandrels of 1.0 mm diameter (McMaster Carr, IL). The control catheters and SNAP catheters were preparing by dip coating 22 coats and 20 coats of polymer solution at 2 min intervals between each coat, respectively. All catheters were allowed to dry overnight under ambient conditions, protected from light, and then removed from the mandrel. Similar to the SNAP-impregnated films, the SNAP-doped catheters were also prepared by soaking in a SNAP solution (120 mg/mL) for 2 h. Then the catheters were removed from the solution, rinsed with MeOH to wash off the residual SNAP solution on the surfaces, and then allowed to air dry overnight to allow the MeOH and MEK solvents to evaporate further, while the

SNAP remains in the catheter. To achieve a smoother surface after impregnation and to prolong NO release, two coats of plain CarboSil polymer solution were applied to the outer surface of the SNAP-impregnated catheters by dip-coating to achieve a total of 22 coats. All the cured films and catheters were dried under vacuum for additional 48 h to remove solvents more thoroughly. The resulting catheters have an i.d. of 1 mm and an o.d. of 2.2 mm.

4.2.3 Characterization of SNAP-impregnated films and catheters

4.2.3.1 UV-Vis

All UV-Vis spectra of solvent dissolved pieces of known mass of the films or catheters (in DMAc) were recorded in the wavelength range of 250 nm - 650 nm with a UV-Vis spectrophotometer (Lambda 35, Perkin-Elmer, MA) at room temperature. The molar absorptivity of SNAP in PBS at 340 nm was determined as ε_{SNAP}= 1075 M^{-1} cm^{-1}. The characteristic absorbance at 340 and 590 nm correlate to the $\pi \rightarrow \pi^*$ and $n_N \rightarrow \pi^*$ electronic transitions of the S-NO functional group.[52,53]

4.2.3.2 NO release measurement from SNAP-impregnated catheters

Nitric oxide release from the SNAP-impregnated CarboSil catheters was measured using a Sievers chemiluminescence Nitric Oxide Analyzer (NOA) 280i (Boulder, CO). For example, a 15 wt% SNAP-impregnated CarboSil catheter with 2 CarboSil topcoats was placed in the sample vial containing 4 mL of 10 mM PBS, pH 7.4, with 100 μM EDTA at 37 °C to mimic physiological conditions. Nitric oxide was continuously generated and immediately purged and swept into the chemiluminescence detection chamber by a N_2

sweep gas and bubbler. All catheters were placed in fresh PBS buffer during NO release measurements and incubated at 37 °C in the absence of ambient light after each measurement. The reported NO flux was the average flux during 4 h of NO release measurements for each time point.

4.2.3.3 Cumulative NAP, NAP disulfide and SNAP leaching from SNAP-impregnated catheters in soaking PBS buffer

The cumulative leaching of NAP, NAP disulfide and SNAP from the impregnated catheters into 10 mM PBS, pH 7.4, with 100 μM EDTA at 37 °C were analyzed using liquid chromatography-tandem mass spectrometry (LC-MS), as previously described in detail.[43] Briefly, 15 wt% SNAP-impregnated CarboSil catheters were incubated in 10 mL PBS buffer, pH 7.4, with 100 μM EDTA in the dark at 37 °C to minimize trace metal catalyzed decomposition of SNAP. At various time points, aliquots (15 μL) of the soaking solution were analyzed for the amount of NAP, NAP disulfide and SNAP in the soaking buffer. The total amount of SNAP-related species is calculated from the following equation 4.2:

$$[\text{all SNAP-related species}]_{total} = [SNAP]_{total} + [NAP]_{total} + 2 \times [\text{NAP disulfide}]_{total.} \quad [4.2]$$

The soaking buffer was replaced with new buffer immediately after the measurement. The total amount of NAP, SNAP and SNAP disulfide leached from the catheter was determined over 14 d consecutive days of measurements.

4.2.3.4 Evaluation of the mechanical properties for catheters before and after impregnation

Four different catheters (5 cm) were prepared for mechanical property tests, including the original CarboSil catheters prepared by dipcoating, CarboSil catheters swelled by solvents only (and then dried), CarboSil catheters impregnated with 7 and 15 wt% SNAP, respectively. Tensile testing of the catheters was performed on an Instron 8800-series machine with Bluehill software (Instron, Norwood, MA). To achieve a better grip on the catheters, the catheters were cut in halves along the axial direction before testing. The catheters had an initial gauge length of 11.55 mm and were pulled at an extension rate of 40 mm/min, corresponding to a strain rate of 0.0593 s^{-1}. The tensile strength (MPa) and maximum elongation (elongated length over the length of the original) were compared for each of the catheter materials tested.

4.2.3.5 Polarized microscope images

SNAP-impregnated polymer films with 5 wt% SNAP loading and a blank reference film of CarboSil, both without topcoats, were prepared as described above. Optical images were captured by a Leica DM2500 LED Microscope (from Leica Microsystems 2016) with a 20× and a 50× objective under crossed polarizers. The images were taken using the Surveyor Software, specifically the 20 x objective image was taken by mosaic imaging and the 50 x objective image (insert) was taken by extended depth of field (EDF) imaging. To better observe the crystal distribution within the impregnated CarboSil polymer, very thin slices (30 μm in thickness) of cross-sections of the 5 wt% SNAP-impregnated CarboSil slices were prepared and observed under the microscope. The film was first cut to expose its cross-section and then embedded into optimal cutting temperature compound (OCT),

allowed to harden at -20 °C, and then cut carefully into 30 μm thick slices by the Leica CM3050S research cryostat. The polymer film slices were then observed under the microscope plate for crystal distribution.

4.2.3.6 Powder X-ray diffraction measurements

SNAP-impregnated polymer films with various wt% SNAP loading and a blank reference film of corresponding polymer, all without topcoats, were prepared as described in Section 4.2.2. Powder X-ray diffraction (PXRD) patterns were collected at room temperature using a Rigaku R-Axis Spider diffractometer with an image plate detector and graphite monochromated Cu-Kα radiation (λ = 1.54187Å) at 40 kV and 44 mA. Synthesized SNAP crystals were finely ground to eliminate preferred orientation, whereas blank CarboSil and SNAP-impregnated CarboSil samples were cut into cubes with dimensions of approximately 250 μm. All samples were mounted on a CryoLoop™ using heavy mineral oil, and images were collected for 15 min with a 0.3 mm collimator. The ω-axis was oscillated between 120° and 180° at 1°/sec, the ϕ-axis was rotated at 10°/sec, and χ-axis was fixed at 45°. The obtained images were integrated from 2.5 to 70° with a 0.1° step size in AreaMax 2.0 software from Rigaku. All powder patterns were processed using Jade 9 XRD Pattern Processing, Identification *&* Quantification analysis software from Materials Data, Inc. The simulated powder patterns of monoclinic and orthorhombic SNAP crystals were calculated in Mercury 3.3 from the CCDC and were compared with the experimental SNAP powder pattern in Jade 9. Quantitation of peak intensity ratios versus SNAP weight percentage was performed in KaleidaGraph 3.5.

4.2.3.7 Effects of ethylene oxide (EO) sterilization

SNAP-impregnated CarboSil films (15 wt%) were prepared and sent to the University of Michigan hospital sterilization facility for ethylene oxide (EO) treatment, a standardized procedure for many medical devices used in clinical applications. Briefly, the films went through 1 h of preconditioning and humidification process, followed by 2-3 h of EtO gas exposure, both performed in a high temperature (54 °C) and high humidity environment (40-80 %). After the 1-2 h of EtO gas evacuation (54 °C), the films were subjected to 12 h of air washes (54 °C). The amount of SNAP remaining in the films was determined by UV-Vis absorbance measurements as previously reported.[43]

4.2.4 Long-term (14 d) in vitro antibacterial experiments

A CDC biofilm reactor system (Biosurface Technologies Corp., Bozeman, MT). was used to test the anti-biofilm properties of SNAP/CarboSil catheters against biofilm formed by *S. epidermidis* and *P. aeruginosa*. The CDC biofilm reactor, its coupon holders and all other connection tubing were autoclaved before use. The EO sterilized catheters were first mounted onto the coupon holders within the reactor and the reactor was then supplemented with sterile nutrient medium (10% Luria Broth) inoculated with overnight bacteria culture (1 to 100 dilution, ~1×10^6 CFU/mL) for 1 h to allow bacterial cell adhesion on the catheter surfaces. The continuous flow of LB broth was controlled at the flow rate of 100 mL/h by a peristaltic pump for 14 days, at 37 °C. The liquid medium was circulated through the vessel and a magnetic stir bar rotated by a magnetic stir plate was used to generate shear force. After incubation for 14 d, the catheters were aseptically removed and each catheter was cut into two 1 cm pieces, that were used for plate counting and imaging, respectively.

For plate counting, the catheter segment was homogenized (OMNI TH, Omni International, Kennesaw, GA) for 30 s in 2 mL of 10 mM sterile PBS (pH 7.4) in order to disintegrate the biofilm to a suspension of isolated cells, which was then diluted by 10-fold each time and plated onto LB agar plates. For imaging, the catheter segment was stained with Live/Dead BacLight Bacterial Vaiability kit (Invitrogen, Carlsbad, CA) for 20 min in the dark, exactly per the kit's instructions. Fluorescence images were acquired with an inverted fluorescence microscope (Olympus IX71, Center Valley, PA) equipped with Fluorescence Illumination System (X-Cite 120, EXFO) and filters for SYTO-9 (excitation = 488 nm/emission = 520 nm) and Propidium Iodide (excitation = 535 nm/emission = 617 nm). Images were obtained using an oil immersed 60× objective lens, in which red indicates dead and green indicates live bacteria.

4.2.5 In vivo antithrombotic evaluation of intravascular catheter in rabbit model

All animal handling and surgical procedures employed in this research were approved by the University of Michigan Committee on the Use and Care of Animals in accordance with university and federal regulations. A total of 3 New Zealand white rabbits (Covance, Battle Creek, MI) were used in this study. All rabbits (2.5-3.0 kg) were initially anesthetized with intramuscular injections of 5 mg/kg xylazine injectable (AnaSed® Lloyd Laboratories Shenandoah, Iowa) and 30 mg/kg ketamine hydrochloride (Hospira, Inc. Lake Forest, IL). Maintenance anesthesia was administered via isoflurane gas inhalation at rate of 1.5-3% by mechanical ventilation via a tracheotomy and using an A.D.S 2000 Ventilator (Engler Engineering Corp. Hialeah, FL). Peek inspiratory pressure was set to 15 cm of H_2O) and the ventilator flow rate was 8 L/min. To facilitate the maintenance of blood pressure

stability, IV fluids of Lactated Ringer's were given at a rate of 10 mL/kg/h. In order to monitor blood pressure and to collect intermittent blood samples for analysis during the experiment, the rabbit's right carotid artery was cannulated using a 16-gauge IV angiocatheter (Jelco®, Johnson & Johnson, Cincinnati, OH). The blood pressure and derived heart rate were monitored by a Series 7000 monitor (Marquette Electronics Milwaukee, WI) while the animal body temperature was monitored with a rectal probe and maintained at 40 °C using a water-jacketed heating blanket. Sample blood analysis (arterial blood pH, PCO_2, PO_2, total hemoglobin and methemoglobin) was conducted using an ABL 825 blood-gas analyzer and an OSM3 Hemoximeter (Radiometer Copenhagen, DK). Prior to the placement of catheters, the rabbit left and right external jugular veins were isolated. Five cm lengths of the catheters (one SNAP and one control) were inserted into the veins. The animals were not treated with anticoagulant systemically during the experiments.

During the experiment, the mean arterial pressure (MAP) of the rabbit was maintained at 35 ± 5 mmHg for 7 h by continuous IV fluid maintenance. The heart rate average was 225 ± 10 beats/min and no significant change was noted for the duration of experiments. The blood gas was measured once every hour and the results were all within the normal ranges. Rabbit whole blood samples were collected in non-anticoagulated 1 cc syringes for activated clotting times (ACT) analysis at the beginning of the experiments. The whole blood samples were also collected by 1 cc heparinized syringes (40 U/mL of sodium heparin) for blood gas analysis every hour for 7 h.

After 7 h of catheter implantation, all animals were first given (400 U/kg) sodium heparin (APP Pharmaceuticals, LLC Schaumburg, IL) systemically to prevent thrombosis during necropsy and were then euthanized with a dose of Fatal Plus (130 mg/kg sodium pentobarbital) (Vortech Pharmaceuticals, Dearborn, MI). The jugular veins were clamped and the catheters were carefully removed from the vein, leaving the thrombus intact on the catheter surface. After rinsing the catheter with saline, any residual thrombus was photographed and quantitated using Image J imaging software provided by the National Institutes of Health (Bethesda, MD).

4.2.6 Statistical analysis

All experiments were conducted in triplicate. Data are all expressed as mean ± SEM (standard error of the mean). Comparison of means using student's t-test was utilized to analyze the statistical differences between SNAP-doped catheters and control catheters. Values of $p < 0.05$ were considered statistically significant for all tests.

4.3. Results and Discussion

4.3.1 Study of SNAP impregnation process of CarboSil polymer films

In order to achieve desired SNAP loading into the CarboSil polymer, an ideal solvent or solvent mixture needs to be employed that has the following properties: 1) high solubility of SNAP; 2) ability to significantly swell CarboSil polymer without harming the material; and 3) evaporate to dryness in a reasonable time period. Therefore, a series of solvents were examined for their ability to swell the CarboSil polymer pellets as well as their SNAP solubility limit. The swell ratio $(R_{after}-R_{before})/R_{before} \times 100$) of solvents were compared and

methyl ethyl ketone (MEK) was found to exhibit the highest swell ratio of 166 ± 9 % (with 155 ± 4 % for acetone, 135 ± 3 % for ethyl acetate and 110 ± 3 % for methanol (MeOH)). However, solubility tests indicated that the SNAP solubility is only 30 mg/mL in MEK, 70 mg/mL in acetone, and 30 mg/mL in ethyl acetate, but 330 mg/mL in MeOH. As a result, a combination of MEK and MeOH was studied in order to determine the optimal solvent composition for maximized SNAP impregnation into CarboSil films and catheters, without destroying the structure of polymer.

To optimize the MEK/MeOH solvent mixture for impregnation, CarboSil polymeric materials (pellets, films or catheters) were totally immersed into various MEK/MeOH swelling solutions (see Figure 4.1), then the material was removed from the swelling chamber, quickly rinsed with MeOH and DI water to decrease any residue on the surface, and then air dried in the ambient environment protected from light exposure.

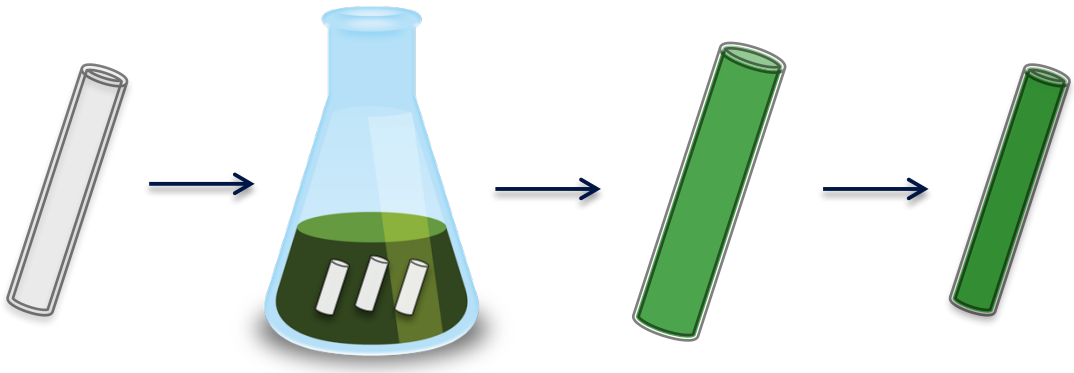

Figure 4.1. The schematic process of SNAP impregnation into CarboSil polymeric material using a CarboSil catheter as an example.

After this process, the polymer material was weighed, and then the impregnated polymer was dissolved in DMAc for UV-Vis absorbance measurements to determine the total amount of SNAP incorporated into the final CarboSil material. The results shown in Figure

4.2 demonstrate that the optimal solvent combination is 70 % MEK and 30 % MeOH (volume ratio). However, 90 % MEK, 10 % MeOH and 80 % MEK, 20 % MeOH can technically incorporate more total SNAP into the CarboSil polymer, but the polymer pellets were easily destroyed and cracked apart during the drying process using these ratios of solvents.

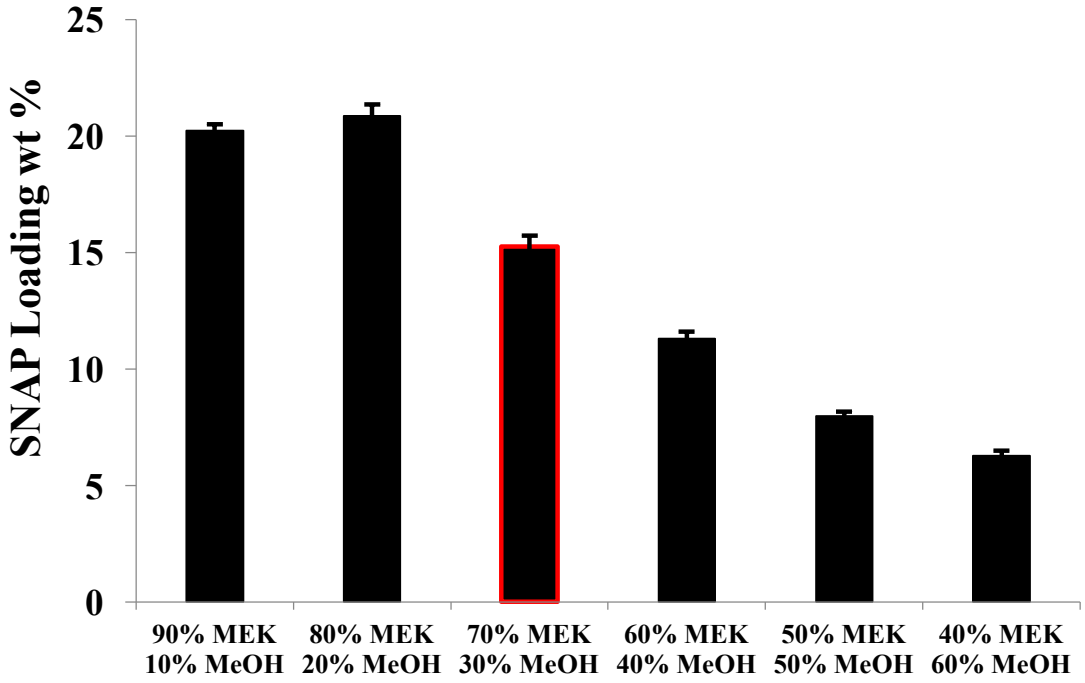

Figure 4.2. The weight percentage (wt%) of SNAP achieved in CarboSil pellets (mg SNAP/mg impregnated CarboSil pellet × 100%) using different solvent mixtures for the impregnation process.

As shown in Figure 4.3, the amount of SNAP impregnated into CarboSil can be modulated and the level directly correlates with the concentration of SNAP employed in the swelling solution (70 % MEK and 30 % MeOH). Indeed, the wt% of SNAP in the final CarboSil material increased from 2.5 % to 15.7 % in near linear fashion when the SNAP concentration increased from 5.5 mg/mL to 120 mg/mL.

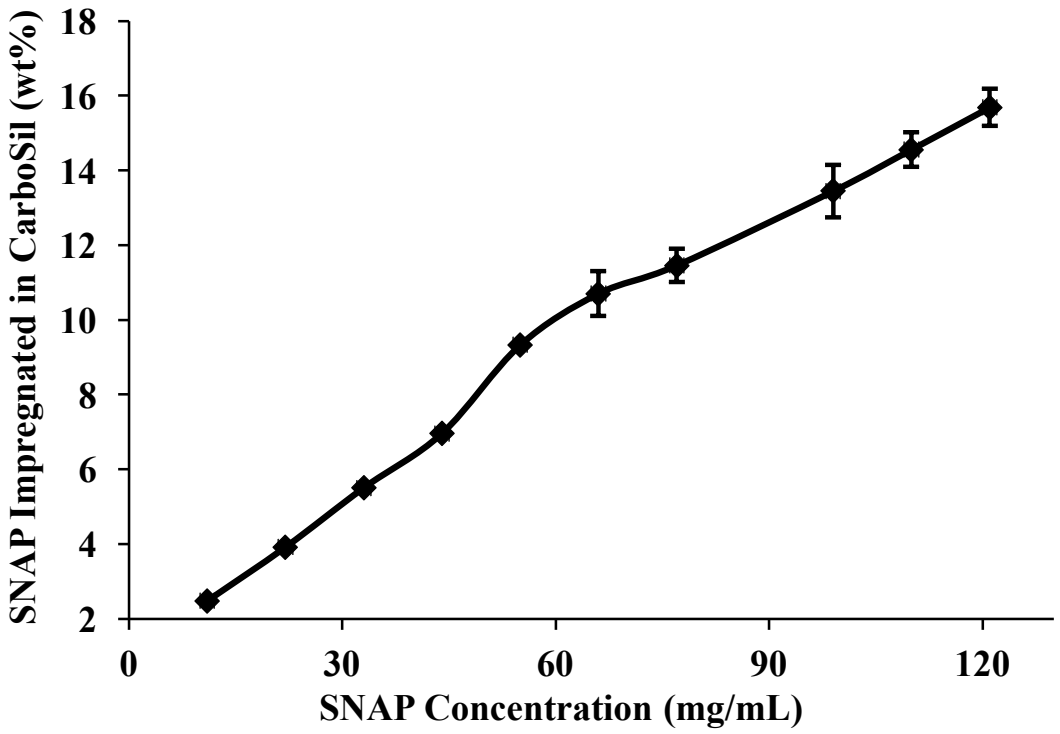

Figure 4.3. The wt % SNAP impregnated in the final CarboSil polymer films correlated with the SNAP concentration in swelling solution consisting of 70% MEK and 30% MeOH and various concentrations of SNAP.

To study the SNAP impregnation kinetics as a function of polymer film thickness and to determine the time required to achieve maximum impregnation, blank CarboSil films of both 250 μm and 500 μm in thickness were prepared. The films were then soaked into a solution of 120 mg/mL SNAP in 70 % MEK/30 % MeOH (n=3 for each condition), for 1, 2, 3, 5, 10, 30, 60, 90, 120 and 150 min, respectively. After thorough drying, the films were weighed and then dissolved in DMAc to quantify the SNAP wt % within the films. The impregnation profile (Figure 4.4) indicated that the maximum impregnation is achieved within 2 h, and there is no significant difference between 250 μm thick films and 500 μm thick films. This suggests that the solvent impregnation process is capable of

incorporating SNAP into various sized catheters (different wall thicknesses, etc.) without requiring any significant additional time to the impregnation process.

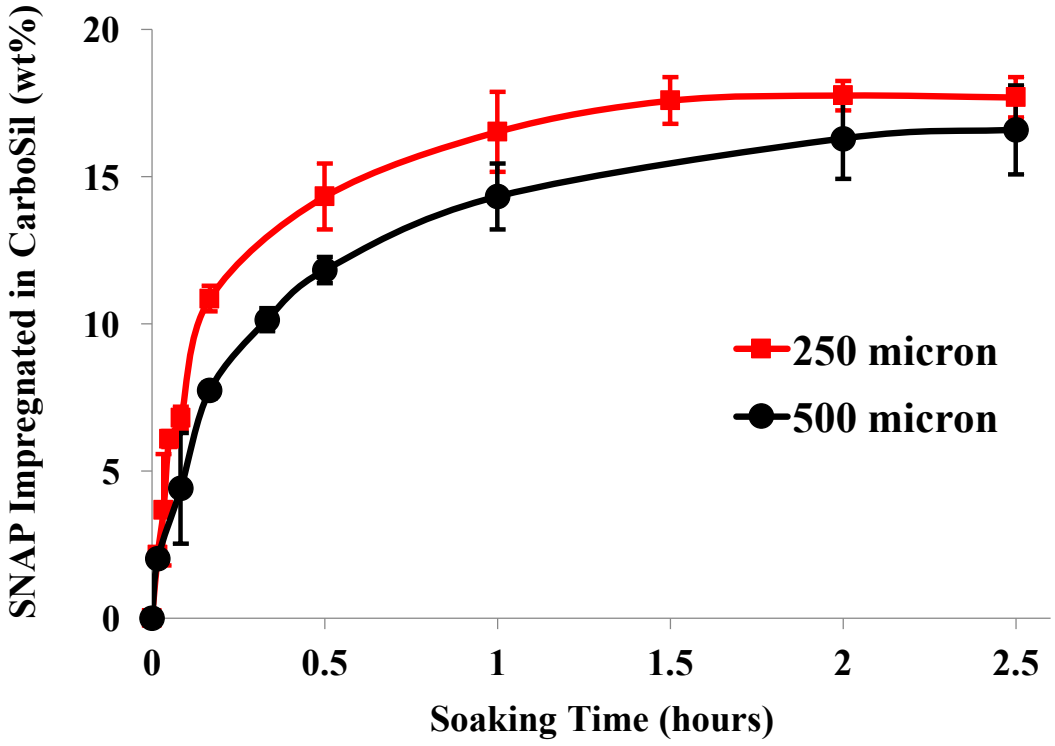

Figure 4.4. The kinetics of SNAP impregnation in CarboSil film using 120 mg/mL SNAP in swelling solution (70% MEK and 30% MeOH), with respect to swelling time and polymer thickness. The results indicate that maximum SNAP incorporation is achieved within 2 h of swelling and there is no significant difference in loading when using films with different thickness (250 μm vs. 500 μm).

4.3.2 Solid-state analysis of SNAP-impregnated CarboSil polymer system

Our group has previously reported solid-state studies of SNAP-doped CarboSil films formed by casting a THF solution containing SNAP and CarboSil polymer into a Teflon plate and allowing the solvent to completely evaporate.[43] The elevated shelf-life stability of SNAP in CarboSil was only observed when the SNAP level within the CarboSil exceeds its solubility in the CarboSil and forms orthorhombic crystals that embed in the bulk of the

polymer matrix. In this work that demonstrates the SNAP impregnation approach using premade CarboSil films, similar solid-state characterizations were conducted to examine the resulting films. As shown in Figure 4.5, clear SNAP crystalline patterns were observed for the 5 wt% SNAP-impregnated samples under a polarized microscope, indicating to the presence of SNAP crystals in the polymer matrix at this SANP concentration.

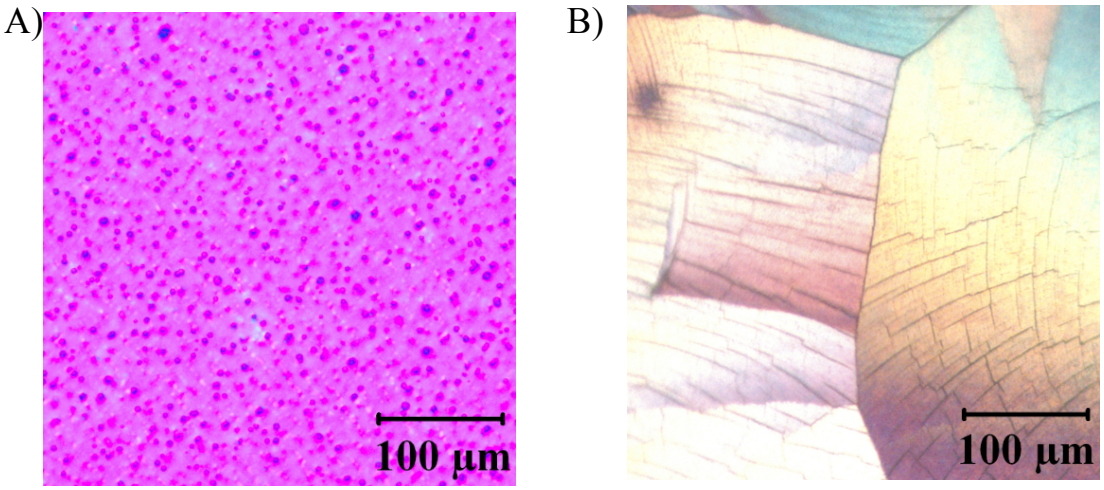

Figure 4.5. Optical image of A) blank CarboSil film and B) 5 wt% SNAP-impregenated CarboSil film surfaces taken under crossed polarizers in combination with a quarter-wave plate. The 5 wt% films present patterns which suggest the presence of crystalline SNAP in the polymer.

Additional microscope images of the cross-section of the SNAP-impregnated CarboSil films were also taken to determine if SNAP impregnated into the bulk polymer matrix or if the crystals exhibit depth dependent distribution when they are formed after the solvent evaporates. Thin slices (30 µm) of the cross-section of 5 wt% SNAP-impregnated CarboSil films were obtained by using the Leica 3050S cryostat. Figure 4.6 shows examples of the optical images of the cross section of the film, which clearly illustrate that SNAP crystals are distributed relatively uniformly within the polymer matrix after impregnation, rather than merely present on the polymer film's outer surfaces.

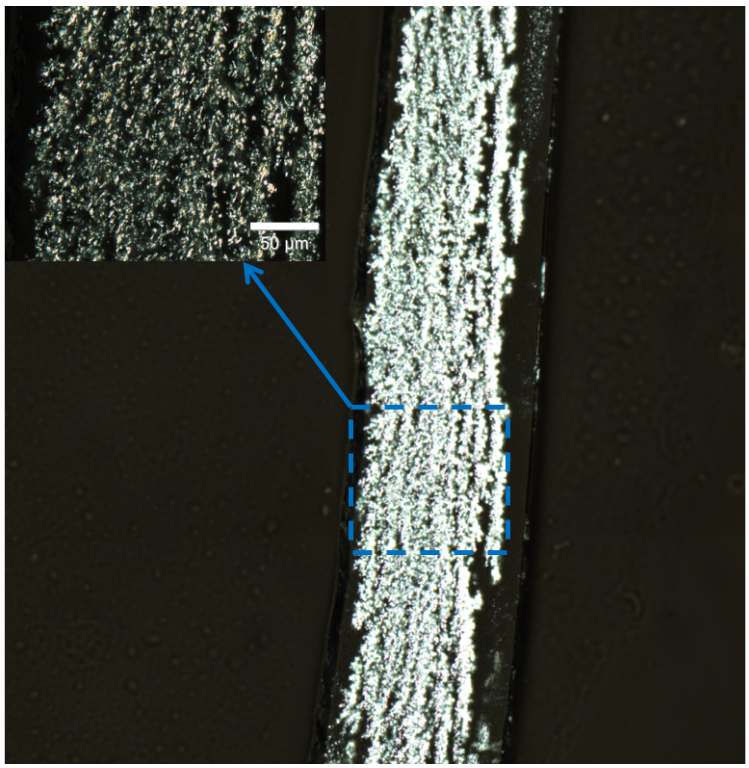

Figure 4.6. Representative optical images of the cross section of 5 wt% SNAP-impregnated. The images were captured by Leica DM2500 LED microscope with a 20× and a 50× (inset) objective under crossed polarizers. The cross-section of film samples was cut into 30 µm thick slices by the Leica 3050S cryostat. The SNAP was impregnated successfully into the bulk of the polymer film and distributed relatively evenly throughout the cross-section.

In principle, SNAP's solubility limit in the CarboSil polymer should be constant regardless of preparation methodology, e.g., casting polymer solution or solvent impregnation. The PXRD patterns of the CarboSil films impregnated with various loading of SNAP were collected and analyzed (Figure 4.7).

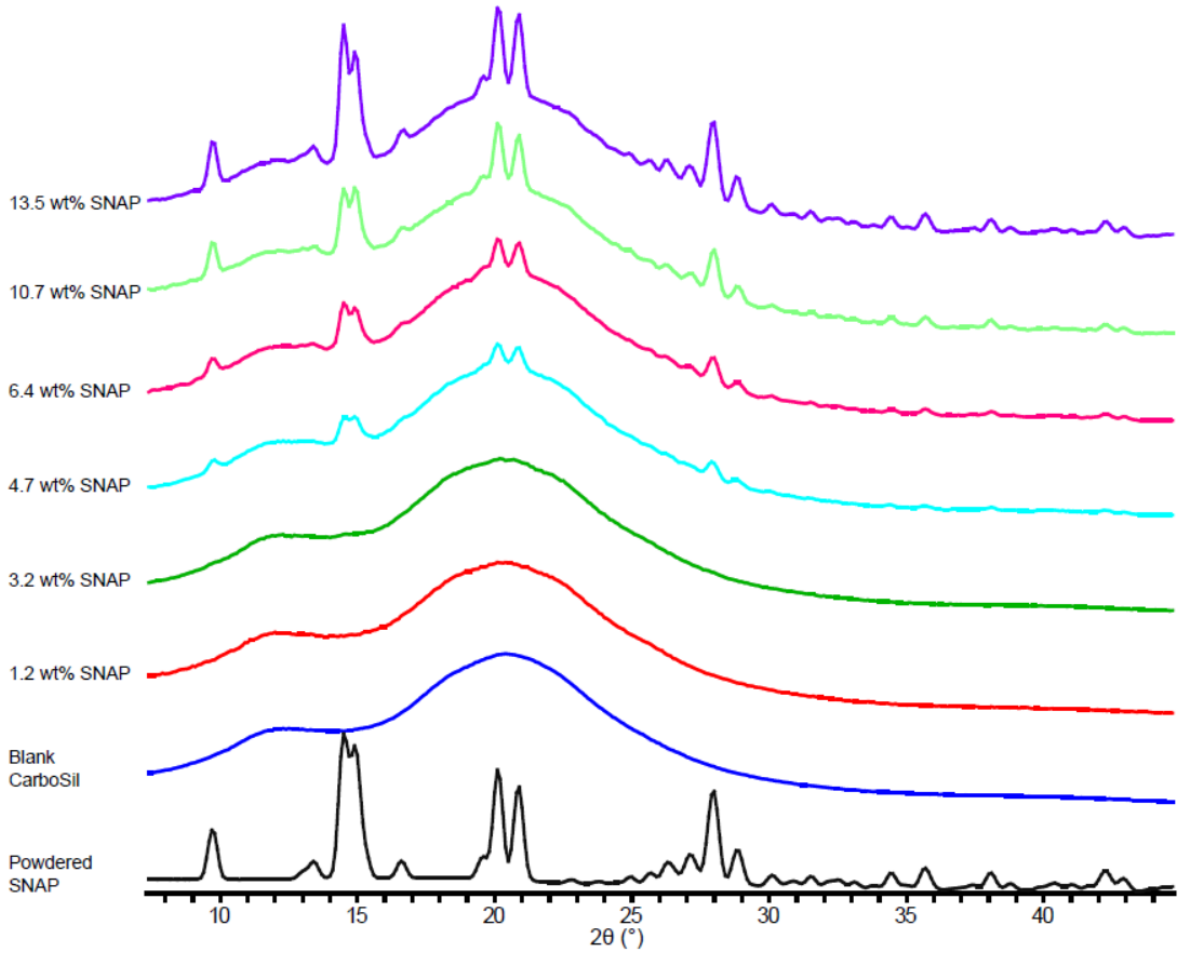

Figure 4.7. Representative PXRD patterns of orthorhombic SNAP crystal, CarboSil blank polymer, and CarboSil impregnated with SNAP of different weight percentages. Characteristic peaks of orthorhombic SNAP were detected in samples. Peak intensity of crystalline SNAP increased with higher loading of SNAP in polymer.

In our previous work, the solubility of SNAP in CarboSil when SNAP was added into polymer solution before casting was calculated by using the ratio of selected SNAP crystalline peak area over the total area of the sample pattern.[43] Herein the method used to calculate the SNAP solubility in the polymers used the ratio of peak heights instead of peak area because this is more generally applicable to various polymers that have broad diffraction peaks. In short, based on the following assumptions that (1) crystalline SNAP is uniformly distributed in the polymer phase, and (2) that the preferred orientation of

SNAP crystals in the polymer could be eliminated by cutting samples into cubes and rotating the samples during data collection, the ratio of a specific SNAP crystalline peak height over the polymer peak height should be proportional to the ratio of crystalline SNAP wt% over the polymer wt % in the sample. By using the height ratio for quantification, all of the other factors that can potentially influence peak intensity (e.g., the volume of the sample irradiated by the X-ray source, the exposure time of sample under the X-ray, etc.) can be eliminated. Here, the SNAP solubility in polymer, represented as x_o, can be calculated from $y_{2\theta}$, the height ratio of a SNAP peak over the height of a polymer peak is calculated using equation 4.3:

$$y_{2\theta} = \frac{I_{SNAP2\theta}}{I_{polymer2\theta}} = \frac{a(x-x_o)}{b(1-x)} \quad [4.3]$$

where $I_{SNAP2\theta}$ and $I_{polymer2\theta}$ are the signal intensities of SNAP and polymer in a SNAP impregnated polymer sample at angle 2θ, obtained in each measurement. For a PXRD pattern of a unit volume sample taken with a unit exposure time, a and b correspond to the peak height of pure orthorhombic crystal and blank CarboSil pattern at a given 2θ, respectively. When the SNAP weight percentage is x, the height ratio of SNAP peak height over CarboSil peak height at a given 2θ ($y_{2\theta}$), should be proportional to the weight percentage ratio of the undissolved SNAP crystal ($x - x_o$) over the weight percentage of CarboSil ($1 - x$). By substituting various x and $y_{2\theta}$ at chosen 2θ angles, the solubility x_o can be determined. Based on this calculation, the solubility of SNAP in the impregnated CarboSil material was found to be 2.4 ± 0.1 wt%, which is significantly lower than the result of 4.3 ± 0.3 wt%, calculated from films obtained by casting SNAP and CarboSil polymer solution (if also using this height based method).[43]

We attribute the decrease in calculated SNAP solubility to insufficient "dissolution" of impregnated SNAP molecules in the polymer to reach its solubility equilibrium in the polymer phase during the solvent impregnation method. When the polymer film is prepared by casting dissolved SNAP in a CarboSil solution (in THF),[43] the SNAP molecules and CarboSil polymer chains are uniformly mixed within the solvent. Therefore, the SNAP molecules are well dispersed in the polymer matrix to form a solid polymer solution before the solvent completely evaporates and the solution reaches its SNAP solubility limit which ultimately leads to the SNAP crystallization (Figure 4.8A). However, during the swelling-impregnation process, SNAP can only be "inserted" into the space between polymer chains when the pre-made CarboSil film is swelled by the MEK/MeOH solvent mixture. The diffusion of SNAP molecules within solid polymers may be less efficient compared to the polymer casting method when SNAP and polymer are all completely dissolved and well mixed. In addition, the swelling effect of solvent mixture may also vary for different polymer segments. For example, the interspace between the soft segments of CarboSil may be swelled more by the solvent and enable easier impregnation of SNAP molecules, which may result in different microenvironments for SNAP crystallization at the different polymer segment sites (see Figure 4.8B). In summary, we hypothesize that SNAP cannot diffuse and reach solubility equilibrium in the polymer during solvent impregnation as easily as it does when SNAP and polymer are well mixed in a solvent, as is in the polymer casting method. Therefore, SNAP aggregates as crystals and forms a polymer crystal composite more readily in the solvent impregnation process that uses pre-made polymer device (e.g., films or catheters).

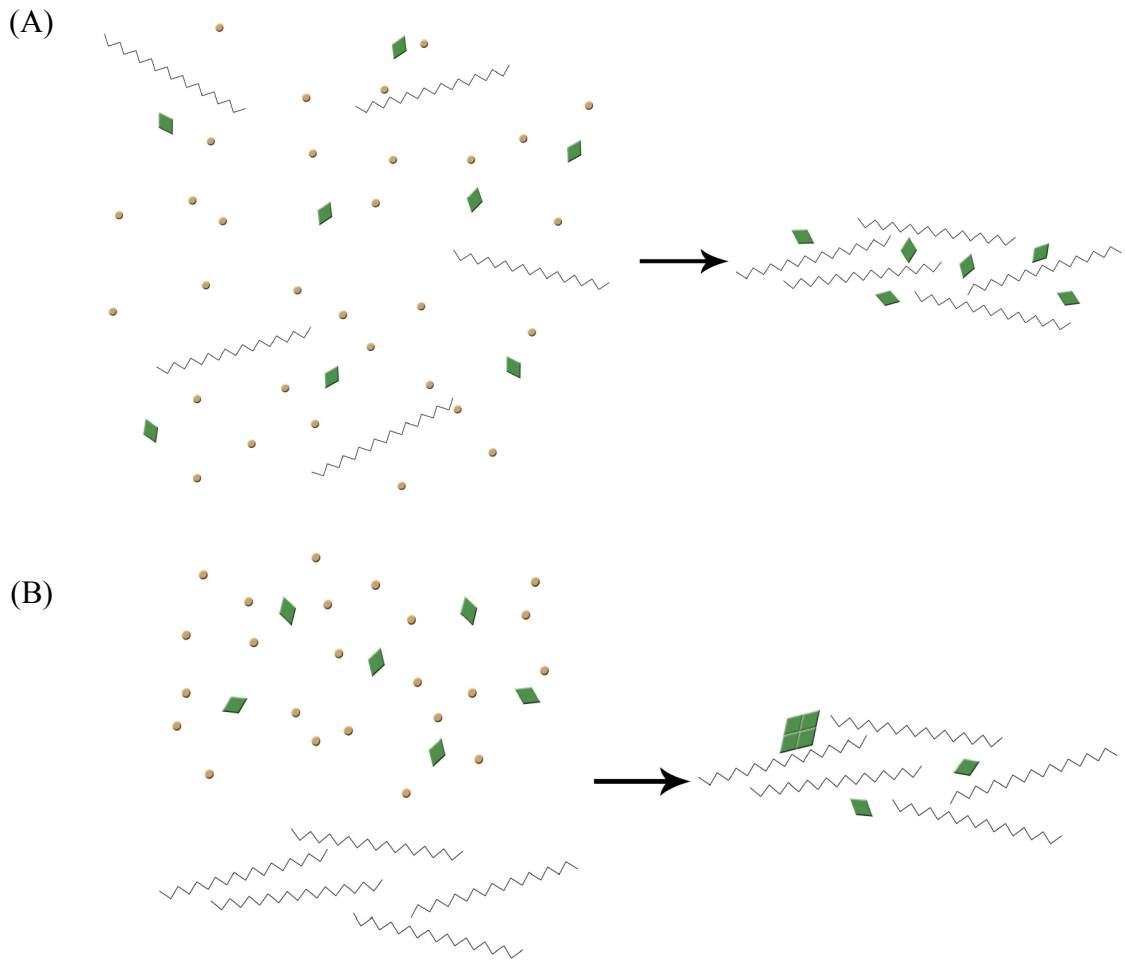

Figure 4.8. Schematic diagram of SNAP distribution in CarboSil polymer prepared by A) casting SNAP and CarboSil polymer solution; and B) polymer solvent impregnation. The lines in the diagram correspond to CarboSil polymer chains, the diamonds correspond to SNAP molecules, and the dots correspond to solvent used in the preparation.

4.3.3 Mechanical properties tests

Tension testing was performed in order to assess the changes in mechanical properties caused by solvent and SNAP impregnation. Of note, the Instron machine was not able to obtain a firm grip on the original CarboSil catheters during the elongation process with the current experimental setup. Thus, the analysis results below only contain three experimental groups; the swelling solvent only, 7 wt% SNAP, and 15 wt% SNAP, with

triplicates of each type of sample tested (n=3). One-way ANOVA results revealed no significant difference in tensile strength (p=0.15) or maximum elongation (p=0.42) among the three groups (see Figure 4.9). The results indicate that the catheters are still mechanically suitable for biomedical use after the impregnation process.

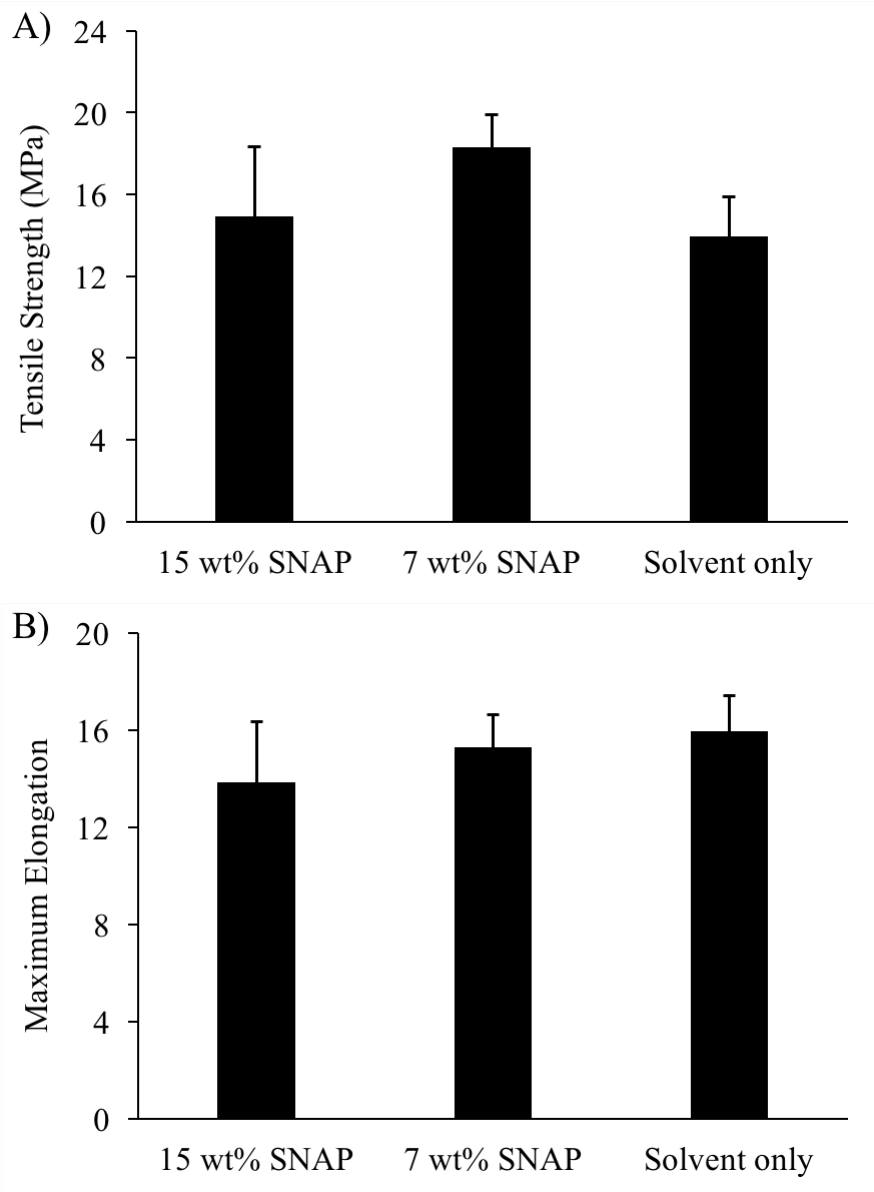

Figure 4.9. Tensile strength testing (A) and the maximum elongation (B) results for CarboSil tubing impregnated by solvents only, and CarboSil tubing with 7 wt% and 15 wt% SNAP loading, respectively. Results are average ± SEM for n=3 for each experiment.

4.3.4 NO release measurement of SNAP-impregnated CarboSil catheters

The 15 wt% SNAP-impregnated CarboSil catheters with CarboSil topcoats release NO above a flux rate of 0.5 x 10^{-10} mol cm^{-2} min^{-1}, for 14 d in PBS buffer at 37 °C. The NO release rate from the catheters was quantitated and recorded by chemiluminescence measurements. A burst of NO release (~4 x 10^{-10} mol cm^{-2} min^{-1}) was observed on day 0, and this correlates with rapid SNAP leaching from the outermost layer of the catheter surface into the buffer. After depletion of the SNAP reservoir in this outermost region, the NO release rate drops to its minimal level at day 2 (~1 x 10^{-10} mol cm^{-2} min^{-1}) and then gradually increases to 4 x 10^{-10} mol cm^{-2} min^{-1} over the next 10 d period (Figure 4.10). The NO release levels then drop below 0.5 x 10^{-10} mol cm^{-2} min^{-1} after d 14, as all the SNAP in the bulk of the polymer has decomposed.

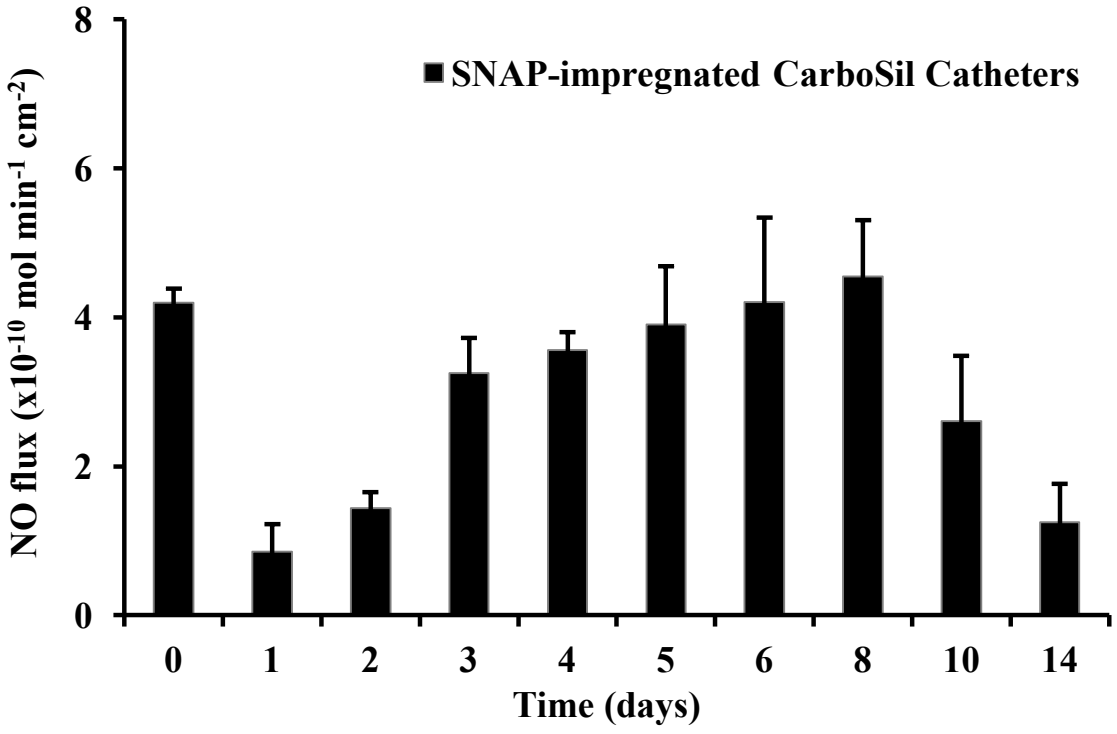

Figure 4.10. The NO release profile of 15 wt% SNAP-impregnated CarboSil catheters over time. The catheters were prepared with CarboSil outer coating (n=3).

As indicated in Section 4.3.2 above, the majority of the SNAP molecules impregnated in the catheters are in their crystalline form, and it takes time for the crystalline SNAP embedded in the bulk of the polymer to dissolve and release its NO. We believe that this slow crystal dissolution process is the reason for the long-term NO release observed from these new SNAP-impregnated CarboSil catheters.

4.3.5 Cumulative leaching of NAP, NAP disulfide and SNAP from SNAP-impregnated CarboSil catheters

The concentrations of NAP, NAP disulfide and SNAP leached from SNAP-impregnated CarboSil catheters were monitored by LC-MS using a method previously reported.[43] As shown in Figure 4.11, 12 % of the initial SNAP (80 nmol/mg polymer) diffuses out of the catheter over the 14 d test period. The rate of SNAP leaching is the greatest in the first few hours after introducing the catheter to the soaking buffer, and then a significant lower amount of SNAP continues to diffuse into the buffer over the following days. Similar leaching patterns were observed for both NAP and NAP disulfide. A total of 12 nmol/mg polymer NAP and 46 nmol/mg polymer NAP disulfide (2 % and 14 % of the initial SNAP present in the catheter, respectively) leached into the buffer over 2 weeks.

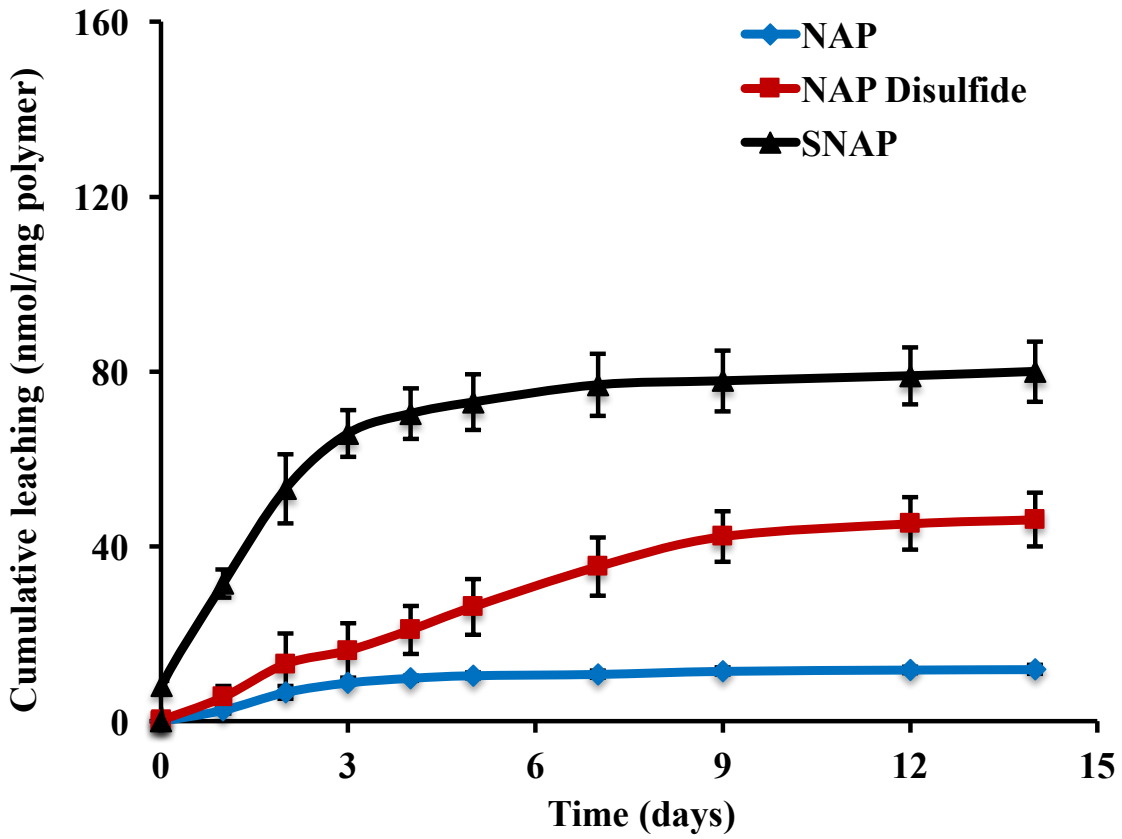

Figure 4.11. Cumulative leaching of NAP, NAP disulfide and SNAP into 1 mL of PBS (soaking buffer) from 15 wt% SNAP-impregnated CarboSil catheters over a period of 14 days, at 37 °C in the dark. Data are mean ± SEM (n=3).

NAP is the parent thiol used in SNAP synthesis, and NAP has been a widely used chelating and detoxifying agent for treating patients with heavy metal ion poisoning (e.g., cadmium, arsenic and mercury) for many years.[54,55] Therefore, NAP and NAP dimer (NAP disulfide) emitted from the SNAP catheter into the buffer or blood stream is considered relatively safe and unlikely to cause any adverse or toxic response in potential clinical applications.[43] Overall, the total moles of SNAP-related species ($[\text{all SNAP-related species}]_{\text{total}}$) leached out over the 14 d test period is approximately 28 % of the total NO (in moles) released from the catheter, which means more than 70 % of the NO is released directly from SNAP

molecules residing within polymeric matrix. Since NO is highly reactive *in vivo* and will be rapidly scavenged by surrounding species (e.g., oxyhemoglobin, oxygen),[56,57] to achieve therapeutic functions of NO, it is essential for the catheters to deliver localized NO release at their surface with minimal NO donor leaching. Based on results from the leaching studies, this appears to be the case for the new SNAP impregnated CarboSil biomaterial.

4.3.6 Prevention of mature microbial biofilm formation

Because stable NO release from biomedical devices is expected to reduce bacterial adhesion and proliferation, *in vitro* antimicrobial experiments were conducted to evaluate the efficacy of SNAP-impregnated Carbosil catheters against bacterial infections caused by microbes, *S. epidermidis* and *P. aeruginosa*, commonly responsible for catheter-related blood stream infections. *S. epidermidis* has always been regarded as an innocuous and commensal inhabitant of healthy mucosal microflora and possesses lower pathogenic potential than *S. aureus* and *P. aeruginosa*,[58] but more recently *S. epidermidis* has been shown to be the most frequent cause of infections on indwelling medical devices.[50,59] This likely stems from the prevalence of *S. epidermidis* on human skin which results in a high probability of contamination during IV catheter insertion. It has also been reported that the primary virulence factor of *S. epidermidis* is its potential capability to form high-biomass biofilm.[44,60–62] Moreover, many studies have shown that treatment of *S. epidermidis* biofilm cells with high dose of antibiotics e.g., rifampicin, vancomycin, etc. accelerates the emergence of highly resistant cells.[16,63,64] Indeed, genome sequence studies of *S. epidermidis* strains isolated from IV catheters in the hospital have expressed specific antibiotic resistance genes and required much higher concentrations of antibiotics for

treatment.[50,59,64,65] The cost related to CRBSIs caused by *S. epidermidis* alone is estimated to $2 billion annually in US.[66] In contrast, gram-negative bacteria account for ~30 % of all episodes of nosocomial bacteremia,[67,68] and *P. aeruginosa* is reported to cause 16 % of all the CRBSIs.[1,69] Infections caused by *P. aeruginosa* often occur in patients with more serious underlying disease, e.g., extensive trauma.[70] Further, it is important to examine the antimicrobial effect of NO release catheters against this particular strain of bacteria because *P. aeruginosa* possesses the NO reductase enzyme which makes the bacteria cells able to metabolize and deactivate NO, and convert NO to nitrous oxide (N_2O) and ultimately nitrogen.[71,72]

The CDC biofilm reactor used in this study provides a model that offers an environment that mimics the bacterial growth on the polymer surface under moderate fluid sheer stress.[73] Therefore this methodology was utilized to stimulate bacterial biofilm development on the surface of IV catheters in the blood stream. All SNAP catheters and control catheters were initially sterilized by ethylene oxide (EO) and kept antiseptic before use. Ethylene oxide sterilization is a routine procedure for sterilizing clinical appliances within hospitals, during which the devices are subjected to high temperature and high humidity level.[74,75] The amount of SNAP remaining in the catheter after EO sterilization was determined to be 97.4 ± 0.8%, suggesting that SNAP is very stable as crystals embedded within the CarboSil polymer during the sterilization process. The sterilized SNAP catheter segments and control catheter segments (n=4) were mounted onto coupons within the CDC bioreactor and bacterial biofilms were formed on the surface of both catheters over a 14 d period at 37 °C. After that time period, the number of live microbes on the surface of the catheters

was determined by plate counting as well as fluorescence imaging. As shown in Figure 4.12 and 4.13, the number of viable *S. epidermidis* and *P. aeruginosa* adhered on the surface of SNAP impregnated catheter segments after 14 d was reduced by 2.0 and 2.5 log units, respectively. These findings were substantiated by the fluorescence imaging data, in which the control catheter surfaces were covered by a high biomass biofilm while the SNAP catheter surfaces had noticeably less bacterial coverage and most of the bacteria on SNAP catheter surfaces were single bacteria cells. The results demonstrate that decreasing bacteria colonization and biofilm formation on the surfaces of SNAP-impregnated CarboSil catheter through continuous NO release may lead to reduced risk of catheter-related bloodstream infections.

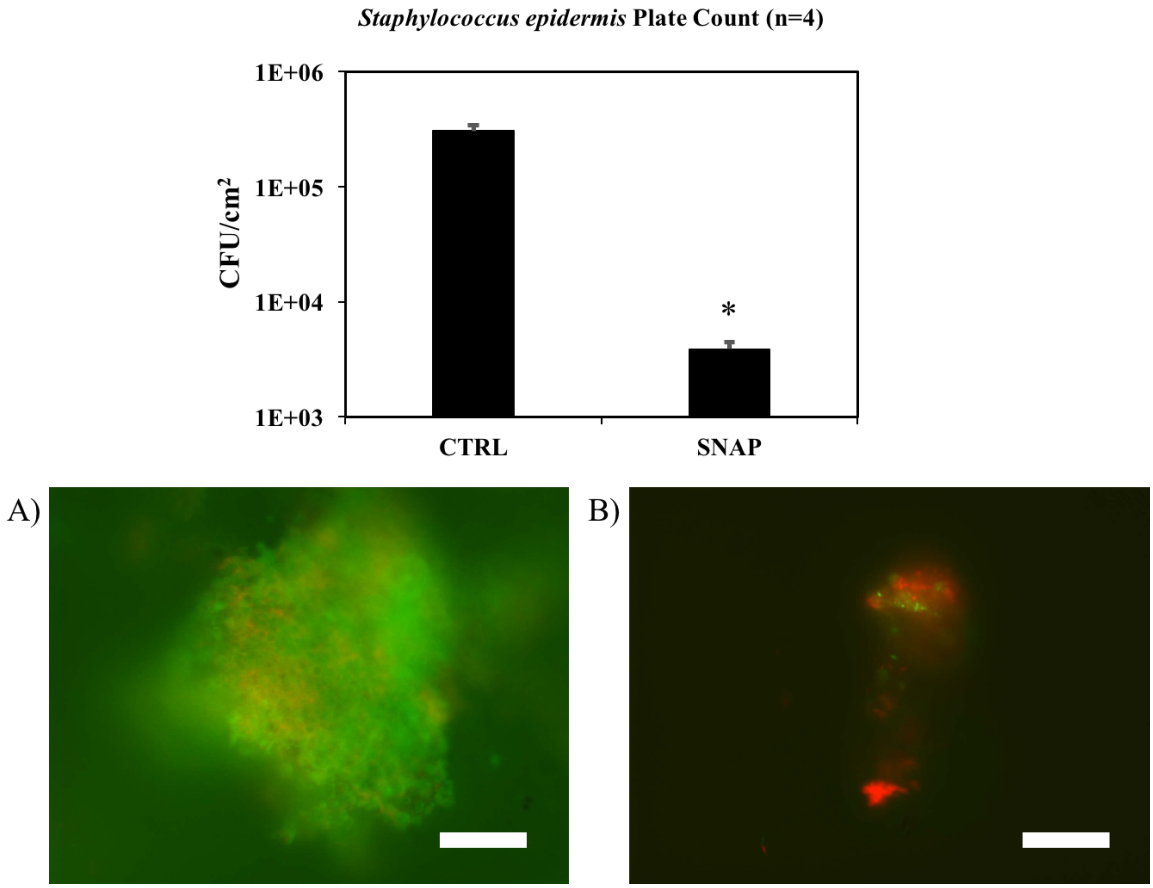

Figure 4.12. *S. epidermidis* biofilms developed on catheter segments in a CDC biofilm reactor for 14 d at 37 °C. Upper image: Bar graph of plate count data for adhesion of viable *S. epidermidis* bacteria to the catheter surfaces. Lower images: Representative fluorescence microscopic images of surface live (green) (A) and dead (red) (B) bacteria on different catheters, acquired by oil immersion 60× objective lens of the biofilms on the surface of the catheter, scale bar 20 μm.

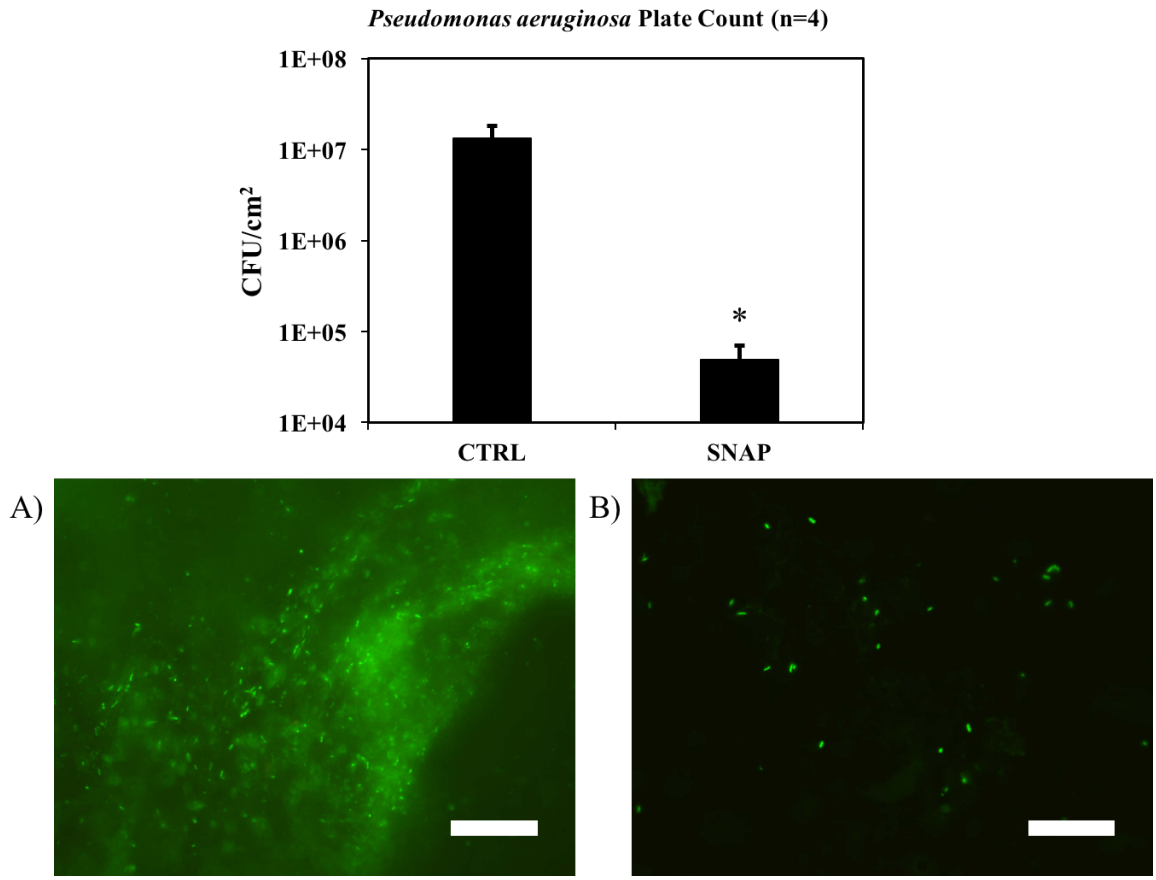

Figure 4.13. *P. aeruginosa* biofilms developed on catheter segments in a CDC biofilm reactor for 14 d at 37 °C. Upper image: Bar graph of plate count data for adhesion of viable *P. aeruginosa* bacteria to the catheter surfaces. Lower images: Representative fluorescence microscopic images of surface live (green) (A) and/or dead (red) (B) bacteria on different catheters, acquired by oil immersion 60× objective lens, scale bar 20 μm.

4.3.7 Reduction of thrombus formation in rabbit model

In vivo experiments using an acute 7 h rabbit thrombogenicity model were conducted to examine the benefits of the SNAP-impregnated CarboSil IV catheters with respect to decreasing clot formation. One SNAP catheter and one control catheter were placed into the external jugular veins of each rabbit (n=3) for 7 h. At the end of the 7 h implantation, the catheters were carefully removed from the blood vessel while any thrombus formation was left intact on the catheter surface. In order to determine the area of clot formation,

digital images of both the SNAP impregnated and control catheters were taken and the two-dimensional representation of the clot areas were quantitated using Image J software from NIH. The clot area on the control catheter was 0.84 ± 0.19 cm^2/catheter while the clot area on the SNAP catheter was 0.03 ± 0.01 cm^2/catheter, considerably less than the controls (see Figure 4.14).

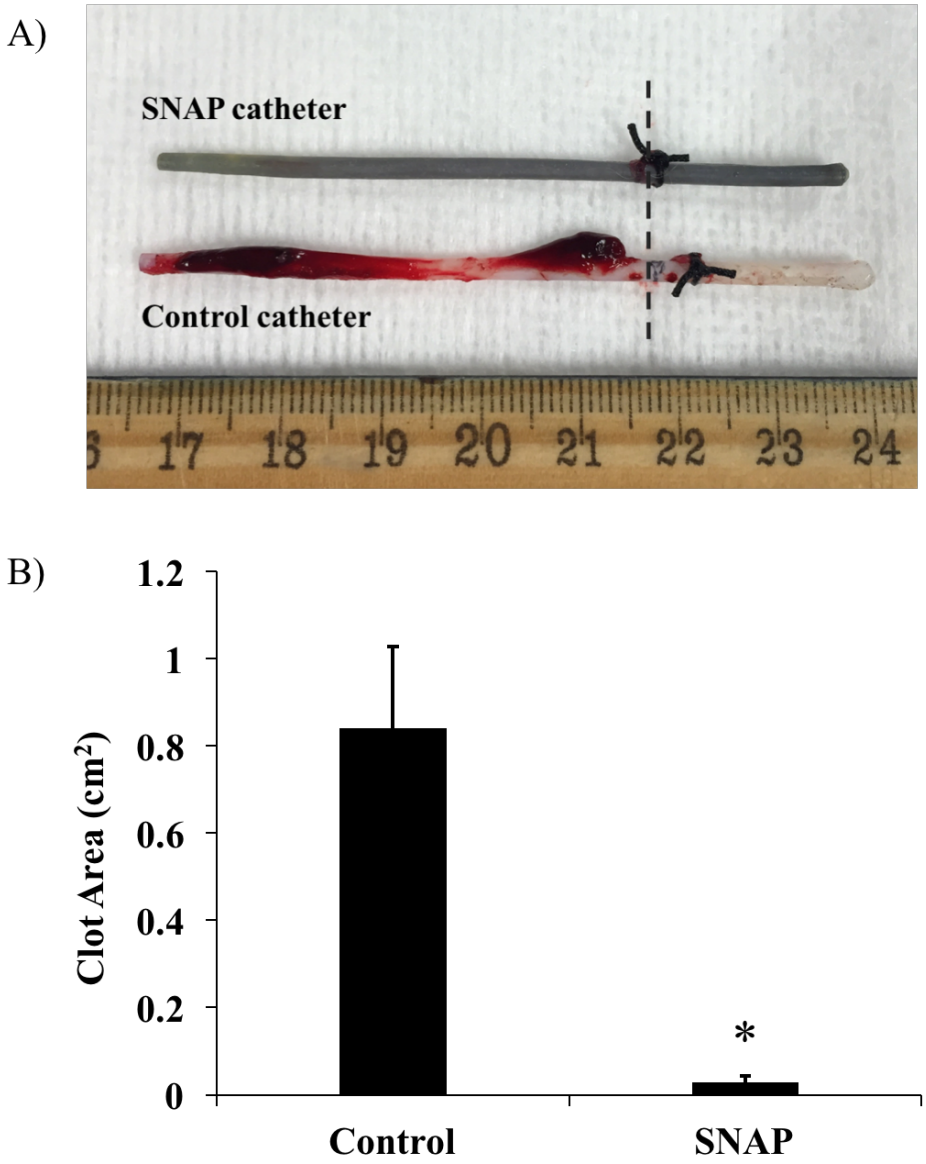

Figure 4.14. Five cm of the catheters (left of the dash line) were inserted into the rabbit external jugular veins for 7 h. (A) Representative pictures of the thrombus formation on the SNAP-impregnated CarboSil and control CarboSil catheters from one rabbit experiment. (B) Two-dimensional representation of the clot area (cm^2) on SNAP and control catheter in rabbit veins for 7 h, as quantitated using Image J software by NIH. Data are mean ± SEM for n=3 animal experiments. * = $p < 0.05$

The NO release rates from the post-surgery SNAP catheters were quantitated using chemiluminescence and the SNAP catheters were shown to maintain NO release at an average flux of $4.4 \pm 1.1 \times 10^{-10}$ mol cm^{-2} min^{-1} at 37 °C. This result clearly illustrates that

continuous localized NO release from the SNAP impregnated CarboSil catheter has the potential to greatly reduce the risk of clot formation on the catheter's surface, thereby maintaining the functionality of IV catheters during use and reduce the risk of stroke or deep vein thrombosis associated with detached blood clots.

4.4. Conclusion

In summary, a simple solvent impregnation procedure has been adapted to incorporate SNAP into CarboSil 20 80A polymer. The impregnation process was optimized to achieve maximized SNAP loading and long-term NO release. The majority of the SNAP incorporated in 15 wt% SNAP-impregnated CarboSil films exists in its crystalline form, and more than 70 % of the total NO release originates directly from the SNAP decomposition within the bulk of the polymer phase. The 15 wt% SNAP-impregnated CarboSil catheters release NO at physiological levels for at least 14 d. The NO release catheters reduce viable *S. epidermidis* and *P. aeruginosa* bacteria adhesion to the surface of the catheters after 14 d was by 2 and 2.5 log units, respectively. The SNAP catheters also exhibit minimal clot formation after 7 h of animal implantation in a rabbit model when compared to the control CarboSil catheters. Overall, both the *in vitro* and *in vivo* studies clearly demonstrate the potential of the SNAP impregnation method to improve the hemocompatibility/antimicrobial activity of IV catheters made with CarboSil polymer. It is anticipated that these results will encourage further pursuit of this strategy in designing the next generation commercial IV catheters and other implantable biomedical devices to greatly reduce risk of infection and thrombosis in patients.

4.5 References

1 R. Parameswaran, J. B. Sherchan, D. Muralidhar Varma, C. Mukhopadhyay and S. Vidyasagar, *J. Infect. Dev. Ctries.*, 2011, **5**, 452–458.
2 E. Venturini, L. Becuzzi and L. Magni, *Case Rep. Vasc. Med.*, 2012, **2012**, 469619.
3 H. Wu, C. Moser, H.-Z. Wang, N. Høiby and Z.-J. Song, *Int. J. Oral Sci.*, 2015, **7**, 1–7.
4 M. L. Linenberger, *J. Natl. Compr. Canc. Netw.*, 2006, **4**, 889–901.
5 P. W. Kamphuisen and A. Y. Y. Lee, *Hematology Am. Soc. Hematol. Educ. Program*, 2012, **2012**, 638–44.
6 K. S. Lavery, C. Rhodes, A. Mcgraw and M. J. Eppihimer, *Adv. Drug Deliv. Rev.*, 2016.
7 J. L. Baskin, C. Pui, U. Reiss, J. A. Wilimas, M. L. Metzger, R. C. Ribeiro and S. C. Howard, *Lancet*, 2009, **374**, 159–169.
8 T. Lee, C. Lok, M. Vazquez, L. Moist, I. Maya and M. Mokrzycki, *Int. J. Nephrol.*, 2012, **2012**.
9 C. Abad and N. Safdar, *Infect. Dis. Spec. Ed.*, 2011.
10 S. Fletcher, *Contin. Educ. Anaesthesia, Crit. Care Pain*, 2005, **5**, 49–51.
11 R. M. Donlan, *Clin. Infect. Dis.*, 2011, **52**, 1038–1045.
12 R. M. Donlan, *Clin. Infect. Dis.*, 2001, **33**, 1387–1392.
13 N. Hoiby, O. Ciofu, H. K. Johansen, Z. Song, C. Moser, P. O. Jensen, S. Molin, M. Givskov, T. Tolker-Nielsen and T. Bjarnsholt, *Int. J. Oral Sci.*, 2011, **3**, 55–65.
14 W. Hengzhuang, H. Wu, O. Ciofu, Z. Song and N. Høiby, *Antimicrob. Agents Chemother.*, 2012, **56**, 2683–2690.
15 L. A. Mermel, M. Allon, E. Bouza, D. E. Craven, P. Flynn, N. P. O'Grady, I. I. Raad, B. J. Rijnders, R. J. Sherertz and D. K. Warren, *Clin. Infect. Dis.*, 2009, **49**, 1–45.
16 M. R. Kiedrowski and A. R. Horswill, *Ann. N. Y. Acad. Sci.*, 2011, **1241**, 104–21.
17 N. P. O'Grady, M. Alexander, E. P. Dellinger, J. L. Gerberding, S. O. Heard, D. G. Maki, H. Masur, R. D. McCormick, L. A. Mermel, M. L. Pearson, I. I. Raad, A. Randolph and R. A. Weinstein, *MMWR. Recomm. Rep.*, 2002, 51, 1–29.
18 D. K. Warren, W. W. Quadir, C. S. Hollenbeak, A. M. Elward, M. J. Cox and V. J. Fraser, *Crit. Care Med.*, 2006, **34**, 2084–2089.
19 D. J. Diekema, S. E. Beekmann, K. C. Chapin, K. A. Morel, E. Munson and G. V Doern, *J. Clin. Microbiol.*, 2003, **41**, 3655–3660.
20 V. D. Rosenthal, S. Guzman and P. W. Orellano, *Am. J. Infect. Control*, 2003, **31**, 291–295.
21 L. Filippi, M. Pezzati, S. Di Amario, C. Poggi and P. Pecile, *Pediatr. Crit. Care Med.*, 2007, **8**, 556–62.
22 S. Smith, S. Dawson, R. Hennessey and M. Andrew, *Am. J. Pediatr. Hematol. Oncol.*, 1991, **13**, 141–143.
23 L. C. Stephens, W. D. Haire, S. Tarantolo, E. Reed, K. Schmit-Pokorny, A. Kessinger and R. Klein, *Transfus. Sci.*, 1997, **18**, 187–193.
24 G. K. Dogra, H. Herson, B. Hutchison, A. B. Irish, C. H. Heath, C. Golledge, G. Luxton and H. Moody, *J. Am. Soc. Nephrol.*, 2002, **13**, 2133–2139.
25 D. Yahav, B. Rozen-Zvi, A. Gafter-Gvili, L. Leibovici, U. Gafter and M. Paul, *Clin.*

Infect. Dis., 2008, **47**, 83–93.
26 M. Vaughn, L. Kuo and J. Liao, *Am. J. Physiol.*, 1998, **274**, 2163–2176.
27 Y. Wo, E. J. Brisbois, R. H. Bartlett and M. E. Meyerhoff, *Biomater. Sci.*, 2016, **4**, 1161–1183.
28 Y. Wang, S. Chen, Y. Pan, J. Gao, D. Tang, D. Kong and S. Wang, *J. Mater. Chem. B*, 2015, **3**, 9212–9222.
29 A. W. Carpenter and M. H. Schoenfisch, *Chem. Soc. Rev.*, 2012, **41**, 3742–52.
30 X. Zhou, J. Zhang, G. Feng, J. Shen, D. Kong and Q. Zhao, *Curr. Med. Chem.*, 2016, **23**, 2579–2601.
31 J. Loscalzo, *Circ. Res.*, 2001, **88**, 756–762.
32 J.-W. Yoo, H. Nurhasni, J. Cao, M. Choi, I. Kim, B. Luel Lee and Y. Jung, *Int. J. Nanomedicine*, 2015, **10**, 3065–3080.
33 A. Ghaffari, C. C. Miller, B. McMullin and A. Ghahary, *Nitric Oxide*, 2006, **14**, 21–29.
34 D. P. Arora, S. Hossain, Y. Xu and E. M. Boon, *Biochemistry*, 2015, **54**, 3717–3728.
35 B. B. McMullin, D. R. Chittock, D. L. Roscoe, H. Garcha, L. Wang and C. C. Miller, *Respir. Care*, 2005, **50**, 1451–6.
36 L. Plate and M. A. Marletta, *Mol. Cell*, 2012, **46**, 449–460.
37 N. Barraud, M. J. Kelso, S. A. Rice and S. Kjelleberg, *Curr. Pharm. Des.*, 2015, **21**, 31–42.
38 E. J. Brisbois, H. Handa and M. E. Meyerhoff, in *Advanced Polymers in Medicine*, ed. F. Puoci, Springer International Publishing, Cham, 2015, pp. 481–511.
39 D. a Riccio and M. H. Schoenfisch, *Chem. Soc. Rev.*, 2012, **41**, 3731–41.
40 M. C. Jen, M. C. Serrano, R. van Lith and G. A. Ameer, *Adv. Funct. Mater.*, 2012, **22**, 239–260.
41 S. Qiao, C. M. Cabello, S. D. Lamore, J. L. Lesson and G. T. Wondrak, *Apoptosis*, 2012, **17**, 1079–1094.
42 E. J. Brisbois, H. Handa, T. C. Major, R. H. Bartlett and M. E. Meyerhoff, *Biomaterials*, 2013, **34**, 6957–66.
43 Y. Wo, Z. Li, E. J. Brisbois, A. Colletta, J. Wu, T. C. Major, C. Xi, R. H. Bartlett, A. J. Matzger and M. E. Meyerhoff, *ACS Appl. Mater. Interfaces*, 2015, **7**, 22218–22227.
44 A. Colletta, J. Wu, Y. Wo, M. Kappler, H. Chen, C. Xi and M. E. Meyerhoff, *ACS Biomater. Sci. Eng.*, 2015, **1**, 416–424.
45 E. J. Brisbois, T. C. Major, M. J. Goudie, R. H. Bartlett, M. E. Meyerhoff and H. Handa, *Acta Biomater.*, 2016, **37**, 111–119.
46 M. L. Clarke, J. Wang and Z. Chen, *J. Phys. Chem. B*, 2005, **109**, 22027–22035.
47 H. Handa, T. C. Major, E. J. Brisbois, K. A. Amoako, M. E. Meyerhoff and R. H. Bartlett, *J. Mater. Chem. B*, 2014, **2**, 1059–1067.
48 J. N. Lee, C. Park and G. M. Whitesides, *Anal. Chem.*, 2003, **75**, 6544–54.
49 L. C. Xu and C. a. Siedlecki, *Acta Biomater.*, 2012, **8**, 72–81.
50 M. Otto, *Nat. Rev. Microbiol.*, 2009, **7**, 555–567.
51 I. Chipinda and R. H. Simoyi, *J. Phys. Chem. B*, 2006, **110**, 5052–5061.
52 K. Szacilowski and Z. Stasicka, *Prog. React. Kinet. Mech.*, 2001, **26**, 1–58.
53 S. M. Shishido and M. G. de Oliveira, *Photochem. Photobiol.*, 2007, **71**, 273–280.
54 K. A. Graeme and C. V Pollack, *J. Emerg. Med.*, 1998, 16, 45–56.

55 M. M. Jones, A. D. Weaver and W. L. Weller, *Res. Commun. Chem. Pathol. Pharmacol.*, 1978, **22**, 581–588.
56 C. Helms and D. B. Kim-Shapiro, *Free Radic. Biol. Med.*, 2013, **0**, 464–472.
57 C. Donadee, N. J. H. Raat, T. Kanias, J. Tejero, J. S. Lee, E. E. Kelley, X. Zhao, C. Liu, H. Reynolds, I. Azarov, S. Frizzell, E. M. Meyer, A. D. Donnenberg, L. Qu, D. Triulzi, D. B. Kim-Shapiro and M. T. Gladwin, *Circulation*, 2011, **124**, 465–476.
58 W. Ziebuhr, S. Hennig, M. Eckart, H. Kränzler, C. Batzilla and S. Kozitskaya, *Int. J. Antimicrob. Agents*, 2006, **28 Suppl 1**, S14-20.
59 L. Zhang, M. Morrison, P. Ó Cuív, P. Evans and C. M. Rickard, *J. Bacteriol.*, 2012, **194**, 6639.
60 L. Hall-stoodley, J. W. Costerton and P. Stoodley, *Nat. Rev. Mcrobiology*, 2004, **2**, 95–108.
61 D. Mack, A. P. Davies, L. G. Harris, R. Jeeves, B. Pascoe, J. K. Knobloch, H. Rohde and T. S. Wilkinson, *Biomaterials associated infection*, Springer New York, New York, NY, 2013.
62 P. D. Fey and M. E. Olson, *Future Microbiol.*, 2011, **5**, 917–933.
63 E. Svensson, H. Hanberger, M. Nilsson and L. E. Nilsson, *J. Antimicrob. Chemother.*, 1997, **39**, 817–820.
64 J. Nakajima, S. Hitomi, H. Koganemaru and Y. Nakai, *J. Infect. Chemother.*, 2013, **19**, 983–986.
65 R. Cabrera-Contreras, R. Morelos-Ramírez, A. N. Galicia-Camacho and E. Meléndez-Herrada, *ISRN Microbiol.*, 2013, **2013**, 1–5.
66 J. W. Costerton, P. S. Stewart and E. P. Greenberg, *Science*, 1999, **284**, 1318–1322.
67 D. L. Dunn, in *Surgery: Basic Science and Clinical Evidence*, eds. J. A. Norton, P. S. Barie, R. R. Bollinger, A. E. Chang, S. F. Lowry, S. J. Mulvihill, H. I. Pass and R. W. Thompson, Springer New York, New York, NY, 2008, pp. 209–235.
68 W. I. Sligl, T. Dragan and S. W. Smith, *Int. J. Infect. Dis.*, 2015, **37**, 129–134.
69 R. Gahlot, C. Nigam, V. Kumar, G. Yadav and S. Anupurba, *Int. J. Crit. Illn. Inj. Sci.*, 2014, **4**, 162–167.
70 D. L. Dunn, *Surg. Clin. North Am.*, 1994, **74**, 621–635.
71 K. P. Reighard and M. H. Schoenfisch, *Antimicrob. Agents Chemother.*, 2015, **59**, 6506–6513.
72 A. W. Carpenter, D. L. Slomberg, K. S. Rao and M. H. Schoenfisch, *ACS Nano*, 2011, **5**, 7235–44.
73 D. M. Goeres, L. R. Loetterle, M. A. Hamilton, R. Murga, D. W. Kirby and R. M. Donlan, *Microbiology*, 2005, **151**, 757–762.
74 G. C. Mendes, T. R. Brandão and C. L. Silva, *Am. J. Infect. Control*, 2007, **35**, 574–581.
75 I. P. Matthews, C. Gibson and A. H. Samuel, *Clin. Mater.*, 1994, **15**, 191–215.

CHAPTER 5

Inhibition of Bacterial Adhesion and Biofilm Formation by Dual Functional Textured and Nitric Oxide Releasing Surfaces

Xu, L.; **Wo, Y**.; Meyerhoff, M.E.; Siedlecki, C.A. "Inhibition of Bacterial Adhesion and Biofilms Formation by Dual Functional Texturing and Nitric Oxide Releasing Surfaces." *Acta Biomater*, *In Press*.*

5.1 Introduction

The long-term use of biomaterials designed for fabricating implantable medical devices such as intravascular catheters, urinary catheters, indwelling blood pumps, vascular assist devices, and orthopedic implants is complicated by the potential for microbial infection due to pathogenic bacterial adhesion and biofilm formation on biomaterial surfaces.[1-3] Due to the difficulty in treating bacterial biofilms via antibiotics and the increasing levels of

* The textured polymer fabrication, material characterization and antibacterial/antibiofilm testing reported in this chapter were conducted by Dr. Lichong Xu, while the SNAP synthesis and all NO release measurements were carried out by this Ph.D. candidate.

antibiotic resistance of pathogens, surgical removal and replacement of the implanted devices is often the only treatment for device-centered infections, causing a significant increase in morbidity and cost.[4] Combatting device-associated infections has been a great challenge in the field of implant-associated health care.[5] Bacterial adhesion to the device surface is the first and critical step in the pathogenesis of implant related infections. As an alternative to traditional methods in which antibiotics or biocides are released or infused (e.g., catheter lock solutions), methods to design and control material properties to reduce/control bacterial adhesion and thereby reduce microbial infection are more attractive approaches.[6, 7] One promising method is the generation of functional surfaces through topographic modifications (e.g., surface texturing) that significantly reduce the initial attachment of microorganisms and the number of persistent pathogens to the surfaces of the implant.[8] By analogy to natural antifouling surfaces such as shark skin, shell or lotus leaf, etc., the physical topographic surface modification with micro- or nano-size features reduces the surface contact area and changes the surface energy, and this approach has been shown to be effective in controlling bacterial adhesion and biofilm formation.[9-12] With interest in this area and the related research increasing, over the past two decades biomimetic or bio-inspired materials have been developed to prepare the sterile biomaterials for the use in medical devices.[13, 14] For example, the topographical features mimicking the shark's skin were applied into polydimethylsiloxane (PDMS) elastomer and it was found that such surfaces disrupt biofilm formation of *Staphylococcus aureus* (*S. aureus*), suggesting the possibility for application of this approach in biomedical devices.[15] Furthermore, an *in vitro* study showed that the micro-patterned surface inhibited the bacterial colonization and migration of uropathogenic *Escherichia coli (E. coli)*; thereby it

could be applied to reduce the risk of catheter-associated urinary tract infection.[16] Our group has previously developed submicron-textured polyurethane biomaterial surfaces featuring patterns with pillars of diameter and spacing of 400/400 nm and 500/500 nm, and demonstrated that both textured surfaces decreased the adhesion of *Staphylococcal epidermidis* (*S. epidermidis*) and *S. aureus* and inhibited biofilm formation under shear and static conditions.[17] Such submicron-textured surfaces have also been shown to reduce platelet adhesion, thereby reducing the potential of implant associated blood clotting/thrombosis of the device if implanted in the blood stream.[18] These *in vitro* successes of textured materials have demonstrated the great potential for their use in clinical applications to combat health-care infections and thrombosis caused by catheters and other implanted devices.

Nitric oxide (NO) releasing biomaterials represent another biomimetic strategy with great potential for clinical use. NO is an endogenous gas molecule and its continuous release from the endothelial cells that line all blood vessels can effectively prevent the adhesion/activation of platelets on normal blood vessel walls.[19] NO also plays an important role in the immune response as an antimicrobial agent and host defense against pathogenic bacteria.[20] As a diatomic free radical, NO can cross the membranes to enter the microbial cell readily and kill the microbe by directly damaging DNA, proteins, and lipids through production of potent nitrosating species or by combining with reactive oxygen species (e.g., superoxide, peroxide) and oxidizing the same targets.[21, 22] Furthermore, the rapid reduction of microbial loads reduces the pressure for the evolution and spreading of variant bacteria and limits the possibility of promoting NO resistant strains.[23] For these reasons, polymeric

materials that mimic endogenous NO release provides a potential solution against medical device-associated microbial infection and also can prevent platelet activation and thereby reduce risk of thrombus formation. Extensive studies have already demonstrated that NO release can effectively inhibit bacterial adhesion and reduce biofilm development on material surfaces.[24-27]

Since NO is highly reactive and short-lived under physiological conditions, NO donor molecules with functional groups that can store and release NO are necessary. These NO donors are incorporated into materials either by blending discrete NO donors within polymeric films, or by covalently attaching them to polymer backbones and/or to the inorganic polymeric filler particles that are often employed to enhance the strength of biomedical polymers (e.g., fumed silica or titanium dioxide).[28] *N*-diazeniumdiolates[26, 29, 30] and *S*-nitrosothiols[30-32] are commonly used to prepare NO releasing polymeric matrices for improved biocompatibility of blood-contacting medical devices. The *N*-diazeniumdiolates are generally synthesized by reaction of amines with NO gas to form relatively stable compounds that release NO when in contact with bodily fluids through proton or thermally driven mechanisms. The *S*-nitrosothiols are generally formed by reaction of nitrous acid with the parent thiol, and undergo thermal decomposition to release NO, which are generally catalyzed by metal ions (e.g., copper), and light.[30] Nitric oxide can also be generated via other techniques, such as electrochemical reduction of nitrite,[33] or reduction of sodium nitroprusside.[34] However, the current NO release strategies have the challenges in terms of storage, stability, costly synthesis or short NO release lifetime. Among the NO donors reported to date, *S*-nitroso-*N*-acetylpenicillamine (SNAP) is among

the most attractive ones in terms of its long-term NO release capability and enhanced stability when incorporated into low water uptake biomedical polymers. Indeed, SNAP has already been incorporated into a number of low water uptake polymers to yield promising new biomaterials, For example, it was reported that SNAP-doped polyurethane Elast-eon E2As polymer retained 82% of the initial SNAP after 2 month storage at 37°C [35] and released NO slowly at the physiological flux level for 3 weeks. Similarly, SNAP in CarboSil 20 80A also exhibits a stability at 88.5 % ± 4.3% of the initial amount after 8 months storage in the dark at 37 °C.[36] The increased stability of SNAP within these polymers is believed to be due to the intermolecular hydrogen bonds between crystallized SNAP molecules. For example, long-term storage stability of SNAP in the CarboSil polymer was found to originate from the formation of a polymer-crystal composite during the solvent evaporation. This composite led to sustained NO release at the physiological flux levels that can last for >3 weeks with the cross-linked silicone rubber as a topcoat.[36]

The SNAP-doped polymers exhibit good blood compatibility. The E2As catheters doped with SNAP significantly reduced the amount of thrombus and bacterial adhesion compared the E2As control catheters when they were implanted in sheep veins for 7 d.[37] An *in vitro* experiment of *S. aureus* biofilm formation over a 7 d period showed that SNAP-doped CarboSil 20 80A intravascular catheters had 5 log units reduction of viable cell count on their surfaces.[36] All results reported to date suggest that SNAP-doped low water uptake polyurethane copolymers could be attractive for clinical applications, providing long-term storage stability, long-term NO release capability *in vivo*, and increased biocompatibility and antimicrobial activity.

Although each biomimetic approach described above (surface texturing modification or NO release) has been shown to exhibit significant antimicrobial and antithrombotic effects, the use of a single approach is still far from ideal for achieving more complete control of thrombosis and microbial infection on implanted biomedical devices. Each strategy has its inherent drawbacks. For example, physical surface defects such as missed pillars during fabrication is always unavoidable, leading to local adhesion and accumulation of platelets or bacteria, while the NO release polymers have the limit of lifetime and storage stability. To overcome the shortcomings of each individual approach, the combination of surface texturing and NO release to control bacterial adhesion and biofilm formation would provide potentially additive or synergetic effects to decrease bacterial adhesion and/or platelet activation. In this study we fabricated new polyurethane films that bear ordered pillar topographies at the top surface as well as a NO releasing material in the sublayer. Such a combination produces dual functional materials with the reduced accessible surface contact area for bacteria adhesion and providing continuous NO release. Experimental data demonstrate that the dual functional surfaces provide a further improvement in the surface antimicrobial activity and anti-biofilm functionality than either of the approaches can provide when employed alone. Results show that textured surfaces with NO release inhibit biofilm formation over a relatively long term (> 28 d) and this provides a practical approach to improve the biocompatibility of current biomimetic biomaterials and reduce the risk of pathogenic infection. The successful implementation of such materials in clinical practice could ultimately reduce costs by decreasing the number of implant replacements and/or amputation/mortality.

5.2 Experimental Section

5.2.1 Materials

CarboSil® 20 80A silicone-polycarbonate-urethane (PU, DSM) was supplied as a solid and dissolved in *N*,*N*-dimethylacetamide (DMAc, Sigma-Aldrich, St. Louis, MO) at a concentration of 15 w/v% (1.5 g PU in 10 ml DMAc) for preparing the films. The SNAP-doped PU solutions were prepared by dissolving SNAP at 5, 10, or 15 w/w% relative to solid polymer within 15 w/v% Carbosil PU DMAc solutions. After extensive mixing, films can then be cast from these solutions by a spin coater (Specialty Coating System Inc., Indianapolis, IN). CarboSil PU contains 4,4'-methylene bisphenyl diisocyanate (MDI) as a hard segment and poly(dimethylsiloxane) (PDMS) and polycarbonate as soft segments. *N*-Acetyl-D-penicillamine was purchased from Sigma-Aldrich for the synthesis of SNAP, which has been described in previous publications.[35, 37] All aqueous solutions were prepared with Millipore water (18.2 MΩ) and phosphate buffered saline (PBS 0.01 M, pH 7.4, Sigma-Aldrich) was used for *in vitro* experiments. All culture media and containers for bacteria study were autoclaved at 121°C for 20 min, and the Carbosil films were sterilized by washing with 70% ethanol prior to experiments. All films were prepared in a clean room to avoid contamination.

5.2.2 Preparation of textured and NO releasing PU films

The CarboSil 20 80A PU film surfaces were textured with ordered arrays of pillars using a modified soft lithography two-stage replication molding technique that has been described previously.[17, 18] Briefly, a master pattern with ordered arrays of pillars was first fabricated

on a silicon wafer. Then a silicone mold (PDMS) was cast against the master pattern to provide the negative silicone mold (see Figure 5.1A). To obtain the highest replication efficiency of surface topography, the PU films were prepared by spin casting CarboSil onto a PDMS mold at 1200 rpm for 1 min in one thin layer first, followed by degassing and curing overnight at room temperature under vacuum. Then, additional layers of CarboSil PU were added by spin casting at 600 rpm for 1 min, respectively. Each layer was degassed and cured at room temperature under vacuum. The CarboSil PU solutions doped with different concentrations of SNAP (5, 10, 15 % (w/w) were repeatedly added on the PU films by spin casting at 600 rpms for 1 min, followed with degassing and curing overnight under vacuum (Figure 5.1B). Finally, the regular CarboSil PU without SNAP was added on the SNAP-PU layer by spin casting, and cured under vacuum, so that the SNAP-doped textured PU films were composed of 3 main layers with a base of PU, a middle layer containing SNAP, and a textured PU top layer with patterns and having a total film thickness of approximately 700 μm (Figure 5.1C). Two patterns of silicon wafers with pillar geometries having diameter (d) and separation (s) and d/s values of 400/400 nm and 500/500 nm were used as the masters for replicating PU films. The height of pillars in both patterns was 600 nm. Textured silicon wafers were fabricated by RTI International (Research Triangle Park, NC) based on requirements.

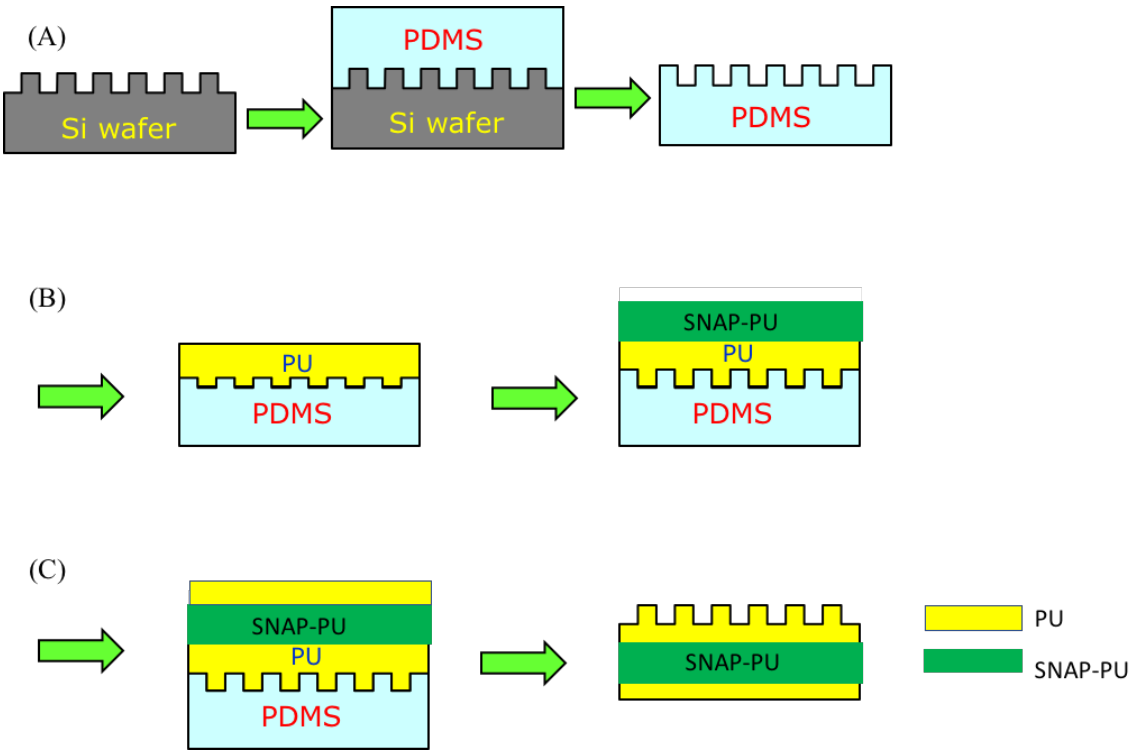

Figure 5.1. Schematic diagrams of a soft lithography two-stage replication molding technique employed to prepare textured films examined in this study.

5.2.3 NO release measurements

Nitric oxide release from the films was measured using a Sievers chemiluminescence Nitric Oxide Analyzer (NOA) 280i (Boulder, CO) using a method described previously.[35, 38] Briefly, films with diameter of ~10 mm were placed in the sample vessel immersed in PBS containing 100 μM EDTA at 37°C. NO was continuously purged from the buffer and swept from the headspace using nitrogen gas and a bubbler into the chemiluminescence detection chamber of the NOA. When not being tested with the NOA, the SNAP-doped samples were incubated in PBS under same conditions avoiding exposure to light. The NO flux was calculated based on assuming a flat surface area of two sides of films exposed to solution. All experiments were conducted in triplicate.

5.2.4 Surface water wettability measurement

The water wettability of CarboSil PU films was determined as the advancing water contact angle measured by sessile drop method using a Krüss contact angle goniometer. All measurements were made using water as a probe liquid and an ~ 8 µl of water droplet was used for the measurement. Advancing contact angles were obtained by a minimum of eight independent measurements and are presented as mean ± standard deviation.

5.2.5 Characterization of surface topography by atomic force microscopy (AFM)

A Multimode AFM with a Nanoscope IIIa control system (software version 5.12r3, Veeco, Santa Barbara, CA) was used to examine the surface textures of PU films operated in tapping mode (intermittent contact) using Si probes having aspect ratio of ~ 4:1 (TETRA, K-Tek Nanotechnology, Wilsonville, OR) in air. AFM was also used to image the bacterial adhesion on CarboSil PU surfaces. AFM images were treated and analyzed by off-line AFM software (version 5.12r3, Veeco, Santa Barbara, CA).

5.2.6 Bacterial growth, adhesion, and biofilm formation on SNAP-doped textured PU surfaces

S. epidermidis RP62A is a strongly adherent, slime-producing, pathogenic strain isolated from a patient with intravascular catheter-associated sepsis.[39] *S. epidermidis* RP62A (ATCC 35984) was used to test the bacterial growth inhibition, and adhesion to various CarboSil surfaces in this study. The culturing and collection of bacteria have been reported in a previous publication.[17] Bacterial colonies of the strain were cultured in tryptic soy broth (TSB) at 37 °C for 24 h and collected by centrifuge at 1360g for 10 min. The pellet

was re-suspended in PBS and the concentration of bacteria was measured via a spectrophotometer at 600 nm (turbidity measurement). To test the effect of NO release on bacterial growth, the polymer films were cut into round disks with 9 mm diameter, and soaked in PBS for 1 h, and placed in 24 well plates. Two ml of TSB culture medium containing S. *epidermidis* RP62A with a concentration of 1×10^6 CFU/ml was added and incubated at 37°C with shaking at 180 rpm. At 6, 24, and 48 h time points, 0.25 ml medium was drawn and diluted into 1 ml with sterile TSB, and the optical density (OD) was measured at 600 nm, where OD_{600} values indicated the growth of bacteria.

To test bacterial adhesion, the bacterial suspension was diluted in PBS to a final concentration of 1×10^8 CFU/ml. PU films were cut into the round pieces with diameter of 10 mm and pre-hydrated in Millipore water for 24 h and conditioned in PBS for 1 h, to fully equilibrate the outermost surface of the polymer films. Such pre-hydration also washes away any SNAP on the surface of the films that would lead to an initial burst of NO release from the surface of the film. This provides a more reliable approach to evaluate the effect of stable NO release on bacterial adhesion over longer periods by removing the initial NO burst. Bacterial adhesion was carried out in a micro-well plate with the volume of ~ 0.5 ml at 37°C for 1 h at near static condition with slight orbital shaking. After adhesion, the bacteria suspension was exchanged with PBS for 3 times, and then the samples were fixed in 2.5 % glutaraldehyde for 2 h. After being rinsed with PBS, bacteria on the PU films were stained with Hoechst 33258 (Invitrogen) and analyzed under a fluorescence optical microscope (Nikon, Eclipse 80i).

Biofilm formation was assessed under static and shear conditions. PU films were incubated with *S. epidermidis* RP62A in tryptic soy broth medium containing bacteria at an initial concentration of 1×10^8 CFU/ml in a 12 well plate for 2 days at 37°C. A rotating disk system with a speed control (model: AFMSRX, Pine Instrument, PA) was used to assess biofilm formation and slime production on surfaces under shear condition.[17] PU films were incubated in TSB under same conditions and run at speed of 431 rpm. Every 2 days, 25 % of media was replaced for supplement of nutrients. After desired time periods, the samples were washed with PBS by sequential addition and aspiration, stained with 100 µg/ml wheat germ agglutinin-FITC (Sigma) for 1 min, and fixed in 1% paraformaldehyde for 30 min. The samples were then examined by fluorescence optical microscopy.

5.2.7 Statistical Analysis

Statistical analysis was performed using SAS software (version 9.4). Means of experimental data were compared by 2-sample t-test and differences were considered statistically significant for $p< 0.05$. Significance is denoted in figures of this paper with one symbol denoting $p< 0.05$, two symbols $p < 0.01$, and three symbols denoting $p< 0.001$. The bacterial adhesion was further regressed with the factors by ANOVA general linear model (GLM), and differences in bacterial adhesion means were analyzed by the least mean square method.

5.3 Results and Discussion

5.3.1 Preparation SNAP- textured polyurethane films

In a previous study,[35] we examined the NO release and stability of 5wt% and 10 wt% SNAP-doped Elast-eon E2As polymers. In this study, we examined a different polymer, CarboSil 20 80A, and combined the SNAP-doped PU in the middle layer and the top layer with textured pattern to make the "sandwich-like" polymer films. To study the NO release profiles and the response of bacterial adhesion to the polymer films that contain different concentrations of NO donor SNAP, a series of SNAP-textured films with CarboSil 20 80A polyurethane, in which the middle layer of PU was doped with 5 wt%, 10 wt%, and 15 wt% SNAP and the top surface layer was textured with patterns of 400/400 nm or 500/500 nm, were fabricated by a soft lithography two-stage replication molding technique. Generally, we obtained regular textured patterns on the outer polyurethane surfaces, similar to the features that we described in previous publications for the regular textured surface (without NO release).[17, 40] Both the diameter of pillars and distance of inter pillars are less than the dimensions of bacterial cells, ensuring a reduction of available contact area when bacterial cells contact the surface, with minimal opportunities for bacteria to become lodged in the spaces between pillars.

Initially we observed some shallow areas on the textured surfaces after we applied only a thin layer at the top surface (composed with PU layers which were spin coated at 1200 rpm and 600 rpm for 1 min, respectively) and with SNAP-doped polyurethane added as the middle layer (Figure 5.2A). The shallow areas are believed to be SNAP that diffused into the thin top polyurethane layers during fabrication, leading to a reduction of pillar height.

To improve the texturing pattern, two more layers were added to the top textured layer by spin coating at 600 rpm for 1 min. The thicker top layer of PU significantly limited the diffusion of SNAP into the textured layer during drying/curing and the resulting textured surface had a more uniform distribution of pillars, with a pillar yield of > 99.8% (see Figure 5.2B).

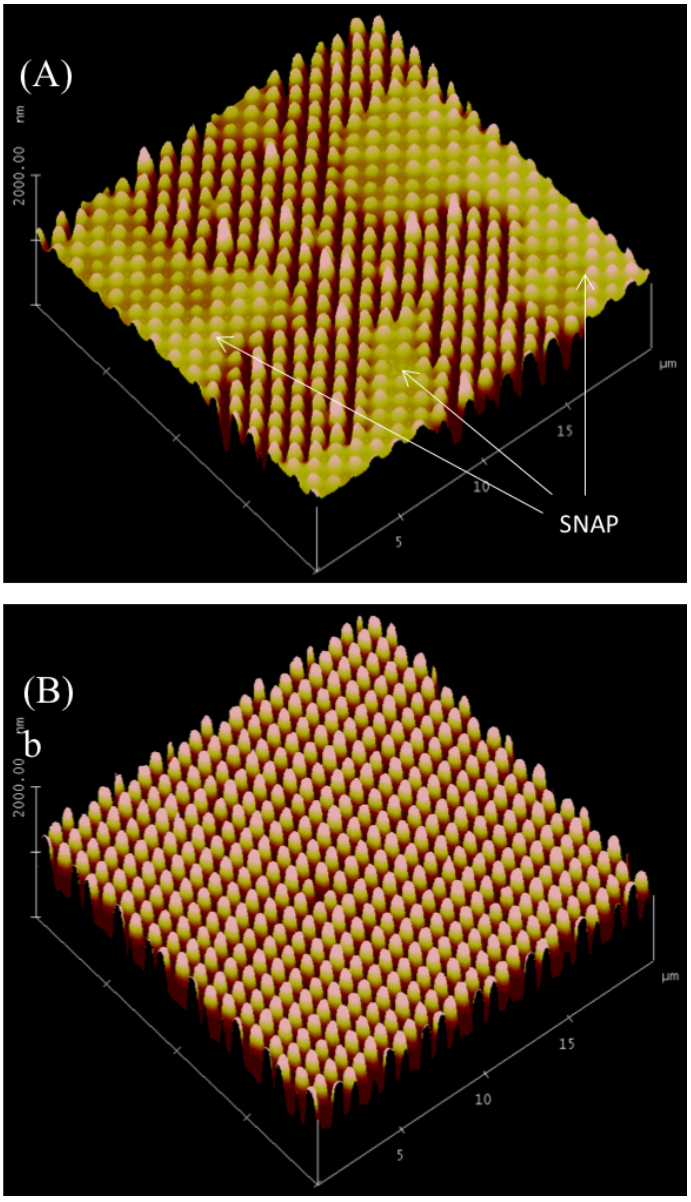

Figure 5.2. 3D AFM image of NO releasing 500/500 nm textured polyurethane film surface; (A) thin top layer showing the diffusion of SNAP onto top surface, and (B) thick top layer showing normal textured surface feature (scan size 20×20 μm^2, height 1000 nm).

To ensure that the NO release can be controlled, a base layer of PU was subsequently applied onto the middle SNAP-PU layer by spin coating at 400 rpm for 1 min, and application of such layers was repeated for 3 times. In this manner, the sandwich-like PU films with SNAP and texturing were fabricated. The subsequent measurement of NO generation showed that a thicker top layer of PU extended the lifetime of NO release, suggesting that the thickness of top layer can control the release rate of NO (see Section 5.3.3). Further, a thicker top layer of PU can also reduce the leaching of SNAP, NAP and NAP dimer from the films.

The SNAP-textured polymer film was prepared by solvent evaporation under vacuum. In this study, DMAc was used as the solvent to dissolve the polyurethane and/or SNAP to form the thin layer on the mold by spin casting. Such process enables easy control of the thickness of films and produces well textured patterns with high yield of pillars, but is time-consuming. Brisbois et al.[35] used the alternative solvent tetrahydrofuran (THF) to prepare the SNAP-doped Elast-eon E2As polymer as a homogenous coating on a Teflon plate. However, it appears that this approach is unsuitable for spin casting in a soft lithography two-stage replication process since the fast evaporation of THF often causes a heterogeneous film thickness during the spinning process. Furthermore, the pattern produced was found to be unacceptable and pillar yield was low because the PU polymer solution did not have good access into the submicron size holes within the PDMS mold.

5.3.2 Surface wettability

The regular smooth CarboSil 2080A PU surface is hydrophobic with a water contact angle of 91.0±1.4°. Surface texturing increased the hydrophobicity with water contact angle of 139.3 ±1.6° due to air captured in the spaces between pillars (Figure 5.3). This is similar to the BioSpan® MS/0.4 polyurethane textured surfaces that have been described elsewhere.[40] Adding the SNAP-doped polyurethane as the middle layer of films did not affect the water contact angle significantly for the smooth surfaces while it appeared to decrease the water contact angles for the textured surfaces as the SNAP content increased. This is probably due to the diffusion of SNAP into top layer of PU film. However, since the observed differences of water contact angles between textured surfaces having 0, 5 and 10 wt% SNAP was only approximately 5°, this is generally within the variability of the measurement method.

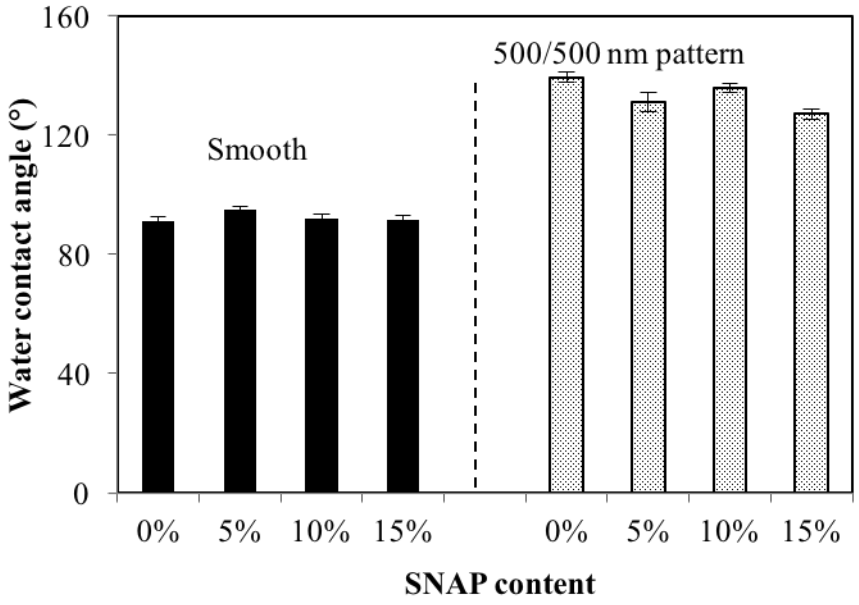

Figure 5.3. Water contact angle of smooth and textured (500/500 nm pattern) PU films with SNAP-doped in middle layer.

5.3.3 NO generation from SNAP-doped PU films

S-Nitrosothiols (RSNOs) are one of the most widely used NO donors. SNAP can decompose into the disulfide, dimer of NAP or $(NAP)_2$, and release NO in the presence of light, heat, or moisture. In the presence of certain metal ions (e.g. Cu(II)) a reductive catalytic reaction is possible that leads to formation of initially NAP (and then $(NAP)_2$ after oxidation of NAP thiols) and NO. SNAP is a synthetic tertiary RSNO and is more stable than most physiological RSNOs due to the steric hindrance of the sulfur atom.[41, 42] Upon placing the SNAP-doped CarboSil PU films into PBS at 37°C, the decomposition of SNAP within polymer film occurs simultaneously to release NO (equation. 5.1) owing to the combination of moisture and temperature.

$$2\ SNAP \rightarrow 2\ NO + (NAP)_2 \qquad [5.1]$$

The NO release flux rate depends on the topcoat polymer layer thickness, the surface topography, and level of SNAP content within the 'sandwich' middle layer of the polymer film. We found that the NO release was fast for the SNAP-polymer with a thin top layer and lasted only 3-4 days. Also, we found that NO flux was generally higher in the presence of the textured surface than on the normal smooth surface, likely due to the increased water contacting surface area of the textured film (Figure 5.4A). To control the NO release flux, we fabricated CarboSil PU films containing 5, 10, and 15 wt% SNAP in a middle layer sandwiched by a base PU and a thick textured PU surface. Figure 5.4B illustrates the NO flux release from 15 wt% SNAP-doped surface in contact with water at 37°C. It was found that the NO flux release was delayed initially, then gradually increased with time and then

reached a peak. The average NO flux was as high as 15 $\times 10^{-10}$ mol min^{-1} cm^{-2} on day 1, and then decreased in the following days. The lifetime of NO release varied with the concentration of SNAP-doped within the films. The NO flux release from SNAP textured surfaces with 500/500 nm patterns was found to last only about 2 and 4 days for 5 wt% and 10 wt% SNAP-doped films, respectively, while the lifetime of NO release for 15 wt% SNAP-doped materials can last up to 10 d at an NO flux > 0.5 $\times 10^{-10}$ mol min^{-1} cm^{-2} (see Figures 5.4C-5.4E). Healthy endothelial cells produce NO fluxes generally in the range of 0.5-4.0 $\times 10^{-10}$ mol min^{-1} cm^{-2} to prevent platelet activation and subsequent thrombosis.[43]

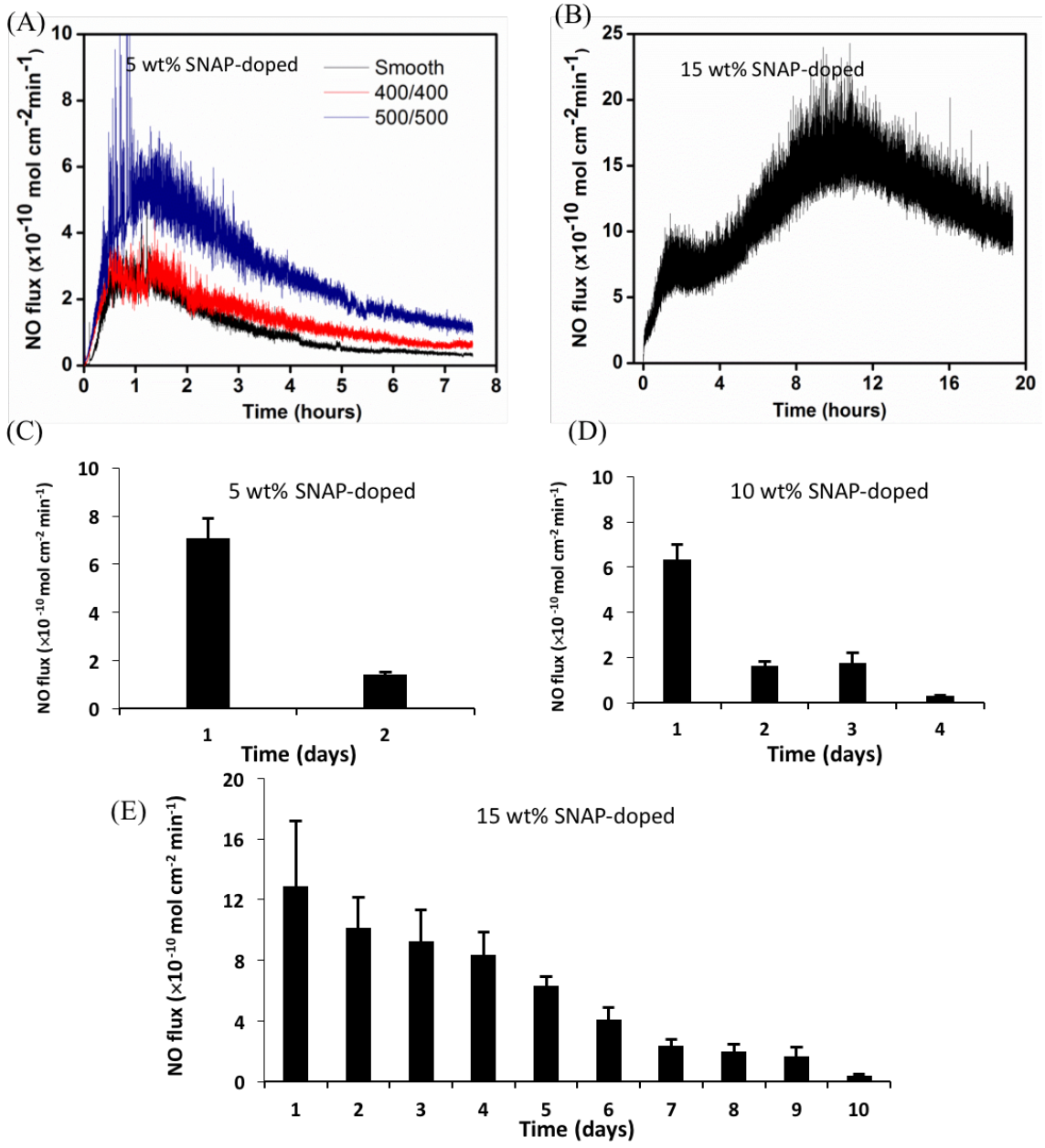

Figure 5.4. NO release from SNAP-doped textured polyurethane film in PBS at 37°C without light. (A) smooth, 400/400nm, and 500/500nm textured PU films with 5 wt% SNAP-doped; (B) NO release on day 1 from 500/500 nm textured PU films with 15 wt% SNAP-doped; and the average NO flux released from surface as the function of time (day) from 500/500 nm textured PU films with (C) 5 wt%, (D) 10 wt%, and (E) 15 wt% SNAP doped. Data collection ended when the flux went below physiological levels of 0.5 $\times 10^{-10}$ mol min^{-1} cm^{-2}.

The sustained NO release originates from the formation of a composite of SNAP crystals within the polymer phase. Wo et al.[36] proposed a 2-step mechanism of NO release from

the SNAP-doped CarboSil polymer. Upon hydration at 37°C SNAP in the polymer matrix decomposes and releases NO, primarily in the water-rich regions near the polymer/solution interface, and the dissolved SNAP in the bulk polymeric phase becomes unsaturated, resulting in the dissolution of crystalline SNAP within the bulk of the polymer. The SNAP-textured CarboSil polyurethane film examined in this study consists of top, middle, and base layers with same CarboSil 20 80A polymer and the SNAP doped in the middle layer. Comparing the long-term NO release from SNAP-doped E2As polymer[35] or silicon rubber top coated CarboSil polymer,[36] the lifetime of NO release from SNAP-textured PU films in this study is relatively shorter (10 d) vs. these prior reports. One probable reason for this is that the top layer in the textured films is a relatively thin film formed by the spin coating process, and SNAP from the underlying layer can enter this outermost layer during the preparation process leading to a greater release rate of NO at the initial time point (e.g., first day). Additional spin coating of layers within the top portion of the film reduces the diffusion of SNAP into top textured layer during film preparation, and increases the lifetime of NO release (Figure 5.4E). Another plausible explanation for reduced longevity of NO release from the textured films that have relatively thin top layers is that the repeated dissolution and recrystallizing of SNAP during fabrication process may lead to the instability and partial decomposition of SNAP within polymer. Clearly, the fabrication process of preparing optimal SNAP-textured films still needs to be optimized.

5.3.4 Surface topography of SNAP-doped PU films

NO release from SNAP-doped polymer film changes the nano-topography of top surface. Figure 5.5 illustrates the AFM surface image of a smooth film containing 15 wt% SNAP

in middle layer before and after hydration. Surprisingly there are particle-like spots distributed on the smooth surface before hydration, and these spots had diameters in the range of 250-350 nm and height of 35-60 nm. These spots were likely due to the SNAP diffusion into the very top thin layer of PU during fabrication and some of SNAP crystals extending out from the surface. We did not observe such particle-like spots on the films in absence of SNAP. After hydration in PBS for 24 h at 37°C, there were few particle-like spots found on surface. Instead, only small pits with a depth of around 5-30 nm were observed, suggesting that SNAP decomposed/dissolved and generated NO flux, which led to the formation of these observed pits.

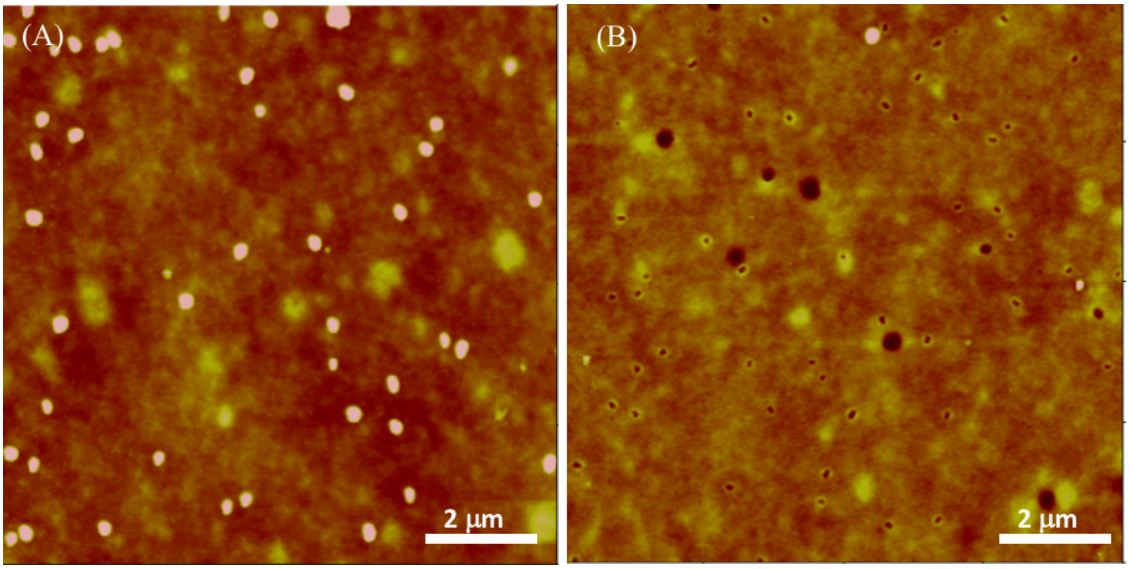

Figure 5.5. AFM images of smooth polyurethane surface with 15 wt% SNAP in the middle layer (a) before hydration and (b) after hydration. (scale bar= 2 µm)

5.3.5 Antimicrobial properties of SNAP-doped PU films

The antimicrobial properties of polymers were evaluated by the measurements of bacterial turbidity of media inoculated with bacterial strains and incubated with polymer films.

Figure 5.6 shows that the values of OD_{600} of media incubated with polymers without SNAP or doped with 5 wt% SNAP increased sharply after 24 h, suggesting that the polymers with 5 wt% SNAP doped in middle layer had no significant inhibition on bacterial growth in the bulk of the culture; however, the OD_{600} values of media incubated with 10 wt% and 15 wt% SNAP-doped polymers increased only slightly at 24 and 48 h. The values were about half of the values of OD_{600} for polymers without SNAP or with 5 wt% SNAP, suggesting that bacteria in the bulk media solution were inhibited by the NO released by the SNAP-doped films. Of interest is that the OD_{600} values of media in contact with the 15 wt% SNAP-doped polymers decreased at 48 h (p-values =0.08 and 0.13 for textured 400/400nm and 500/500 nm surfaces, respectively) compared to the values at 24 h, indicating that bacteria were inhibited by the high NO flux released from these polymers during the initial 2 d of incubation.

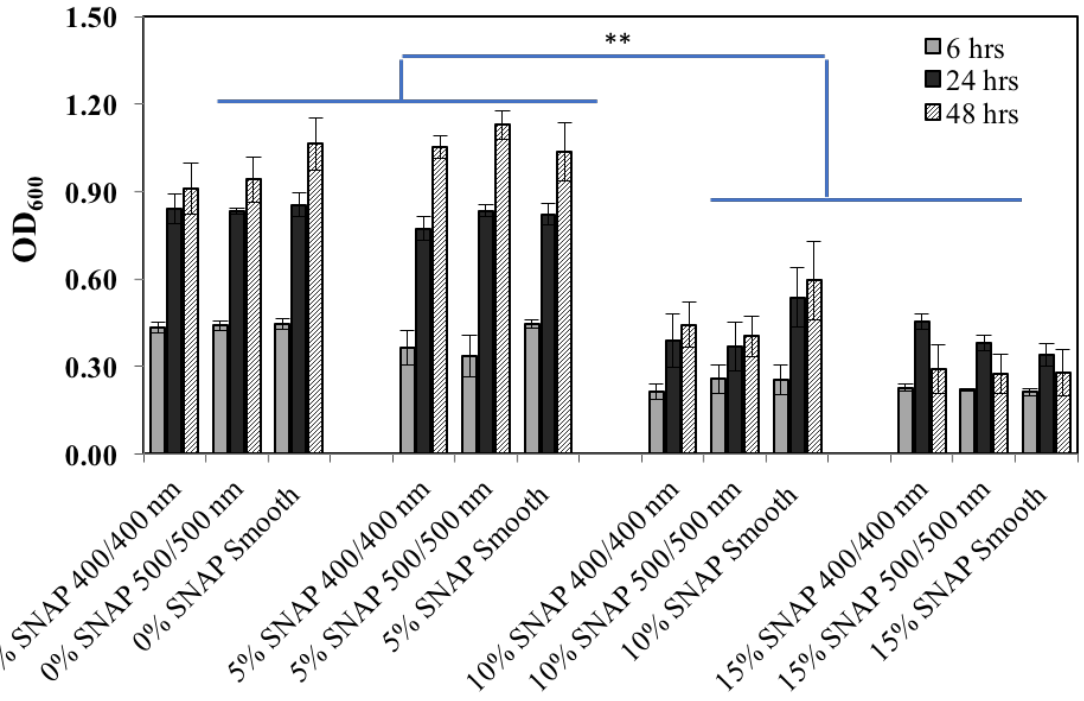

Figure 5.6. Optical density of bacterial culture medium measured at 600 nm wavelength after being incubated with various CarboSil films for 6, 24, and 48 h.

5.3.6 Bacterial adhesion on SNAP-doped PU film surfaces

Bacterial adhesion to the various PU film configurations was assessed under static condition in PBS and evaluated by the bacteria counts per unit area. Generally, both the textured surfaces alone and the use of SNAP alone (without texturing (smooth), significantly reduced bacterial adhesion on CarboSil PU film surfaces (Figure 5.7a). Without NO release from polymers (0% SNAP), surface texturing alone (400/400 nm and 500/500 nm) reduced bacterial adhesion by ca. 61-64%, when compared to the smooth samples. With SNAP present in the middle layer of the polymer films, the reduction rate increased to up to 88% on the films containing 15 wt% SNAP and the 500/500 nm pattern surface texture. The response of bacterial adhesion to the NO release is dependent on the concentration of SNAP doped in the middle layer of polymer films. Bacterial adhesion generally decreased with the increase of SNAP concentration due to the increase of NO release level, as expected (Figure 5.7b). We used the general linear model (GLM) to regress the factors of SNAP content, surface texturing, and interaction of SNAP×texturing, and found that both surface texturing and SNAP were significant factors influencing *S. epidermidis* bacterial adhesion (both p-values <0.0001). Furthermore, the interaction of SNAP and texturing also significantly affected bacterial adhesion (p-value <0.0001), strongly suggesting that the bacterial adhesion linearly decreased with increasing SNAP concentration, but the slopes for different surfaces (Smooth, 400/400 nm, and 500/500 nm patterns) were significantly different (Figure 5.7b), suggesting that the combination of texturing and SNAP produced synergistic effect on inhibition of *S. epidermidis* bacterial adhesion.

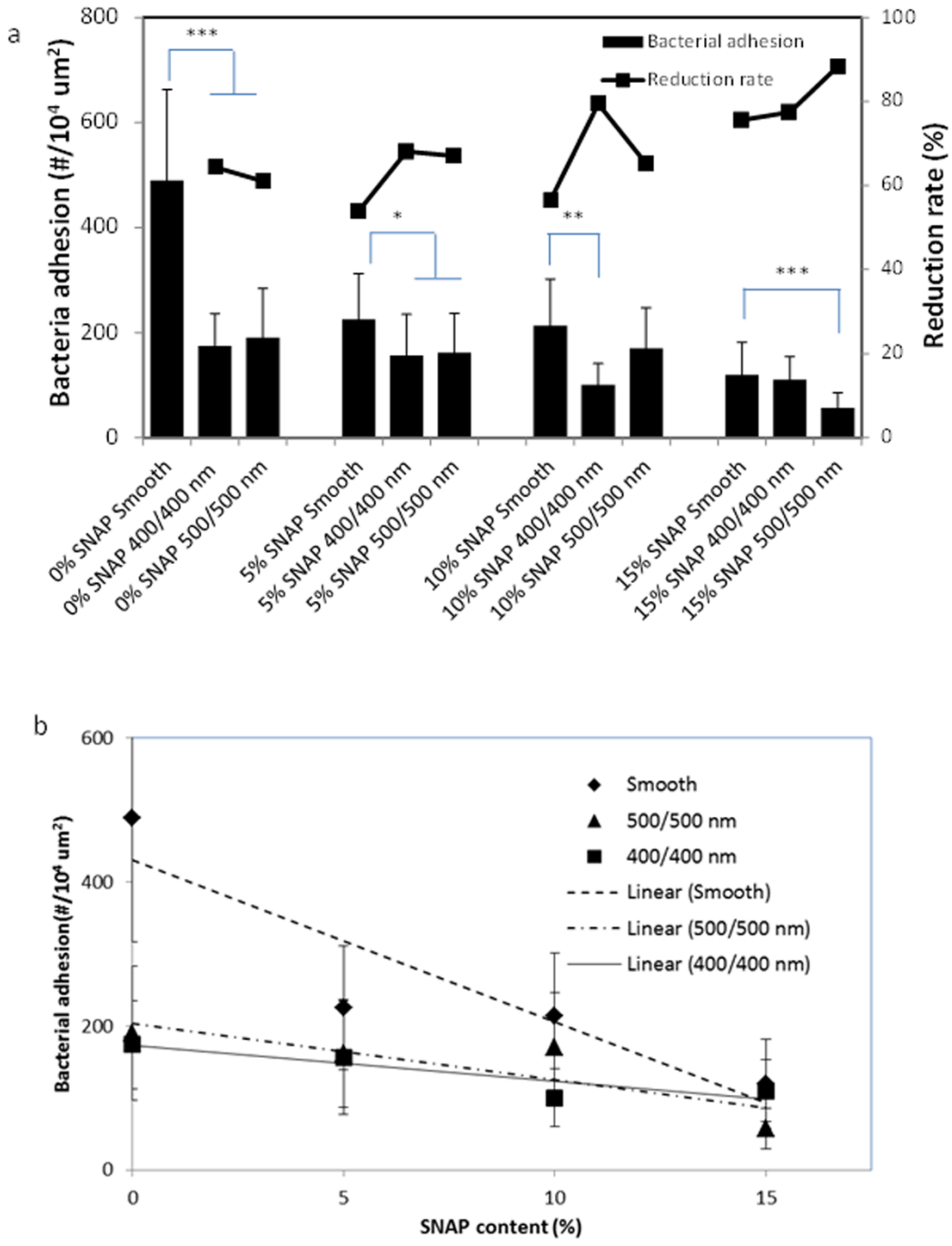

Figure 5.7. (a) Bacterial adhesion and reduction rates (against smooth regular PU polymer) on NO releasing textured polyurethane surfaces under static condition at 37°C for 1 h; (b) linear regression of bacterial adhesion against SNAP content.

These differences in bacterial adhesion were further compared by the least square means method. Table 5.1 shows that the differences of means between smooth and textured

surfaces (either 400/400 nm or 500/500 nm) at SNAP levels of 0 wt%, 5 wt%, and 10 wt% are significant, but not significant at SNAP level of 15 wt% (all p-values >0.05 for smooth and textured surfaces). Results suggest that both NO release and texturing contributed to inhibition of bacterial adhesion at lower levels of SNAP content, but the NO release dominates the degree of reduction in bacterial adhesion at high levels of SNAP (15 wt%), indicating that the effect of surface texturing becomes less significant when the concentration of SNAP is as high as 15 wt%. A comparison of bacterial adhesion between two textured surfaces with different dimensions, 400/400 nm and 500/500 nm, indicates that there is no statistically significant difference of mean for these two differently patterned films (all p-values >0.05) regardless of the levels of SNAP concentration present. This is due to the similar pillar geometry of the patterns with each having the submicron dimensions (400 nm and 500 nm). The effect of significantly larger or smaller pattern sizes on bacterial adhesion in combination with NO release still needs to be examined in the future.

Table 5.1. Statistical analysis of difference of least square means in bacterial adhesion *Staphylococcus epidermidis* between every two groups of biomaterial surfaces examined in this work.

SNAP (wt%)	Comparison	P value
0	Smooth vs 400/400	< 0.0001
	Smooth vs 500/500	< 0.0001
	400/400 vs 500/500	0.2841
5.0	Smooth vs 400/400	< 0.0001
	Smooth vs 500/500	< 0.0001
	400/400 vs 500/500	0.4711
10.0	Smooth vs 400/400	0.0002
	Smooth vs 500/500	< 0.0001
	400/400 vs 500/500	0.8381
15.0	Smooth vs 400/400	0.9991
	Smooth vs 500/500	0.4598
	400/400 vs 500/500	0.4605

The above bacterial adhesion experiment was carried out in PBS, although the presence of proteins are potentially quite important in influencing bacterial adhesion on implanted medical devices surfaces. When a foreign material is implanted in the body, plasma proteins rapidly adsorb on the surfaces and form a layer of proteins. The nature of adsorbed proteins modulates the bacterial adhesion, aggregation and biofilm formation. *In vitro* studies have shown that the presence of the serum proteins generally suppresses the initial bacterial adhesion due to the nonspecific interactions of albumin and the surfaces of bacteria [44] while adhesive proteins (e.g., fibrinogen and fibronectin) were reported to increase adhesion via forming the specific ligand/receptor bonds between proteins and the surfaces of bacterial cells.[45, 46] In our previous study of bacterial adhesion on submicron textured polyurethane surfaces, a greater decrease in adhesion was observed when textured surfaces were incubated in solutions containing plasma or serum compared with the adhesion in PBS.[17] Similarly, we expect a decrease in bacterial adhesion on SNAP-textured PU surfaces in the solution containing serum proteins compared to the adhesion in PBS (Figure 5.7). We also expect that surface texturing and NO release could exert the similar ability in controlling bacterial growth and adhesion on SNAP-textured surfaces in solutions containing plasma proteins. Such studies will be conducted during the next phase of this research project.

5.3.7 Biofilm formation on SNAP-Textured PU films

S. epidermidis RP62A biofilm formation on dual functionalized CarboSil films was assessed in TSB culture under static conditions as well as shear conditions over different

periods, respectively. Under static conditions, biofilm was observed on un-doped (0 wt% SNAP) and 5 wt% SNAP doped CarboSil film surfaces, either smooth or textured, within 2 d (Figure 5.8); however, there were only a few of clusters of bacteria or small biofilms formed on 10 wt% SNAP (both smooth and textured surfaces), and no biofilms were observed on the film surfaces with 15 wt% SNAP, for both smooth and textured surfaces. This suggests that the higher rates of NO release inhibit the growth of bacteria biofilm on the polymeric surfaces.

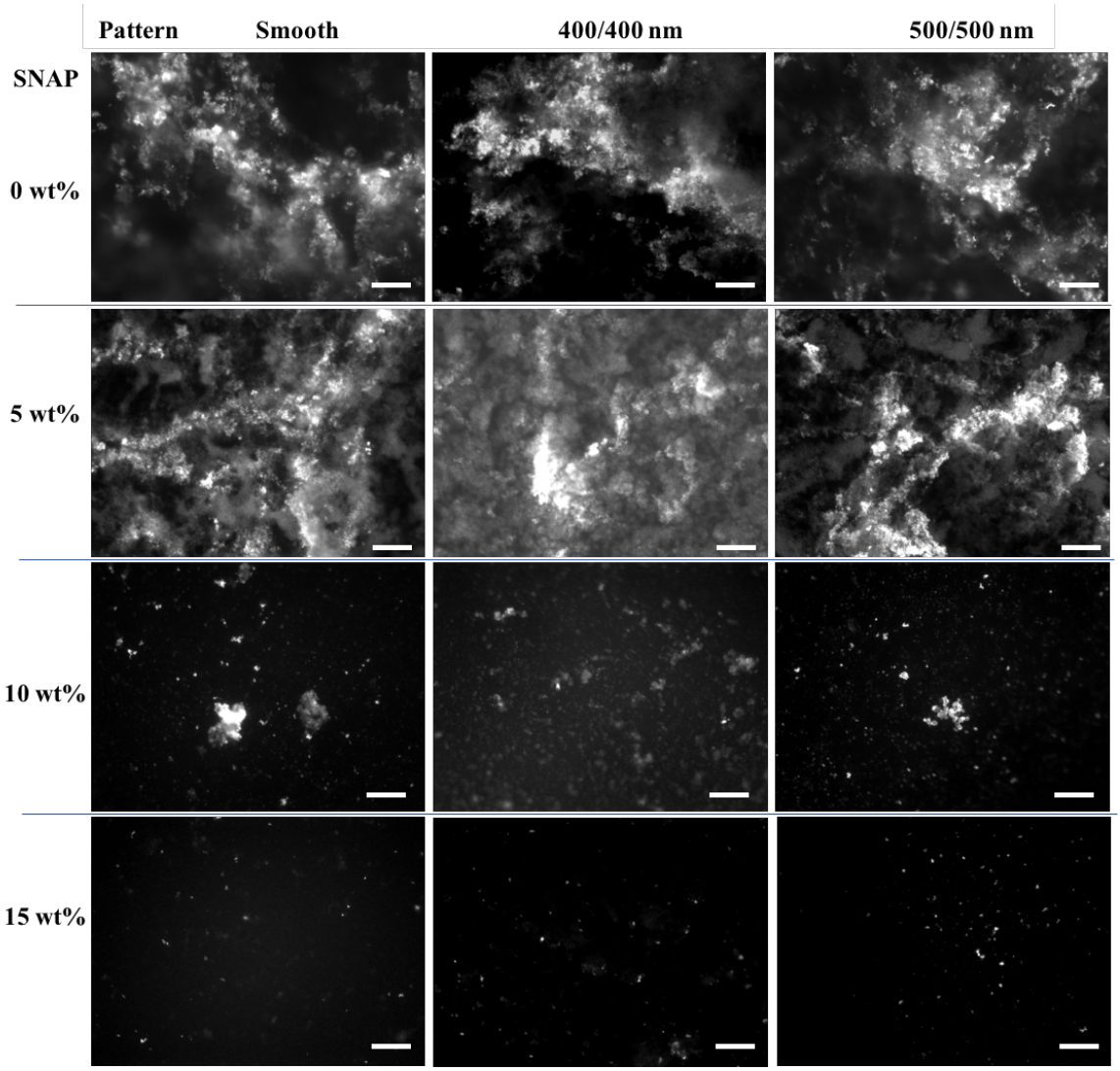

Figure 5.8. Fluorescent optical microscopy images of biofilms formed on a variety of PU film surfaces under static condition for 2 d at 37°C. (Scale bar= 50 μm).

This is consistent with the antimicrobial properties of these new materials (Figure 5.6), where bacteria growth was inhibited in culture medium. Similar bacterial growth and biofilm formation were observed on PU surfaces with the same SNAP-doping level, suggesting that texturing had no significant effect on inhibition of biofilm formation under static conditions. Under static conditions, NO release exerts the more powerful ability to inhibit bacterial growth. In contrast, the combination of texturing and NO release is much more effective in controlling bacterial growth and biofilm formation under shear conditions (see Figure 5.9).

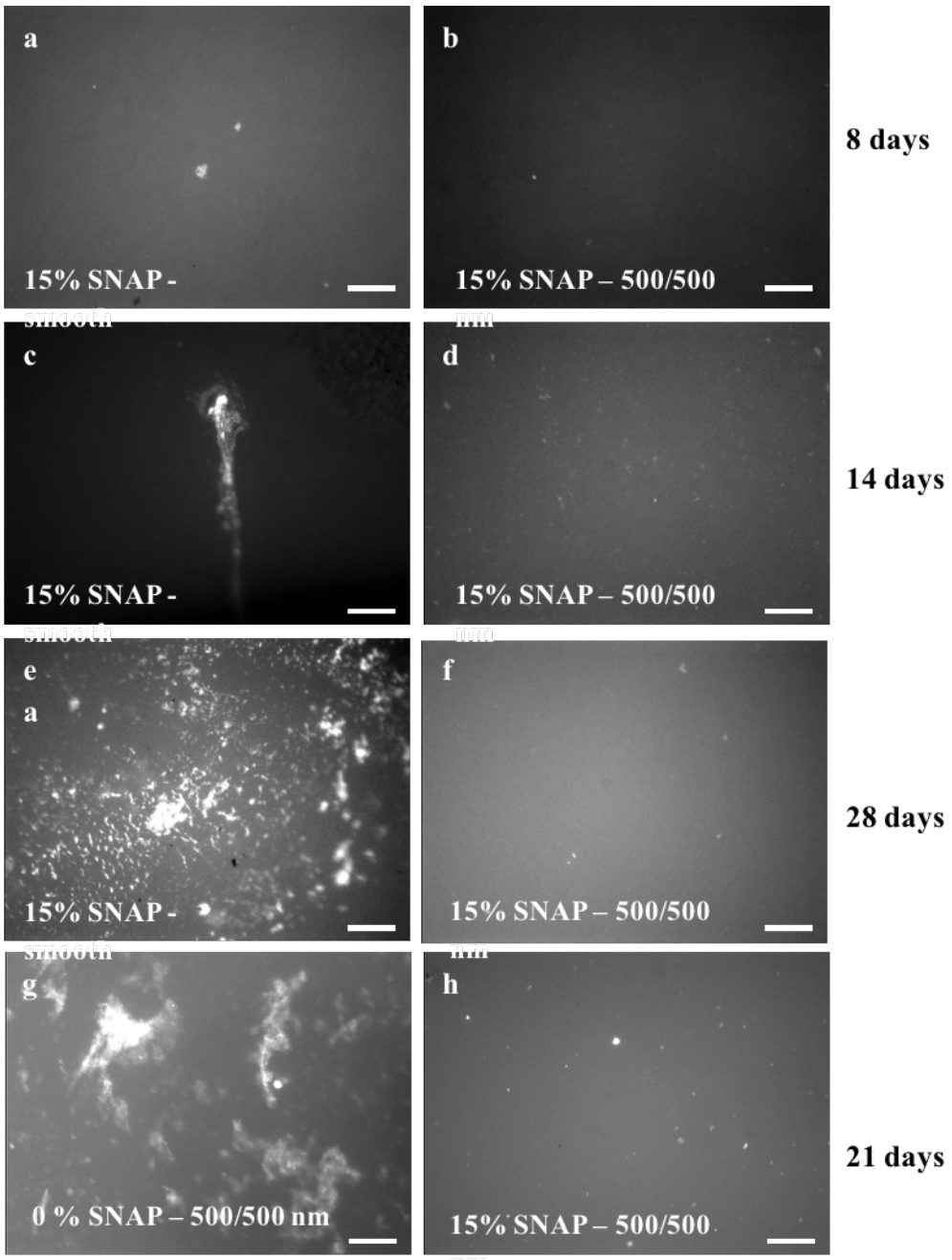

Figure 5.9. Fluorescent optical microscopic images show the biofilm formation on polyurethane film surfaces at 37°C under shear, (a) 15 wt% SNAP – smooth and (b) 15 wt% SNAP and 500/500 nm textured surfaces for 8 d; (c) 15 wt% SNAP – smooth and (d) 15 wt% SNAP and 500/500 nm textured surfaces for 14 d; (e) 15 wt% SNAP smooth and (f) 15 wt% SNAP-500/500 nm textured surfaces for 28 d; (g) regular textured 500/500 nm surface and (h) 15 wt% SNAP-500/500 nm textured surface for 21 d. (image size: 432 μm × 323 μm, scale bar= 50 μm).

The polymer films were further examined for biofilm formation under shear conditions by using a rotating disk system for different periods. There was no significant biofilm observed on 15 wt% SNAP-doped CarboSil film surfaces that were either smooth or textured (with 500/500 nm pattern) over an 8 d period (Figure 5.9a and 5.9b). A small area with biofilm slime was observed on the 15 wt% SNAP smooth surface (Figure 5.9c) after sample was run in culture medium for 14 d, while no biofilm was observed on the 15 wt% SNAP-textured surface under same condition (Figure 5.9d). The duration of experiments was extended to 28 d with the smooth and textured films containing 15 wt% SNAP. It is obvious that there was no biofilm formation on the textured surface while biofilm did form on the smooth surfaces (see Figures 5.9e and 5.9f). To further examine the effect of NO release on biofilm formation, the textured films with or without SNAP were run in culture medium for 21 d. Results show biofilm/slime formed on the regular (0 wt% SNAP) textured surface while no biofilm/slime was observed on 15 wt% SNAP-textured surface (Figures 5.9g and 5.9h). Overall, CarboSil 20 80A PU films containing 15 wt% SNAP doped in the middle layer and the 500/500 nm textured pattern as the top layer can inhibit the biofilm growth for > 28 d. Since the NO release from 15 wt% SNAP-doped PU films can only last up to 10 d, the long term (> 28 d) inhibition of biofilm growth is attributed to the combination of early NO release and the physical surface topography modification created by the pillars. The high NO flux inhibits or kills the bacteria in the initial period and protects the material from biofilm formation. As the NO flux decreases, the surface textured topography continues reducing the bacterial adhesion and inhibiting biofilm formation on surface for longer periods. Results suggest that the combination of NO

release and topography modification provides a promising approach to greatly inhibit biofilm growing for long-term on the polymer surface.

This study has demonstrated the fabrication of the PU films that bear ordered pillar topographies at the top surface and NO release PU in the sublayer. Such a unique combination of surface texturing and NO release can provide a biomimetic surface that exhibits substantial antimicrobial/antibiofilm activity. On one hand, the topographical feature reduces the accessible surface contact area for potential bacterial adhesion. The fractions of total top surface areas for these textured patterns are ~ 25% of the nominal surface area and these textured surfaces alone reduce adhesion of *S. epidermidis* by 61-64% under near static condition in PBS solution for 1 h. The reduction of bacterial adhesion by topographical surface modification may also be attributed to the change of surface energy and surface wettability. The textured pattern makes the surface more hydrophobic due to the Cassie – Baxter effect.[47] Our previous studies showed that the increase of surface hydrophobicity is necessary for the inhibition of bacterial adhesion and biofilm formation on textured surfaces, especially when the size of textured pattern is larger than the dimension of bacterial cells.[40] The submicron textured CarboSil PU surface examined in this study physically reduced the availability of surface contact area and increased the surface hydrophobicity, which both contribute to lowering bacterial adhesion. On the other hand, the addition of SNAP-doped sublayer between base layer and the outer textured surface layer can provide controlled release of NO over an extended period of time. This NO release largely inhibited the growth of bacteria (Figure 5.6) and reduced the bacterial adhesion on the surface overall. Without surface texturing, the 15 wt% SNAP

in middle layer increased the bacterial adhesion inhibition rates up to 75 % after 1 h (Figure 5.7a) and there was no biofilm formed on smooth surface after 2 d under static conditions (Figure 5.8). This clearly suggests the importance of NO release in control of bacterial adhesion and biofilm formation on biomaterial surfaces. Under shear conditions, biofilm formation was found on the smooth surfaces with 15 wt% SNAP within 14 d and on the textured 500/500 nm surface within 21 d, suggesting that each individual treatment alone, either NO release or physical topography modification, can only protect polymer materials less than 21 d. However, integration of NO release and surface texturing together can synergistically inhibit *S. epidermidis* biofilm formation for the longer 28 d period. Since the lifetime of NO release from SNAP-textured films employed in this study only lasted about 10 d, much shorter than the NO release lifetime in other studies,[35, 36] there is also room for improvement in the preparation and design of these new biomimetic polymeric surfaces that may further increase useful lifetime.

Bacterial adhesion is the critical step in the pathogenesis of biomaterial associated infection. Once implanted, a biomaterial surface faces a competition between integration of the material into the surrounding tissue and the adhesion of bacteria. As a successful implant, tissue integration should occur prior to bacterial adhesion and colonization. Therefore, the prevention of bacteria adhesion within the initial hours following implantation, especially in the first 6 h of post-implantation "decisive period", is critical for the long-term success of an implant since the implant is particularly susceptible to surface colonization during this period.[48, 49] The NO possesses a broad-spectrum antibacterial activity against both Gram-positive and Gram-negative bacteria. The NO flux

released from SNAP doped films controls the bacteria growth and inhibits the bacterial adhesion within the initial hours (Figure 5.6), and this helps accelerate the integration of tissue onto the material's surface thereby inhibiting microbial infection. The other benefit of using NO to control bacterial adhesion is the very limited possibility of it promoting bacterial resistance, a common issue for the antibiotic therapy. It has not been reported that NO treatment would cause potential antibiotic resistance.[50] Therefore, the controlled release of NO over a long period (>10 d) is desirable and will provide additional benefits for the long-term success of polymeric implants.

5.4 Conclusion

SNAP-doped and textured CarboSil 20 80A polyurethane films were fabricated with the top layer bearing ordered submicron pillars and a SNAP-doped sublayer for NO release, via a two-stage replication process. Controlling the thickness of top layer can limit and control the diffusion of SNAP during fabrication process and produce the desired uniform pillars on the outermost surface. The NO release rate depends on the SNAP concentration in the sublayer. The 15 wt% SNAP-doped textured polyurethane film release NO for up to 10 d above the lower end of the physiological flux level, 0.5×10^{-10} mol min^{-1} cm^{-2}. The combination of NO release and surface texturing produced a synergistic effect on inhibition of *S. epidermidis* bacterial adhesion, significantly greater than the inhibition of bacterial adhesion achieved by either the use of NO release or texturing alone. The long-term study of biofilm formation on biomaterial surface showed that the biomimetic SNAP-textured CarboSil PU surface reduced the bacterial adhesion and inhibited biofilm formation for at least 28 d, providing a practical approach to improve the biocompatibility of current

biomaterials to control and potentially reduce the rate of pathogenic infections caused by implanted polymeric biomedical devices.

5.5 References

1. R. M. Donlan, *Emerging Infectious Diseases*, 2001, **7**, 277-281.
2. I. Francolini and G. Donelli, *Fems Immunology and Medical Microbiology*, 2010, **59**, 227-238.
3. L. Zhang, J. Gowardman and C. M. Rickard, *International Journal of Antimicrobial Agents*, 2011, **38**, 9-15.
4. R. M. Klevens, J. R. Edwards, C. L. Richards, T. C. Horan, R. P. Gaynes, D. A. Pollock and D. M. Cardo, *Public Health Reports*, 2007, **122**, 160-166.
5. R. P. Wenzel, *Clinical Infectious Diseases*, 2007, **45**, 85-88.
6. D. Campoccia, L. Montanaro and C. R. Arciola, *Biomaterials*, 2013, **34**, 8018-8029.
7. D. Campoccia, L. Montanaro and C. R. Arciola, *Biomaterials*, 2013, **34**, 8533-8554.
8. A. B. Estrela, M. G. Heck and W. R. Abraham, *Current Medicinal Chemistry*, 2009, **16**, 1512-1530.
9. A. J. Scardino, D. Hudleston, Z. Peng, N. A. Paul and R. de Nys, *Biofouling*, 2009, **25**, 83-93.
10. A. J. Scardino, H. Zhang, D. J. Cookson, R. N. Lamb and R. de Nys, *Biofouling*, 2009, **25**, 757-767.
11. W. Barthlott and C. Neinhuis, *Planta*, 1997, **202**, 1-8.
12. B. Bhushan and Y. C. Jung, *Progress in Materials Science*, 2011, **56**, 1-108.
13. T. Sun, G. Qing, B. Su and L. Jiang, *Chemical Society Reviews*, 2011, **40**, 2909-2921.
14. S. Shin, J. Seo, H. Han, S. Kang, H. Kim and T. Lee, *Materials*, 2016, **9**, 116.
15. K. K. Chung, J. F. Schumacher, E. M. Sampson, R. A. Burne, P. J. Antonelli and A. B. Brennan, *Biointerphases*, 2007, **2**, 89-94.
16. S. T. Reddy, K. K. Chung, C. J. McDaniel, R. O. Darouiche, J. Landman and A. B. Brennan, *Journal of Endourology*, 2011, **25**, 1547-1552.
17. L.-C. Xu and C. A. Siedlecki, *Acta Biomaterialia*, 2012, **8**, 72-81.
18. K. R. Milner, A. J. Snyder and C. A. Siedlecki, *Journal of Biomedical Materials Research Part A*, 2006, **76A**, 561-570.
19. M. W. Radomski, R. M. J. Palmer and S. Moncada, *Biochemical and Biophysical Research Communications*, 1987, **148**, 1482-1489.
20. C. Bogdan, *Nat Immunol*, 2001, **2**, 907-916.
21. F. C. Fang, *Journal of Clinical Investigation*, 1997, **99**, 2818-2825.
22. M. L. Jones, J. G. Ganopolsky, A. Labbé, C. Wahl and S. Prakash, *Applied Microbiology and Biotechnology*, 2010, **88**, 401-407.
23. B. J. Privett, A. D. Broadnax, S. J. Bauman, D. A. Riccio and M. H. Schoenfisch, *Nitric Oxide*, 2012, **26**, 169-173.
24. A. B. Seabra, D. Martins, M. Simoes, R. da Silva, M. Brocchi and M. G. de Oliveira, *Artificial Organs*, 2010, **34**, E204-E214.
25. J. Park, J. Kim, K. Singha, D.-K. Han, H. Park and W. J. Kim, *Biomaterials*, 2013, **34**, 8766-8775.
26. W. Cai, J. Wu, C. Xi and M. E. Meyerhoff, *Biomaterials*, 2012, **33**, 7933-7944.

27. N. Barraud, M. J. Kelso, S. A. Rice and S. Kjelleberg, *Current Pharmaceutical Design*, 2015, **21**, 31-42.
28. M. C. Frost, M. M. Reynolds and M. E. Meyerhoff, *Biomaterials*, 2005, **26**, 1685-1693.
29. H. Handa, E. J. Brisbois, T. C. Major, L. Refahiyat, K. A. Amoako, G. M. Annich, R. H. Bartlett and M. E. Meyerhoff, *Journal of materials chemistry. B, Materials for biology and medicine*, 2013, **1**, 3578-3587.
30. V. N. Varu, N. D. Tsihlis and M. R. Kibbe, *Vasc Endovascular Surg*, 2009, **43**, 121-131.
31. P. N. Coneski and M. H. Schoenfisch, *Polymer Chemistry*, 2011, **2**, 906-913.
32. J. R. Laver, S. McLean, L. A. Bowman, L. J. Harrison, R. C. Read and R. K. Poole, *Antioxid Redox Signal*, 2013, **18**, 309-322.
33. H. Ren, J. Wu, C. Xi, N. Lehnert, T. Major, R. H. Bartlett and M. E. Meyerhoff, *ACS Appl Mater Interfaces*, 2014, **6**, 3779-3783.
34. C. M. Moore, M. M. Nakano, T. Wang, R. W. Ye and J. D. Helmann, *Journal of Bacteriology*, 2004, **186**, 4655-4664.
35. E. J. Brisbois, H. Handa, T. C. Major, R. H. Bartlett and M. E. Meyerhoff, *Biomaterials*, 2013, **34**, 6957-6966.
36. Y. Wo, Z. Li, E. J. Brisbois, A. Colletta, J. Wu, T. C. Major, C. Xi, R. H. Bartlett, A. J. Matzger and M. E. Meyerhoff, *ACS Appl Mater Interfaces*, 2015, **7**, 22218-22227.
37. E. J. Brisbois, R. P. Davis, A. M. Jones, T. C. Major, R. H. Bartlett, M. E. Meyerhoff and H. Handa, *Journal of materials chemistry. B, Materials for biology and medicine*, 2015, **3**, 1639-1645.
38. A. Colletta, J. Wu, Y. Wo, M. Kappler, H. Chen, C. Xi and M. E. Meyerhoff, *ACS Biomaterials Science & Engineering*, 2015, **1**, 416-424.
39. S. R. Gill, D. E. Fouts, G. L. Archer, E. F. Mongodin, R. T. Deboy, J. Ravel, I. T. Paulsen, J. F. Kolonay, L. Brinkac, M. Beanan, R. J. Dodson, S. C. Daugherty, R. Madupu, S. V. Angiuoli, A. S. Durkin, D. H. Haft, J. Vamathevan, H. Khouri, T. Utterback, C. Lee, G. Dimitrov, L. Jiang, H. Qin, J. Weidman, K. Tran, K. Kang, I. R. Hance, K. E. Nelson and C. M. Fraser, *J Bacteriol*, 2005, **187**, 2426-2438.
40. L. C. Xu and C. A. Siedlecki, *Biomedical Materials*, 2014, **9**, 035003.
41. P. G. Wang, M. Xian, X. Tang, X. Wu, Z. Wen, T. Cai and A. J. Janczuk, *Chemical Reviews*, 2002, **102**, 1091-1134.
42. C.-E. Lin, S. K. Richardson, W. Wang, T. Wang and D. S. Garvey, *Tetrahedron*, 2006, **62**, 8410-8418.
43. M. W. Vaughn, L. Kuo and J. C. Liao, *Am J Physiol*, 1998, **274**, H2163-2176.
44. J. D. Patel, M. Ebert, R. Ward and J. M. Anderson, *Journal of Biomedical Materials Research Part A*, 2007, **80A**, 742-751.
45. C. P. Xu, N. P. Boks, J. de Vries, H. J. Kaper, W. Norde, H. J. Busscher and H. C. van der Mei, *Applied and Environmental Microbiology*, 2008, **74**, 7522-7528.
46. O. M. Hartford, E. R. Wann, M. Hook and T. J. Foster, *Journal of Biological Chemistry*, 2001, **276**, 2466-2473.
47. A. Cassie and S. Baxter, *Transactions of the Faraday Society*, 1944, **40**, 546-551.
48. K. A. Poelstra, N. A. Barekzi, A. M. Rediske, A. G. Felts, J. B. Slunt and D. W. Grainger, *Journal of Biomedical Materials Research*, 2002, **60**, 206-215.

49. E. M. Hetrick and M. H. Schoenfisch, *Chem Soc Rev*, 2006, **35**, 780-789.
50. Y. Wo, E. J. Brisbois, R. H. Bartlett and M. E. Meyerhoff, *Biomaterials Science*, 2016, **4**, 1161-1183.

CHAPTER 6

Dual Functioning Antibacterial Surface via Controlled Delivery of Nitric Oxide Combined with Submicron-Textured Surface Topography

Wo, Y. [†]; Xu, L**.** [†]; Meyerhoff, M.E.; Siedlecki, C.A. *Biomater Sci*, *submitted.*

[†] These authors have contributed equally to this work.[*]

6.1 Introduction

Bacterial attachment and biofilm formation play a substantial role in causing health-care related infections in the hospital, especially those associated with the use of implanted biomedical devices, such as intravascular (IV) catheters, urinary catheters, prosthetic heart valves, and orthopedic implants.[1–3] Such biomaterial-associated infections are extremely difficult to treat by use of antibiotics alone due to formation of microbial biofilm that consists of an extracellular polymeric substance (EPS), also known as the "house of biofilm cells". EPS is known to be a physical barrier that protects bacteria in mature biofilm from

[*] The SNAP synthesis, polymer impregnation, NO release measurements and statistical analysis were conducted by the Ph.D. candidate, while the preparation of the textured materials, AFM characterization and antibacterial testing reported in this chapter were conducted by Dr. Lichong Xu.

traditional antibiotic treatment.[4,5] It has been suggested that the slow penetration rate of antibiotics can thus foster the expression of genes in the bacteria that mediate antibiotic resistance.[6] Thus, surgical removal and replacement of an infected implanted devices often is the only option in this situation, causing significant morbidity and mortality, and this greatly influences patient outcome and healthcarecost.[7,8] Several bacteria are commonly found to be associated with catheter-related bloodstream infections (CRBSIs), including *Staphylococcus aureus* (*S. aureus*), *Staphylococcus epidermidis* (*S. epidermidis*), *Pseudomonas aeruginosa* (*P. aeruginosa*) and *Escherichia coli* (*E. coli*).[9–12] Table 6.1 summarizes the four bacteria's characteristics based on their shape, gram staining, with or without coagulase, virulence and % responsible for CRBSIs.

Table 6.1. Summary of four bacteria and their shape, gram staining, virulence and % responsible for CRBSIs.

Bacteria Strain	Shape	Gram Staining	With or without coagulase	Virulence and % responsible for CRBSIs
S. aureus	grape	positive	coagulase positive	40 % [9,10] 25 % in children [39,40] 22 % [41] 20 % is responsible for CLABSIs [42] ** MRSA accounts for >50 % of all S.aureus infection [43] 1 in 4 *S.aureus* colonization on IV catheters develop to bacteremia if not treated w/antibiotics [39,44]
S. epidermidis	grape	positive	coagulase negative	< 34 % in children [39,40] * < 37 % [41] * < 8 % [10] * < 31 % is responsible for CLABSIs [42] ** 22 %, repsonsible for BSIs in ICU in US, causing 2 billion annually in US [12]
P. aeruginosa	rod	negative	coagulase negative	16 % [10] 5.5 % [41]
E. coli	rod	negative	n/a	8 % [10] 6 % is responsible for CLABSIs [42] **

* The data reported in the papers are for coagulase negative *Staphylococci* (CoNS) in general, in which one of the most important strain is *S. epidermidis,* therefore the % responsible for CRBSIs by *S. epidermidis* is reported as "< % for CoNS".
** CLABSIs is central line associated blood stream infections.

The first step of biofilm formation on the surface of medical devices is bacteria attachment. For a successful long-term implant, the device should ideally be able to prevent bacterial colonization, especially in the most susceptible initial 6 h of post-implantation which is termed the "decisive period".[13] Therefore, developing biomaterial surfaces that can resist bacteria attachment represents one of the most straightforward solutions to this problem.[8] Bacteria can adhere to biomaterial surface via either nonspecific interactions or indirect binding to molecules adsorbed on the material. Therefore, one strategy is to mediate bacterial adhesion by modifying the material's surface property and reduce the initial bacterial attachment. Surface texture manufacturing techniques can be applied to biomaterials as a means to obtain topographical features that mimic the skin of a shark.[14,15] This physical modification of the polymer surface can reduce the surface contact area and the availability of binding sites of bacteria cells. Xu et al. have demonstrated that submicron-textured surface featuring patterns with pillars of diameter and spacing of 400/400 nm and 500/500 nm can decrease the adhesion and bacterial colonization of *S. aureus* and *S. epidermidis*.[8] Helbig et al. have also reported ordered surface structure with dimensions (holes, posts or lines) in similar range as bacterial cell size can decrease *S. epidermidis* and *E. coli* bacterial adhesion, regardless of contact time (minutes to hours) or surface hydrophobicity.[16]

Antibacterial biomaterials that can release nitric oxide (NO), which mimics the NO release from nasal epithelial cells, macrophage anti-inflammatory cells and endothelial cells, etc.,[3,17–21] have also gained great research interest over the past two decades. NO serves as an indispensable antimicrobial agent in our immune response system to combat infectious

diseases.[21–23] NO possesses broad-spectrum antibacterial activity against both gram-positive and gram-negative bacteria, including methicillin-resistant *S. aureus* (MRSA), without any known antibiotic resistance.[24] Low levels of NO (picomolar to nanomolar in solution phase) are also an important signaling molecule in bacterial quorum sensing to minimize bacterial adhesion and disperse mature biofilm.[25,26] Many NO releasing polymeric materials, where NO is released/generated via decomposition of various NO donors (e.g., *N*-diazeniumdiolates or *S*-nitrothiols, etc.) or reduction of nitrite through electrochemical modulation, have been evaluated for their antibacterial and antibiofilm efficacy *in vitro*.[27–33] *S*-Nitroso-*N*-acetylpenicillamine (SNAP) is a particularly attractive *S*-nitrothiols for incorporation into biomedical grade polymers for NO release application because of its low cost, safety and potential for long-term NO release.[6,30,34,35] SNAP also exhibits long term stability during 8 months storage in the dark at 37 °C when incorporated into CarboSil 20 80A, a low water uptake silicone-polycarbonate-urethane tri-block copolymer (see Chapter 2 of this dissertation).[30] Polyurethane block copolymers have been widely used for blood-contacting medical devices due to their relatively good biocompatibility, that partly result from the micro-phase separation between the thermodynamic immiscibility of hard segments and soft segments.[8,36,37] Specifically, SNAP-doped CarboSil IV catheters exhibited potent antibacterial effect *in vitro* against *S. aureus* with 5-log unit reduction of viable bacteria count on SNAP catheter surface than the corresponding controls, in a 7 d study using a drip-flow biofilm reactor.[30] These results have demonstrated that NO releasing materials represent an attractive antibacterial biomaterial for use in preparing IV catheters and other blood contacting medical devices.

Although either physical surface modification (topographical surface textures) and chemical modification (nitric oxide release) have both been proven to be effective approach to inhibit bacterial adhesion and biofilm formation in prior studies, a very promising approach would be to combine these two techniques to create enhanced dual functioning antibacterial polymer surfaces for clinical use. Since both approaches can reduce bacterial attachment and thus prevent biofilm formation, the single cells either adhered onto catheter surface or in bulk of blood, are subject to antibiotic treatment without the physical barrier and protection from EPS, which would greatly reduce the possibility of CRBSIs. Therefore, a submicron textured surfaces with reduced surface area that would decrease bacteria adhesion coupled with long-term NO release can better inhibit biofilm formation than either of these two methods alone.

Previously, we have reported our effort to prepare CarboSil films that bear ordered pillar topography at the top surface using a soft lithography two-stage replication process using by layer-by-layer spin-coating technique and formed a ”sandwich-like” film configuration with SNAP-doped CarboSil in middle layer and top thin layer textured with pattern (see Chapter 5). Obviously such a process is time-consuming, often requiring 1-2 weeks to reach the desired thickness. Furthermore, the repeated spin-coating of new SNAP-polymer solution onto the dried SNAP-polymer surface may lead to the re-dissolution and re-crystallization of SNAP, causing undesired SNAP degradation during fabrication.

Therefore, herein, a simple solvent impregnation approach to incorporate NO donor SNAP into the bulk of a surface textured polymer film is described. Textured CarboSil films

without SNAP were first fabricated by spin-coating[8] and dried. Then the polymer film bearing the ordered pillar topography was immersed in an optimized SNAP/solvent solution for SNAP impregnation. After thorough drying, the resulting material is shown to achieve long-term NO release. StreamLine High Resolution (HR) Raman mapping characterization was utilized to elucidate the chemical constituent of crystals inside of the SNAP-impregnated CarboSil films in combination with the 2D representation of crystal distribution. *In vitro* bacterial adhesion studies were conducted to examine the anti-bacterial adhesion efficacy and analyze if there is any interaction between surface texturing and NO release and whether the antibacterial efficacy from SNAP-impregnated textured CarboSil films are additive or synergistic against the four microorganisms mentioned above.

6.2 Experimental Section

6.2.1 Materials

N-Acetyl-D-penicillamine (NAP), sodium nitrite, L-cysteine, sodium chloride, potassium chloride, sodium phosphate dibasic, potassium phosphate monobasic, copper (II) chloride, ethylenediaminetetraacetic acid (EDTA), tetrahydrofuran (THF) and *N*,*N*-dimethylacetamide (DMAc) were purchased from Sigma-Aldrich (St. Louis, MO). Methanol (MeOH), methyl ethyl ketone (MEK), hydrochloric acid, sulfuric acid were products of Fisher Scientific (Hampton, NH). CarboSil 20 80A was obtained from DSM Biomedical Inc. (Berkeley, CA). All aqueous solutions were prepared with 18.2 MΩ-deionized water using a Milli-Q filter from EMD Millipore (Billerica, MA). Phosphate buffered saline (PBS), pH 7.4, containing 138 mM NaCl, 2.7 mM KCl, 10 mM sodium

phosphate, and 100 μM EDTA was used for all *in vitro* experiments. Textured silicon wafers were fabricated by RTI International (Research Triangle Park, NC) based on requirements. *S. epidermidis* ATCC 35984, *S. aureus* ATCC 25904, *P. aeruginosa* ATCC 27853 and *E. coli* ATCC 11775 were obtained from the American Type Culture Collection (ATCC) (Manassas, VA).

6.2.2 Preparation of smooth and textured CarboSil film

The CarboSil 2080A PU film surfaces were textured with ordered arrays of pillars using a modified soft lithography two-stage replication molding technique that has been described previously.[8] Briefly, textured silicon wafers with different ordered array of pillars, either fabricated by RTI International (Research Triangle Park, NC) or Penn State Nanofabrication Lab (State College, PA), were used as the master patterns to prepare the master PDMS molds and the corresponding CarboSil films were then fabricated. CarboSil pellets were dissolved in *N*,*N*-dimethylacetamide (DMAc) at concentration of 15 w/v% (1.5 g PU in 10 ml DMAc) and was spin-coated onto the silicon mold to prepare the textured CarboSil films. To obtain the highest replication efficiency of surface topography, the films were prepared by spin casting CarboSil onto a PDMS mold at 1200 rpm for 1 min in one thin layer first, followed by degassing and curing overnight at room temperature under vacuum. Then, additional layers of CarboSil were added by spin casting at 600 rpm for 1 min, respectively, until reaching the desired thickness of 700 μm. Each layer was degassed and cured at room temperature under vacuum. The master silicon wafers with pillar geometries having diameter (d), separation (s) and height (h) values of 400/400/600 nm, 500/500/600 nm and 700/700/300 nm were used as the masters for replicating CarboSil

textured films for AFM images, but only 700/700/300 nm textured films were used in all *in vitro* experiments. Smooth CarboSil films were also prepared by spin-coating against a smooth PDMS mold.[8]

6.2.3 SNAP impregnation of textured CarboSil film

Small disks of films (10 mm in diameter) were punched out from both the smooth and textured CarboSil films. As described previously in Chapter 4, the films were impregnated in solutions (70 % MEK and 30 % MeOH) with different SNAP solution concentrations (35, 65 and 110 mg/mL) to achieve 5, 10 and 15 wt% SNAP loading, respectively. After 2 h of impregnation, the films were removed from the impregnation solution, quickly wash with methanol to remove any residual SNAP solution on the film surface, and allowed to dry thoroughly in an ambient environment protected from light exposure.

6.2.4 Characterization of surface topography by atomic force microscopy (AFM)

Multimode AFM with a Nanoscope IIIa control system (software version 5.12r3, Veeco, Santa Barbara, CA) was used to examine the surface textures of CarboSil films operated in tapping mode (intermittent contact) using Si probes having aspect ratio of ~ 4:1 (TETRA, K-Tek Nanotechnology, Wilsonville, OR) in air. AFM was also used to image the bacterial adhesion on CarboSil PU surfaces. AFM images were viewed and analyzed by off-line AFM software (version 5.12r3, Veeco, Santa Barbara, CA).

6.2.5 Surface water wettability measurement

The water wettability of all CarboSil PU films was determined as the advancing water contact angle measured by the Sessile drop method using a Krüss contact angle goniometer. All measurements were made using water as a probe liquid and an ~ 8 µl of water droplet was used for the measurement. Advancing contact angles were obtained by a minimum of eight independent measurements and are presented as mean ± standard deviation.

6.2.6 NO release measurement by nitric oxide analyzer (NOA)

Nitric oxide release from the CarboSil films was measured by a Nitric Oxide Analyzer (NOA) 280i (Boulder, CO) via chemiluminescence. Briefly, films with diameter of ~10 mm were placed in the sample vessel immersed in 4 mL PBS containing 100 µM EDTA at 37°C. NO was continuously purged from the buffer and swept from the headspace using nitrogen gas and a bubbler into the chemiluminescence detection chamber of the NOA. When not being tested with the NOA, the SNAP-doped samples were incubated in PBS under same conditions, protected from light exposure.

6.2.7 Characterization of SNAP-impregnated and SNAP-doped CarboSil films by Raman spectroscopy

StreamLine High Resolution (HR) Raman mapping characterization was utilized to map the two-dimensional SNAP crystal distribution at the cross-section of a 5 wt% SNAP-impregnated CarboSil film and a 5 wt% SNAP-doped CarboSil film. The film was first cut to expose its cross-section and then embedded into optimal cutting temperature compound (OCT), allowed to harden at -20 °C, and then cut carefully into 30 µm thick

slices by a Leica CM3050S research cryostat. StreamLine HR Raman Mapping experiments were conducted by using a Renishaw inVia Raman microscope equipped with a Leica microscope, a RenCam CCD detector and a 785nm laser employing a 1200 lines/nm grating and a 50 μm slit. The obtained spectrum of each spot was fitted with pure orthorhombic SNAP spectrum as the reference, and the green areas in the presented figures correspond to regions fitting the characteristic peaks of orthorhombic SNAP.

6.2.8 Bacterial adhesion on the surface of CarboSil films with different configuration

The methods used for culturing and collection of bacteria have been reported previously.[8] Bacterial colonies of four different strains were cultured in tryptic soy broth (TSB) at 37 °C for 24 h and collected by centrifuge at 1360g for 10 min. The collected bacteria were then re-suspended in PBS and diluted to a final concentration of 1×10^7 CFU/mL, as determined by turbidity measurement at 600 nm using a spectrophotometer. All CarboSil films, both smooth or textured, with increasing SNAP concentration (0, 5, 10, 15 wt%), were pre-hydrated in Millipore water for 24 h and conditioned in PBS for 1 h before use. Bacterial adhesion studies were conducted by placing the CarboSil films in a 12-well home-made microwell containing 0.5 mL of bacteria suspended in PBS solution at 37°C for 1 h under static conditions. After the experiment, the film was washed with PBS 3 times, and then the bacteria remaining on the film surface were fixed in 2.5% glutaraldehyde for 2 h. The bacteria on the films were washed with PBS again before being stained with Hoechst 33258 (Invitrogen) and analyzed under a fluorescence optical microscope (Nikon, Eclipse 80i). Nine optical microscopy images of each film were taken

(50 μm × 50 μm) and the number of bacteria adhered on the surface was counted and average ± standard error or means were used for statistical analysis.

6.2.9 Statistical Analysis

Statistical analysis of the bacterial adhesion data was performed using IBM SPSS statistics 22. The data were analyzed using a univariate general linear model to determine the significance of SNAP, surface texturing, and the interaction of SNAP×texturing on the reduction of bacterial adhesion. Briefly, the 700/700/300 texture topography property of the film was set as covariate X1 (depicted as 0 or 1), and the SNAP concentration in the film was set as fixed factors X2 (depicted as 0, 1, 2 or 3). The number of bacteria adhered on the surface was the dependent variable, Y. The analysis was conducted to determine if X1 or X2 have significant impact on the outcome, and also to determine if there is any significant interaction between X1 and X2. The data analysis was always first conducted assuming there is interaction between the two factors, then if the significance p is <0.05, then there is interaction between the factors, suggesting that texturing and NO release have a synergistic effect on reducing bacteria adhesion. If the significance p is > 0.05, then there is no interaction between surface topography and NO release and they have only an additive effect on reducing bacteria adhesion.

6.3 Results and Discussion

6.3.1 Characterization of SNAP-impregnated textured CarboSil films

CarboSil films were textured with ordered arrays of pillars using a soft lithography two-stage replication molding technique. Initially, Carbosil films with different dimensions,

including 400/400/600 nm, 500/500/600 nm, 700/700/300 nm patterns, depicted by their diameter/separation/height, were prepared Textured silicon wafers were used as the master patterns to prepare the master PDMS molds (Figure 6.1A) and the corresponding CarboSil films were then fabricated using the PDMS molds (Figure 6.1B). Textured Carbosil film bearing different topographical patterns were punched out and impregnated with 5, 10 and 15 wt% SNAP loading. However, further topography images showed that the cylinder pillars with dimensions of 400 or 500 nm in diameter and 600 nm in height were collapsed due to the solvent during impregnation, while the shorter and larger pillars with 700 nm in size and 300 nm in height remain intact, which suggested that the solvent impregnation process is more suitable for the pillars with low aspect ratio of height to diameter. As a result, 5 wt%, 10 wt% and 15 wt% SNAP-impregnated smooth and textured (700/700/300 nm) CarboSil films were fabricated for further characterization and bacterial adhesion studies.

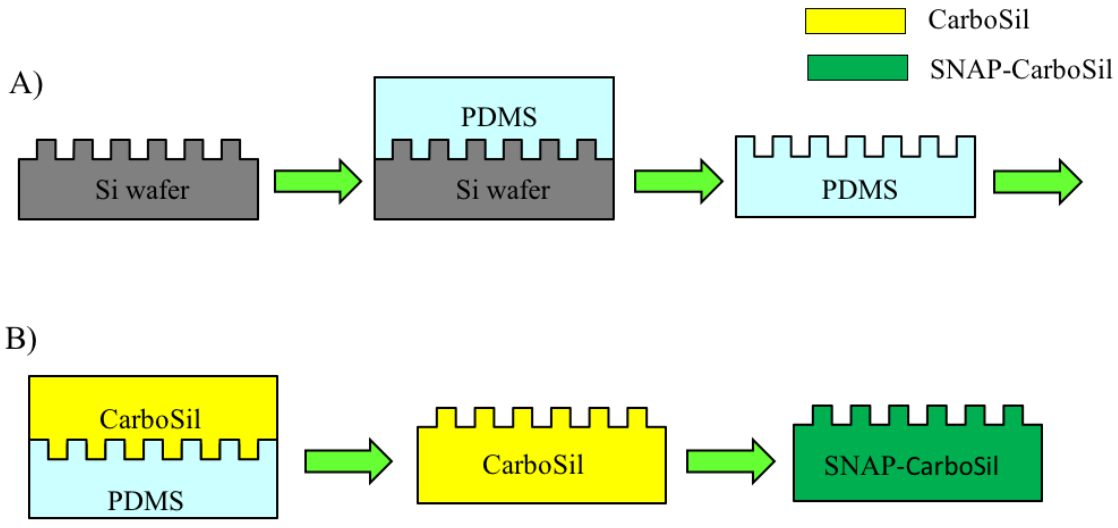

Figure 6.1. Schematic diagrams of the steps in the soft lithography two-stage replication molding technique employed to prepare textured CarboSil films, followed by SNAP impregnation of the CarboSil films.

The topographical surface texture and pillars remain intact in all SNAP-impregnated textured CarboSil films (5, 10 and 15 wt%), as shown in the atomic force microscopy (AFM) images. Representative AFM images of the textured film before and after 10 wt% SNAP impregnation are shown in Figure 6.2.

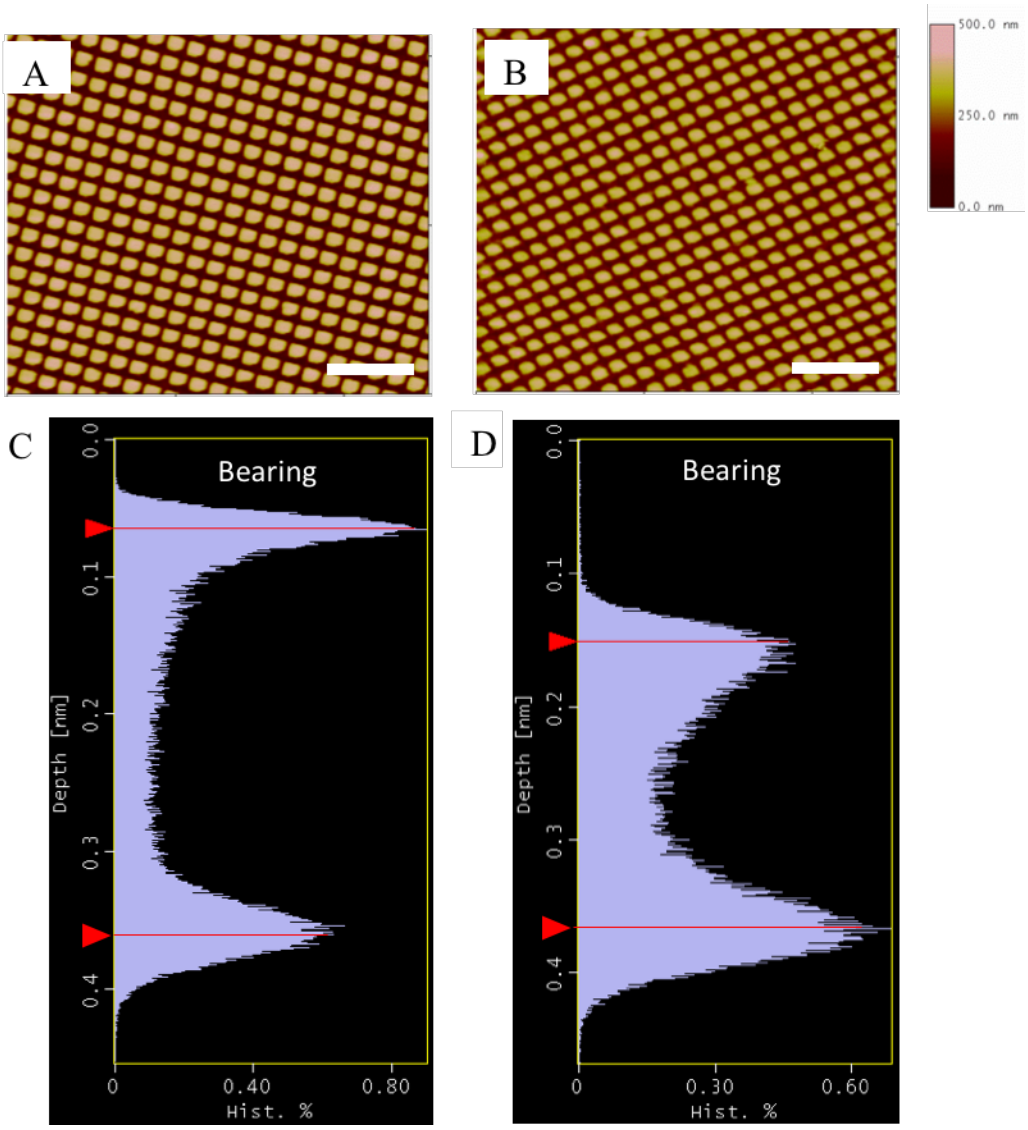

Figure 6.2. 2D AFM images of textured PU surface (A) before and (B) after impregnation of SNAP. Bearing analysis showing the overall height difference of pillars (C) before and (D) after impregnation of SNAP (scale bar = 5 μm). The red cursors represent the height levels of surface features with maximum bearing area fraction. The distance between two cursors represents the average height of pillars.

The bearing analysis of surface topography shows that the average height of pillars of films before impregnation is about 300 nm, while the height of pillars reduced to about 220 nm after impregnation. The reduction in pillar height is believed to be due to the impregnation of SNAP that lifts the level of the base. The regular smooth CarboSil films and CarboSil films with SNAP impregnation are hydrophobic, with the water contact angle of ~90.5°. Surface texturing increased the hydrophobicity of the polymer films to 122.5° due to air trapped in between pillars (Figure 6.3), but lower than the contact angle of regular textured films (~145°). The results demonstrate that SNAP impregnation into polymer films decreased the hydrophobicity of the polymer surface.

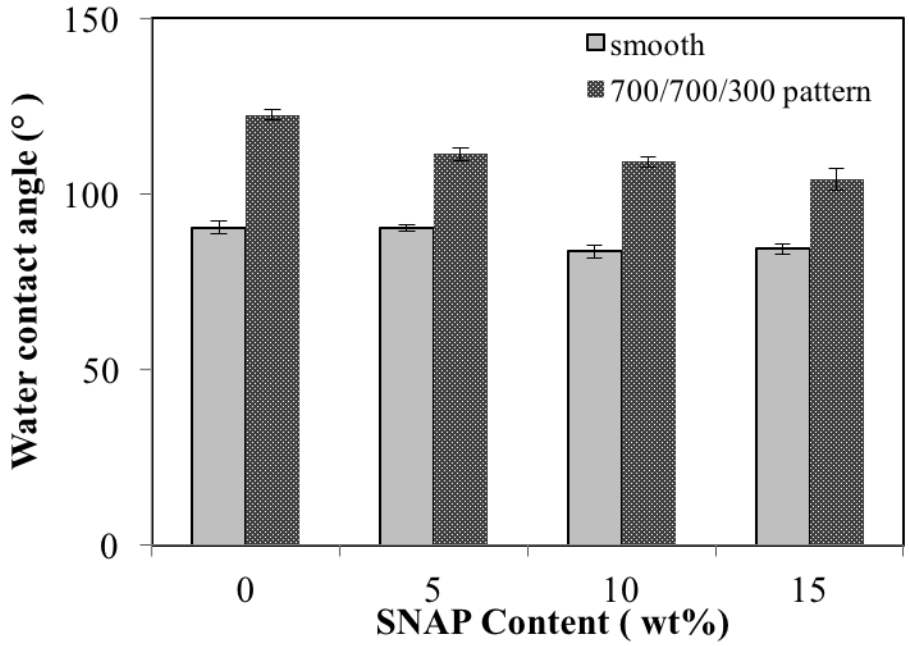

Figure 6.3. Water contact angle of smooth and textured (700/700/300 nm pattern) CarboSil films with different concentration (0, 5, 10 and 15 wt%) of SNAP impregnation.

NO release varied with the concentration of SNAP incorporated into the PU films. NO release of 5 wt%, 10 wt% and 15 wt% SNAP-impregnated textured CarboSil films were

measured by the nitric oxide analyzer (NOA) via chemiluminescence. Briefly, the NO release from films in PBS buffer at 37°C was measured at various time points for 4 h each time, and the average NO flux over the 4 h period was used to represent the average NO flux of the film during that day. The films were incubated in PBS buffer at 37 °C and protected from light when not being tested, and the buffer solution was changed daily. NO release from SNAP-impregnated textured films can last up to 9, 19 and 38 d at physiological conditions (with flux > 0.5 x 10^{-10} mol cm^{-2} min^{-1}, the lower end of physiological NO level released by endothelial cells) for the 5 wt%, 10 wt% and 15 wt% films, respectively (see Figure 6.4).

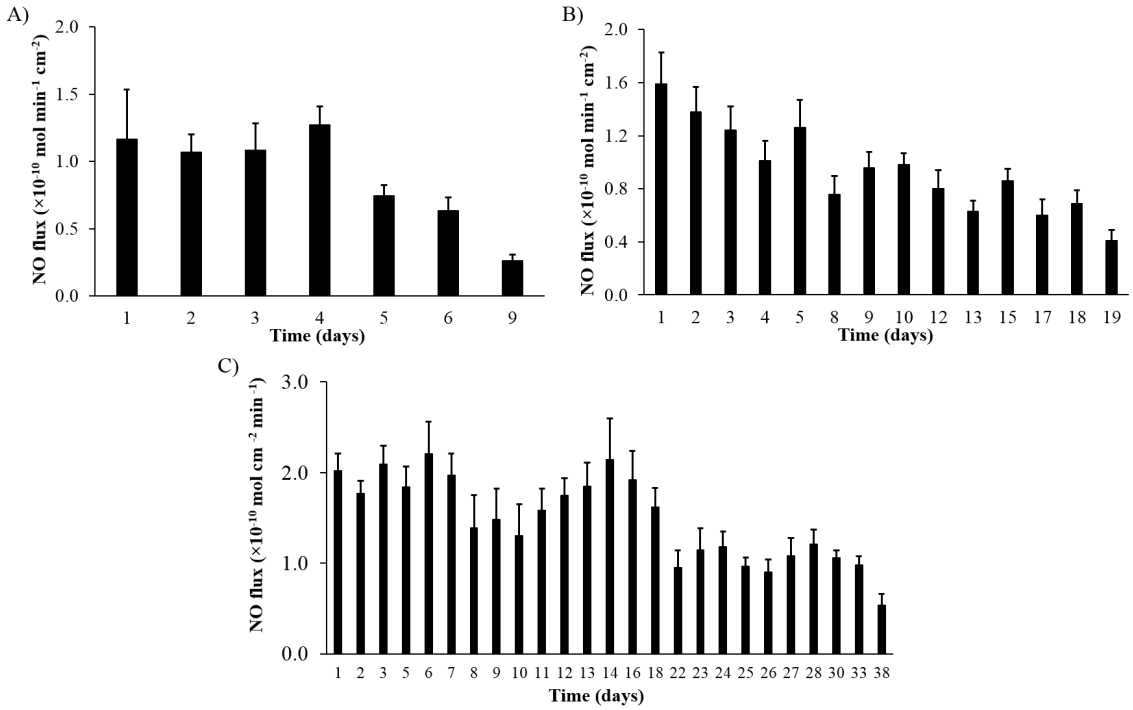

Figure 6.4. NO release profile at physiological conditions from 5 wt% (A), 10 wt% (B) and 15 wt% (C) SNAP-impregnated CarboSil films with 700/700/300 nm surface textures.

The main advantage of SNAP impregnated textured CarboSil films is its preparation time efficiency, stability and extended NO release lifetime. In the previous study, we have

prepared SNAP-textured CarboSil film by a layer-by-layer type spin-coating procedure where SNAP is doped in the middle layer of the sandwich like CarboSil film bearing textured pattern on the top (Chapter 5). However, not only is that process extremely time-consuming, but also the repeated dissolution of crystalized SNAP may lead to SNAP degradation during fabrication and shorten the NO release lifetime. The solvent impregnation technique allows SNAP incorporation into the CarboSil polymer via a one step method following polymer solvent swelling, and the impregnated SNAP will crystallize in the bulk of the material as the solvents evaporate (see Chapter 4). It is known that SNAP can partially dissolve in CarboSil polymer with a solubility limit of ~3.4-4 wt%[30] and SNAP exceeding this concentration will form a stable polymer-crystal composite that can lead to stable, long-term NO release from the polymer film.

In order to compare the SNAP crystal distribution in textured CarboSil film prepared by the spin-coating and solvent impregnation methods, Raman mapping was conducted to compare the crystal distribution in 5 wt% SNAP-doped and 5 wt% SNAP-impregnated CarboSil films. It was hypothesized that SNAP molecules were "inserted" into the interspace between the layers of the CarboSil 20 80A polymer (see Chapter 4), within a lamellae structure of the PDMS phase and the polycarbonate/polyurethane hard segment mixed phase,[38] during solvent impregnation. This process may result in a slightly less uniform crystals distribution in the 5 % SNAP-impregnated films when compared to the 5 wt% SNAP-doped films that are prepared by the traditional spin coating technique employed in Chapter 4. Two-dimensional Raman spectra of the cross-section of 5 wt%

SNAP-doped textured CarboSil film (A) and 5 wt% SNAP-impregnated film (Figure 6.5) indeed validate this hypothesis.

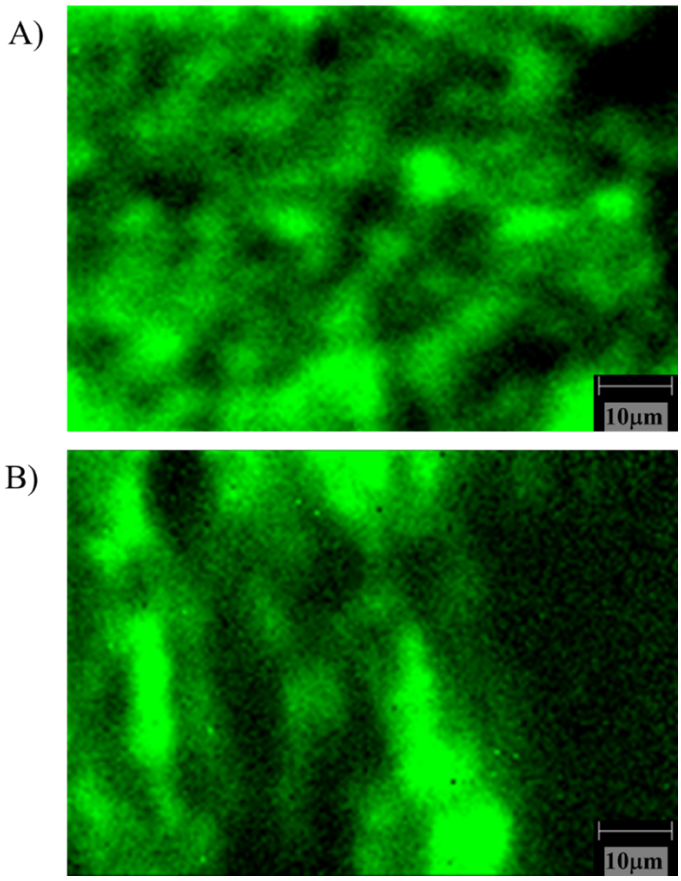

Figure 6.5. StreamLine HR Raman mapping results for fitting of cross section of A) 5 wt% SNAP-doped CarboSil films and (B) 5 wt% SNAP-impregnated CarboSil films, under 50× objective. Green areas represent the distribution of crystalline SNAP, which is less uniform in the 5 wt% SNAP-impregnated CarboSil films.

6.3.2 Evaluation of the antibacterial adhesion properties of NO releasing textured films

To evaluate the anti-bacterial adhesion properties of CarboSil films with respect to surface topography and SNAP concentration, all films with different configurations were incubated with different strains of bacteria in PBS buffer (with a concentration of 1×10^7 CFU/mL) at 37°C for 1 h, respectively. At the end of each experiment, the films were

observed under fluorescent optical microscope and the average of bacterial count on the surface of the films per unit area (10^4 μm^2) were compared (see Figure 6.6).

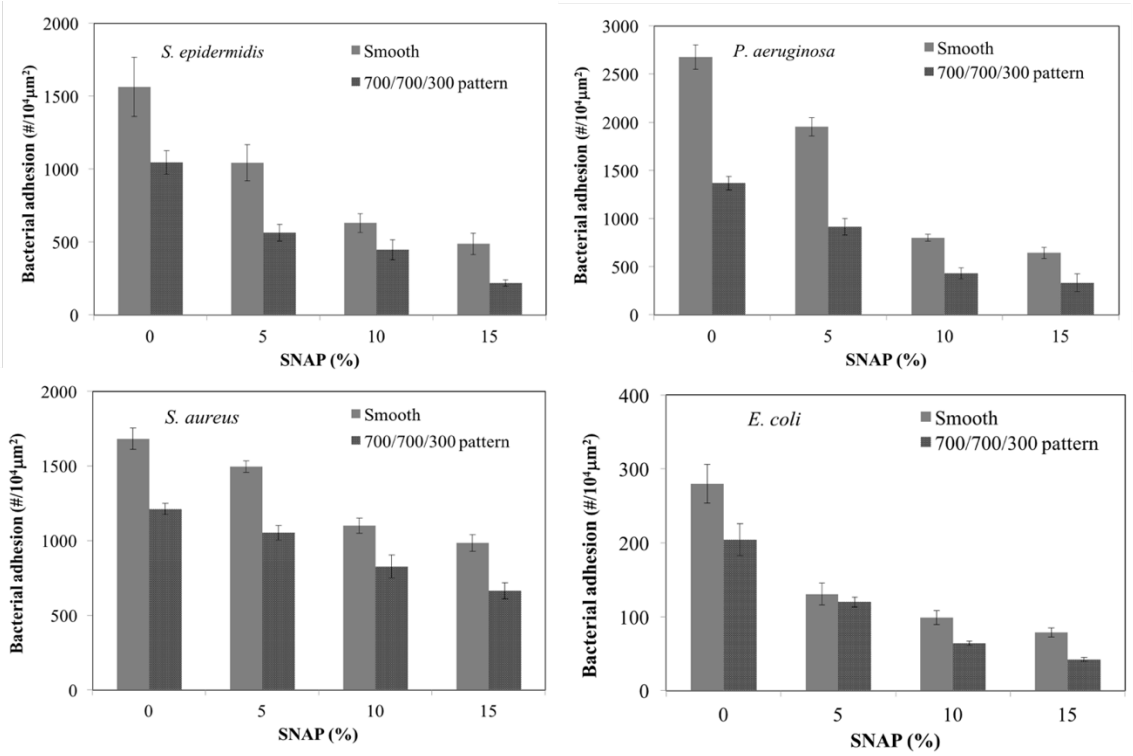

Figure 6.6. Summary of bacterial adhesion on CarboSil films with different configurations under static conditions at 37°C for 1 h, represented as the number of adhered bacteria per 10^4 μm^2 of polymer film.

Without any NO release from the polymer film (0 wt% SNAP), the 700/700/300 nm surface texture alone reduced the bacteria count by 28 %, 33 %, 49 % and 27 % for *S. aureus*, *S. epidermidis*, *P. aeruginosa* and *E. coli*, respectively. However, with NO release from polymer film (15 wt% SNAP), the reduction rate of textured surface increased to 61 %, 86 %, 88 % and 85 %, respectively. Bacterial adhesion generally decreases with an increase of SNAP concentration and the concomitant increase of NO release rate. A univariate general linear model was utilized to analyze the significance of surface texture and NO release (SNAP) on reduction of bacteria adhesion as well as to determine if there is any

interaction between surface texturing and NO release with respect to the observed bacteria count reduction. The results are summarized in Table 6.2 and indicate that either surface texturing or NO release alone have a significant effect on reduced bacterial cell adhesion to the surface, regardless of bacteria strain tested. There was significant interaction between the two factors for *S. epidermidis* ($p=0.037$) and *P. aeruginosa* ($p<0.001$), but a non-significant interaction for *S. aureus* ($p=0.199$) and *E coli* ($p=0.089$). This means that surface texturing and NO release produced a synergistic effect on bacterial adhesion reduction for *S. epidermidis* and *P. aeruginosa* but the effect was only additive for reducing adhesion of *S. aureus* and *E. coli*. But the mechanism of synergy between texturing and NO release on preventing bacterial adhesion in a short period of time is not entirely clear and the different effects of these two factors on different bacteria stains still need careful investigation in the future.

Table 6.2. Statistical analysis of the bacterial adhesion result, in which X1 represents texture and X2 (0, 1, 2, 3) represents 0, 5, 10 and 15 wt% of SNAP in films.

Significance				
Parameter	***S. aureus***	***S. epidermidis***	***P. aeruginosa***	***E. coli***
X1*X2	0.199	0.037	<0.001	0.089
X1	<0.001	0.031	<0.001	<0.001
[X2=0]	<0.001	<0.001	<0.001	<0.001
[X2=1]	<0.001	0.041	<0.001	0.001
[X2=2]	0.013	0.101	0.108	0.492
[X2=3]	0[a]	0[a]	0[a]	0[a]
[X2=0] * X1	n/a	0.049	<0.001	n/a
[X2=1] * X1		0.577	0.004	
[X2=2] * X1		0.527	0.136	
[X2=3] * X1		0[a]	0[a]	

a. This parameter is set to zero because it is used as reference.

AFM surface images of CarboSil films after bacterial adhesion were also taken in order to examine the distribution and orientation of adhered bacteria on polymer film surfaces. The representative images of *S. epidermidis* and *P. aeruginosa* adhesion on CarboSil films with different configurations are presented in Figure 6.7 A and B, respectively. Similar to the optical microscopic images, the bacteria count on polymer surfaces visibly decrease with increasing SNAP concentration (0, 5, 10, 15 wt%), for both smooth and textured films. For CarboSil films with the same SNAP concentration, bacteria attach less to the surfaces with a textured pattern than the smooth surfaces. Of note, the grape shape *S. epidermidis* bacteria were mostly present in 2 or 3 or more cell clusters on the film surface and no cell clusters were trapped in the space between pillars, for films either with or without SNAP impregnation (see Figure 6.7A). However, as shown in the enlarged AFM images (Figure 6.7B), the larger rod shaped *P. aeruginosa* species on the film surfaces were mostly single microbes, and hence this bacteria can be trapped in between the grooves of the pillars on the surface of the textured films without NO release and their orientation is aligned with the pattern features. Surprisingly, the *P. aeruginosa* were merely adhered on the surface but not trapped in between pillar spaces on the textured films when the films do not have NO release, and this indicates the importance of NO in reducing bacterial adhesion via its role as a signaling molecule. In the future, it will be important to examine and compare the influence of different parameters of the pillar arrays in surface topographical designs, including pillar diameter (d), separation distance (s) and pillar height (h), on the bacterial adhesion properties.

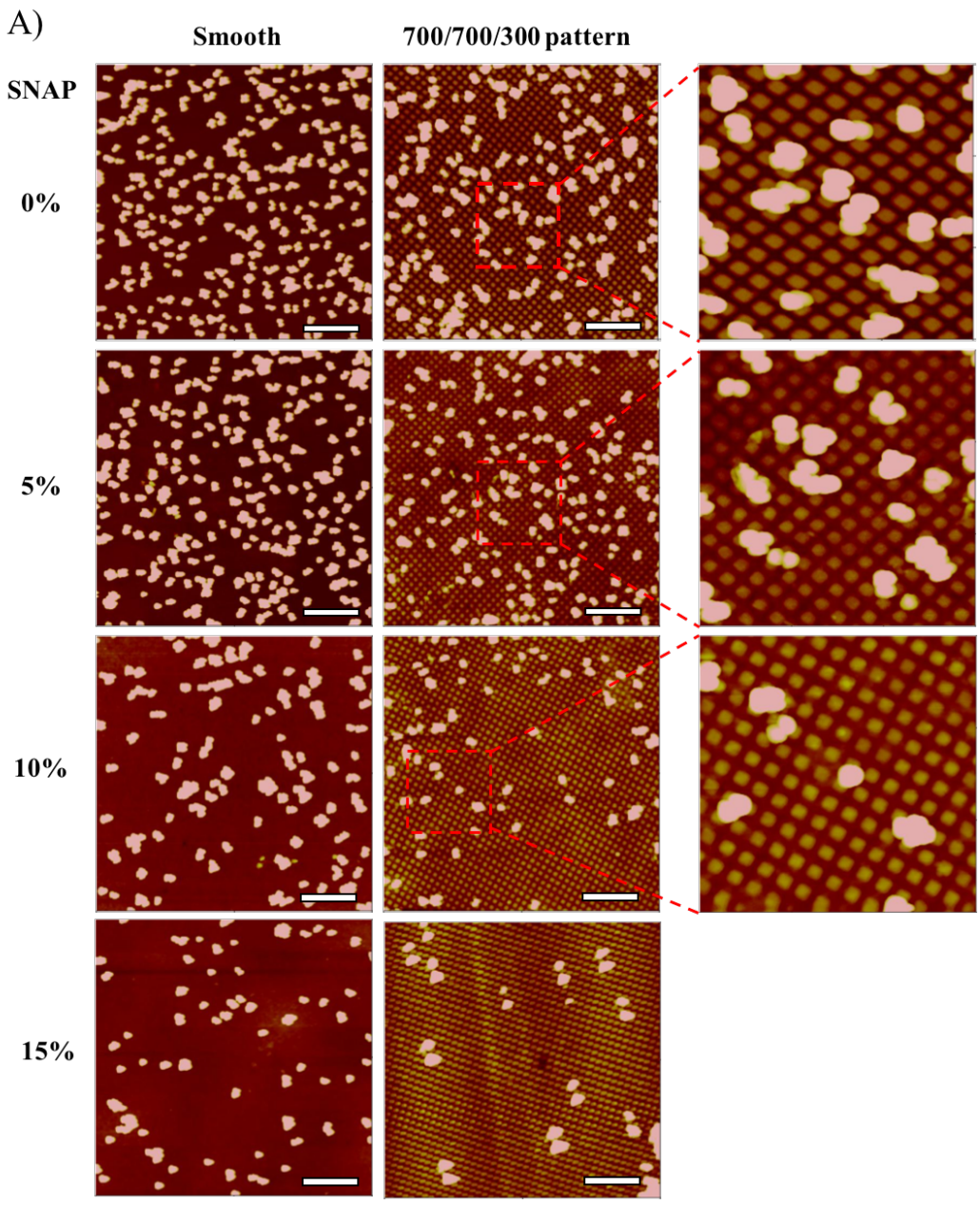
A)
Smooth
700/700/300 pattern
SNAP
0%
5%
10%
15%

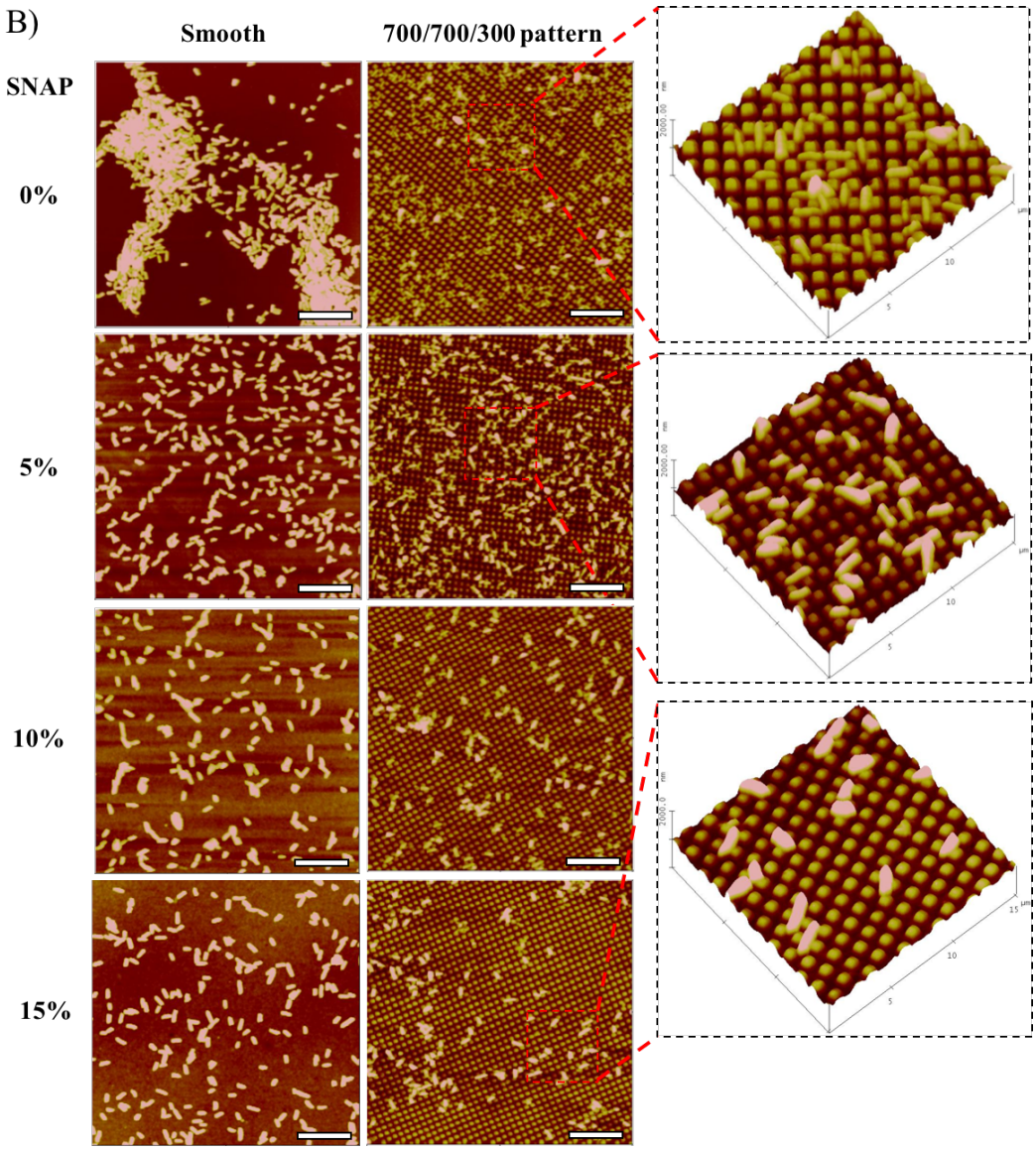

Figure 6.7. Representative AFM images of A) *S. epidermidis* and B) *P. aeruginosa* adhesion on CarboSil films with different configuration after 1 h incubation, scale bar is 10 μm. To better observe the bacterial orientation on the textured pattern surface, he magnified images for *S.epidermidis* (top-view) and *P. aeruginosa* (side-view) are provided (15 μm ×15 μm).

6.4 Conclusion

In summary, a novel dual functioning CarboSil polymer surface with texturing and NO release have been prepared by fabricating polymeric films bearing ordered submicron (700/700/300 nm) pillars on top surface first and subsequently impregnating the films with the NO donor SNAP to achieve NO release. This preparation approach is much more time-efficient and produces more stable and longer-term NO release at physiological conditions, compared to sequential spin coating method described in Chapter 5. Both surface texture and NO release alone can significantly reduce bacterial adhesion of S. aureus, S. epidermidis, P. aeruginosa and E. coli, respectively. Moreover, synergy was observed between texturing and NO release against S. epidermidis and P. aeruginosa microbial adhesion. Such a dual functionality surface should provide a promising approach to devise new biomaterials that can significantly reduce bacterial adhesion, and thus potentially reduce the possibility of medical device-related infections.

.

6.5 References

1 R. M. Donlan, *Clin. Infect. Dis.*, 2001, **33**, 1387–1392.
2 R. M. Donlan, *Clin. Infect. Dis.*, 2011, **52**, 1038–1045.
3 Y. Wo, E. J. Brisbois, R. H. Bartlett and M. E. Meyerhoff, *Biomater. Sci.*, 2016, **4**, 1161–1183.
4 L. Chen and Y. Wen, *Int. J. Oral Sci.*, 2011, **3**, 66–73.
5 C. R. Arciola, D. Campoccia, P. Speziale, L. Montanaro and J. W. Costerton, *Biomaterials*, 2012, **33**, 5967–5982.
6 A. Colletta, J. Wu, Y. Wo, M. Kappler, H. Chen, C. Xi and M. E. Meyerhoff, *ACS Biomater. Sci. Eng.*, 2015, **1**, 416–424.
7 M. A. Almuneef, Z. A. Memish, H. H. Balkhy, O. Hijazi, G. Cunningham and C. Francis, *J. Hosp. Infect.*, 2006, **62**, 207–213.
8 L. C. Xu and C. a. Siedlecki, *Acta Biomater.*, 2012, **8**, 72–81.
9 R. Parameswaran, J. B. Sherchan, D. Muralidhar Varma, C. Mukhopadhyay and S. Vidyasagar, *J. Infect. Dev. Ctries.*, 2011, **5**, 452–458.
10 R. Gahlot, C. Nigam, V. Kumar, G. Yadav and S. Anupurba, *Int. J. Crit. Illn. Inj. Sci.*, 2014, **4**, 162–167.
11 L. Lorente, A. Jiménez, M. Santana, J. L. Iribarren, J. J. Jiménez, M. M. Martín and M. L. Mora, *Crit. Care Med.*, 2007, **35**, 2424–7.
12 M. Otto, *Nat. Rev. Microbiol.*, 2009, **7**, 555–567.
13 E. M. Hetrick and M. H. Schoenfisch, *Chem. Soc. Rev.*, 2006, **35**, 780–789.
14 A. J. Scardino, H. Zhang, D. J. Cookson, R. N. Lamb and R. de Nys, *Biofouling*, 2009, **25**, 757–767.
15 A. J. Scardino, D. Hudleston, Z. Peng, N. A. Paul and R. de Nys, *Biofouling*, 2009, **25**, 83–93.
16 R. Helbig, D. Günther, J. Friedrichs, F. Rößler, A. Lasagni and C. Werner, *Biomater. Sci.*, 2016, **4**, 1074–1078.
17 M. Rosselli, P. J. Keller and R. K. Dubey, *Hum. Reprod. Update*, 1998, **4**, 3–24.
18 J. MacMicking, Q. W. Xie and C. Nathan, *Annu. Rev. Immunol.*, 1997, **15**, 323–350.
19 D. a Riccio and M. H. Schoenfisch, *Chem. Soc. Rev.*, 2012, **41**, 3731–41.
20 E. M. Hetrick and M. H. Schoenfisch, *Annu Rev Anal Chem (Palo Alto Calif)*, 2009, **2**, 409–33.
21 C. Bogdan, *Nat. Immunol.*, 2001, **2**, 907–16.
22 J. O. Lundberg, *Anat. Rec. (Hoboken).*, 2008, **291**, 1479–1484.
23 E. Weitzberg and J. O. N. Lundberg, *Am. J. Respir. Crit. Care Med.*, 2002, **166**, 144–145.
24 B. J. Privett, A. D. Broadnax, S. J. Bauman, D. A. Riccio and M. H. Schoenfisch, *Nitric Oxide - Biol. Chem.*, 2012, **26**, 169–173.
25 L. Plate and M. A. Marletta, *Mol. Cell*, 2012, **46**, 449–460.
26 N. Barraud, M. J. Kelso, S. A. Rice and S. Kjelleberg, *Curr. Pharm. Des.*, 2015, **21**, 31–42.
27 A. Pegalajar-Jurado, K. A. Wold, J. M. Joslin, B. H. Neufeld, K. A. Arabea, L. A. Suazo, S. L. McDaniel, R. A. Bowen and M. M. Reynolds, *J. Control. Release*, 2015, **220**, 617–623.
28 M. C. Frost and M. E. Meyerhoff, *J. Am. Chem. Soc.*, 2004, **126**, 1348–9.

29 G. E. Gierke, M. Nielsen and M. C. Frost, *Sci. Technol. Adv. Mater.*, 2011, 12, 55007.
30 Y. Wo, Z. Li, E. J. Brisbois, A. Colletta, J. Wu, T. C. Major, C. Xi, R. H. Bartlett, A. J. Matzger and M. E. Meyerhoff, *ACS Appl. Mater. Interfaces*, 2015, **7**, 22218–22227.
31 H. Ren, J. Wu, C. Xi, N. Lehnert, T. Major, R. H. Bartlett and M. E. Meyerhoff, *ACS Appl. Mater. Interfaces*, 2014, **6**, 3779–83.
32 H. Ren, A. Colletta, D. Koley, J. Wu, C. Xi, T. C. Major, R. H. Bartlett and M. E. Meyerhoff, *Bioelectrochemistry*, 2015, **104**, 10–16.
33 H. Ren, J. Wu, A. Colletta, M. E. Meyerhoff and C. Xi, *Front. Microbiol.*, 2016, **7**, 1–8.
34 E. J. Brisbois, H. Handa, T. C. Major, R. H. Bartlett and M. E. Meyerhoff, *Biomaterials*, 2013, **34**, 6957–66.
35 C. W. McCarthy, J. Goldman and M. C. Frost, *ACS Appl. Mater. Interfaces*, 2016, **8**, 5898–5905.
36 L. C. Xu and C. a. Siedlecki, *J. Biomed. Mater. Res. - Part A*, 2010, **92**, 126–136.
37 L. C. Xu, P. Soman, J. Runt and C. a Siedlecki, *J. Biomater. Sci. Polym. Ed.*, 2007, **18**, 353–368.
38 H. Ren, J. L. Bull and M. E. Meyerhoff, *ACS Biomater. Sci. Eng.*, 2016, acsbiomaterials.6b00215.

CHAPTER 7

Conclusion and Future Directions

7.1 Conclusion

As demonstrated within this dissertation, nitric oxide (NO), an endogenously produced small gas molecule, has many favorable physiological functions that can be used for improving the biocompatibility of implanted medical devices, such as intravascular catheters, urinary catheters, etc. The term "biocompatibility" is interpreted differently under different circumstances. The ideal biocompatible surface should prevent any protein adsorption, which is almost impossible to achieve. Protein adsorption to device surfaces is considered the first critical step that occurs to promote platelet activation and also the colonization of the device surface with bacteria. NO releasing materials cannot eliminate protein adsorption; however, they can directly inhibit platelet activation and thus disrupt the coagulation cascade which can ultimately prevent thrombus formation. Localized NO release can also kill microbes and prevent bacterial biofilm formation on surfaces. Clearly, a stable and cost-effective polymeric matrix that can provide continuous, long-term NO release would significantly facilitate the applications of the NO release technology in various medical settings. This thesis has focused on the study and applications of SNAP-incorporated polymeric matrices for various biomedical applications.

In Chapter 2, it was demonstrated that doping SNAP into CarboSil 20 80A polymer, a commercial tri-block copolymer of polydimethylsiloxane, polycarbonate and polyurethane, generates a very attractive material for biomedical application. The mechanism of the long-term stability and NO release capability was elucidate using solid-state analysis. This work showed that most of the SNAP crystalizes via hydrogen bonding within the bulk of the CarboSil polymer phase that has very low water uptake and that slow dissolution of the crystals leads to the long-term NO release upon solution contact. SNAP-doped CarboSil catheters with a silicone rubber top-coating showed reduced clotting when implanted in blood vessels of rabbits 7 h and prevented the *S. aureus* bacterial biofilm formation on its surface during 7 d *in vitro* experiments using a drip-flow bioreactor.

In Chapter 3, studies of the real-time crystallization process of SNAP within CarboSil 20 80A were reported. It was also demonstrated that the unique NO release mechanism from this polymer-crystal composite material is directly correlated with the surface area of the polymer that is exposed to aqueous solution, suggesting that a water rich layer within the outermost surfaces of the polymer is the likely site where most of the NO is liberated from soluble SNAP within the polymer. SNAP-doped CarboSil catheters with CarboSil coating exhibited significant bactericidal effects against *P. aeruginosa* and *P. mirabilis* in 14 d anti-biofilm experiments in the CDC bioreactor, when compared to the controls of NAP-doped catheters, as well as just the CarboSil catheters and commercial silicone tubing.

Chapter 4 provided a significant follow-up report to a paper[1] that was initially published that demonstrated, for the first time, that existing commercial urinary silicone Foley catheters can be impregnated with SNAP via a solvent swelling method. In Chapter 4, the SNAP impregnation process was optimized for use with CarboSil 20 80A, a polymer that has better innate biocompatibility compared to silicone rubber and other common biomedical polyurethanes. The SNAP impregnation process was optimized using using dip-coated CarboSil catheters that can be impregnated with a SNAP solution (120 mg/mL in 70 % MEK and 30 % methanol) to achieve 15 wt% SNAP loading within 2 h at room temperature. After thorough drying to remove the impregnating solvent system, the resulting catheters impregnated with SNAP have were found to exhibit significant antimicrobial activity with respect to reducing mature biofilm formation by *S. epidermidis* and *P. aeruginosa*. Testing these SNAP impregnated catheters within a rabbit model also demonstrated their greatly improved hemocompatibility when compared to the control catheters of the same material without NO release.

Chapter 5 reported on a collaboration project between our group and Dr. Lichong Xu and Dr. Christopher A. Siedlecki at the Penn State Medical School. We demonstrated, for the first time, on our effort to combine physical modification (topographical surface texture) and chemical modification (NO release) to create dual-functional antibacterial polymeric surfaces. A CarboSil polymer surface with ordered pillar topographies (400/400/600 nm and 500/500/600 nm patterns) at the top surface and a SNAP-doped layer in the middle was created by spin-coating via a soft lithography two-stage replication process. The NO release from the underlying 15 wt% SNAP-doped CarboSil with 500/500/600 nm texture

on the top can last 10 d at or above the lower end of the physiological flux level. Synergy was observed between surface texture and NO release for the inhibition of *S. epidermidis* bacterial adhesion on the pillared surface. This new polymer surface can inhibit *S. epidermidis* biofilm formation for up to 28 d and provides an exciting approach to improve the antibacterial functionality of current biomimetic biomaterials.

Chapter 6 provided a follow-up to Chapter 5 studies regarding the development of dual-functional biomaterial surfaces with enhanced antibacterial properties. Spin-coating a tri-layer film configuration with SNAP-doped CarboSil within the middle layer can be time-consuming, and the repeated spin-coating of new polymer solution might lead to dissolution and decomposition of the previously dried SNAP layer. Hence in Chapter 6, the combined NO release/textured CarboSil polymer film bearing 700/700/300 nm pillars was made first and then the NO release capability was incorporated to the material using the solvent impregnation technique described in Chapter 3. Raman mapping demonstrated a slightly less uniform SNAP distribution in CarboSil films prepared by this impregnation approach (Chapter 6) compared to the spin-coating method (Chapter 5). The NO releasing textured surfaces displayed a synergistic effect in reducing bacterial adhesion by *Staphylococcus epidermidis* and *Pseudomonas aeruginosa*.

Overall, this thesis work demonstrated that SNAP-incorporated within CarboSil has tremendous potential in improving the hemocompatibility and antibacterial properties of the blood contacting biomedical devices currently used in hospitals. One of its biggest advantages is the stability of this composite material during long-term storage. The lack

of need for precise temperature control during storage and shipping is very beneficial for any future commercialization of medical device products that would employ this technology.

7.2 Future Directions

7.2.1 The Cytotoxicity Test of SNAP on Mammalian Cells

One important aspect that remains to be examined is whether SNAP-impregnated polymeric materials are safe in applications when they are not in contact with blood, such as when employed to create antimicrobial urinary catheters.[1] In this application the NO release would occur in direct contact with urothelial cells that line the urethra, and unlike blood, such cells would not immediately scavenge the NO (via reaction with oxyhemoglobin). Therefore, A follow-up study is needed to examine whether NO releasing SNAP-impregnated silicone Foley urinary catheters might potentially have cytotoxic effect on the urothelial cells.

Very preliminary experiments toward this end were recently conducted by treating cells with SNAP solutions of different concentrations to evaluate their cytotoxicity. Of note, AD-293 cells, a human embryonic kidney cell line, rather than urothelial cells were used as the subject cells in this preliminary study because of easy access.

SNAP solution (7.5 mM) was prepared in PBS buffer first and then diluted by Dulbecco's modified eagle medium (DMEM) cell culture media with 2 % BSA added to the desired SNAP concentrations of 0, 3.75, 7.5, 15, 150, 300, 500, 750 and 1500 μM. The AD-293

cells were then plated (~10,000 cells/well) into the wells of the sterile 96-well cell culture plate in 200 μl of cell culture medium. When the cells reached 90-95 % confluence, the cells were treated with the different dosages of SNAP solution. Finally, at different time points (1, 2, 3, and 5 d), the cytotoxicity test was performed using the standard lactate dehydrogenase (LDH) assay kit[2] and the results are shown in Figure 7.1.

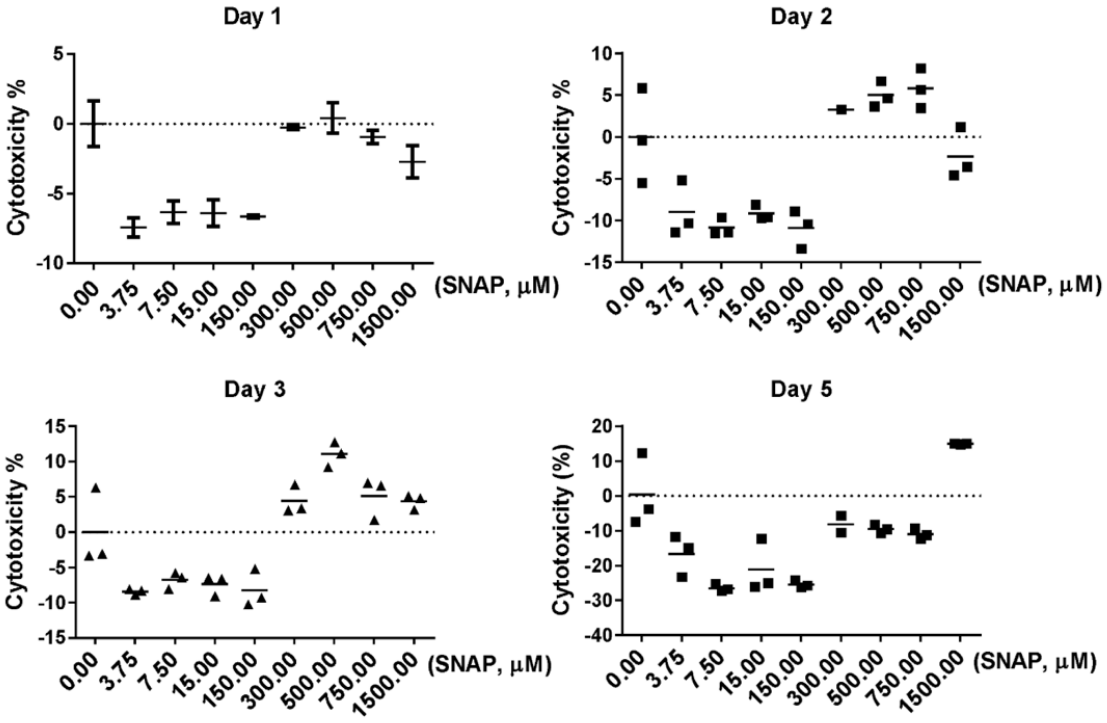

Figure 7.1. The cytotoxicity effect of SNAP solutions with different concentrations on AD-293 cells.

The results indicated that SNAP has very minor cytotoxic effect on AD-293 cells within 5 d culture period and that low doses of SNAP (<300 μM) could decrease cytotocixity and potentially protect the AD-293 cells. Clearly, more cytotoxicity studies like this are needed in the future, especially using urothelial cells, and perhaps also using polymeric films with NO release placed on the surface of the cells, rather than solution phase SNAP.

7.2.2 SNAP-Impregnated PDMS Microfluidic Device for Continuous Blood Analysis

One potential application of SNAP-impregnated PDMS membranes/tubing is for the use in fabrication of hemocompatible microfluidic devices. Dr. Shuichi Takayama's research group in the Biomedical Engineering Department at U of M is interested in taking advantage of this material in order to pump whole blood at low flow rates through PDMS tubing and microchannels.[3] This would be particularly useful in continuous monitoring of many important blood analytes, such as glucose, lactate, pH, etc. For preliminary studies, in order to fabricate the NO releasing microfluidic devices, heat curable PDMS Sylgard® 184 (Dow Corning Corporation) was spin-coated on microfluidic molds and cured to form thin membranes with embedded microchannels.[4] These membranes were then impregnated in a solution of SNAP THF solution (50 mg/mL) for 24 h[4] and the final membranes were allow to dry in ambient conditions for several days for complete removal of residual solvent. Then one PDMS membrane with channels and one without channels were first treated with plasma oxidization,[5] which can functionalize the PDMS surface and allow for bonding, and then baked at 60 °C for 120 s. After bonding, holes were punched out at the inlets/outlets, and SNAP-impregnated silicon tubing was connected in place to allow continuous flow of sample solution through the device. The ultimate goal of this approach would be to use an integrated microfluidic pump[6] to continuously withdraw patient blood at a constant low flow rate through an NO release SNAP doped catheter, which will then flow over different sensors for analyte detection (see Figure 7.2). By minimizing sample volume, this device would minimize the impact of continuous blood

withdrawal and analysis on the patient. A braille display based pump was first proposed as the peristaltic pump for continuous blow withdrawal (see Figure 7.3).

Further studies are now needed to test this system for its ability to be coupled with a tiny SNAP impregnated catheter tubing for sampling blood continuously at very low flow rate without observing any clot formation in the tubing and pump. Animal studies to pursue such testing will hopefully take place soon.

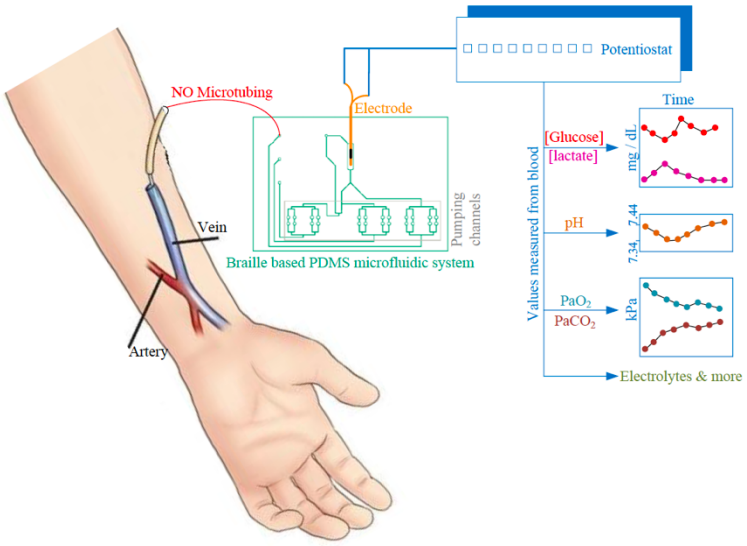

Figure 7.2. The schematic of the integrated microfluidic pump for continuous blood withdrawal from patient and analyte monitoring.

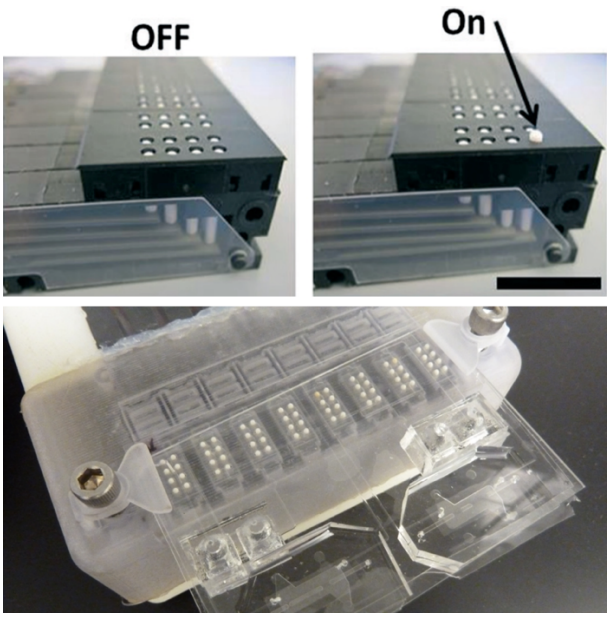

Figure 7.3. The braille-based microcirculatory channels for peristaltic pump. Upper images: braille display at ON and OFF mode; lower image: the connection between PDMS channels and the braille nodules.

7.2.3 Development of Dual-functional Antibiotic and NO Releasing Catheters

It is known that bacteria are sensitive to most broad spectrum antibiotics before they are protected by the extracellular polysaccharide matrix, also known as biofilm. Cook Medical has manufactured catheters with the antibiotics rifampin and minocycline impregnated within peripherally inserted central line (PICC) catheters, with the aim of reducing the risk of catheter-related bloodstream infections. However, after bacteria colonize the catheter surfaces, they can form biofilm that protect them from antibiotic penetration. Therefore, it may be of interest to develop dual-functioning catheters that can release antibiotics as well as nitric oxide (NO), so we can utilize the function of NO as a signaling agent to prevent biofilm formation and the efficient bactericidal function of antibiotics against various bacteria strains, without the physical protection from biofilm.

So to pursue the preliminary feasibility of this conept an impregnation method for incorporation of two antibiotics, structures shown in Figure 7.4, rifampin (A) and minocycline (B) as well as NO donor SNAP, into commercial silicone tubing was pursued.

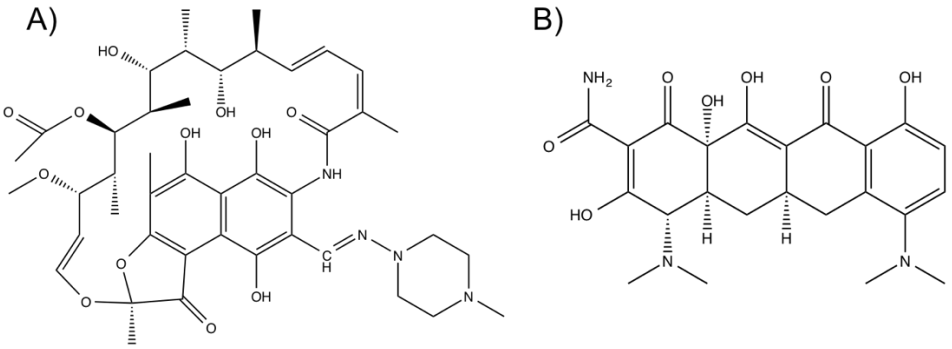

Figure 7.4. The structures of antibiotics rifampin (A) and minocycline (B).

Before screening the solvents system that can dissolve rifampin, minocycline and SNAP, and also be able to impregnate silicone rubber material, it is very important to optimize characterization method for accurate detection and quantification of the two antibiotics separately when the impregnated polymer is in contact with physiological solution. The accurate qualification and separation of the antibiotics is essential for determination of the total loading of antibiotics within the silicone tubing. UV-Vis spectra of rifampin and minocycline (50 μg/mL in methanol for each analyte), were obtained separately (see Figure 7.5).

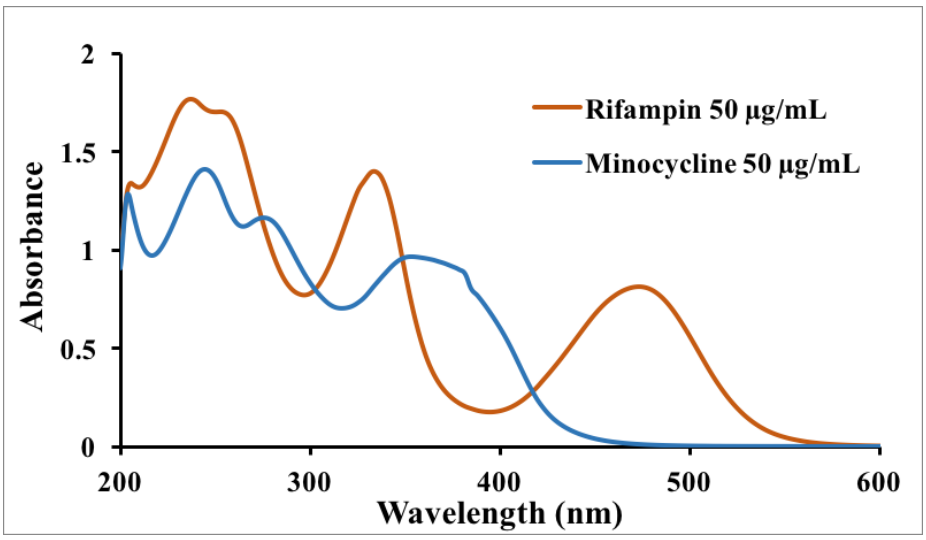

Figure 7.5. The UV-Vis absorbance spectra of rifampin and minocycline at 50 µg/mL.

To avoid signal overlap in absorbance when both compounds are present in the soaking solution, 475 nm and 350 nm can be used as the characteristic wavelengths for identification and quantification of rifampin and minocycline, respectively. Each antibiotic stock solution (50 µg/mL) was diluted with PBS buffer to the desired concentration for standard calibration. Calibration curves for both rifampin (at 475 nm) and minocycline (at 350 nm) were conducted by measuring the UV-Vis absorption of solutions containing different concentration of each antibiotic (see Figure 7.6 and Figure 7.7 for the absorbance data (A) and calibration curves (B) for rifampin and minocycline, respectively).

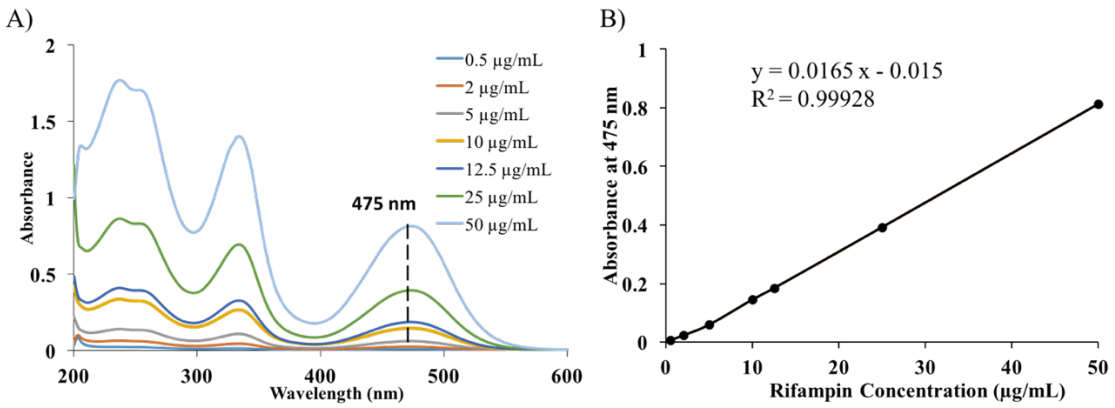

Figure 7.6. The UV-Vis absorbance spectra of rifampin solutions with different concentrations (A), and the resulting calibration curve of absorbance at 475 nm vs. concentration (B).

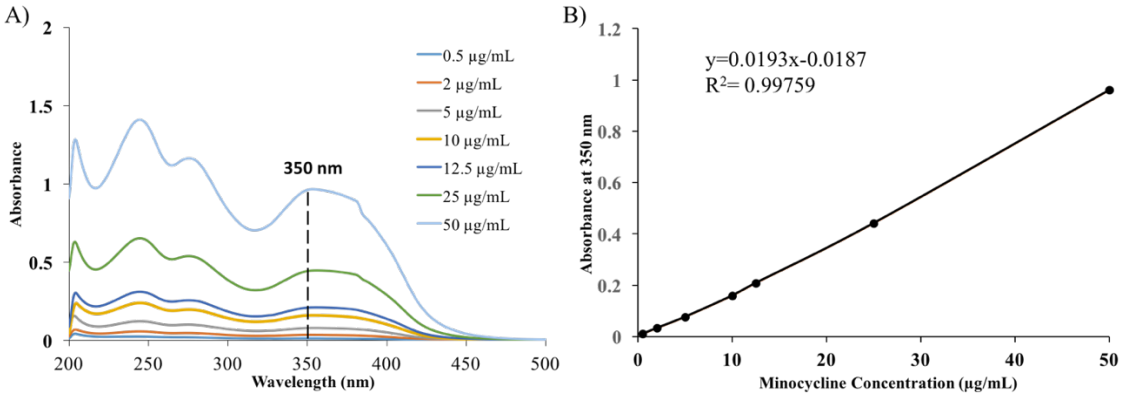

Figure 7.7. The UV-Vis absorbance of minocycline solutions with different concentrations (A), and the resulting calibration curve of absorbance at 350 nm vs. concentration (B).

Liquid chromatography-tandem mass spectrometry (6520 Accurate-Mass Q-TOF LC/MS, Agilent Technologies, CA) can also be optimized as a detection and qualification method for analyzing soaking solutions containing both antibiotics. In preliminary studies toward use of this approach, the mass spectrometer used electrospray ionization in the positive ion mode, and the detected species were $[M+H]^+$. The m/z for rifampin ion is 823.4119, while the m/z for minocycline is 458.1922. A reversed-phase column (ZORBAX RRHD Eclipse Plus C18, 1.8 µm, 2.1 x 50 mm) was used in order to separate the two antibiotics. The

gradient was obtained with eluent A (water with 0.1% formic acid) and eluent B (95% acetonitrile, 0.1% formic acid). After sample injection (15 μL), a linear change of eluent mixtures from 95% A to 40% A over 7.5 min was carried out with a flow rate of 0.4 mL/min. Minocycline, log P = 0.20 (obtained by Marvin Sketch software) was separated from rifampin and eluted from the column first, between 2 to 2.2 min; rifampin, with log P = 1.91, instead, eluted from the column at between 6 to 6.3 min, see Figure 7.8 for the chromatography result.

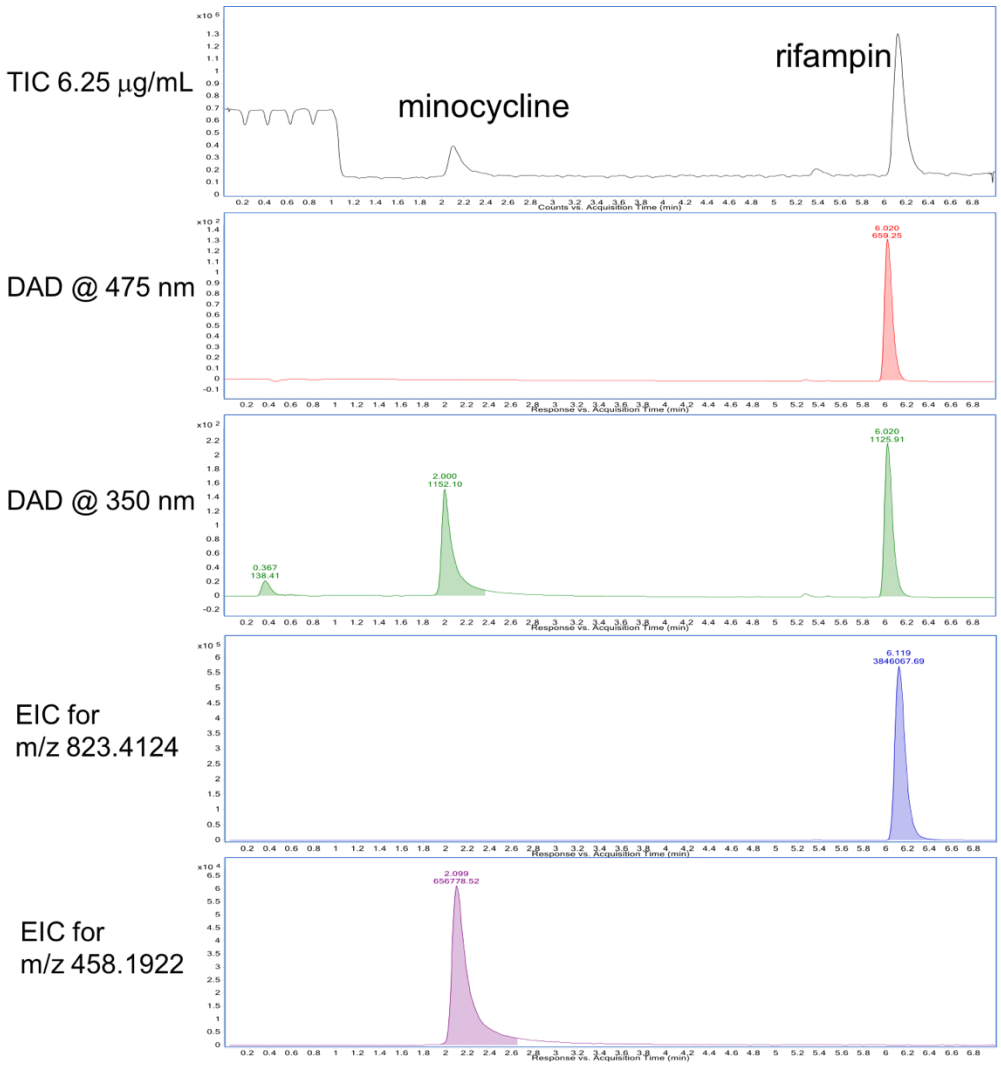

Figure 7.8. The total ion chromatography (TIC) of the separation result for a solution containing minocycline and rifampin, each at 6.25 μg/mL. The UV-Vis measurements using diode array detection (DAD) and the extracted ion chromatography results (EIC) of both antibiotics were also obtained.

In order to eventually quantify the concentration of antibiotics in the solution using MS, calibration curves of concentration and peak area were plotted for samples detected by MS (see Figure 7.9).

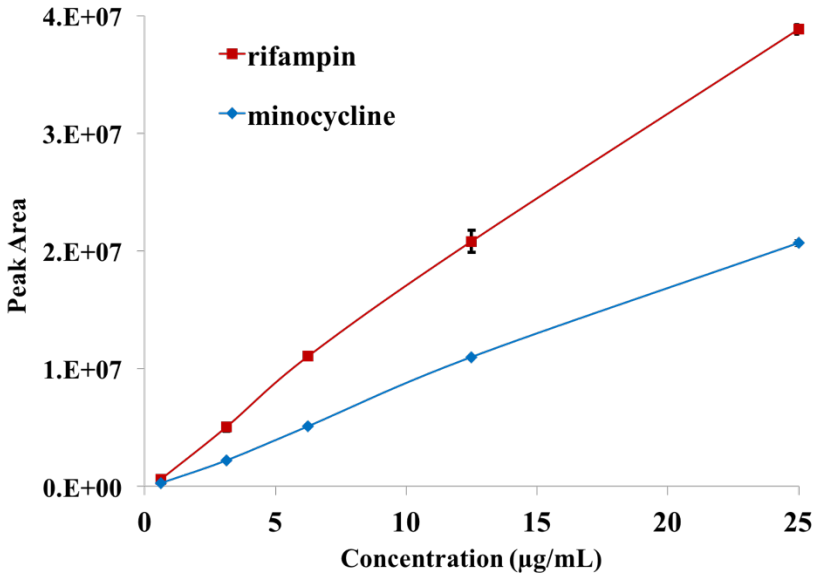

Figure 7.9. The calibration curves of peak area vs analytes concentration, for solutions containing 0.625, 3.125, 6.25, 12.5 and 25 µg/mL of both rifampin and minocycline.

The ultimate goal of for future research would be to optimize the solvent system for impregnation of both of the antibiotics and SNAP into silicone tubing (and potentially other catheter tubing (e.g., CarboSil), and fabricate dual-functioning antibiotic and NO releasing polymeric tubing that might exhibit enhanced antibacterial efficiency. After characterizing the NO and antibiotic release rates from such tubing, the device can then be tested in existing bioreactor models for antimicrobial activity, and compared to tubing that only release NO (via SNAP impregnation) or only both antibiotics only. This would enable us to determine whether the combination of NO with the antibiotics significantly increases the antimicrobial/antibiofilm activity of the catheter tubing compared to each approach alone.

7.3 References

1 A. Colletta, J. Wu, Y. Wo, M. Kappler, H. Chen, C. Xi and M. E. Meyerhoff, *ACS Biomater. Sci. Eng.*, 2015, **1**, 416–424.

2 F. K.-M. Chan, K. Moriwaki and M. J. De Rosa, *Methods Mol. Biol.*, 2013, **979**, 65–70.

3 Z. Zhang, J. Borenstein, L. Guiney, R. Miller, S. Sukavaneshvar and C. Loose, *Lab Chip*, 2013, **13**, 1963–1968.

4 A. Mata, A. J. Fleischman and S. Roy, *Biomed. Microdevices*, 2005, **7**, 281–293.

5 M. J. Owen and P. J. Smith, *J. Adhes. Sci. Technol.*, 1994, **8**, 1063–1075.

6 W. Gu, X. Zhu, N. Futai, B. S. Cho and S. Takayama, *Proc. Natl. Acad. Sci. United States Am.* , 2004, **101**, 15861–15866.